THERMAL AND DAYLIGHT PERFORMANCE OF DOUBLE-SKIN FACADES; CASE STUDY OF AN OFFICE BUILDING

A Thesis

by

Hadil H. S. Alsafadi

Submitted to the
Graduate School of Sciences and Engineering
In Partial Fulfillment of the Requirements for
the Degree of

Masters in Architecture

in the
Department of Architecture

Özyeğin University
December 2021

THERMAL AND DAYLIGHT PERFORMANCE OF DOUBLE-SKIN FACADES; CASE STUDY OF AN OFFICE BUILDING

Approved by:

Asst. Prof. Dr. Turaj Arda Aşrafi,
Advisor,
Department of Architecture
Özyeğin University

Asst. Prof. Dr. Ece Özdemir
Department of Architecture
Özyeğin University

Asst. Prof. Dr. Nazanin Moazzen
Department of Architecture
Maltepe University

Date Approved: 28 December 20

To my parents and Abu Elyas

ABSTRACT

Depending on the climatic region, double-skin facade structures can aid in achieving human comfort and save building energy through controlling the interaction between indoor and outdoor environments. Sustainable designs aim to maximize admitted indoor daylighting to help reduce energy consumption.

The study analyses different variables of double-skin facades that may affect the thermal performance and daylighting of the building. The main objective is (a) investigate the thermal effect in office buildings (b) analyze admitted daylight into the building (c) propose a flexible model that contribute to the overall performance and formation of the building façade.

The framework consisted of investigating an office building located in Eskisehir, Turkey. The research evaluates performance-based computational simulations using Rhinoceros, Ladybug, and climate studio combined with Energy-Plus. The assessment focuses on the various characteristics of the façade, such as; façade distance, solid to void ratio and rotation degree. Four different façade iteration were designed and tested on all four façade directions of the office building.

The results of all four different proposals have reduced the highest radiation value indoors significantly in both seasons. The highest radiation reduction reached 32.12% in summer and 22.82% winter. The highest increase in daylighting reached 83.78% in summer and 45.58% in winter. The results confirm that the use of wider panels provides lower concentrated solid areas of panels and admits more radiation and daylight levels into the building.

ÖZETÇE

İklim bölgesine bağlı olarak, çift cidarlı cephe sistemleri, iç ve dış ortamlar arasındaki etkileşimi kontrol ederek, konforun sağlanmasına ve bina enerjisinden tasarruf edilmesine yardımcı olabilir. Sürdürülebilir tasarımlar, enerji tüketimini azaltmak için, binaya giren gün ışığını arttırmayı amaçlar. Ancak kontrol altına alınmamış güneş ışınları, yetersiz gün ışığı veya uygun olmayan ısıl koşullar oluşturarak iç ortamda olumsuz etkilere yol açabilir.

Çalışmanın öncelikli amacı, çevreye duyarlı bir tasarım için ısıl konforsuzluğunu azaltmak ve iç mekâna ulaşan gün ışığını kontrol etmek için kullanılacak çift cidar cephe yapılarını analiz ederek farklı senaryoların etkisini ortaya koymaktır. Çalışma, çift cidarlı cephelerin binanın termal performansını, binaya giren gün ışığını etkileyebilecek temel yönlerini ve farklı değişkenlerini analiz etmektedir. Ayrıca bu çalışmanın genel amacı (a) ofis binalarında çift cidarlı cephelerin ısıl etkisini araştırmak (b) binaya giren gün ışığını analiz etmek (c) bina cephesinin genel performansına ve oluşumuna katkıda bulunan esnek bir model önermektir.

Çalışma kapsamında, Eskişehir'de tasarlanan bir ofis binası ele alınmıştır. Araştırmada, Rhinoceros, Ladybug ve Energy-Plus ile ClimateStudio yazılımları kullanılarak, performansa dayalı hesaplama simülasyonları gerçekleştirilmiştir. Çift cidarlı cepheler, birçok parametre sebebiyle performansları etkilendiği için sıradan cephelere göre oldukça karmaşıktır. Değerlendirmede, cephe cidarları arasındaki mesafe, doluluk-boşluk oranı ve modüllerin dönme derecesi gibi çeşitli cephe özelliklerine odaklanmıştır. Bu özellikler dikkate alınarak, sıradan bir ofis binasının dört cephesini kapsayan dört farklı çift cidar cephe tasarlanmış ve analiz edilmiştir.

Dört cephe önerisinin analiz sonuçunda da, yaz ve kış mevsimlerinde iç mekanlardaki en yüksek radyasyon değerini önemli ölçüde azalttığı görünmüştür. Bu konu kamaşmaya olasılığını azaltılmış olduğu anlamına gelmektedir. Yaz aylarında, en yüksek radyasyon en çok%32.12 ve en az %18.50 azaldığı görünmüştür. Kış aylarında ise, en yüksek radyasyon en çok %22.82 ve en az %7.59 azaldığı görülmüştür. Öte yandan, hemen hemen tüm katlar için ortalama radyasyon değerinin arttığı gözlendi. Bu konu ise içerideki yeterli ve gerekli aydınlık seviyesine ulaşmak için gereklidir ve yarar sağlamaktadır. Elde edilen bulgulara göre dört önerinin tamamında ortalama ve ortanca (medyan) gün ışığı değerlerinde bir artış kaydedilmiştir. Yaz aylarında, ortalama gün ışığındaki en az artış %36,47'ye, en yüksek artış ise %83,78'e ulaşmaktadır. Kış aylarında ise, ortalama gün ışığındaki en düşük artış %19.90'a, en yüksek artış ise %45.58'e ulaşmaktadır. Sonuçlara göre, daha geniş panellerin kullanımının, panellerde daha çok boşluk kullanıldığında, binaya daha fazla homojen gün ışığı sağlandığı ve ayrıca dönüş açısının da bu konu üzerinde önemli bir rol oynadığını görünmektedir.

ACKNOWLEDGEMENTS

All praises to Allah Almighty who has seen me through my journey in Master of Architecture Program, in the Graduate school of Engineering and Science in Ozyegin University.

I would like to express my special gratitude to my advisor Dr. Touraj Ashrafian, who has shown his unconditional support, patience, motivation, and consistent guidance throughout the years, especially when I was confused and distressed. His efforts and encouragement to ensure my successful accomplishment of this research were invaluable and contributed to the success of many of my studies in general and this dissertation in particularly.

My sincere gratification for my beloved parents, amazing brother Abdullah and my lovely family, whom without I would not be where I am today. Thank you for your constant support, encouraging words and care, I am forever in debt to you. I would like to express my appreciation for my dear friend, Farah Al-Kilani and Kamile Ozcan who have supported me even long before the beginning of my study and always believed in me.

A special thanks to all my friends and colleagues who have stood by me through the most distressing and confusing times, and for their support during my studies.

TABLE OF CONTENTS

LIST OF TABLES

LIST OF FIGURES

CHAPTER I

INTRODUCTION

1.1 Argument and Theoretical Frame:

More than half of the energy consumed in the building sector is utilized to achieve thermal comfort through heating and cooling systems [1]. The building envelop forms a relationship between indoors and outdoors by controlling the transmission of exterior environmental elements to the indoor environment. That provides environmentally efficient interactive buildings through fulfilling 80% of environmental solutions [2]. Double Skin Façades (DSFs) are considered one of the solutions to achieve energy efficiency and sustainability in the building sector [3]. DSFs contribute to energy reduction, enhancing aesthetics, achieving thermal performance, improving ventilation and acoustics [4].

A proper solar shading technique should provide the building with an envelope that balances daylight levels and solar radiation, controls the thermal exchange, and contributes to the annual energy savings [5] . However, this process is complicated due to the challenges that DSFs encounter, particularly with buildings that possess a higher proportion of curtain walls as the facade. Buildings with higher glazing ratio that adapt shading devices to overcome natural ventilation and thermal comfort face other challenges. That adaptation had minimized natural daylighting and increased reliance on artificial lighting, consequently increasing heat gain. In that case, artificial cooling can be a solution to overcome the heat

gained from the excess use of artificial lighting, which results in high energy consumption and cost [4] .

The integration of shape, size and distribution of the building envelope's pattern plays a crucial role in minimizing thermal gain and maximizing daylight [6]. Artificial lighting usage can be reduced by depending on the renewable energy of daylight as the primary lighting resource during the day [7]. Natural daylight provides the occupants with positive mental, psychological, and physiological effects [8]. However, some aspects must be considered, such as the visual comfort and heat gain to enhance the quality of the interior space because "nature is always in motion, never at a standstill" [9]. To provide a climatic adaptive design, it is necessary to analyze the relationship between the space and other aspects that concern daylighting in the area, such as: the amount of lighting and radiance [10]. Other parameters, such as the regional climate and building function, affect the building envelope efficiency [11].

In architecture, the form of the building determines the building identity and defines the environmental interaction. It will also determine the admitted daylight amount into the building [12]. With technological, innovative passive design techniques, which became readily available [13], enlarging these opportunities at early design stages will increase investment in environmentally high-performance solutions.

'Parametric' is originally coming from ‘parameter’ which mean “measurable factors that define or limit a system” [14]. The concept of parametric designs is mainly concerned with a software that creates and recognizes the relationship between different sets of

parameters and allows the designer to adjust those parameters to analyze the model's reaction according to the modified data [15]. Therefore, parametric designs are known as defining a problem using variables in order to alter those variables to determine the most suitable solution to the problem. Parametric designs are widely used in contemporary design practices as they depend highly on computers. The parameters are generated through code writing and unique programming language [16]. Parametric skin façade patterns are still being developed to yield solutions in interdisciplinary processes [17] .

The impact of parametric skin on building daylighting and thermal performance has not been widely researched. These types of facades present a complex geometry, making it harder to model using conventional simulation tools and software, which results in a more intricate design process. Energy consumption tools like Energy Plus are used mainly to evaluate an entire building's energy performance. Still, those software's lack accuracy in describing the energy transformation through sophisticated geometry [18]. The software came short in providing daylight prediction in the space, especially if the gap between the façade and space increases [19]. A study by Lagios et al. tried to develop methods to overcome this limitation using software programs such as Rhinoceros and Grasshopper [20]. Few researchers had combined both Parametric designs (Glapagos/Grasshopper) with energy performance tools (Diva) to assess daylighting, energy consumption and CO2 emissions [21].

Previous works were dedicated to studying the effect of fixed shading systems like overhangs, fins, and louvres on thermal performance [22] using TRNSYS; an energy simulation software along with Engineer Equation Solver (EES) and Energy Plus [5]. A few studies have focused on creating stability between reducing solar gains and efficient

daylighting through solar control systems [23] [24]. Few studies analyzed the balance between daylighting and thermal performance to reach design optimization through perforated skin facades [25] and with interactive kinetic skin facades [26] and parametric patterns on office spaces [27].

1.2 Problem statement:

According to previous literature, the rapidly growing energy consumption has called out the researchers' concerns to develop extensive studies dedicated to façade thermal and daylight performance in accordance with energy conservation.

The impact that parametric skin façade has on daylighting and thermal performance has not been widely studied. Most DSF studies are limited to colder climates of Europe and North America, but they lack accuracy in describing the strategical application of a sophisticated façade design. Few studies have investigated the interaction between thermal performance levels regulated by double-skin façade in the Mediterranean and temperate climates.

1.3 The purpose and objectives of the study

Shape integration, size and distribution of the building envelope's pattern plays a crucial role in minimizing glare and maximizing daylight [6]. The research underlines the role of the parametric façade in performance-based design. The research aims to assess and evaluate recent developments related to DSFs applied on office buildings and realize a

flexible model configuration that contributes to the overall performance and formation of the building façade.

In this procedure, the study investigates an energy-efficient approach driven by double façade patterns through the strategic application of different iterations. The iterations tested in the parametric skin façade are based on the distance between panels and the rotation degree of the panels and the overall solid to void ratio. The research analyses different façade patterns on office building units by evaluating their environmental performances to identify the optimum façade pattern. The optimized design aims to find an equilibrium between available daylighting and total radiation in an office building in Turkey. The study mainly focuses on façade distance optimization and façade rotation optimization to balance energy consumption and occupants' comfort.

1.4 Thesis hypothesis

This research hypothesis states that for the selected office building in Eskisehir, the larger the void to solid in the façade pattern applied to the building, the higher the heat transfer and the higher the daylight that penetrates the building. On the other hand, the smaller the void to solid rate, the lower the heat transfer and the lower is the daylight is going to be. Therefore, this thesis focuses on studying different designs of façade dimensions, rotation rate and gap optimization to analyze their effect on heat transfer, daylighting and achieving occupants' comfort in this office building.

Chapter II

AN OVERVIEW ON DOUBLE-SKIN FAÇADE

The first part of this chapter reviews different definitions of DSFs by various authors and researchers. Then it explains the basic concept and components of the system, followed by a brief timeline of the most notable DSF buildings and their development through time.

DSFs existed way back in most European houses in the form of box-like windows that were utilized to improve the thermal insulation of the house [28] [29]. In literature, DSFs have many definitions. They are defined by the Belgian Building Research Institute (BBRI) as an impermeable or air separated and penetrated systems that create one or more layers. The system allows the air to circulate the building sides and adapts the building to the surrounding weather conditions [30]. It may have either active or passive ventilation techniques, and sometimes both techniques are integrated. Claessens and DeHerde identify DSF as additional second skin to the original surface, and it is primarily translucent. The gap and the air in-between both skins work as a buffer zone that insulates the building. Hendriksen stated that the main aim of DSF is to achieve large transparent and glazed openings while decreasing energy consumption [31]. DSF in architecture filters direct sunlight through its translucent panels [32]. The panels control the radiation and reflect direct sunlight while providing a clear exterior view [33].

Oesterle defines the DSF as a multi-layer system with a buffer zone between the inner and outer layer that protects the building from direct sunlight and provides ventilation [28].

Ding et al. added that the external façade layer offers sound insulation against the surrounding environment [34]. Kim & Song comprehensively grouped the construction of DSF process into; “Shaft-box façade, multi-story façade, Box Window façade and Corridor façade [35]. Chan debated that the outer layer should consist of a specific type of glass compatible with the surrounding weather and environment, and the cavity ranges between 200mm and 2 meters, sometimes more. The cavity contributes to reducing heat loss and therefore maximizing the thermal performance of the building. Moreover, the ventilated DSF envelops the heat and prevents heat transference into the buildings, eventually reducing solar gain [36].

In 1978, Richard Rogers expressed his vision of buildings with DSF “A building becomes a chameleon which adapts. A properly equipped and responsively clothed building would monitor all internal and external variables, temperature, hygrometry and light levels, solar radiation etc., to determine the best energy equation by given these conditions and modify the building and its internal systems accordingly. It is not too much to ask of a building to incorporate, in its fabric and its nervous system, the very basic vestiges of an adaptive capability” [37].

2.1 Technological development of Double Skin Facade

DSF buildings started being built at the beginning of the 1900s but were not so developed or popular at that time. They were designed to maximize human comfort and energy efficiency in the existing and new buildings [38]. The evolution of manufacturing and technology had a deep, direct connection with the development of DSF. The concept and development of the systems can be tracked down through architecture history. Building

envelopes started being considered since the 20th century as a form of aesthetic structures that add protection for the residents and contribute to saving energy usage inside the building. Previously, the envelop used to have many limitations concerning the amount, capacity, and design of the window, but not anymore. [39].

The first DSF building was created by the Architect Richard Steff and constructed around 1903 in Gienge, Germany. The building was called after its designer; The Steiff toy Factory. The DSF system's main goal focused on achieving maximum daylighting in defiance of the cold climate and improve thermal insulation. [40] (Figure 1).

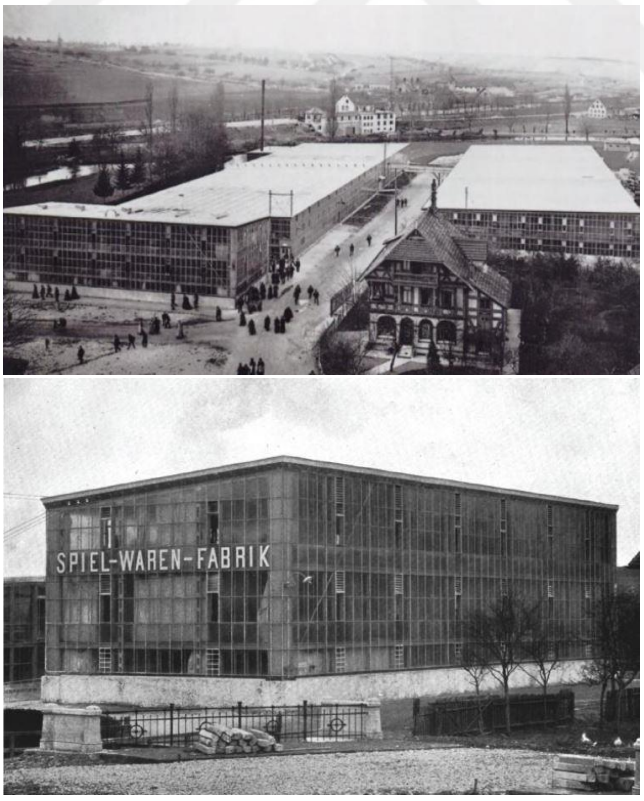

Figure 1: The first DSF building: Steiff toy factory. Source: (Fissabre & Niethammer, 2009).

The Steiff factory building dimensions are 30 m x 12 m x 9.4 m and consists of three floors. The building is embraced by a total DSF envelope that extends from ground to ceiling, topped by a flat roof. The inner shell expands between the upper borders of each floor until the lower border of each ceiling. The building skin façade system can be considered a more developed and innovative than the building structure, as the façade bears its weight and defies the wind pressure [41] (Figure 2).

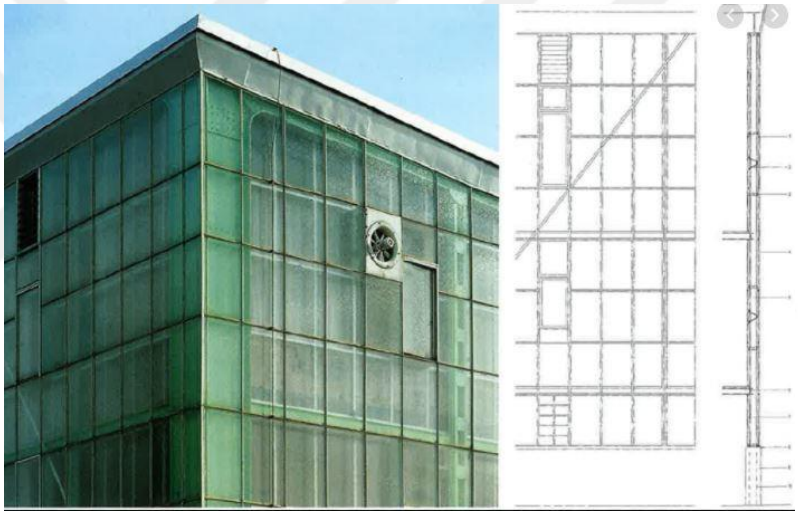

Figure 2 : Façade section of Steiff Factory. (Source: Alessi, 2008)

The building façade generally saves electricity by providing a well-lit office space that creates a productive working environment. Although the design aimed to utilize maximum daylighting, the Planning authorities was worried about excessive summer glare which might blind the workers. That concern was settled by installing sun-protection drapes with several inspection holes and a 25cm cavity gap [42].

In Austria, Vienna, a double skin skylight in a Post Bank was built in 1912 by Otto Wanger and was named after him. The building was founded in two phases within 8 years,

from 1904 to 1912. The central skylight is situated at the central hall of the building as a double skin to reduce heat loss. The double skin skylight is fixed together and attached with a steel structure. Although the building went through some renovations in the 70s to enhance the lighting and install air-conditioning, the original skylight had not been altered [43].

Experimentations and studies started being conducted in the 1920s to improve DSFs' heating and cooling potential as well as aesthetics [42] [44]. Le Corbusier was amongst the earliest contributors to further improve the DSFs structures. He designed many buildings using DSF systems; Centrosoyus in Moscow, in 1928, Cite de Refuge and Immeuble Clarte in 1929. DSFs started being highly implemented in buildings in the late 1970s as they became further improved [45].

The energy crisis that occurred in 1973 was the reason that the concept of sustainability was born. Natural resources, such as solar, wind and geothermal power were needed to be practically and effectively utilized. Those renewable resources gained prominence and became high in demand. Utilization of natural energy resources contributed to reducing the overall cost of energy, minimizing energy consumption, and producing the required energy for the building. Subsequently, DSFs became very popular and gained importance as they have the potential to utilize renewable energy resources and merge technology and energy-saving with aesthetics [38] [39].

Climate responsive architecture was first documented back in 4BC [46]. This type of vernacular architecture incorporated the regional climate effectively and seek unique design techniques which maintained the microclimate of the building and the occupants' thermal comfort [46]. However, an International Style had been introduced in architects' training

curriculum which encouraged the application of active methods to achieve thermal comfort and disregarded passive techniques that were used in the past. This curriculum generated a dependency on energy-consuming solutions which produced high cost buildings [47]. The high reliance on active methods had only worsened the climate change and magnified global warming [48]. Therefore it is essential for architects to be informed by climate-responsive architecture and should operate responsibly and promote environmental sustainability.

Occidental Chemical Center office in New York was designed by Cannon Design and was the first modern building designed to embody and embrace Le Corbusier's DSF approach. It was considered to be the earliest energy-conscious DSF building located in Northern America by many studies. The building envelope has double layers of protection from direct sunlight, "intelligent" light sensor white metal Venetian blinds, and a green-tinted double-skin façade layer with a 1200 mm distance from the inner layer. The building ventilation is handled through two systems; interior spaces are well-ventilated using a ventilation chimney, and a 300 mm DSF gap which provides natural ventilation on the sides of the building [49]. The system protected the building from over-heating, and the louvers stopped the direct sun from penetrating the building (Figure 3).

Figure 3: Occidental Chemical Center. (Source: Harrison &Meyer-Boake, 2003)

One of the earliest and best examples of high-tech DSF building was designed by Richard Rogers in 1978; The Lloyd's headquarters building in London. The building has a 76 meters high central atrium called "The room", surrounded by six towers (figure 4). Roger's vision embodied the capability of the skin to react to the changing weather. He designed 3 layered ventilated windows that are solar adaptive [30].

Figure 4: Lloyd's headquarters in London. (Source: arcaidimages.com)

In the 90s, the EU determined limitations on the energy costs of the buildings. Architects complied and responded by designing low energy cost buildings. One of the most notable examples was designed by Norman Foster in 1994, the Commerzbank building in Frankfurt. The Tower was recorded as Europe's tallest building as well as the first ecological office in the world. It has a garden in a central atrium that is as high as the building and surrounded by DSF (Figure 5). The atrium acts as a vertical ventilation system and provides lighting for the interior spaces. [50].

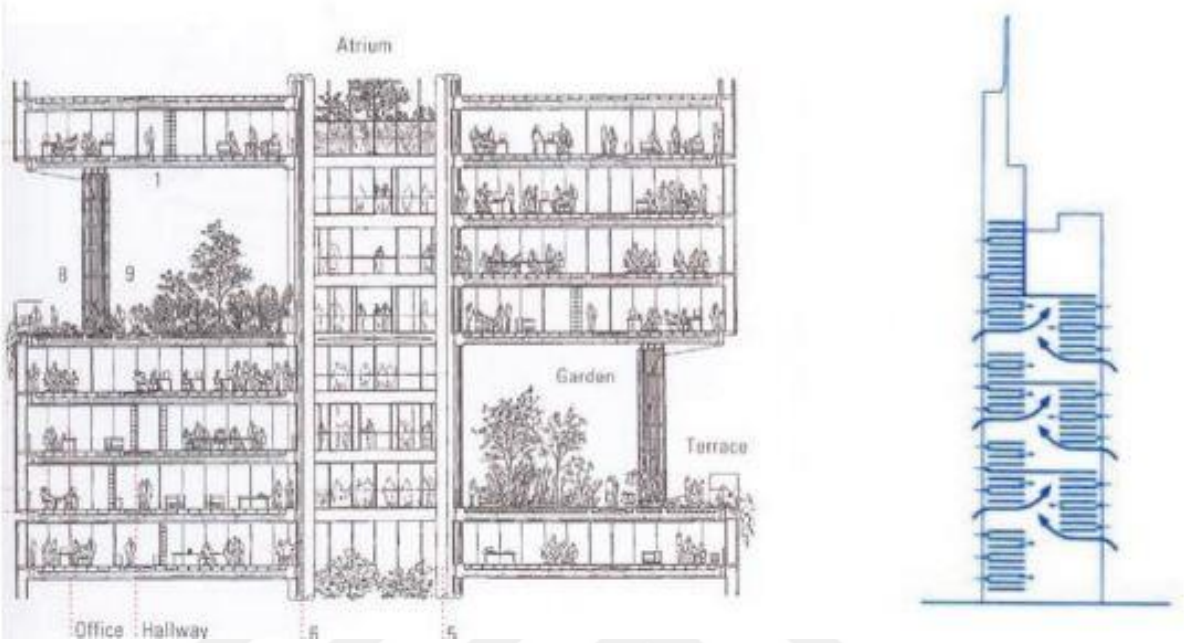

Figure 5: Commerzbank atrium section. (Source: Gissen, 2002).

Another example is RWE Corporate Headquarters AG in Esse, built by Ingenhoven and Overdiek in 2000. The DSF gap is 500 mm and was designed with remotely controlled louvres located between the inner and outer layers. That way, the louvres are sheltered from any exterior forces, wind, and rain [51]. The building had a specific window frame called "Fish Mouth", exclusively designed to function as an air vent. This air inlet admits air intake inside the cavity in order to get it heated and ejects the upcoming air outside (Figure 6) [52].

Figure 6: RWE Corporate Headquarters fish mouth. (Source: Wigginton &Harris, 2002).

Over the past 50 years, DSF structures were being thoroughly studied and developed. This technology has proved to be essential in contributing to energy-saving and reducing energy consumption within buildings. According to previous studies, DSFs contribute roughly to 25% less energy consumption in high-rise and low-rise buildings. The systems are more prevalent in the high-rise building sector as they provide maximum natural ventilation through the low pressure in the façade gaps. They also work mainly as sun shading devices that protect from direct sunlight and heat [28].

2.2 Classification of Double Skin Façade System

DSFs had been categorized in various classifications throughout the years. Most of DSFs categorizations were mainly according to the specifications of the geometry of the skin. The classifications range between; operation/construction mode, ventilation mode/airflow method, cavity partition and window type systems. Although these categorizations are recognized, some of these typologies are contradictory. Therefore, creating inclusive DSF systems classifications is essential in order to be able to evaluate all types of DSFs and achieve the required performance.

The first most well-known classification distinguished by Maria Szell, is divided in two main categories; ventilation mode (mechanical/ natural) and operation mode/ cavity partitioning [53]. This classification is mainly focused on the size and distribution of the cavity. However, it is not inclusive of all types of DSF, and there are some vague lines in the categories.

Pottgiesser proposed a classification based on the construction type. This classification considers critical aspects of the DSF, ventilation system position and openings division. However, it does not consider the potential shift in performance due to openings modification within active opening elements in the façade system [54].

The Belgian Building Research Institute (BBRI) conducted a research project that aimed to offer a summarized and coherent classification of Ventilated Double Façade VDF. This classification is divided into three main features; ventilation mode, cavity partitioning and ventilation type (Table 1) [55]. This classification gives a comprehensive summary of

different types of façade construction and operation. It also tackles the opening elements changes within active façade systems. However, this typology does not offer an interrelationship between façade operation and its mechanical demeanor.

Table 1: BBRI Classification of DSF. (Lancour et al., 2004).

Type of ventilation	**Mechanical**	**Hybrid**	**Natural**
Partitioning of the cavity	- Ventilated double window - VDF with juxtaposed modules - Corridor VDF per storey - Multi-storey VDF		- Multi-storey louver VDF - Shaft-box VDF
Ventilation mode	- Indoor air curtain - Outdoor air curtain - Air Supply - Air exhaust - Buffer zone		

Another classification by Herzoge et al. is according to the ventilation process and the capacity to reduce annual energy consumption. The system was divided into three main categories; Extract Air system, Twin Face System and Buffer System [56].

Gelesz and Reith proposed a comprehensive classification for a double skin façade system formed on Pottgiesser's typology with some modifications (Table 2) [57]. This typology depends mainly on the façade ventilation mode rather than the building's ventilation mode. Secondarily, it focuses on the façade operation mode and the partitions of the openings.

Table 2: Gelesz and Reith DSF classification (Gelesz & Reith, 2011).

Ventilation mode		**Mechanically ventilated exhaust-air systems**	**Non-ventilated buffer systems**	**Double-skin systems, partly or fully naturally ventilated**
Operation mode/ construction type		Indoor air curtain (air exhaust)	Buffer zone	Outdoor air curtain Air supply Air exhaust (Buffer zone)
Window type system		Exhaust air-window	Compound window	Box-type window
Double skin facades	**Vertically and horizontally partitioned**	Exhaust air façade	Buffer façade	Box-type window façade
	Horizontally partitioned			Corridor façade
	Multi-storey	Multi-storey exhaust-air facade		Multi-storey DSF
	Mixed partitioning mode	-	-	Shaft-box-type façade
Double skin roofs		-	-	Multi-layered glass roof

2.2.1 Classification of DSF according to the ventilation mode

According to Saelens, DSF is a two-layered envelope separated by an air cavity. These layers minimize energy demand in both winter and summer by improving thermal performance [58].

Ventilation mode classification is categorized according to the origin of the circulating air in the cavity and its destination. Some facades may endorse different ventilation modes at different times, depending on the façade components. Therefore, the

same façade may adopt different ventilation modes at different times. The primary distinction between a non-ventilated and a ventilated DSF is the controlled and calculated ventilation of VDF, despite providing the air cavity with a shading device. Façade ventilation mode is independent of the types of ventilation applied in the façade (Natural/ Mechanical/ Hybrid).

2.2.1.1 Non-ventilated buffer systems

This type of ventilation mode offers buffer facades with buffer zones.

- **Buffer façade:** this system provides airtight and insulating glass that improves thermal insulation and admits natural daylight into the interior spaces. It is a closed cavity façade that operates as a buffer zone and receives no ventilation [59]. The two enclosed skins are usually placed at a range of 250mm to 900mm [60].

2.2.1.2 Ventilated buffer systems (Partly/Fully/ Mechanically)

- **Outdoor Air Curtain:** the system facilitated air towards DSF cavity and evacuated it outside the cavity without admitting the air back indoors. The method creates an air curtain outdoors (Figure 7).
- **Indoor Air Curtain:** this system contradicts Outdoor Air Curtain. This system supplies air from indoors then circulates it back into interior spaces through the cavity space. This method creates an air curtain indoors.
- **Air Supply:** this system utilizes outdoor air and facilitates it through the cavity. The building is supplied by air by being admitted into the interior spaces and the mechanical ventilation systems.

- **Air Exhaust:** this system contradicts the Air Supply system as the air is supplied from the interior spaces of the building then released outdoors. This façade system allows the air to be evacuated outside the building.

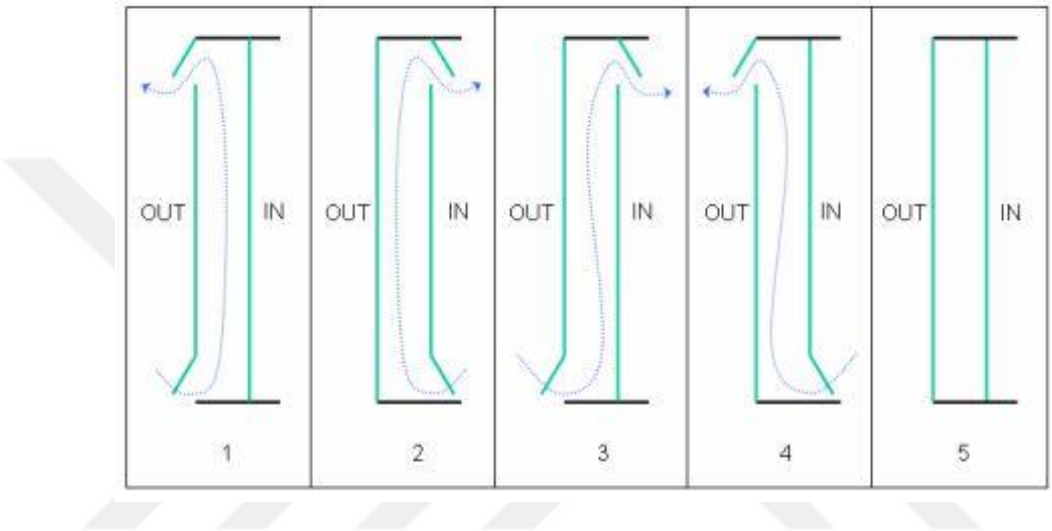

Figure 7: five main ventilation modes; 1- Outdoor Air Curtain, 2- Indoor Air Curtain, 3- Air Supply, 4- Air Exhaust, 5- Buffer Zone. (Loncour et al., 2004)

2.2.2 Classification of DSF according to the type of ventilation

Type of ventilation necessarily means the causing factors for ventilation of the air space is located at the cavity between the two glazed layers. This classification divides DSFs into three categories:

- Natural Ventilation
- Mechanical Ventilation
- Hybrid Ventilation

Standard NBN EN 12792 summarizes the characteristics of these three categories:

- **Natural Ventilation:** relies on fresh air flow, without any need for any external factors or generators. Several factors may contribute to the generation of natural ventilation, such as; different temperature levels, different pressure levels and the stack effect [61].
- **Mechanical Ventilation:** depends on the aid of the external factors that generate air force and movement. This method improves the performance and distribution of the transported air [62].
- **Hybrid Ventilation:** this type of ventilation balances between the controlled use of Natural and Mechanical Ventilation. The dominant method of ventilation is Natural Ventilation. When Natural Ventilation is insufficient or lacking, Mechanical Ventilation is relied on to fulfil the required performance. The controlled motors are installed in the window frames to supply fresh air by opening the window frames at determined times [63].

The type of ventilation wields a significant influence on the façade thermal performance. Mechanical ventilation can have an assured thermal performance as it can be controlled; however, oftentimes, it is harder to determine or manage the thermal performance of the natural ventilation system.

2.2.3 Classification of DSF according to the partitioning of the cavity

It is a classification where the façade is divided into smaller, independent boxes by horizontal and vertical partitioning and depends on where the cavity is located in-between the two layers of the DSF. Endless possibilities and types of partitioning can be designed for

the ventilated double façade [55]. Partitioning in the façade is different from partitioning in the windows. In practice, there are 4 groups of DSF according to partitioning (Figure 8).

- **Box type window:** in this type of partitioning, the façade is divided into smaller, independent boxes by horizontal and vertical partitioning. The glass panes of this façade are usually mounted with a unique frame called 'fish-mouth'. In literature, this type of façade is also named Ventilated Double Windows (VDW) and considered to be the oldest type of DSF. This façade consists of a ventilated double window either inside or outside the skin, separated by a gap creating a cavity. Usually, there is a 200 mm to 400 mm cavity gap between the two layers [55]. This type of façade is considered to be a good solution for sound, air, and smell insulation. Box windows are commonly applied to buildings located in noisy districts [64].
- **Multi-storey DSF:** this type of partitioning does not have vertical nor horizontal dividing. It is rather one large cavity volume providing the building with natural ventilation. Typically, multi-storey DSFs are naturally ventilated; however, they can be mechanically ventilated, allowing the installation of HVAC systems and creating atriums with an undivided space. This type of façade is considered to provide an excellent acoustic insulation performance [55].
- **Corridor DSF:** this type of partitioning depends on the horizontal partitioning of a large cavity at each floor height. It forms independent floor-height corridors along the façade that contribute to minimizing the over-heat in the upper levels. The corridors are supplied with air inlets and outlets on each floor, providing natural ventilation. The system is considered to be more intricate than Multi-storey DSF as each floor

requires separate ventilation openings. Typically, those corridors are considered as separating space utilized for cleaning and maintenance needs [65]. This system has the most efficient structure for fire prevention, thermal performance, sound insulation purposes [28].

- **Shaft-box DSF:** in this type of partitioning, a set of window boxes is fixed on the vertical shafts located in the skin to guarantee that the shaft effect occurs. The shaft utilizes natural ventilation to boost the stack effect. Thus, this type of DSF is exclusively relevant to naturally ventilated facades. The vertical shaft shifts the warm air captured in the façade and facilitates it to the upper areas to be released outside. Shaft-box facades provide better ventilation than corridor facades. The main disadvantage of this system is that the continuous air gap along the building height makes it prone to noise transmission and provides insufficient fire protection [66].

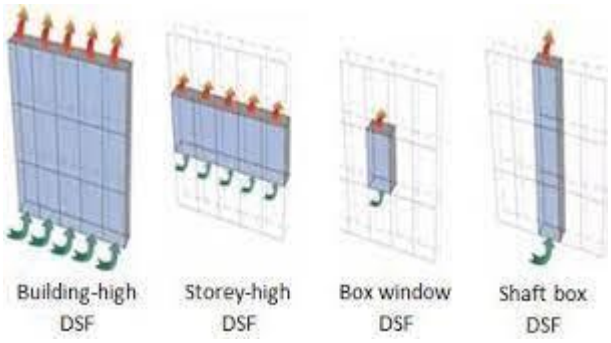

Figure 8: Double skin facade classification according to the partitioning of the cavity.

2.3 Thermal Performance and heat transfer

Two main component and characteristics of an energy-efficient building are thermal efficiency and air permeability. In DSFs, the thermal barrier consists of the façade skin and

the air barrier consisting of the cavity. The proper installation of suitable insulation material will reinforce the building's thermal performance. On the other hand, the inaccurate selection of suitable insulation material will significantly reduce thermal performance by 30%. [67]. Understanding the mechanism of how glass behaves with radiation is crucial. The light spectrum contains several wavelengths. The longer the wavelength, the less energy it bears. Therefore, heat waves are travel on short wave/ high frequency through infra-red and visible light waves [68].

Conventional glass windows are almost transparent to high radiation frequencies and transmit approximately 90% radiation into the interior spaces. Thus, it is essential to incorporate thermally efficient windows to reduce energy consumption significantly [29]. In conventional glazing systems, the glass allows the transmission of solar radiation and interior spaces are heated by absorption. The warmed-up surfaces turn into radiators, and the admitted heat trapped in the room increases the temperature (Figure 9) [69].

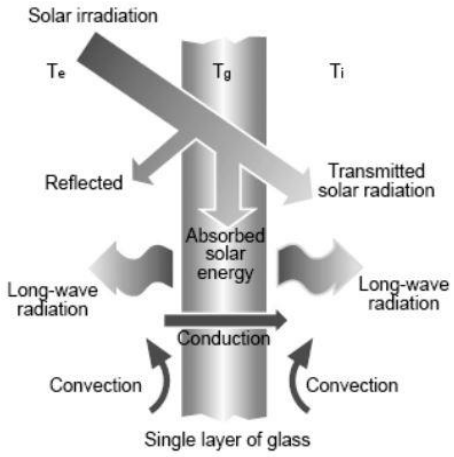

Figure 9: Heat transfer through normal glazing. (Source: www.buildingenvelopes.org).

DSFs control the transmission of solar heat through shading devices and cavities. The cavity aids in absorbing some solar radiation heat. The shading devices main aim is to reflect short-wave radiation and absorb the remaining high-frequency solar radiation. The second layer of the glass reflects the remaining low-frequency radiation, and the inner spaces are not warmed up (Figure10) [69].

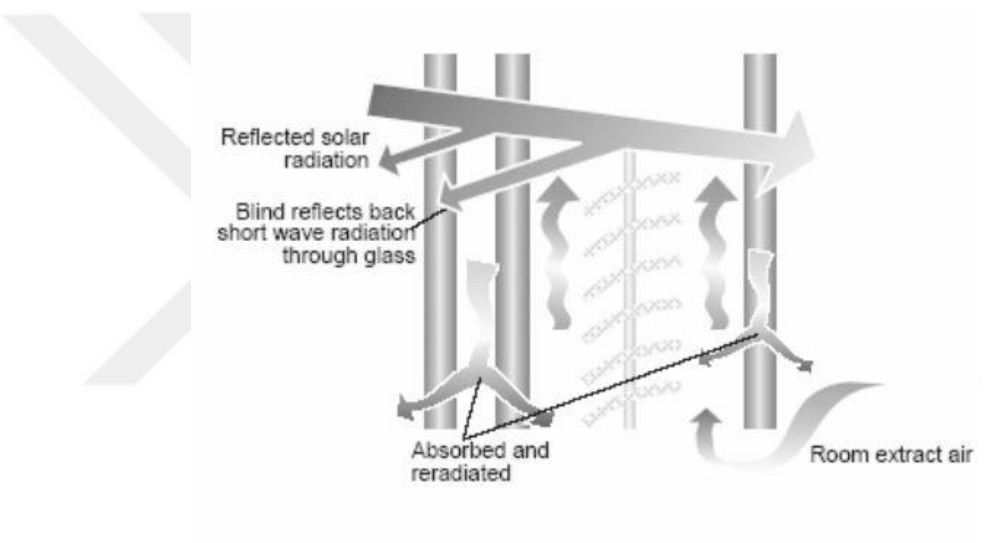

Figure 10: Heat Transfer through Double Skin Facade. (Source: www.buildingenvelopes.org).

Thermal transmittance is the heat transfer through the structure and it is referred to as U-value (W/m2K). Lower levels of U-value mean higher insulation performance. Low U-value levels mean that the building components possess high thermal resistance. Thermal resistance is referred to as R-value. Highly insulated building elements are the ones that have a higher R-value. High R-values mean that the insulation defies heat transfer, which in turn in a building with low internal gain and can provide high energy efficiency [67]. Figure 11 shows recommended R-values for each building element (walls, floors, and roofs).

Researchers' concerns regarding the climate change happening around the world are growing due to higher insulation values on buildings overheating [70]. The higher the insulation of the building, the lower its ability to disperse heat, which in turn will result in overheating, especially when the temperature outdoors is lower than indoors temperature. Comprehensive research has been carried out where it encompasses various parameters including building insulation, thermal mass, glazing ratio, shading, ventilation etc. and their effect on insulation. The results show that all other parameters amongst insulation account for overheating in the building, and insulation alone accounts for up to 5 % of overall heating [70]. Research conducted by Gupta and Gregg reinforced these results by concluding that overheating relies on how the parameters are integrated [71]. Therefore, a holistic building model would have to take into consideration all of those parameters as they are all equally critical in affecting the building over-heating.

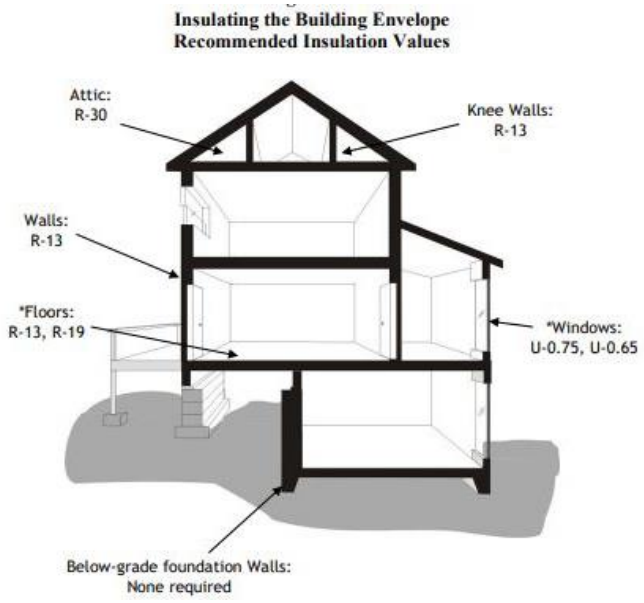

Figure 11: Elements of energy-efficient buildings and their R values. Source: [67].

Indoor Environmental quality faces several problems in different building sectors, including schools, offices, etc. Those issues range from high energy demand for cooling and heating purposes, high humidity rates and increasing carbon monoxide and radon emissions. Previous studies listed a few elements that control the quality of indoor environment properties, such as temperature, air quality, ventilation, humidity, and structural integrity [67].

DSFs are designed according to different weather conditions to achieve the required thermal performance that maintains the thermal comfort on the interior spaces in the building, in both seasons, summer and winter.

- **In the winter season:** properly insulated materials significantly decrease the rate of heat transfer. Ventilated DSF tend to have lower U-values in comparison to closed or partly ventilated facades. The higher resistance of heat transfer is due to the controlled intake and exhaust of the air, where the rate of the airflow is decreased, and the air temperature collected in the cavity is maintained. Therefore, heat loss and heat transfer are lower at closed/ partly ventilated facades [67].
- **In the summer season**: DSFs act as cooling systems. The continuous airflow in the cavity allows the air to transfer to adjacent places. This airflow keeps the inner glazing temperature low, therefore, reduced conduction, convection, and radiation. The application of DSFs reduces the rate of heat transfer from the exterior environment into interior spaces and requires lower energy demand to cool the interior spaces. Shading systems that are installed in the cavity contribute to absorbing and reflecting high and low-frequency radiation waves [72].

2.4 Daylighting Features of Double Skin Façade

DSFs have been under development throughout the years. The rapidly growing application of these systems enlarged the glass surface ratio on buildings and restored the concept of effective application of daylighting. DSFs made it achievable to cut artificial lighting significantly and depend on daylighting to illuminate deep spaces in the buildings [72]. Daylighting combines two fields, art, and science while illuminating interior spaces. Previous studies highlighted how daylighting directly and indirectly affects human behavior and office arrangement [73]. Daylighting affects thermal comfort, visual comfort, and energy consumption. [74].

There are many ways to enhance daylight performance, for example, by applying components that contribute to the absorption and reflective values, such as reflective glass, colored glass, or thin filmed glass [55]. Those systems tackled other issues that came with daylighting applications, such as glare. The cavity in DSF allows the installation of other shading systems to prevent glare. The glare can be controlled by altering the angle of the horizontal shading devices, either manually or mechanically. Avoiding glare using DSF achieves visual comfort for the occupants in the building [65].

2.5 Daylighting Strategies for DSF in offices

In the architecture field, studies regarding daylighting are gradually increasing as they are crucial to the industry. Those studies focus on creating advanced tools for mathematical formulas, coding, simulation, and modeling programs. [75]. Providing adequate lighting is crucial for the occupants' mental health and for them to properly carry out their tasks [76].

Occupants in offices usually occupy the building during the daytime. Therefore, the utilization of daylight during those hours is crucial to achieving visual comfort [77]. Daylighting utilization can be achieved through multiple solar control elements. Outdoor lighting can be receiver through transparent windows, roof skylights and other openings. The interior spaces receive light in three forms: direct sunlight, externally reflected light (ERC) and internally reflected light (IRC) [78].

Illuminance is referred to the luminous flux density at a surface, which means; how much light illuminates the surface. It is used to describe the lighting performance according to the activity. Illuminance is measured in Lux (lx); lumens per square meter (lm/m2). Sky conditions determine the lighting level. The typical conditions range from 5000lx to 40000lx outdoors and 300lx to 500lx indoors [79]. The purpose of the Area determines the recommended lighting levels as particular tasks require different levels (Table 3) [80].

Table 3: Lighting levels recommendation (lx). Source: [80].

Area	**Recommended Lighting Level (lx)**
General	500
Computer Workstations	300-500
Filing Rooms	300
Print Rooms	300
Drawing Office	500
Drawing Boards	750
CAD Design Areas	300-500

2.6 Advantages and disadvantages of DSF in offices

Compared to buildings with single-skin façade systems, a DSF system can positively or negatively impact the building. In general, DSF contributes numerous merits in comparison with conventional building facades (Table 4). However, those systems do not come without any disadvantages (Table 5).

Advantages of Double Skin Facades:

- **Thermal insulation:** DSF systems can achieve better thermal performance than conventional facades in both seasons, summer, and winter.

  - In winter: shutting the cavity partially or entirely reduces airflow inside the cavity and trap the air. It would slow down the heat exchange process, maintaining higher temperature levels inside the corridor [28].

  In summer: a cavity between the two layers allows the air's transmission either by natural or mechanical ventilation. The proper selection of ventilation method, type of pane and shading devices directly affect the airflow ventilation within the cavity. It, in turn, influences the overall thermal performance of internal spaces as well as the cavity [59].

- **Construction Costs:** Compared with specially treated glass such as thermochromics, photochromic and other glass solutions, DSF is more efficient and durable. Although those solutions are favorable, climatic conditions and environmental conditions greatly influence their quality and performance.

- **Solar, Wind and Rain Protection:** the installation of shading devices in the cavity helps the DSFs minimize direct heat received, which enhances the shading coefficient. The external skin creates a shield that protects the building from strong wind and rain and minimizes the winter cooling effect
- **Acoustic Insulation:** These devices may minimize room-to-room sound transmission (Internal Noise) as well as outside noise transmission (External Noise). For effective acoustic insulation, the minimum gap is 100 mm [28]. Many buildings in urban settings resort to the application of DSFs for acoustic insulation [72].
- **Energy Savings:** the proper design and installation of the Double Skin façade save energy by reducing solar loads admitted into the building. The system also provides the building with natural ventilation, which would reduce energy demand. [72]. Reducing the reliance on mechanical ventilation will cause the overall electricity bill to be substantially reduced, and total energy consumption will be saved [28].
- **Thermal comfort:** DSF traps warmer air inside the cavity than the air surrounding the building exterior. The cavity space maintains temperature levels that are near comfort levels. DSF contributes to achieving lower heat gain (G-value) and effective thermal transmission (U-value). Energy savings through DSFs is acquired by reducing heat gain inside the building. It will result in minimizing the solar factor and U-Value in the overall space and surrounding areas [72].

Table 4: Advantages of Double Skin Facade according to different literature studies. (Source: (Poirazis & Harris, 2004).

Advantages mentioned by the author	Oesterle et al., 2001	Compagno 2002	Claessensa et al.,	Lee et al,.	B.B.R.I., 2002	Arons, 2000	Faist, 1998	Kragh, 2000	Jager, 2003
Lower construction cost (comparing to electrochromic, thermochromics photo-chromic panes	X	-	-	-	-	-	-	-	-
Acoustic insulation	X	-	-	X	-	X	X	X	X
Thermal insulation during winter	X	X	-	X	X	-	X	X	-
Thermal insulation during summer	X	X	-	X	-	-	X	X	-
Nighttime ventilation	X	X	X	X	-	X	-	-	-
Energy savings and reduced environmental impacts	-	-	-	-	-	X	-	-	-
Better protection of the shading or lighting devices	X	X	-	X	-	-	-	-	X

Reduction of the wind pressure effects	X	X	X	-	-	-	-	-	X
Transparency-Architectural design	-	-	-	X	X	X	-	X	-
Natural Ventilation	X	X	-	X	-	X	X	-	X
Thermal comfort, temperature of the internal wall	X	X	-	X	X	X	X	X	-
Fire escape	X	-	-	-	-	-	-	-	-
Low U-value and G-value	-	X	-	-	-	X	-	X	-

Disadvantages of Double Skin Façade:

- **Maintenance Costs:** As DFSs systems are more complex than conventional façade systems, the maintenance operations costs are increased [28].
- **Construction Costs:** DSFs hold a high construction cost compared to conventional façade construction cost. *"There is not any dispute in saying that double-skin facades are more costly than single skin forms"* [28].
- **Fire Protection Issues:** DSFs connect the space through the cavity, making it harder to extinguish the fire quickly [72].

- **Overheating Problems:** in DSFs systems, the air temperature in the cavity is usually warmer than the outside air. The improper design, as well as improper installation of those systems, may cause an excessive rise in the temperature. The minimum cavity depth in the DSF is 200mm. Cavity width and ventilation openings are the two main factors in over-heating issues [65].

- **Acoustic problems:** Although DSFs provide adequate Exterior noise insulation, these systems may also act as an acoustic channel if not installed properly. The channels may use the cavity as a path to transmit sound [72].

Table 5: Disadvantages of DSF according to different literature studies. Source: (Poirazis & Harris, 2004).

Disadvantages mentioned by the author	Oesterle et al., 2001	Compagno 2002	Claessensa et al.,	Le et al,.	B.B.R.I., 2002	Arons, 2000	Faist, 1998	Kragh, 2000	Jager, 2003
Higher construction costs	X	-	-	-	X	X	-	-	X
Fire protection	X	-	-	-	X	-	-	-	X
Reduction of rentable office space	X	-	-	-	-	-	-	-	X
Additional maintenance and operational costs	X	-	X	-	X	-	-	-	X

Overheating problem	X	X	-	-	X	-	X	-	X
Increased air flow speed	-	-	-	-	X	-	-	-	-
Increased weight of the structure	-	-	X	-	-	-	-	-	X
Daylight	X	-	-	-	-	-	-	-	-
Acoustic insulation	X	-	-	-	X	-	-	-	X

In General, DSFs contribute positively by serving as great sound insulators as well as reducing the cost and power consumed within the building. The systems reduce heat loss, permitting the occupants on higher floors to open windows, consequently diminishing the need to use air-conditioning systems. On the other hand, DSFs may have disadvantages concerning high construction cost, ventilation limitation between the two skins, constraining the space for offices, disbanding sound between skins, and increasing energy load to overcome ventilation issues between layers [81].

2.7 Samples of Office buildings with DSF:

2.7.1 Helicon Finsbury Pavement, London.

Helicon was designed by Sheppard Architect in London. The building was designed to provide maximum daylighting through the application of full-height glazing. The DSF external skin is a 12 mm single frameless glazing, and the internal skin is double glazing.

The cavity includes automatically controlled vents that allow it to be naturally ventilated through stack effect in order to dismiss unrequired solar gain. Automatically controlled tilted blinds were included in the cavity to respond to the solar intensity and different temperatures to maintain thermal comfort. The full-height glazing allows the light to reach deep areas in the interior spaces. Each floor was designed with wide maintenance walkways that grant solar protection (Figure 12). The building was built with an atrium using 50% reflective glass. [52]. The heating system is implemented by finned tubes and a boiler in the basement. The boiler heats up domestic hot water to run through the pipes and warm up the surrounding air. In summer, chilled water is distributed through chilled ceiling panels to achieve a cooling effect. These cooling and heating methods reduce the building's energy demand [52].

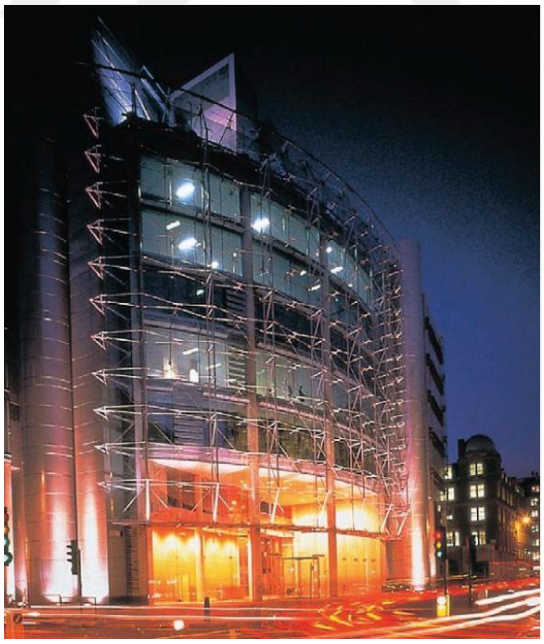

Figure 12: Helicon Finsbury Double Skin Façade. Source: (Wigginton & Harris, 2006).

2.7.2 Debis building, Berlin, Germany

Debis Building is a high-rise office building built by Renzo Piano Architect in Berlin, Germany. The building has a 14 m wide central atrium that extends for 82 m from north to south. The building eastern, southern, and western façades were covered with an outer DSF to protect it against high solar exposure. The skin can be automatically controlled in order to adapt to different weather conditions. In summer, the skin can open up to 70 degrees in order to simulate natural ventilation. The cooling system depends mainly on chilled ceilings. In winter, the façade closes entirely to create an insulating layer from the cavity (Figure 13). The DSF also protects the internal glass from wind, rain, and solar radiation. The building is provided with a generous amount of natural daylighting. It only requires electrical lighting less than 40% of the year [52].

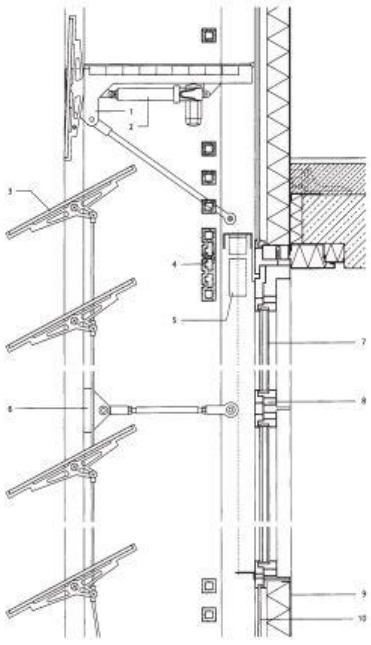

Figure 13: Debis Building DSF details. Source (Wigginton & Harris, 2006).

2.7.3 Suva Insurance Company, Switzerland.

Suva Insurance Company is an office building designed by Heroz and de Meuron, located in Base, Switzerland. This building was built in the 1950s, then later was cladded with DSF to improve the thermal and visual performance. The new over-cladding contained operable automatically controlled windows that adapt to solar angles. The windows closed shut in winter to seal the building and create a thermal buffer to save energy. Air conditioning is forbidden in Switzerland; therefore, the operable windows open to admit airflow into the cavity and ventilate the stone walls, in summer. The glazing is divided into three sections, each section with its function. The lower glazing consists of insulation glass that protects the interior stone walls. The middle glazing consists of insulating glass that covers office windows to enhance ventilation and view-out. The upper glazing consists of operable bands that adjust their opening angle to adapt to the solar intensity. The glass panes operate according to the air temperature recorded by a computer sensor between both skins (Figure 14) [52].

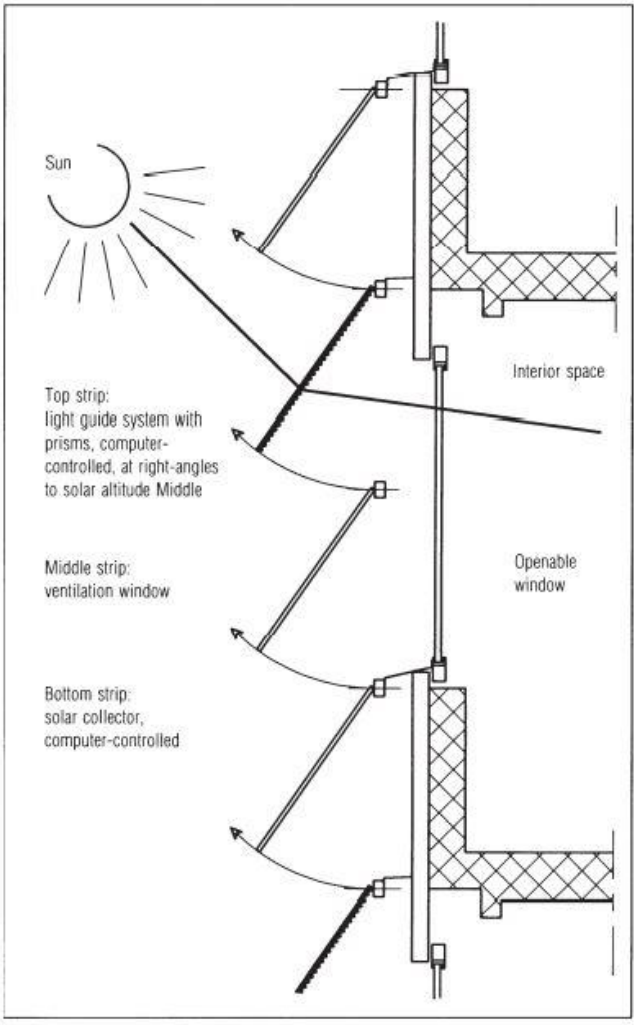

Figure 14: Suva building glazing system; three bands. Source: (Wigginton & Harris, 2006).

2.7.4 Design Office for Gartner, Germany

Kurt Ackermann Architect designed the design office for Gartner in 1997 in Germany. The building was designed with innovative curtain walls in the northern and southern facades to improve thermal performance (Figure 15). The curtain wall consists of semi-transparent louvres automated by computer sensors that track solar movement and intensity. The skin facade consists of triple glazing covering all four elevations. The cavity

is filled with argon gas on the south and the north and krypton gas on the east and the west. The innovative façade integrates 'water-carrying profiles' that assess the heating and cooling process. The heated water circulates in a framework that warms up the room, thus provides thermal comfort in winter. Cool water is run through the framework to counter the solar heat gain in the summer. The adjustable louvres contain reflecting characteristics utilized to reflect the light to the ceiling then into the deeper parts of the building [52].

Figure 15: Design office for Gartner DSF System. Source: (Wigginton & Harris, 2006).

CHAPTER III

METHODOLOGY

This chapter dissects the study conducted so it meets the aims and objectives of this dissertation. It thoroughly explains the research strategy, design and methods applied. This research is conducted based on a qualitative method and investigated multiple quantitative experiments. The experiment conducted amalgamates both qualitative and quantitative characteristics of daylighting and radiation and its effect on the users' well-being and their comfort. A comprehensive thermal and daylighting analysis simulation is conducted to analyze the performance of DSF within a warm and temperate climate region. The study investigated various effective variables and characteristics of DSF on a proposed building model in Eskisehir, Turkey.

3.1 Data collection and instruments

This research was based on the approach categorized by Gliner, Morgan and leech, which divides the research design into three categories: Exploratory, Descriptive and Experimental (Figure 16) [82].

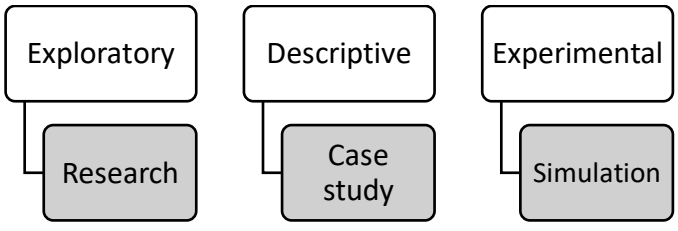

Figure 16: Research Design (Gliner et al., 2017).

The basic source of the exploratory part of this research depended on the theoretical information collected from many research specialized in studying indoor thermal and daylighting conditions within a similar building typology. The data collection depended on several qualitative instruments aside from the theoretical study, such as photos, drawings, graphs, and computational tools.

The second step of data collection concerning the 'Descriptive' step focused on the selected Case study: a proposal of an office building in Eskisehir. The comprehensive building data concerning weather, location and plans were collected from multiple resources and simulations and explained in detail in the Case Study Chapter.

The practical step was conducted through multiple simulations using different software and computational tools; ACAD, Rhino, Grasshopper, ClimateStudio, Energy-Plus and Ladybug. Each tool and software are explained thoroughly later in this chapter.

3.2 Methodology outline graph

The presented methodology includes four main stages (Figure 17). Firstly, the modelling of the selected office building using Rhinoceros software where all simulations will be conducted on. The second stage consists of coding the radiation analysis code using grasshopper [83] a parametric modelling plug-in for the 3-D modelling program Rhinoceros [84]. The different skins facades are each applied separately on the case study building on all four facades. The following step consists of an environmental analysis conducted using EnergyPlus [85]. Lady-Bug [86] calculates solar radiation levels using energy-Plus weather files and the cumulative sky approach [87]. The four façade iterations are then tested for their

daylight performance using ClimateStudio [88]. The presented methodology and tools had been used in prior studies and verified through them [84] [83].

The simulation calculates the radiation performance of each façade on the original building model (highest radiation and median radiation). The daylight simulation calculates the lux that each façade provides inside the building (median and average daylight). All results include comparisons between the four different skin façade iterations and their performance in both seasons, winter and summer.

The plans were divided into 4 sections: east, west, north and south, in order to study the effect each façade has on the interior wing inside the building. This method was used to help determine the most suitable façade performance that is needed to be applied on each side.

Lastly, a comprehensive analysis of the results was conducted. The radiation results are analyzed in accordance with the daylight performance of all simulations for the best overall environmental performance. The presented steps are outlined in (Figure 17).

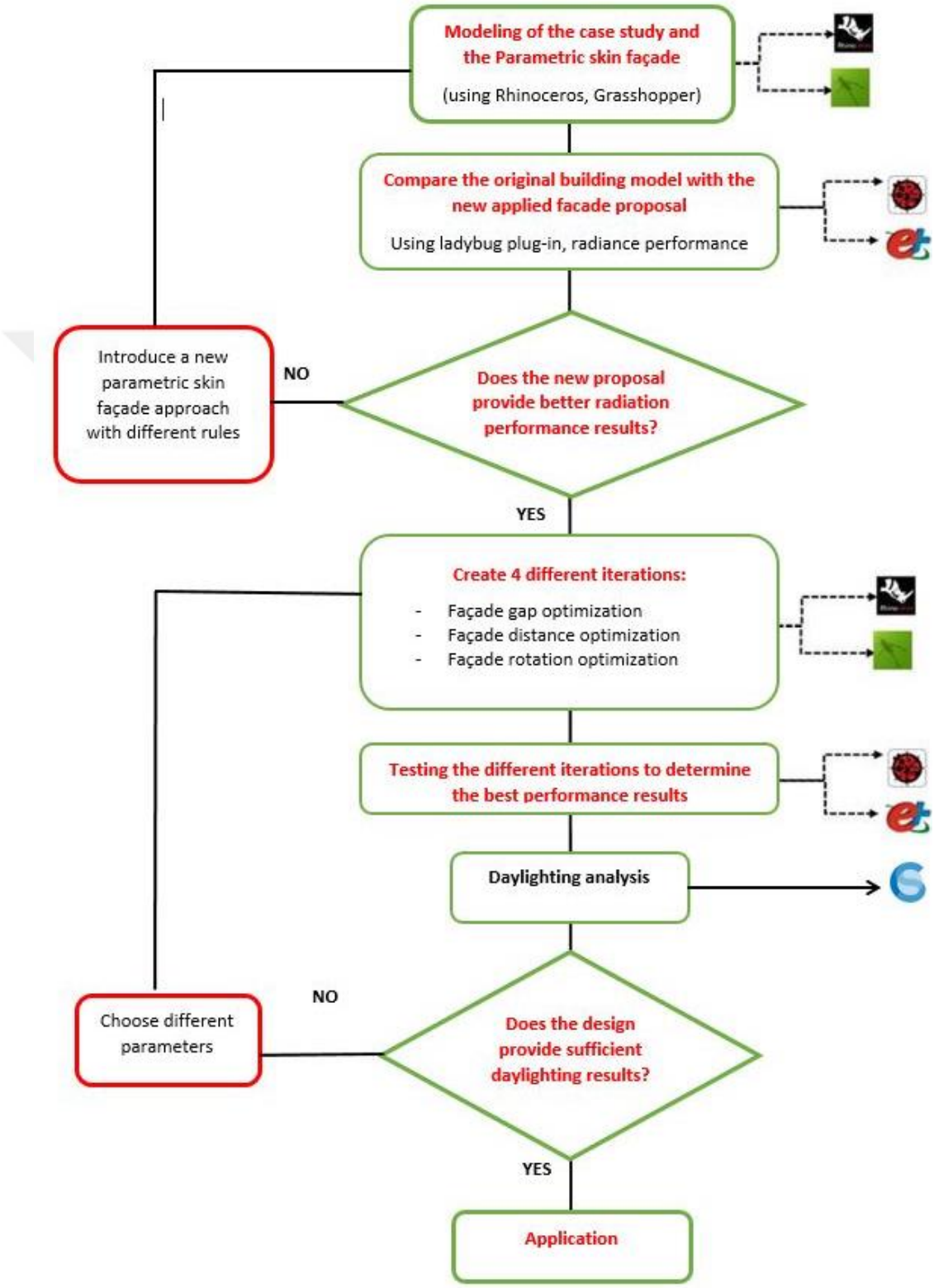

Figure 17: Methodology workflow

3.3 *Software and simulation tools*

- **Grasshopper, ClimateStudio, Ladybug and Energy-Plus**

The methodology workflow starts with the creation of the 3D model of the office building using Rhinoceros software. The case study is explained in more detail in chapter 4. The primary modeling of the façade was conducted by coding in Rhinoceros using Grasshopper. This computational tool allows the parametric visualization of rather more complex geometry than usual, as is the case in this research. The façade code is explained in detail in 3.4.1.

The Ladybug is a computational tool that aids in environmental design assessment. It allows the designer to study the correlation between different design assets and the environment by providing graphical data outputs. Ladybug was used to evaluate radiation performance inside the office building. It provides thermal performance results calculated in kWh/m2 through carpet dotted graphs of the radiation levels. The tool is supported by EnergyPlus weather files (EPW), which provides 3D communicative climate data. It conducts the simulation through accurate weather data, graphics, temperature, sun paths and humidity levels. Those weather data files are vital as they contribute to the overall analysis and generate a rather innovative workflow and accurate assessment. The thermal performance code is explained in more detail in 3.4.4. The selected patterns were further developed in terms of the void to solid ratio and distance in Grasshopper to reach the optimum design that admits proper radiation and sufficient daylighting evenly indoors.

The Daylight simulation was carried out using ClimateStudio; an advanced Rhinoceros plug-in that carried out daylight modeling and simulations. The software generally provides a series of environmental analysis developed by Robert McNeel & Associaes in Solemma LLC. The software calculated annual illuminance and distribution of daylight indoors in Lux. The daylight performance is explained in more detail in 3.4.4. This method is essential in designers and architects' early design and decision-making stages.

3.4 Model construction

3.4.1 Façade model construction and details

The parametric façade model pattern was coded and modelled using Grasshopper plugin in Rhinoceros (Figure 18-A). The code starts with a simple flat surface covering the entire façade, with 30 m width and 8 m height on the first and second floors on, and 21 m width and 8 m height on the southern and western façade. The northern and Southern façade surface dimensions on the first and second floor are 50 m width x 8 m height and on the third floor are 40.5 m width x 4.5 m height. The flat surface (façade design) is the same dimension as the façade fronts of each floor. A horizontal line that controls the openings was added to the surface. The flat plane was then divided into vertical strips into smaller parts. Then the surface is cut and extracted to divide the strips into two different sections horizontally. The horizontal line is then controlled through the Z-axis and rotated. The vertical strips rotation is controlled through a Number Slider and each strip is given an opening. The middle line location can be adjusted by altering both ends' Point On Curve command. Lastly, the code is converted to the solid surface and converted to 3D.

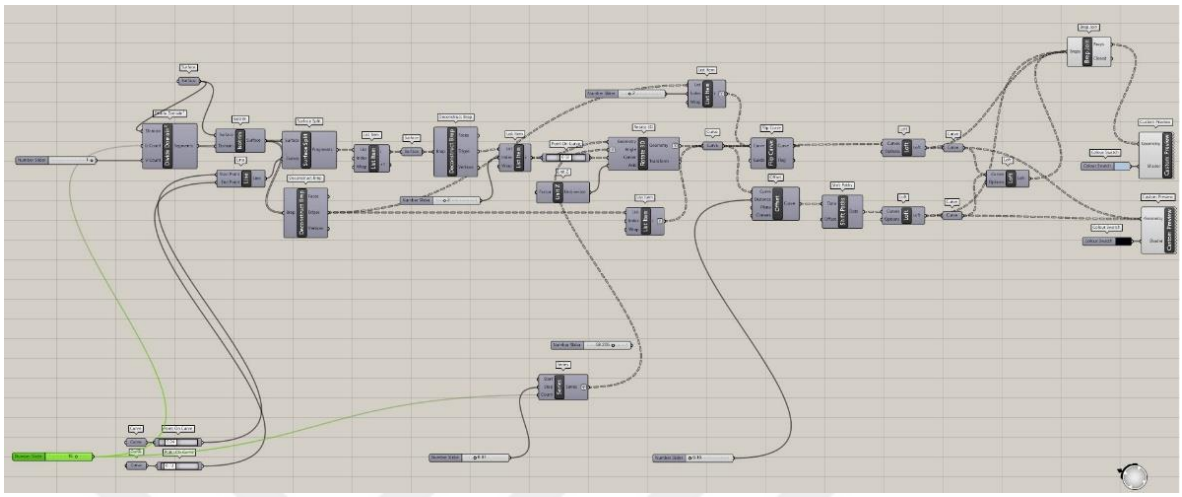

Figure 18-A: Parametric skin facade code using Grasshopper.

According to ventilation mood, the selected façade type for this thesis study is Buffer façade according to ventilation mood. This façade consists of a closed cavity that traps the air, improves thermal insulation, and admits daylightto the building. This façade was selected for this case study due to the climate conditions of Eskisehir, which requires a high level of insulation, especially during the cold winter and warm summer. Façade construction details are available in (Figure 18-b).

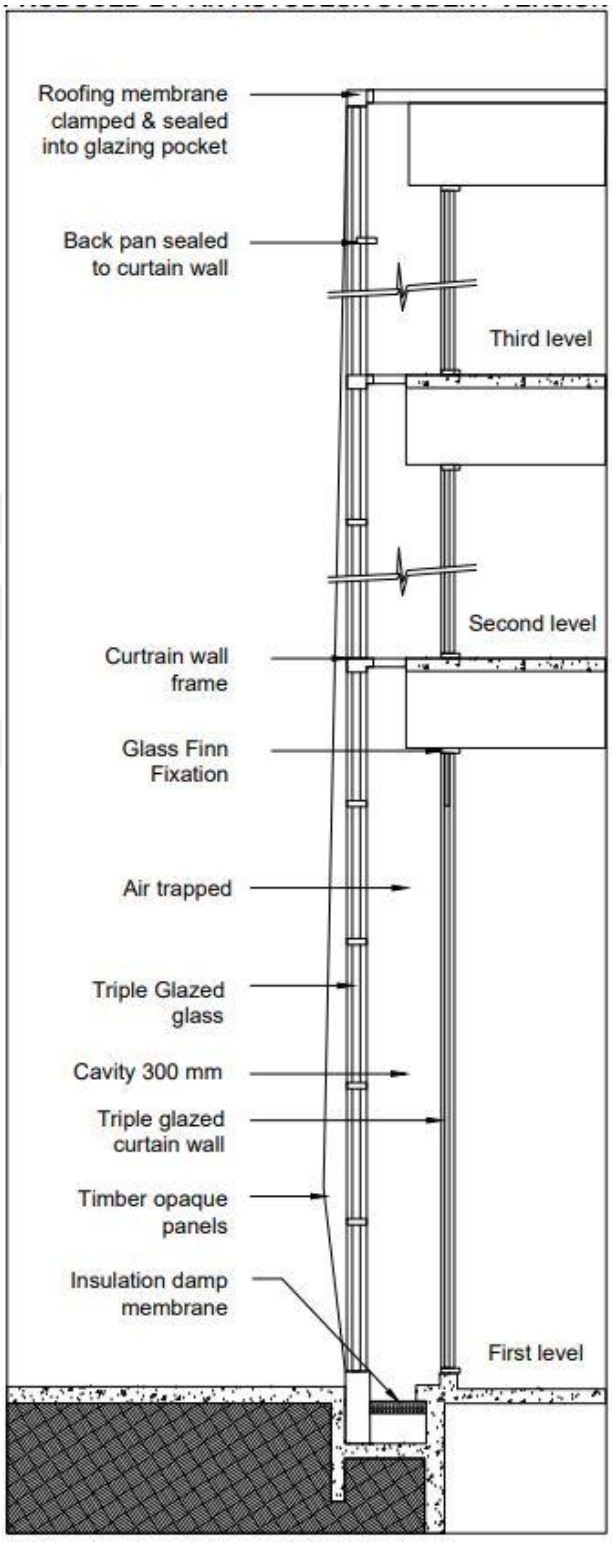

Figure 19-B: Parametric skin facade code using Grasshopper.

3.4.2 Defining Variable

The influential variables in this simulation will be exclusively related to the parametric Double skin façade parameters applied to the office building facade exteriorly. There are also several changing parameters and variables in the simulation environment, such as; the Month, Day and Time. The simulation records the radiation performance in summer and winter. The daylight simulation will be recorded in summer and winter on the 21st of July and December on three different timings in the day; 10 am, 12 pm and 2 pm (table 6).

Table 6: changing variables in the simulation (time and date).

Variable	Radiation Simulation	Daylight Simulation
Day	21st	21st
Month + Sky conditions	December (Overcast sky) July (Clear sky)	
Time	All-day	10 am, 12 pm, 2 pm

The parametric skin façade developed will exhibit changing configurations to provide different results and values based on the variable value (Table 7). The maximum width of panels was set to 800 mm and the minimum reached 400 mm. The distance for the panels was ranged from 200 mm to 400 mm. The lowest panel rotation started from 4°, and the highest started from 8°.

Table 7: Defining Variables and their values.

Variable	Minimum Value	Maximum Value
Width of each panel	400 mm	800 mm
Distance between each panel	200 mm	400 mm
Panel Rotation rate	4°	8°

3.4.3 Model Geometry and Surface properties

The parametric skin facade designed for the office building is comprised of buffer DSF filled with Argon. The DSF was added to the case study building and fixed externally at 300mm on all elevations. Previous studies have concluded that the placement of sun-shading elements on the interior is not an efficient way to reduce solar gains [55]. Multiple studies proposed that the shading system's most efficient distance and placement would be exteriorly placed approximately 1/3 section of the cavity. This placement promotes and encourages air movement inside the cavity and minimizes solar energy gains [28] [89]. A recent study has concluded that the shading device color had a very insignificant effect on the simulation results [90]. Therefore, the materials of the skin facade were not considered in this simulation. The performance of the skin façade is evaluated and determined by three main factors; panel size, the distance between panels, and panel rotation degree. The simulation had been run on all façade iteration; A, B, C and D (Figures 19, 20, 21 and 22).

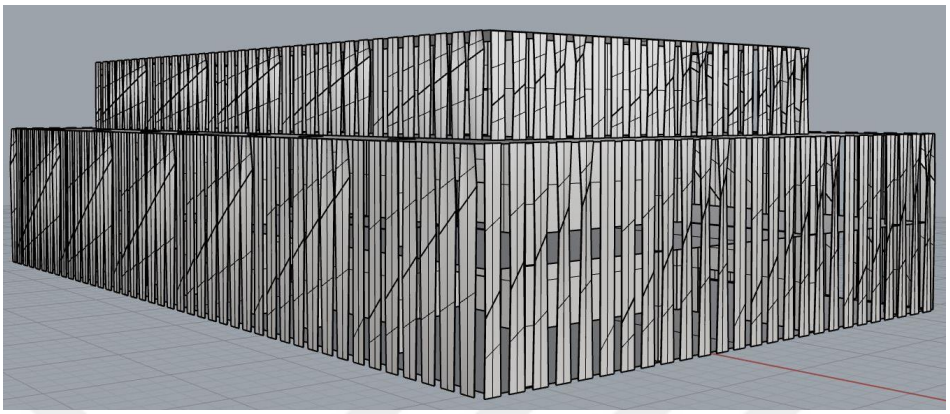

Figure 20: Facade A

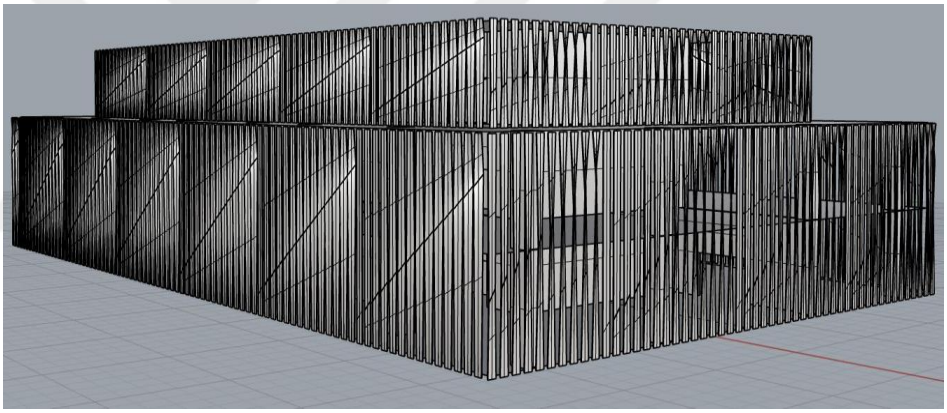

Figure 21: Facade B

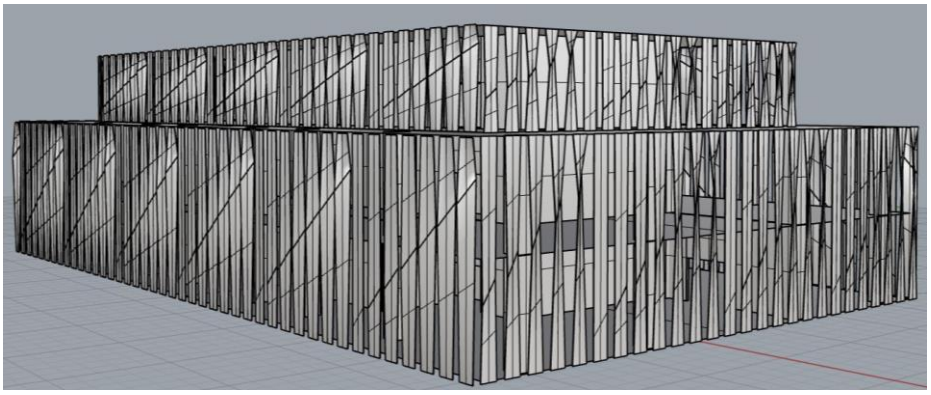

Figure 22: Facade C

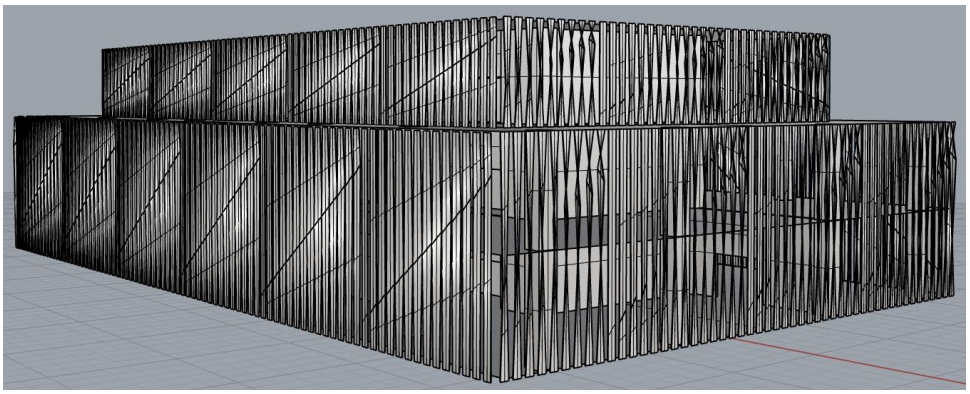

Figure 23: Facade D

Table 8 shows the main characteristics of each skin iteration. It explains the distinction in the number of panels, the dimensions, the distance between panels, and each panel's rotation degree on all of the different iteration designs A, B, C, and D (Table 4).

Table 8: The distinction between facade patterns. Facade materials and characteristics were not considered in this simulation.

Pattern number	Width of each panel	Distance between panels	Façade panels Rotation rate
Pattern A	800 mm	400 mm	4°
Pattern B	400 mm	200 mm	4°
Pattern C	800 mm	400 mm	8°
Pattern D	400 mm	200 mm	8°

The distinction between facades is modeled according to the information provided in table 8. Façade A width was set to 800 mm with a void of 400 mm between panels and a 4° rotation degree for each panel (figure 23). Façade B was designed to have 400 mm of width and 200 mm of gaps between each panel with a rotation degree of 4° for each panel (figure 24). Façade C is similar to façade A in terms of panel width and voids, but with a higher

rotation degree of 8° (figure 25). Façade D is similar to façade B in terms of panel width and voids, but with a higher rotation degree of 8° (figure 26).

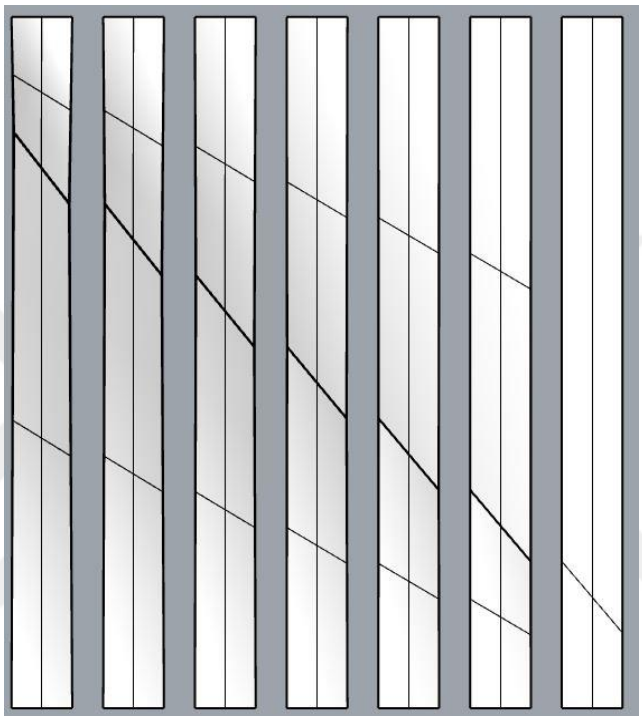

Figure 24: Facade A pattern close-up.

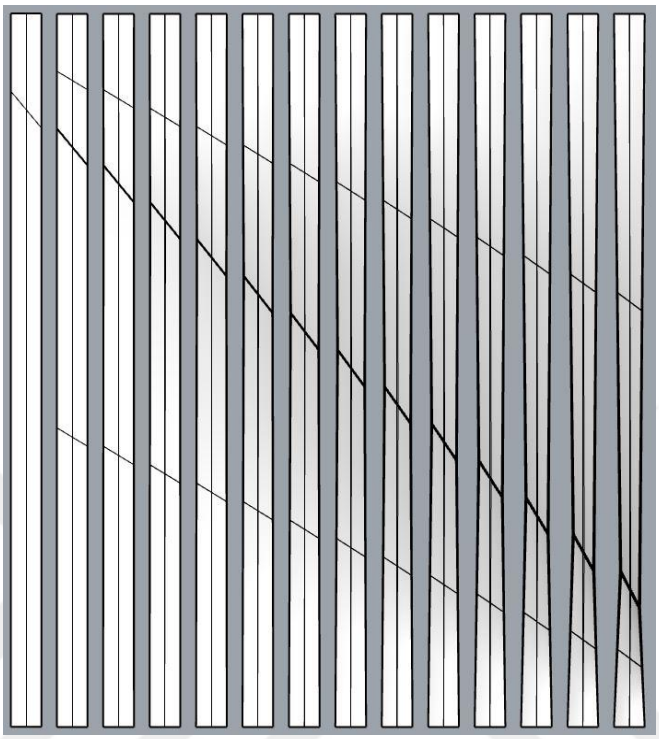

Figure 25: facade B pattern close-up.

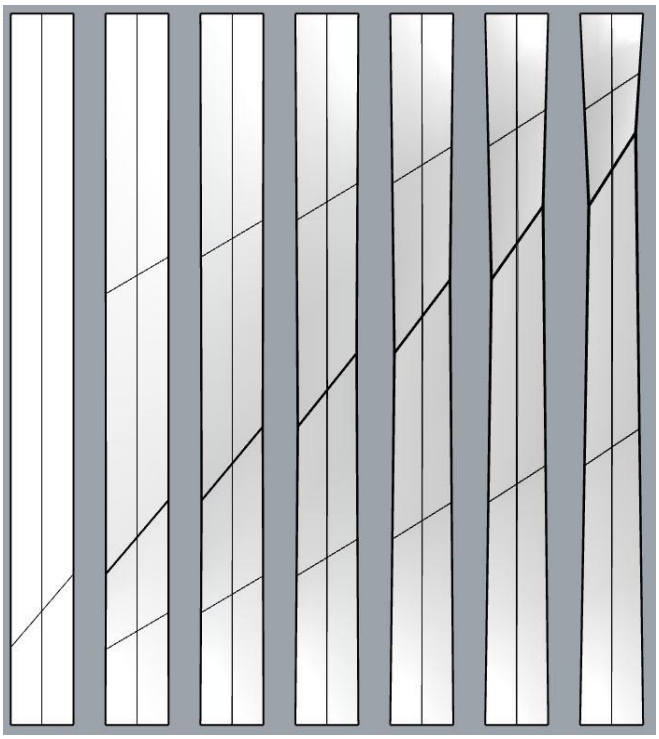

Figure 26: Facade D pattern close-up.

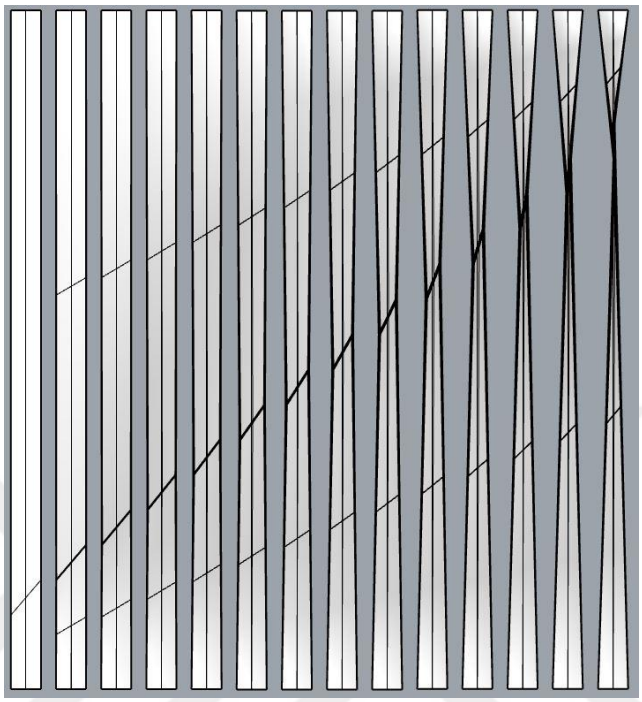

Figure 27: Facade C pattern close up.

The materials set to the DSF were obtained from the material library assigned by the modeling software. The role of the material played a crucial role, but the overall effect was dismissed as the materials for the DSF were set the same for all simulations. Material properties are explained in table 9.

Table 9: DSF material, the materials are consistent for all simulations to cancel out their effect on the results.

Outer Layer Material	Clear Float Glass 6 mm
Middle Layer	Argon- 13 mm
Inner Layer Material	Sungate 400 6mm
U factor (W/m2K)	1.53
SHGC	0.637
TVIS	0.754
Embodied Energy (MJ/m2)	432.6
Embodied Carbon (kgCO2/m2)	74.9625

3.4.4 Model Application through Simulation

Simulations are an alternative to reality, providing the designers with particular models that create certain outputs that visualize reality. Unlike other research methods, this research design provides actual experimentation system standards and values. Models and simulations are a crucial part of the comprehensive apprehension of the research field. Comparing the model results makes model validation possible and the analysis closer to reality [91] [92].

- **Sun path study**

Sun path Diagrams aid in locating the position of the sun in the sky at any time of the day, at any day of the year. Those graphical models provide quick, practical, and efficient results to estimate where the extra shading on the building is needed [93]. Solar charts and diagrams are sufficient tools that help the designers in visualizing the sun latitude and highlight the different angles of movement [94].

There are two types of Sun Charts: Cartesian and Polar Coordinates. The Cartesian Coordinates have two axis's: X-axis and Y-axis. X-axis plots azimuth and Y-axis plots the solar elevation. Polar Coordinate is a circular graph that plots the azimuth (sun's angle) around the circle starting from 0° to 360° and the altitude lines. The angles surround the edge of the diagrams. The attitude lines run from the center of the diagram out and are dotted lines.

This research will conduct the Sun Path Study using Polar Coordinates. This observation would assist in studying the solar sun direction to determine whether it was suitable to place the DSF on all of the four facades or not. The simulation was conducted in

two different seasons, summer and winter, in three different timings; 9 AM, 12 PM and 3 PM and the graphs were documented for analysis.

- **Solar Radiation Direction (Radiation-Rose)**

Solar radiation Direction calculates the radiation emitted from the sun that reaches the building. Total solar radiation includes both defused radiation and Direct Radiation. Rad-Rose simulation provides diagrams that capture the radiation magnitude that originates from various directions.

- **Radiation Analysis (Incident Study)**

Radiation study is able to incorporate the sun location for every hour of the year and calculate radiation levels indoors and as well as on the surface of the building. The analysis includes the building surrounding environment as well as the shading. There is a clear relationship between the quantity of radiation a building receives and the orientation and angle of the DSF.

The radiation incident simulation was conducted on the entire building on a mesh size of 0.2 m x 0.2 m. The annual incident value was recorded for every point on that mesh exteriorly on all of the four elevations of the case building and the roof. Grasshopper possesses a parametric nature that allows the researcher to examine an endless number of methods and results. The simulation provided a numerical database for 35 different settings and recorded in kWh/m2. The average and median value of each façade, level, façade pattern and season were calculated and summarized for comparison. The thermal simulation in this research was conducted through ladybug coding (figure 27). The code is divided into seven

segments: Weather Files (EPW), Cumulative SkyMix, Analysis Period, Selected Sky Mix, Sun Path, Radiation Direction and Radiation.

The weather files were obtained from EnergyPlus and imported into the design day parameters. The first simulation action is to create a clear sky around the case study using the imported EPW files. The simulation creates a skydome that visualizes the Peak solar hours and the sun path. Few inputs are required for the code to run, such as; determining the north point direction, selection of the hour, day and month, including the geometry for the analysis, adding context (Skin façade), determining the grid size. The Radiation study simulation is run after determining the Grid size, for every 20 cm. The simulation provides numerical output data for all 5 simulations in both summer and winter.

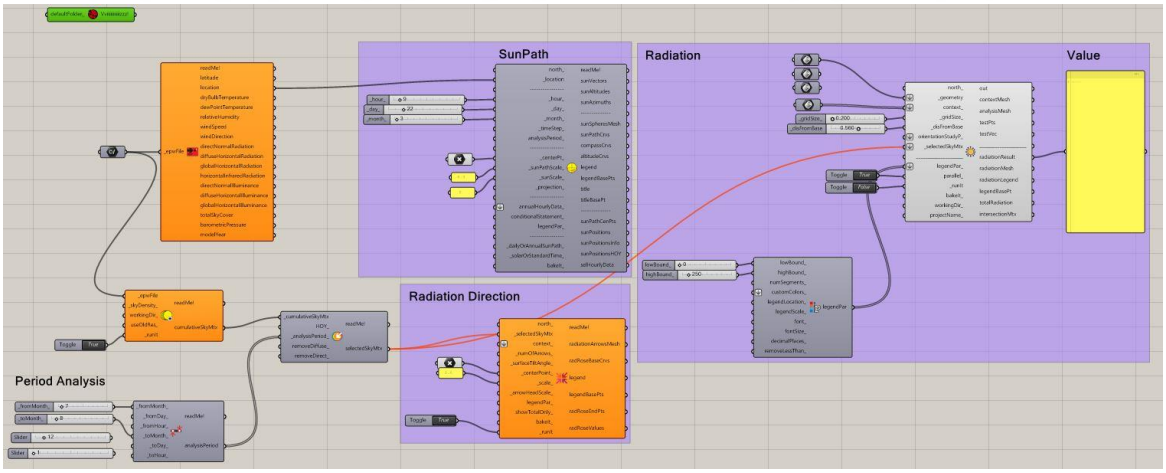

Figure 28: Ladybug code for radiation analysis.

- **Daylight Study (Visual Performance)**

The daylight study was conducted using ClimateStudio plug-in in Rhinocerous. The software assesses the available illuminance indoor and calculates total daylight. The goal of

this simulation is to determine whether the amount of daylight provided by each façade iteration is sufficient for each office floor. The simulation prepares the model to go through four stages/subpanels; location, materials, blinds, and occupied areas.

The daylight simulation was conducted on the entire building on a mesh size of 0.5 x 0.5 m. The simulation took different values under different weather settings; Sunny clear sky and overcast sky. The simulation provided a numerical database of daylight values for all different settings and recorded them in lux. The average and highest value of each level provided by the façade pattern and season were calculated and summarized.

CHAPTER IV

CASE STUDY

This chapter presents the selected case study. The case study selected for this dissertation is an office building proposal submitted as urbanism and planning to the Ministry of Environment and Urbanism in Eskisehir, Turkey. The project was designed to take part in the 1.016 Ha ecological settlements. The office building is constructed of three storeys comprised mostly offices, labs, cafeteria, dining hall, and a rooftop terrace. The architectural drawings of the building and 3D modeling were acquired from the designers to take part in this research. The materials set to the base model and the 4 cases were obtained from the material library assigned by the modeling software. The role of the material played a crucial role in the building design, but the overall effect was dismissed as the materials were set the same for all 5 models. The material reflection and transmittance are chosen directly from the material library of the software. All materials were fixed for all simulations, except for the glazing material. Further characteristics of the building are explained in table 10.

Table 10: case study building characteristics.

Building location (figure 28)	**Country**	Turkey
	Direction	North-west
	Province	Eskisehir
	Elevation	792 meters above sea level
Building type	Office building (Proposal)	
Year	2015- 2016	
Building area	3834.3 sqm	
Building capacity	120 thousands occupants.	

Location climate (figure 29 and 30)	**Climate**	Warm and temperate.	
	Koppen-Geiger specification	Csb (warm summer Mediterranean climate) [95]	
	Average temperature	18°C	
	Highest temperature	**Months**	July- August
		Degree	31°C to 32°C
	Lowest temperature	**Months**	December- January
		Degree	-3°C
	Average sun hours	**Highest**	11.6 hours
		Lowest	5.1 hours
	Total sun hours	3047.19 hours	
Site specifications (figure 31)	**Location**	South of the main road	
	Setback	5 meters	
	Green area	1099 sqm	
	Orientation	30°	
Building layout (figure 32, 33, 34 and 35)	**Plan layout**	Rectangular	
	Number of floors	3 floors	
	Zoning	**First level**	Public
		Second level	Semi- Private
		Third level	Private
	Dimensions	**First level**	50 x 30 x 4.5 m
		Second level	50 x 30 x 4.5 m
		Third level	40.5 x 20.60 x 4.5 m
Building ventilation system		Mechanical ventilation	
Building materials			
Building component	**Material**	**Reflectance**	**Transmittance**
Exterior walls	White Plaster Facade	83.27 %	0.00 %
Interior floors	Ceramic Tile floor	53.82 %	0.00 %
Interior walls	White Plaster Wall	86.62 %	0.00 %
Ceiling	White paint	72.32 %	0.00 %
Tables	Dark brown timber	4.77%	0.00%

Glazing	Clear	8.4 %	86.6 %
	Double Glazing	7.3 %	70.7 %

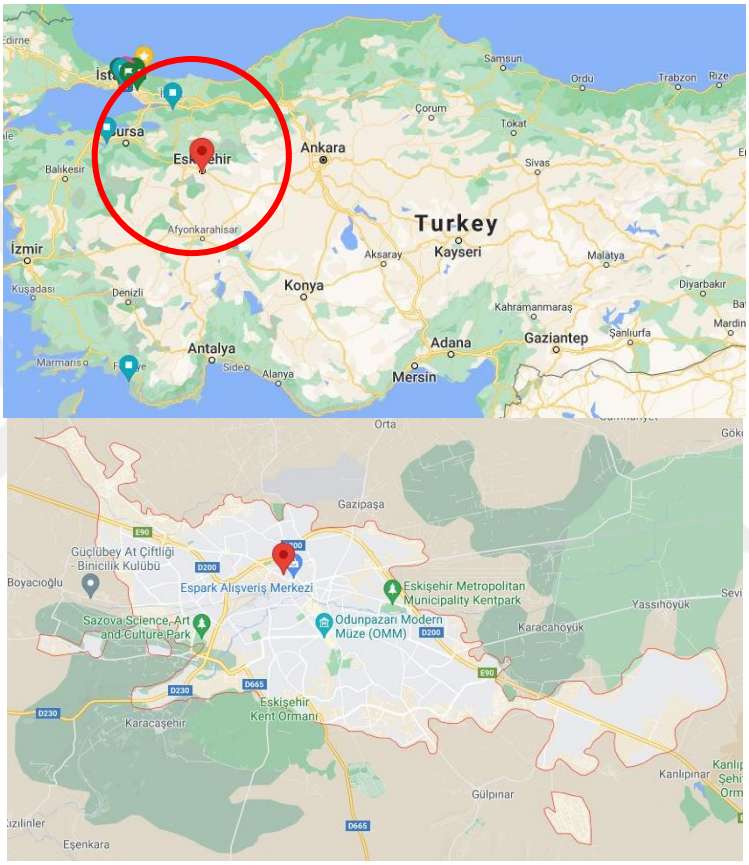

Figure 29: Location of the case study. (Source: Google Maps)

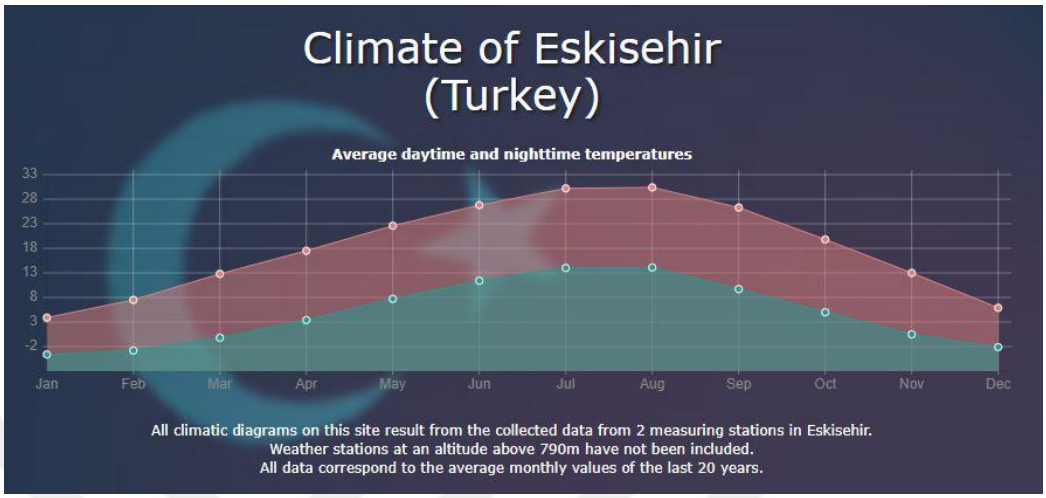

Figure 30: Climate of Eskisehir. Source: Worlddata.info

	January	February	March	April	May	June	July	August	Septem-ber	October	Novem-ber	Decem-ber
Avg. Temperature °C (°F)	-0.1 °C (31.8) °F	1.6 °C (35) °F	5.2 °C (41.4) °F	9.7 °C (49.4) °F	14.6 °C (58.2) °F	18.5 °C (65.4) °F	21.7 °C (71) °F	21.7 °C (71.1) °F	17.6 °C (63.8) °F	12.2 °C (54) °F	6.4 °C (43.5) °F	1.6 °C (34.9) °F
Min. Temperature °C (°F)	-4.2 °C (24.5) °F	-3.1 °C (26.4) °F	-0.6 °C (31) °F	3.2 °C (37.8) °F	8 °C (46.4) °F	12.1 °C (53.7) °F	14.7 °C (58.4) °F	15.2 °C (59.3) °F	11.4 °C (52.5) °F	6.8 °C (44.2) °F	1.3 °C (34.4) °F	-2.3 °C (27.9) °F
Max. Temperature °C (°F)	4.7 °C (40.5) °F	7 °C (44.7) °F	11.2 °C (52.2) °F	15.9 °C (60.7) °F	20.8 °C (69.5) °F	24.8 °C (76.7) °F	28.8 °C (83.8) °F	29 °C (84.2) °F	24.6 °C (76.3) °F	18.5 °C (65.3) °F	12.5 °C (54.5) °F	6.6 °C (43.8) °F
Precipitation / Rainfall mm (in)	48 (1.9)	47 (1.9)	54 (2.1)	53 (2.1)	49 (1.9)	34 (1.3)	12 (0.5)	14 (0.6)	16 (0.6)	36 (1.4)	35 (1.4)	54 (2.1)
Humidity(%)	77%	72%	66%	62%	58%	56%	51%	51%	54%	62%	68%	76%
Rainy days (d)	7	7	8	7	7	5	2	3	3	4	5	7
avg. Sun hours (hours)	5.1	5.9	7.5	9.1	10.5	11.2	11.6	10.7	9.2	7.2	6.7	5.3

Figure 31: weather data of Eskisehir. Source: climate-data.org

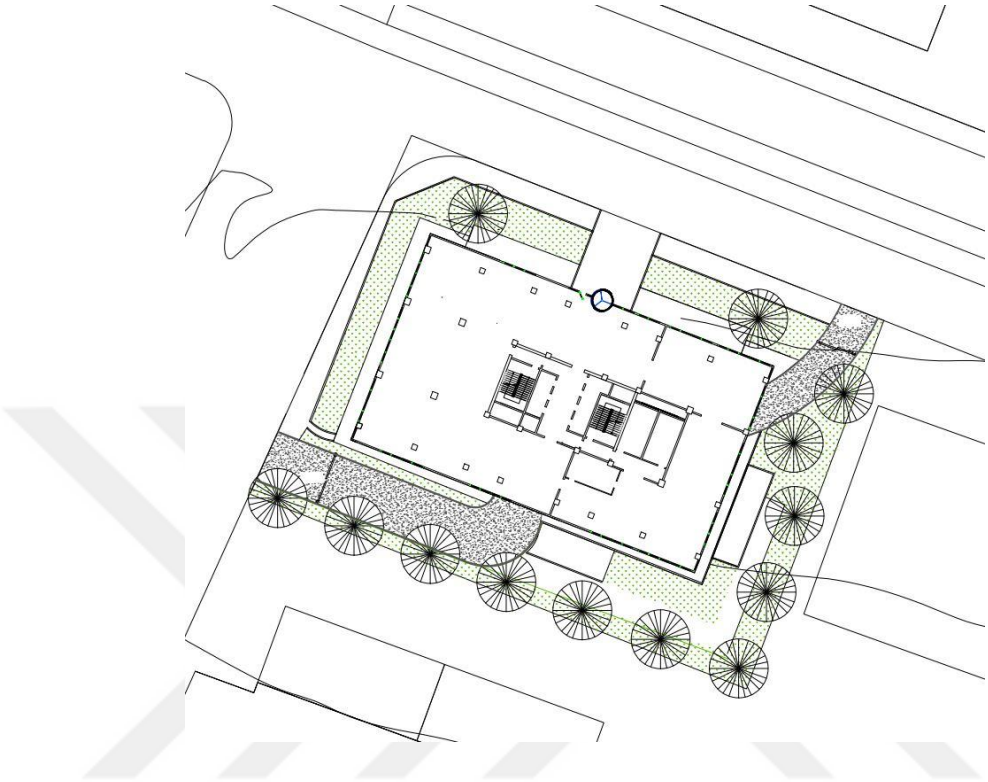

Figure 32: Case Study site plan.

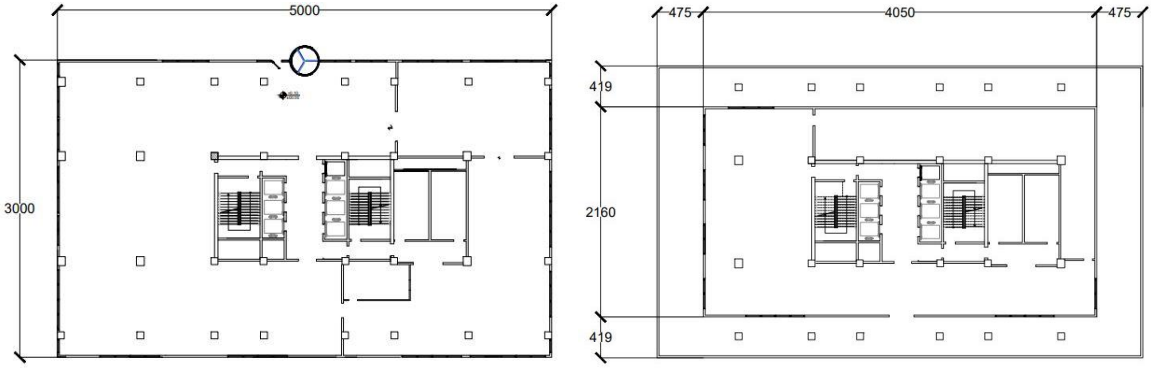

Figure 33: First, second plan layout (Left) and Third-floor plan (right) overall dimensions.

The building entrance is located on the ground floor, the northern façade side (Figure 33). The main vertical circulation inside the building is located at the core of the space, where there are elevators and staircases. The circulation route inside the building is fluid and ample. The open spaces provide seamless movement for the building occupants except for certain

private zones such as storage and mechanical rooms. The open space layout also permits the light to penetrate the windows into deep areas inside the building. The second floor exhibits a much similar layout to the Ground floor (Figure 34). The third-floor plan floor has a terrace on the rooftop that occupies about half of the space (Figure 35). Each floor plan had been divided into four wings with a (dashed line) in order to study the effect each pattern has on each side of the building as illustrated below.

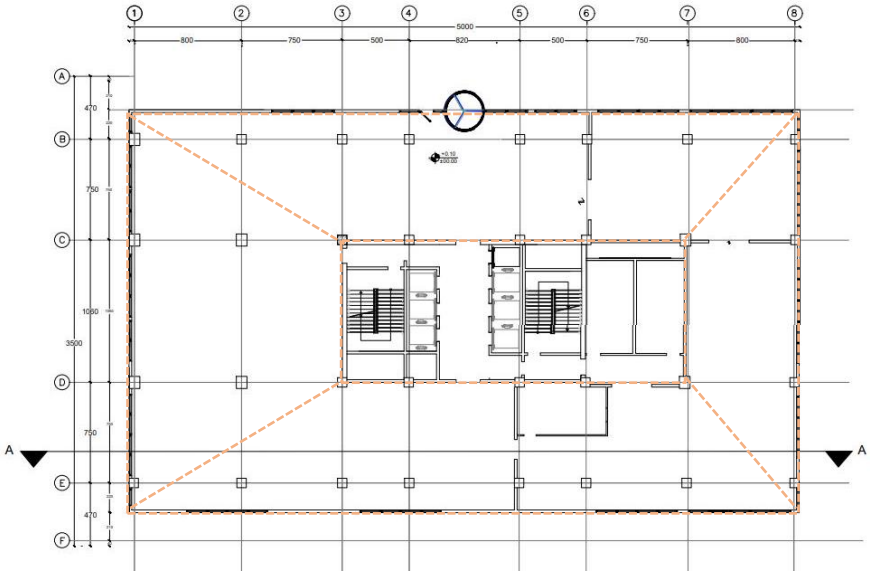

Figure 34: Ground Floor Plan

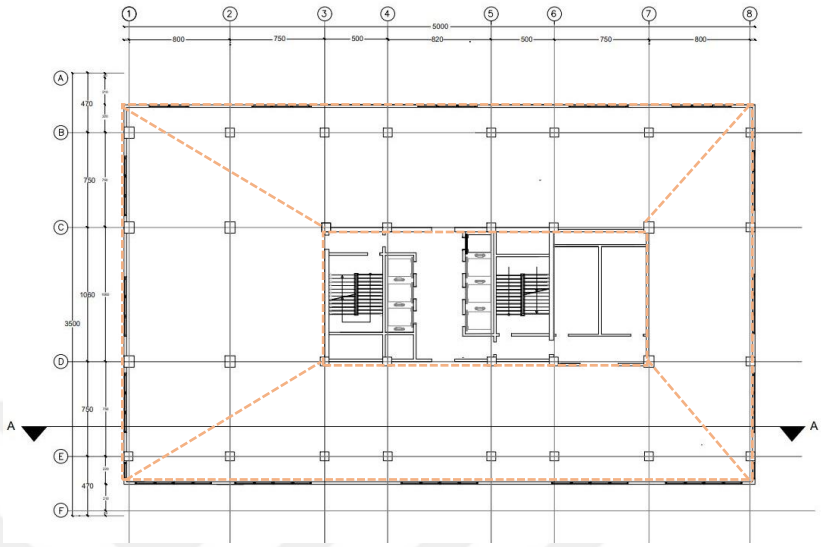

Figure 35: Second Floor plan.

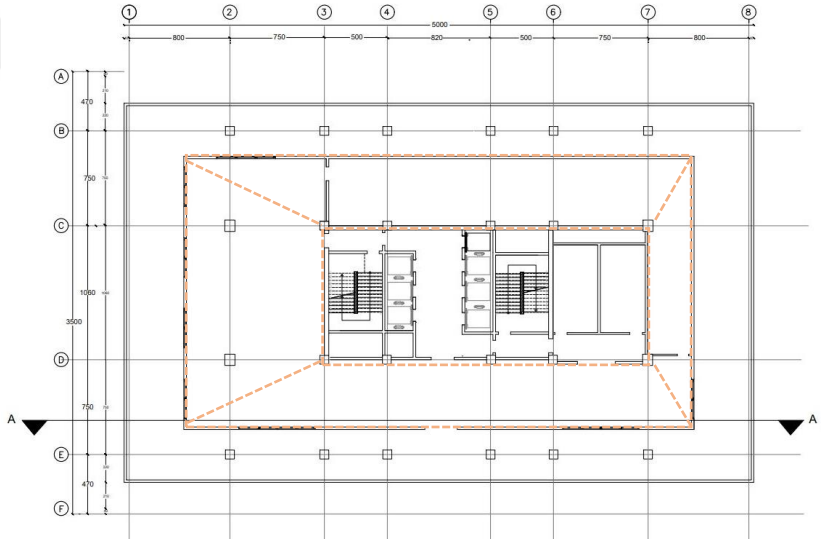

Figure 36: Third-floor plan.

- **Base case model**

A reference model of the case study building was modelled following the original measurements (figure 36 and 37). The boundary space for the windows facing the south and east are 100 cm from the floor and 250 cm in height (Figure 38).

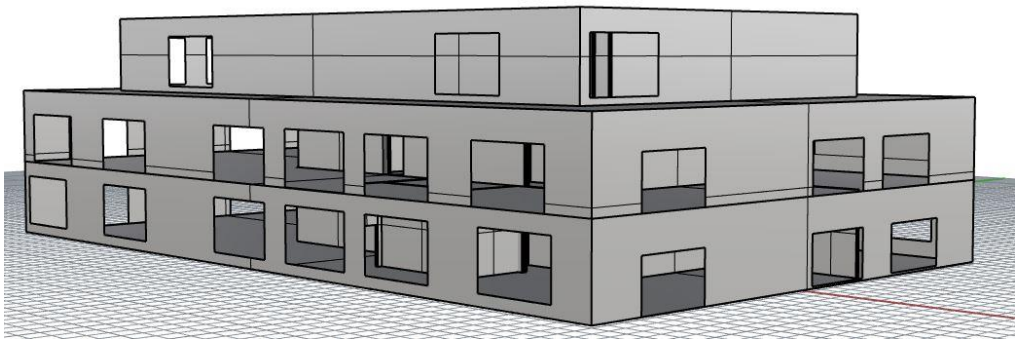

Figure 37: Office Building model. Built with Rhinoceros.

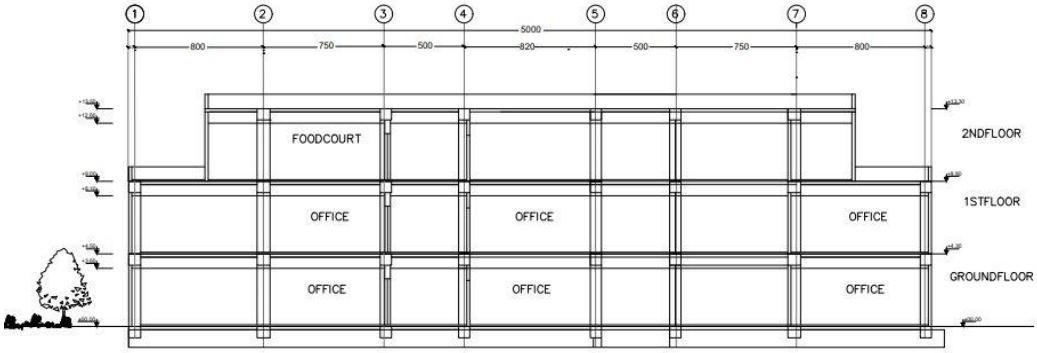

Figure 38: Case study Building Section.

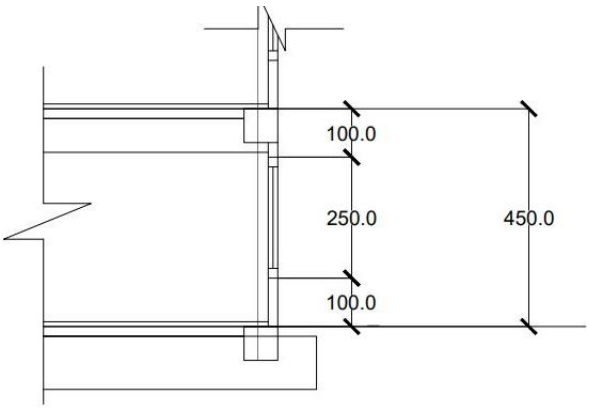

Figure 39: Glazing second of the southern and eastern facades.

CHAPTER V

RESULTS

5.1 Sun Path:

The study records the sun path, movement, and attitude in both summer and winter seasons at three different times (9 AM, 12 PM & 3 PM).

a- Summer Sun Path:

The results record the sun path at 9 AM on the 1st of July (Figure 39) impacts the roof and the Eastern Façade, leaving the Northern, Southern and Western facades shaded.

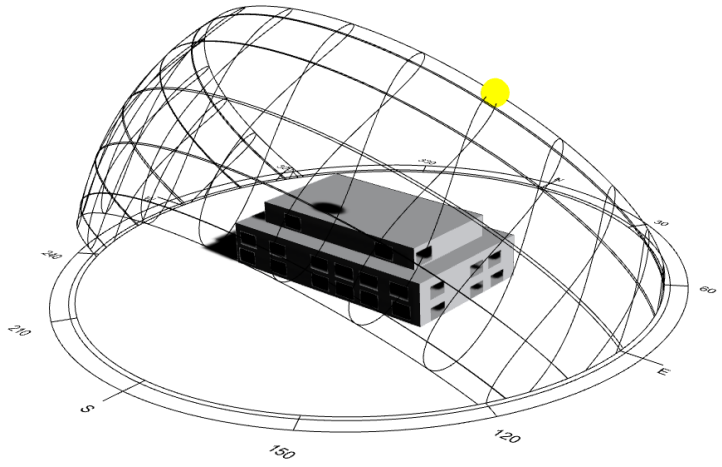

Figure 40: Summer Sun Path at 9 AM.

The sun path result recorded at 12 PM in 1st of July (Figure 40) impacts the roof and the Southern Façade directly leaving the Northern façade to be the least exposed to the sun.

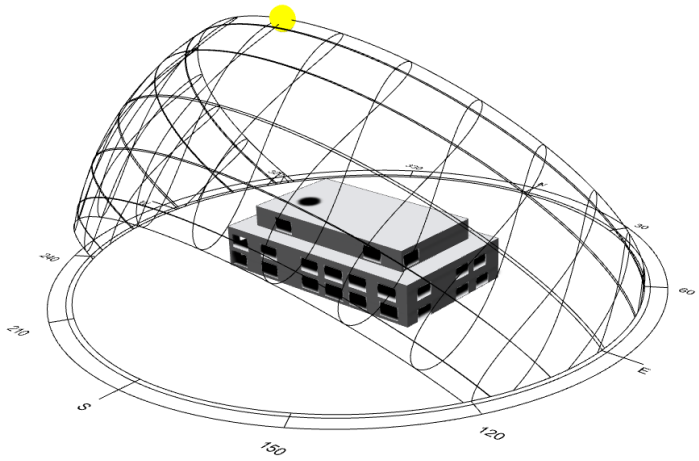

Figure 41: Summer Sun Path at 12 PM.

The results record the sun path at 3 PM on the 1st of July (Figure 41) impacts the roof and the Western, and Southern Façade, leaving the Northern and eastern facades shaded.

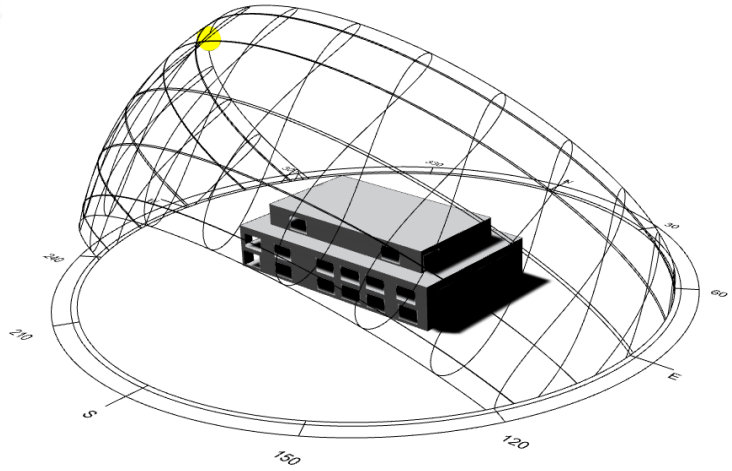

Figure 42: Summer Sun Path at 3 PM.

b- Winter Sun Path:

The results of the sun path at 9 AM on the 1st of December (Figure 42) has a lower attitude. It impacts the Eastern and Southern facades the most, casting a big shadow on the Northern and Western facades as they are the least exposed to the sun.

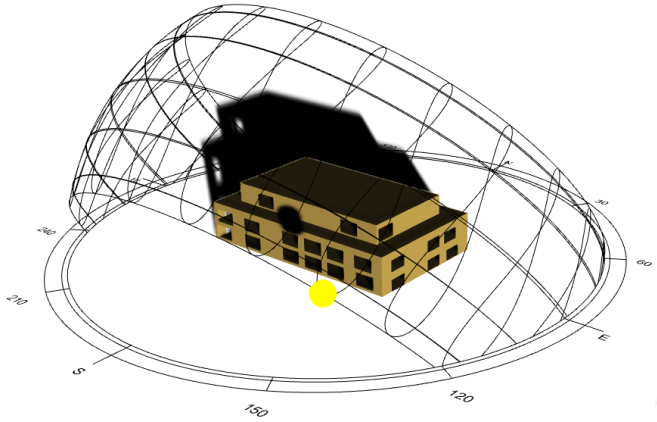

Figure 43: Winter Sun Path at 9 AM.

The results of the sun path at 12 PM on the 1st of December (Figure 43) impacts the Southern façade and roof the most, casting a shadow on the Northern, Eastern and Western facades.

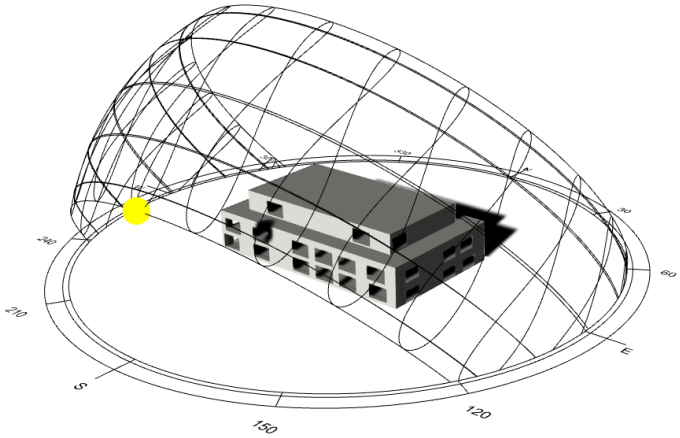

Figure 44: Winter Sun Path at 12 PM.

The results of the sun path at 3 PM on the 1st of December (Figure 44) impacts the Southern façade, Western façade and roof the most, casting a big shadow on the North and East.

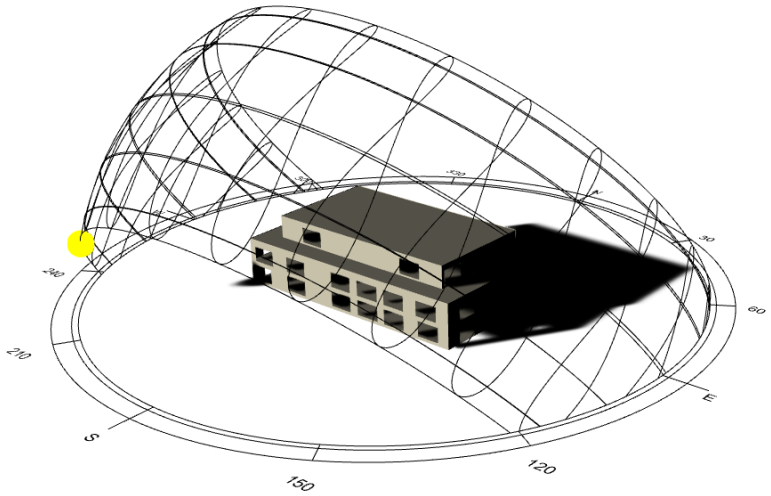

Figure 45: Winter Sun Path at 3 PM

The results in Table 6 are extracted from the sun paths diagram, aid in determining the critical areas where the DSF needs to be applied.

Table 11: Sun Path Diagram data; Azimuth and Elevation results.

Season/ Time	**9 Am**		**12 Pm**		**3 Pm**	
	Azimuth	**Elevation**	**Azimuth**	**Elevation**	**Azimuth**	**Elevation**
Summer	89°	36°	136°	67°	242°	60°
Winter	126°	4°	164°	23°	208°	19°

The results recorded at 9 AM and 12 PM in the summer have higher Elevation and lower Azimuth than winter results. This exposes the eastern façade the most to the sun in the summer and the eastern and southern façade in winter. The lower elevation of the sun in winter admits more sunlight into the building, but the higher sun elevation recorded in summer exposes the roof to the higher solar radiation.

The results recorded at 3 PM are a little different as the Azimuth value for the summer is higher than winter. Yet, the elevation of the winter is lower. The original case study model depends mainly on self-shading.

5.2 Solar Direction (Radiation-Rose)

a- Summer Solar Direction

Figure 45 shows that the highest radiation the area receives is mainly from the southeast direction. The radiation is the highest between 100° to 140° as it reaches up to more than 203.41 kWh/m2. The building receives the lowest radiation on the northern side.

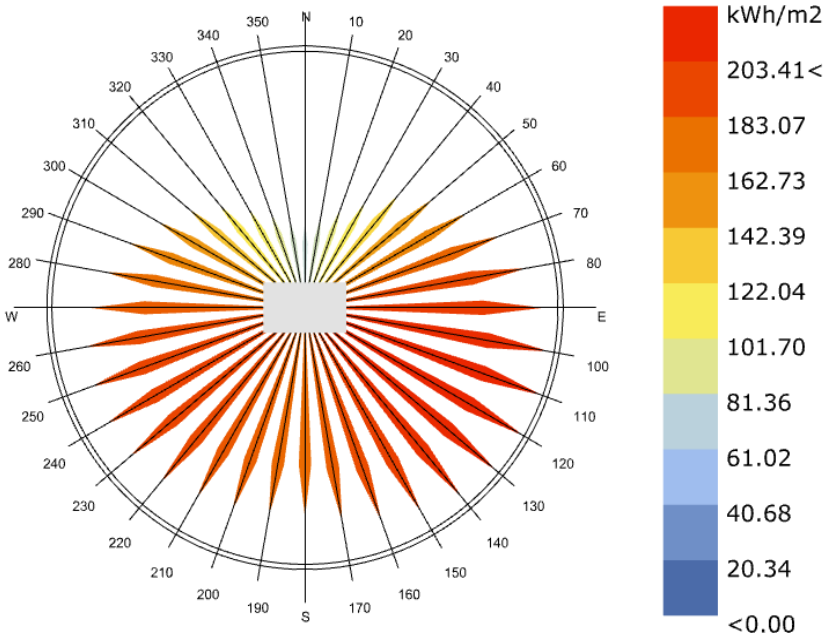

Figure 46: Summer Solar Direction, recorded from 21st of June until 20th of September.

b- Winter Solar Direction:

Figure 46 shows that the area's highest radiation is from the southern direction. The radiation is the highest between 160° to 210° as it receives more than 96.59 kWh/m^2. The building receives little to no radiation on the Northern side. The radiation on the Eastern and Western Façade is less than 57.95 kWh/m2.

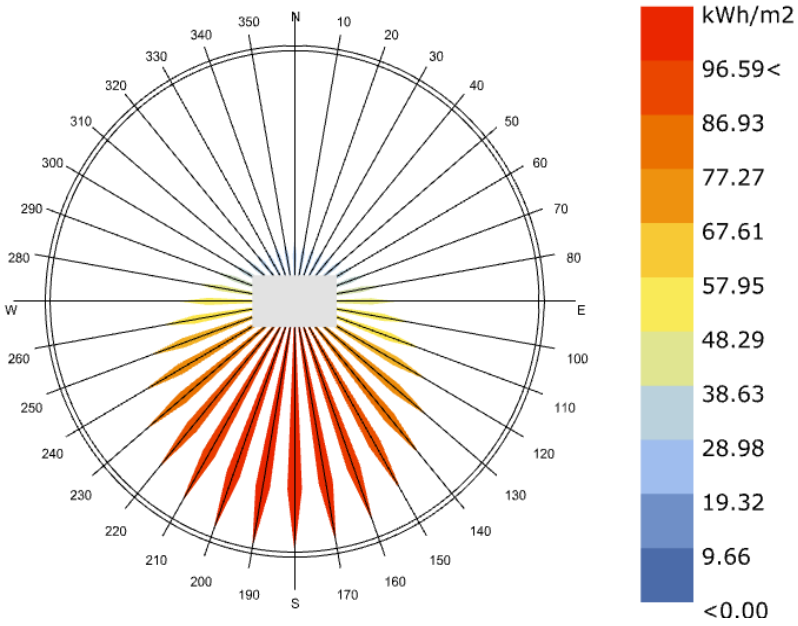

Figure 47: Winter Solar Direction recorded from 21st of December until 20th of March...

The simulation results support the decision taken in this research methodology of placing the DSF on the building façade.

5.3 Annual Solar Incident (Radiation Simulation):

The western and eastern facades receive up to approximately 750-900 kWh/m2 (Figure 47). The Southern façade receives a relatively higher radiation value than all other

three facades. It reaches between 900- 1050 kWh/m2. The Northern façade is the least exposed to the sun (figure 48).

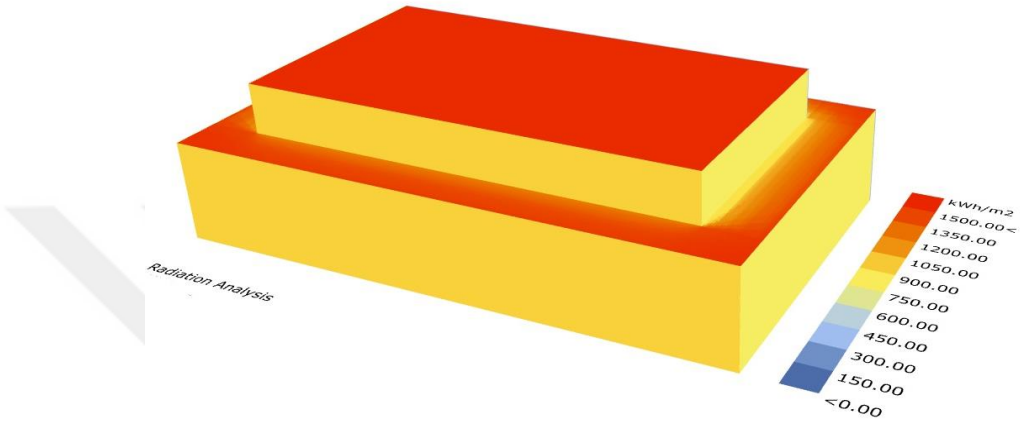

Figure 48: Annual Building (Incident) Radiation graph on the Eastern and Southern facade.

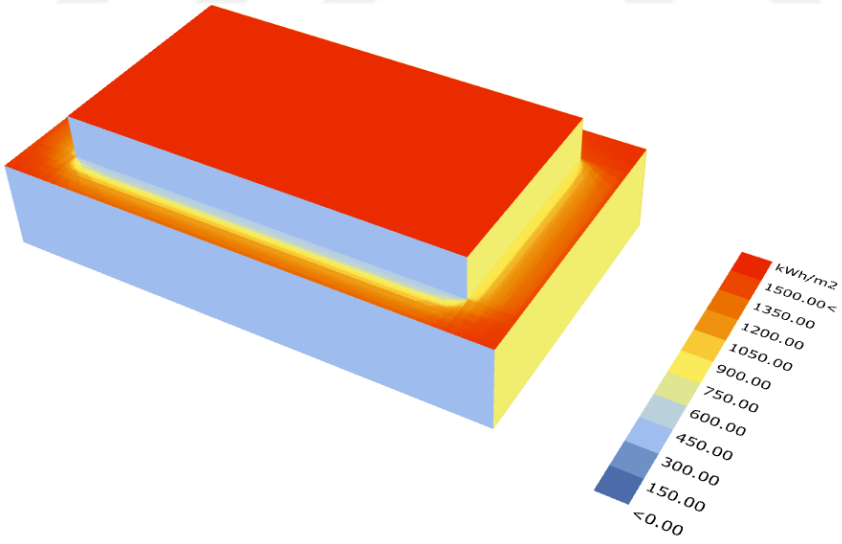

Figure 49: Annual Building (Incident) Radiation graph on the western and northern facade.

5.3.1 Case Study Building Base Model:

Each floor plan had been divided into four wings with a (dashed line) in order to study the effect each pattern has on each interior part of the building.

a- Summer (Incident) radiation graphs:

The carpet plot graph of the first level indicated the highest levels of radiation received, represented in red plots, is on the Southern side, which reached 4.69 kWh/m2. The Eastern and western windows receive between 2.82 kWh/m2 and 3.28 kWh/m2 (Figure 49).

On average, the second level receives lower radiation levels than the first level. The southern areas record a radiation value of 3.52 kWh/m2. Radiation reaches up to 2.47 kWh/m2 on the east and up to 3.17 kWh/m2 on the west (Figure 50).

On the third level, the highest radiation levels are received from the south 5.07 kWh/m2, followed by the western side of almost 3.55 kWh/m2 to 4.06 kWh/m2, then the eastern side receives up to 3.04 kWh/m2 (Figure 51).

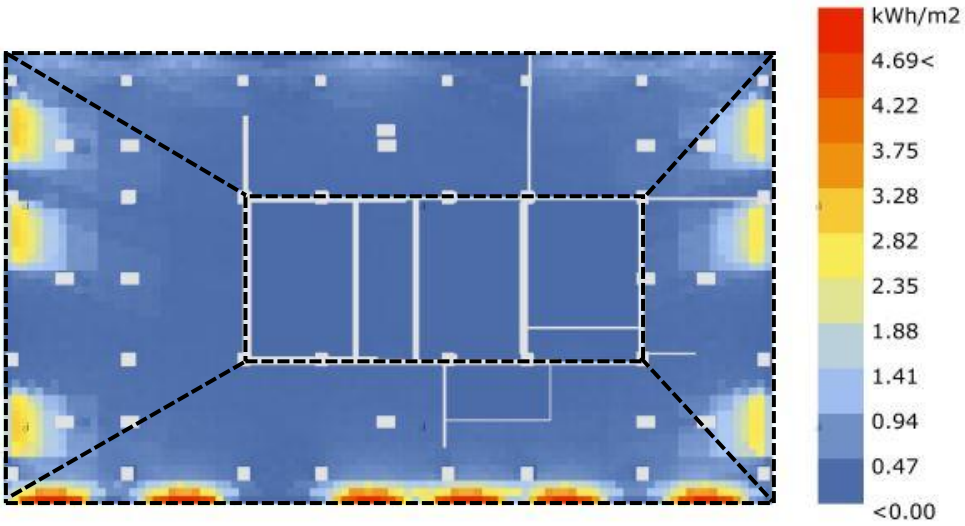

Figure 50: Base Building Summer Radiation Graph (21st of June); Level 1.

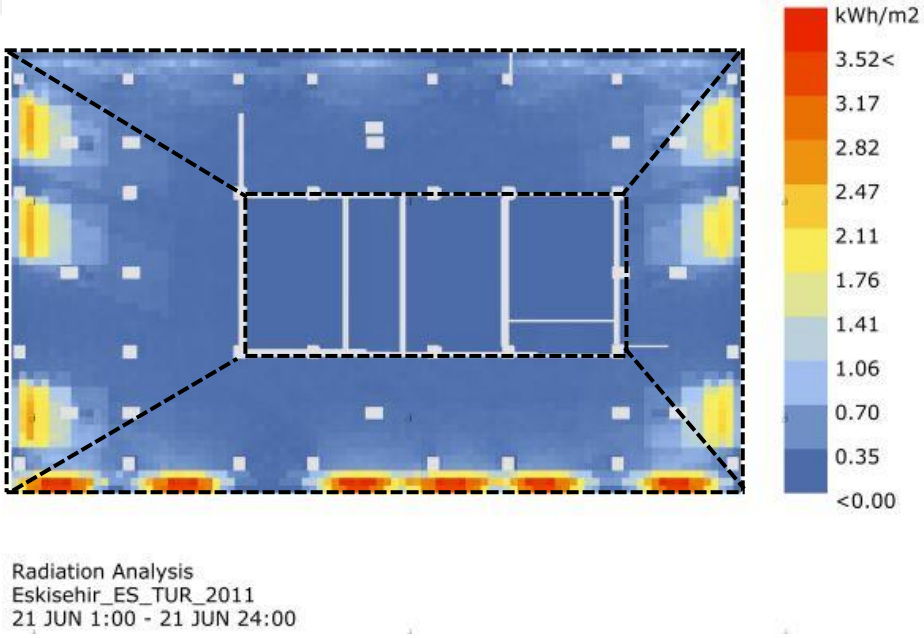

Figure 51: Base Building Summer Radiation Graph (21st of June); Level 2.

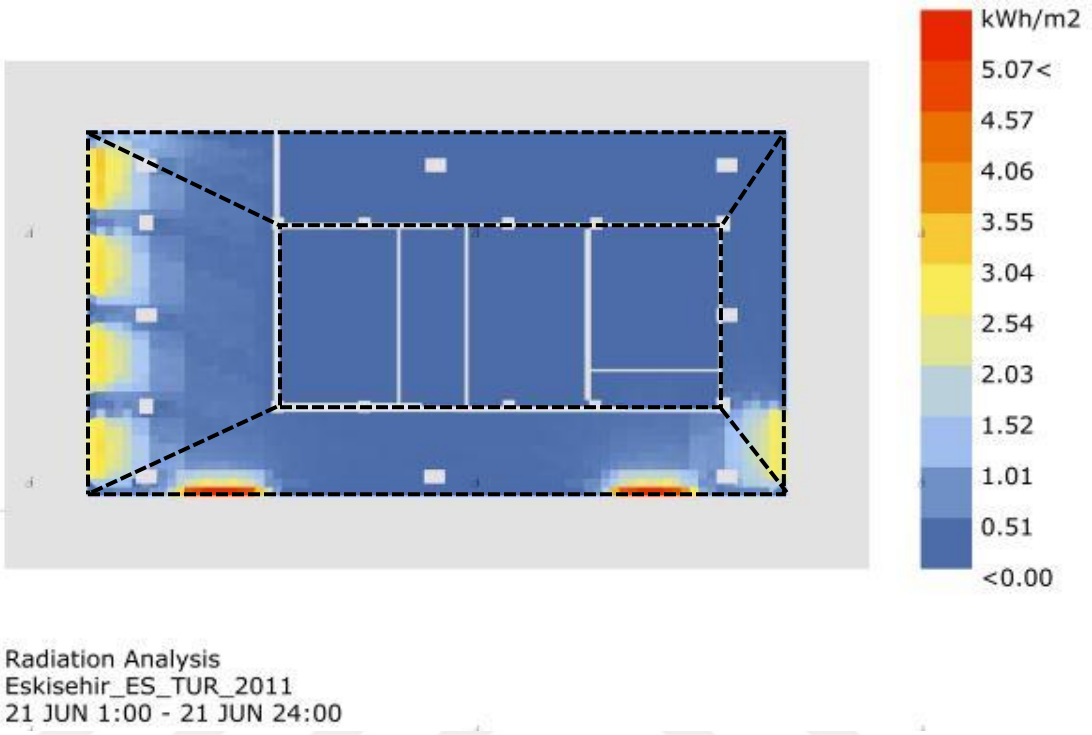

Figure 52: Base Building Summer Radiation Graph (21st of June); Level 3.

b- Winter (Incident) radiation graphs:

The graph of the first level indicated the highest levels of radiation received are on the southern wing, which reached 1.19 kWh/m2. Level 1 receives relatively higher radiation than level 2. The Eastern and western windows receive between 0.60 kWh/m2 and 0.83 kWh/m2 (Figure 52).

On average, the second level receives fewer radiation levels than the first level. The southern areas record a radiation value of 1.08 kWh/m2. Radiation reaches between 0.32 to 0.75 kWh/m2 on the east and up to 0.65 kWh/m2 on the west (Figure 53).

Unlike the first and second levels, the radiation in winter penetrates deeper spaces in the office on the third level, especially on the southern and western wing, because there are

more windows. The highest radiation levels are received from the south, more than 1.26 kWh/m2, followed by the western side of almost 0.88 kWh/m2, then the eastern side up to 0.76 kWh/m2 (Figure 54).

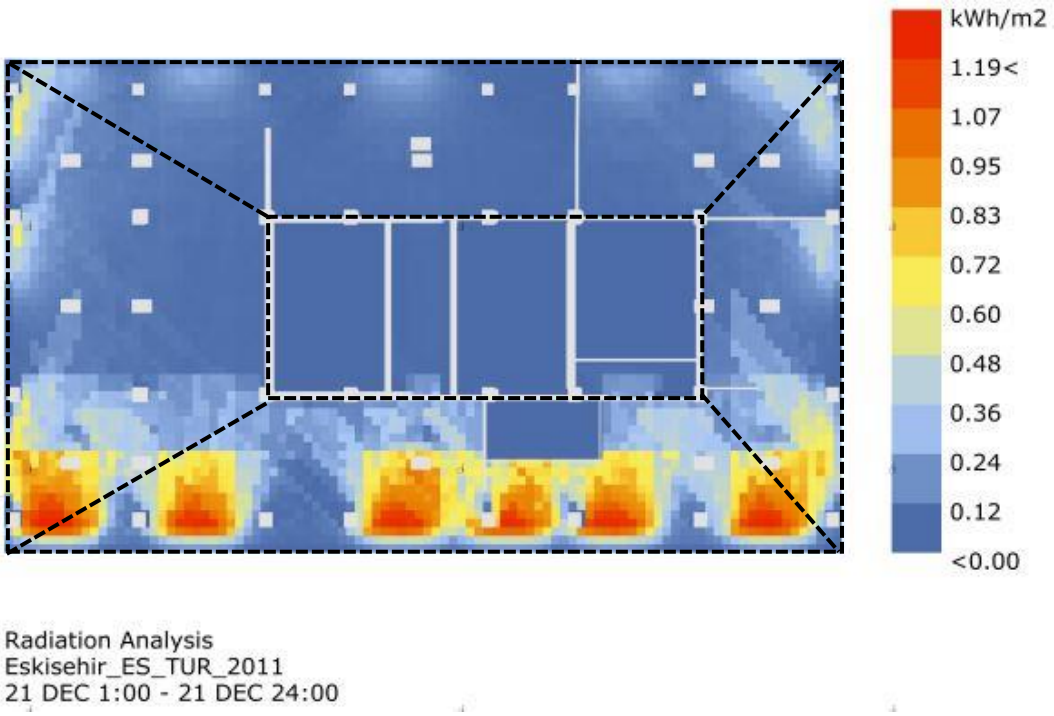

Figure 53: Base Building Winter Radiation Graph (21st of December); Level 1.

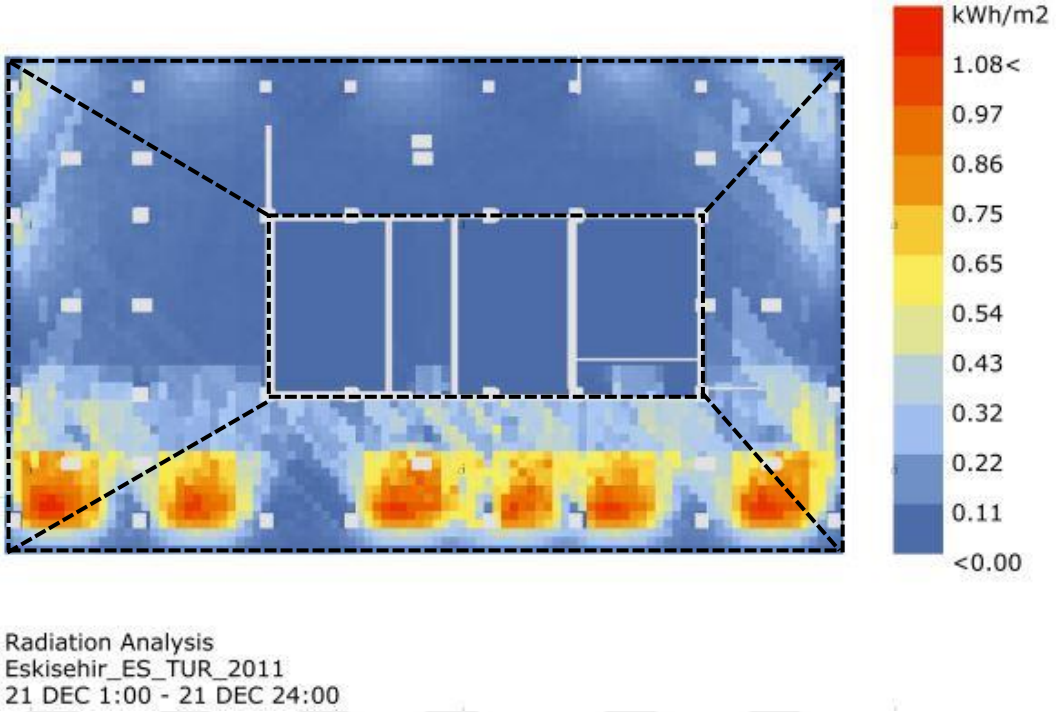

Figure 54: Base Building Winter Radiation Graph (21st of December); Level 2.

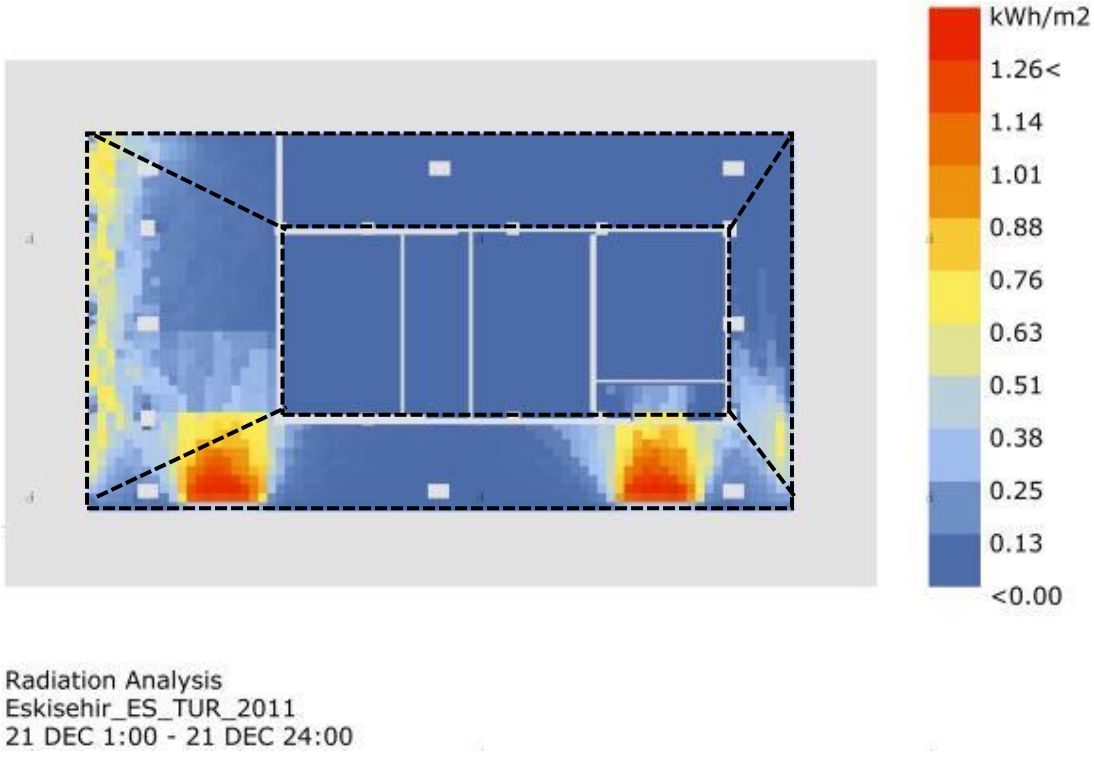

Figure 55: Base Building Winter Radiation Graph (21st of December); Level 3.

The variations in the following four simulation incident graphs result from DSF shading, unlike the first case building radiation simulations, which depended on self-shading. A table of more accurate results for each floor average and highest radiation recordings is provided after analyzing all radiation graphs at the end of the chapter.

5.3.1 Type-A Facade Building Model

a- Summer (Incident) radiation graphs:

Figure 55, the first level, recorded a notable decrease in the red-carpet plots than the original model. The radiation levels were reduced to 4.31 kWh/m2 on the south. The first level has an even radiation distribution, as presented in figure 55. The western side values were reduced to 2.15 kWh/m2. The northern side radiation reached almost 1.29 kWh/m2.

The second level shows a significant decrease in the radiation values compared to the original base model, especially on the southern and western sides of the building. The southern areas recorded radiation of less than 2.22 kWh/m2. The eastern wing recorded a decrease of incident value, less than 1.98 kWh/m2, and the western wing 1.48 to 1.98 kWh/m2 (Figure 56).

The third level recorded a significant decrease in radiation levels, especially on the southern and western facades, in comparison to the base study model. On the other hand, the northern and eastern facades received more radiation levels. The radiation levels on the southern side decreased to 2.80 kWh/m2 (Figure 57).

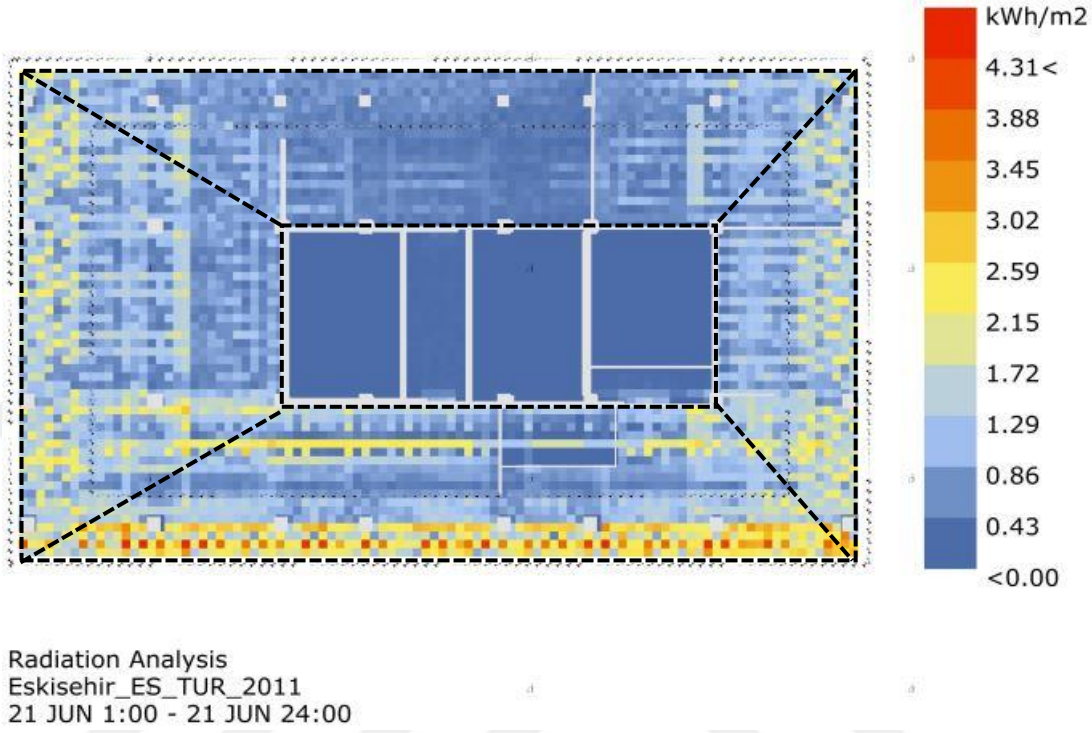

Figure 56: Type A Facade, Summer Radiation graphs (21st of June), Level 1.

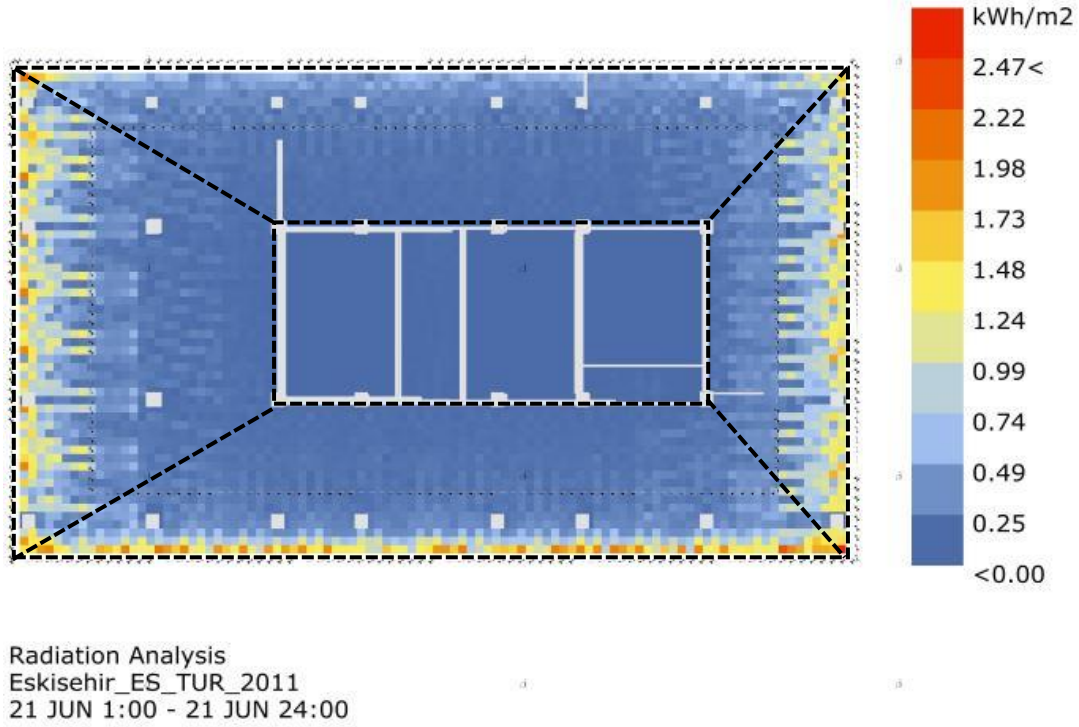

Figure 57: Type A Facade, Summer Radiation graphs (21st of June), Level 2.

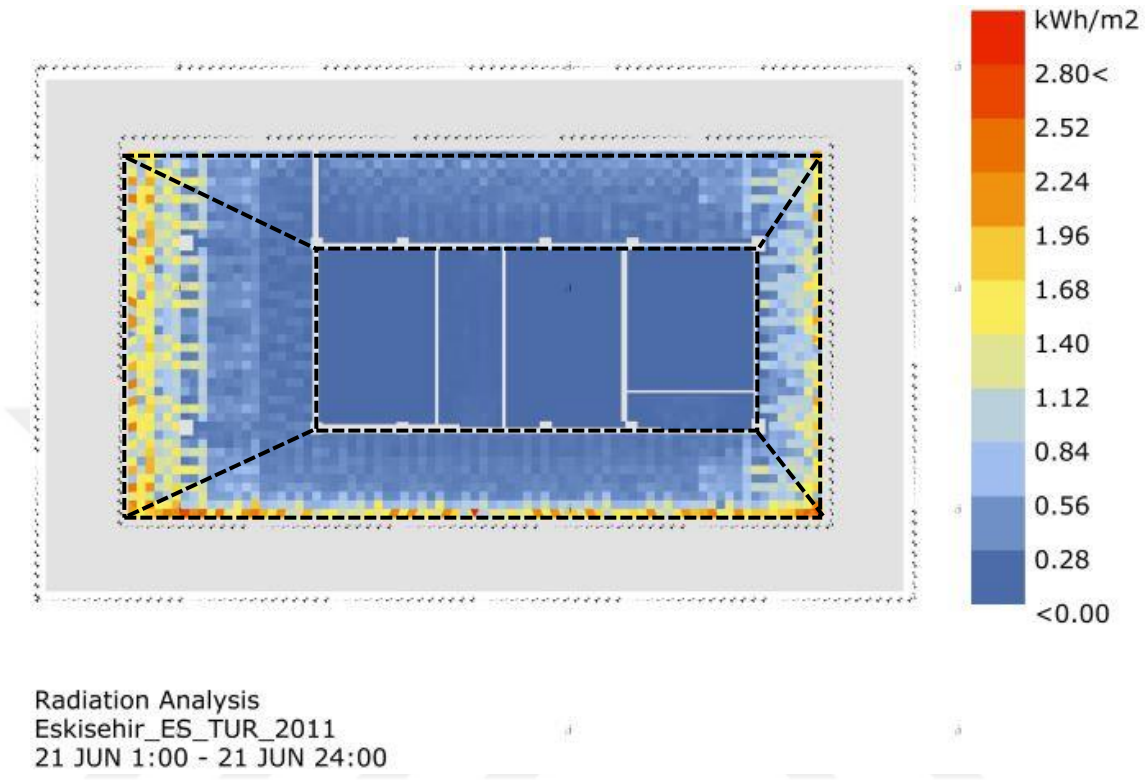

Figure 58: Type A Facade, Summer Radiation graphs (21st of June), Level 3.

The overall results for façade A recorded more radiation distribution on the interior spaces of the building, where the radiation decreased in value, but on some levels reached deeper parts of the office.

b- **Winter (Incident) radiation graphs:**

In comparison to the base model in winter, level 1 for this façade pattern allows radiation to penetrate into deeper areas in the form of long strips of red plots on the graph. However, the radiation values are significantly lower than the base model. On the southern wing, the radiation reaches 0.56 kWh/m2 to 0.94 kWh/m2. The western and eastern facades record radiation values around 0.66 kWh/m2 (Figure 58).

Like the first level, the northern spaces receive the lowest radiation levels, less than 0.26 kWh/m2. The southern part records radiation of 0.87 kWh/m2. The radiation reaches shallower parts than the first level. The eastern and western wings receive relatively similar radiation levels, but slightly higher on the eastern wing. Radiation reaches 0.52 kWh/m2 on the east and up to 0.43 kWh/m2 on the west (Figure 59).

The third level of this simulation allows the radiation to reach deeper parts than the base case model. The highest radiation levels are received from the south 0.91 kWh/m2, followed by the eastern side of almost 0.55 kWh/m2, then the western side, which records 0.37 kWh/. The northern part receives the lowest radiation of 0.27 kWh/m2 (Figure 60).

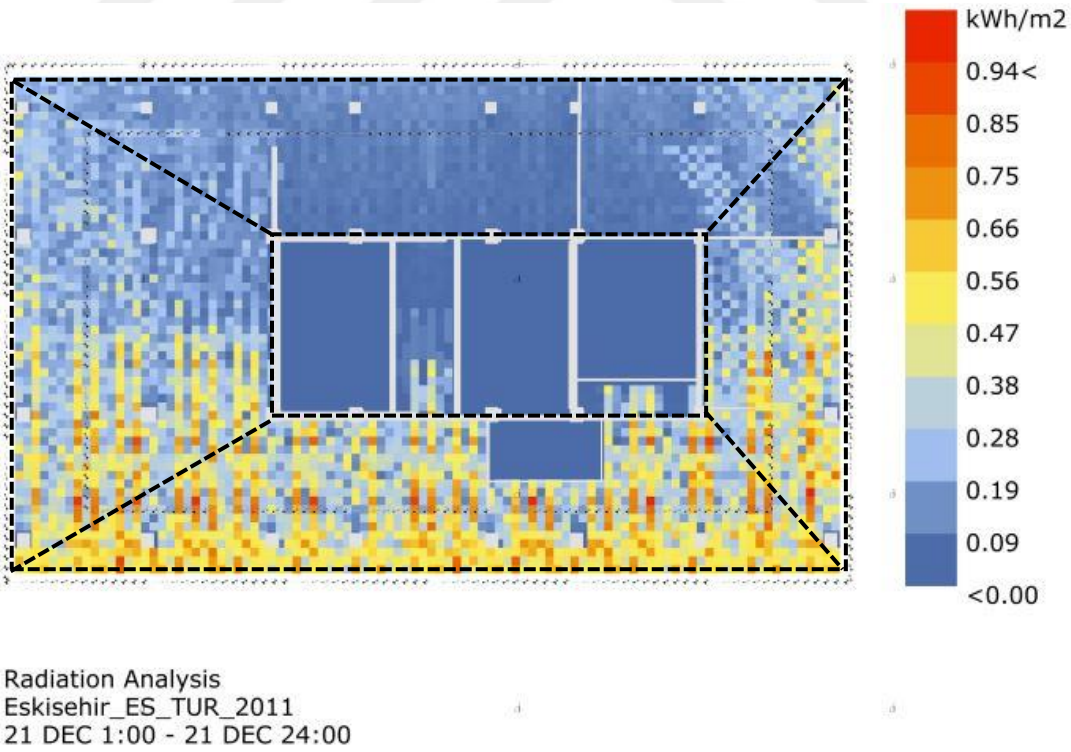

Figure 59: Type A Facade, Winter Radiation graphs (21st of December), Level 1.

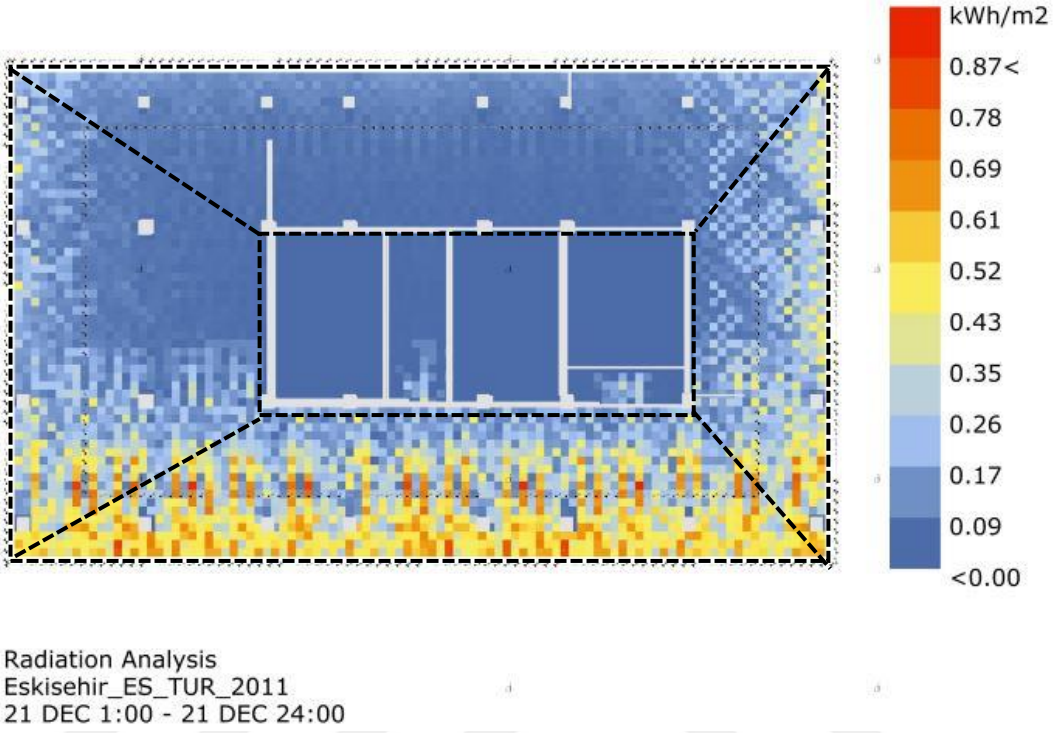

Figure 60: Type A Facade, Winter Radiation graphs (21st of December), Level 2.

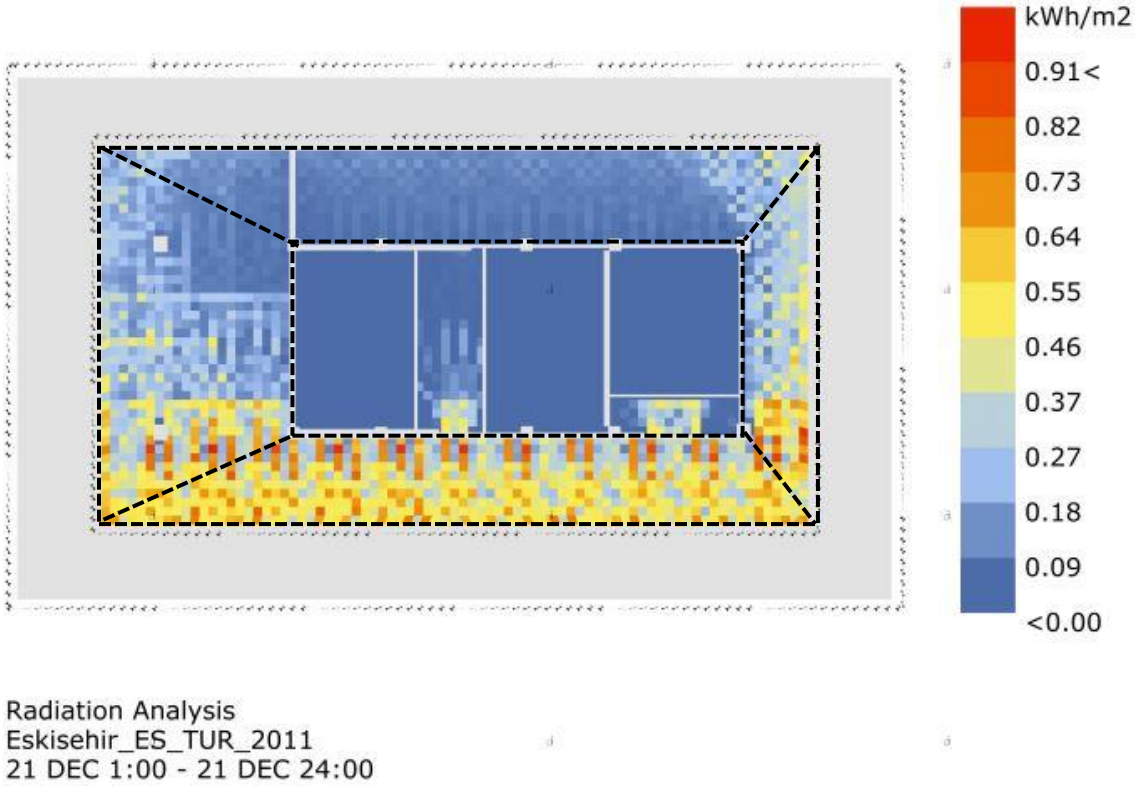

Figure 61: Type A Facade, Winter Radiation graphs (21st of December), Level 3.

The overall radiation results on winter for façade A recorded more radiation distribution on the interior spaces of the building compared to the base model, where the radiation, although decreased in the average value significantly,reached deeper parts of the office.

5.3.3 Type B Facade Building Model

a- Summer (Incident) radiation graphs:

The first level of this simulation, like pattern A, allows the radiation to reach deeper interior areas in the office building. In pattern B simulation, the first level graph results have a lower average of radiation levels compared to the original building, especially on the southern area of the office (figure 61). The western side values were reduced down to 2.46 kWh/m2. The northern radiation reached 1.23 kWh/m2 to 0.92 kWh/m2.

Compared to the first level, the second level shows a significant decrease in the average radiation values compared to the original building. The southern areas recorded radiation levels less than 2.81 kWh/m2. The eastern recorded a decrease of incident value, down to 2.25 kWh/m2, and the western wing was between 1.68 kWh/m2 to 2.53 kWh/m2 (Figure 62).

Compared to the base model, the third level recorded a significant decrease in average radiation levels, especially on the southern facade. The radiation levels on the southern side recorded 2.97 kWh/m2. On the other hand, the northern and eastern facades received more radiation levels than the base model (Figure 63).

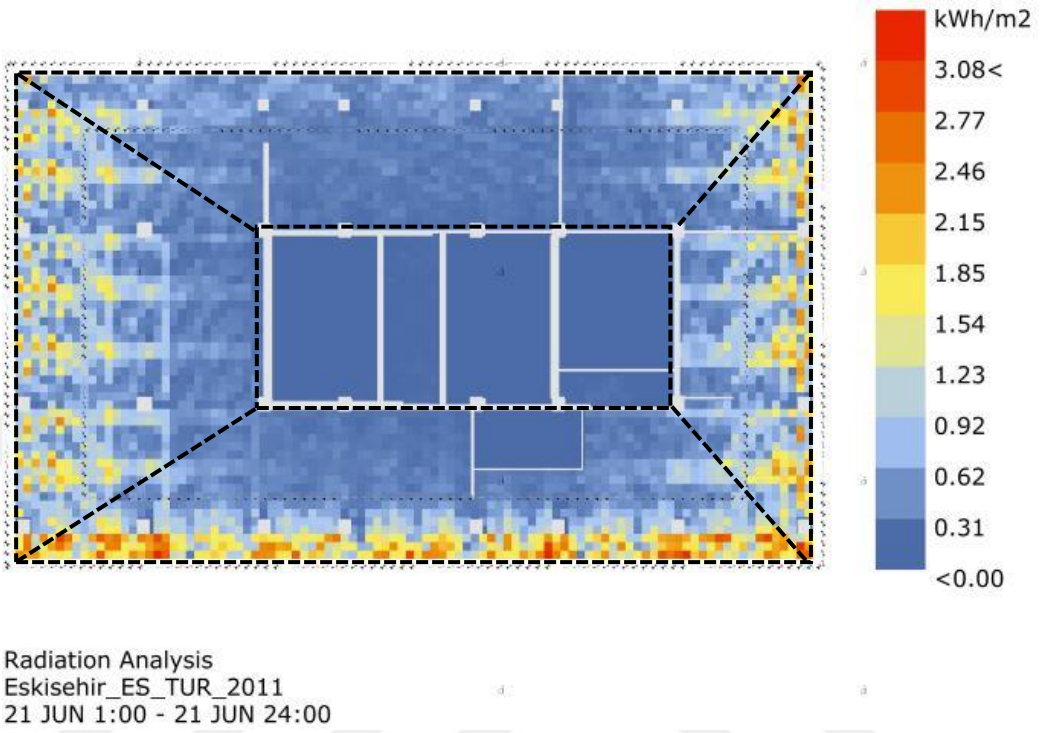

Figure 62: Type B Facade, Summer Radiation graphs (21st of June), Level 1.

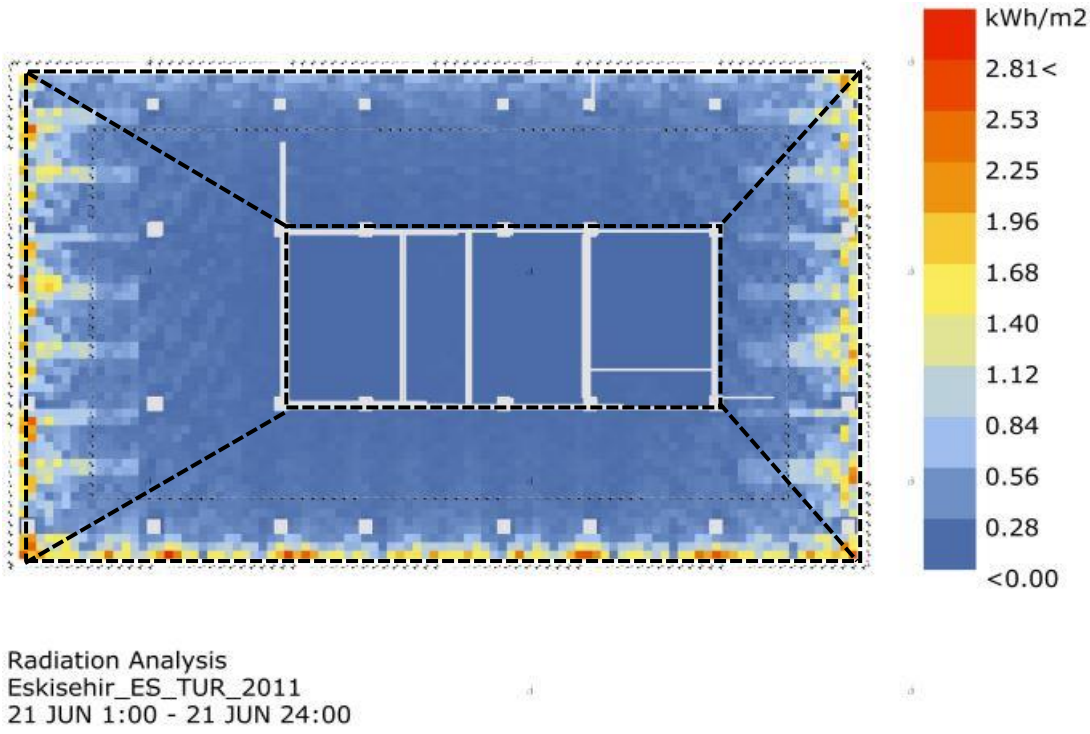

Figure 63: Type B Facade, Summer Radiation graphs (21st of June), Level 2.

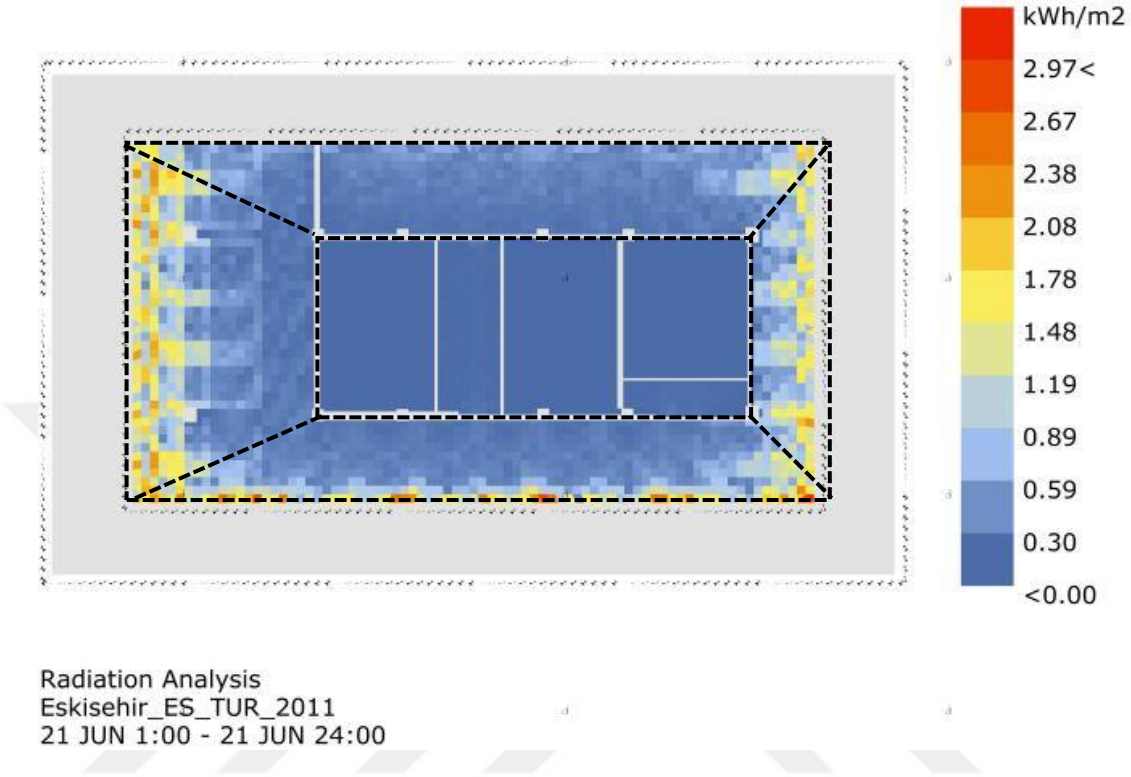

Figure 64: Type B Facade, Summer Radiation graphs (21st of June), Level 3.

Pattern B provides lower radiation values on the first level than Pattern A. This is due to the fact that pattern B consists of thinner panels with smaller gaps that provide a higher ratio of solid areas. However, the radiation values recorded on the second level of pattern B were slightly higher than pattern A. The third-level radiation results for patterns A and B were almost similar.

b- Winter (Incident) radiation graphs:

Compared with the original base model winter graphs, Pattern B decreased the radiation levels notably (figure 64). Radiation levels on the first level do not exceed 0.94 kWh/m2 on the southern side. The western wing records radiation values up to 0.56 kWh/m2. The eastern wing receives radiation of 0.84 kWh/m2 (Figure 64).

The second level receives, on average lower radiation than the base model. The southern part records radiation of 0.89 kWh/m2. Radiation reaches 0.69 kWh/m2 on the east and up to 0.49 kWh/m2 on the west (Figure 65).

The third level of this simulation allows the radiation to reach deeper parts than the base case model but with a lower average radiation value. The highest radiation levels are received from the south of 0.92 kWh/m2, followed by the eastern side of almost 0.64 kWh/m2, then the western side, which records almost 0.37 kWh/m2. (Figure 66).

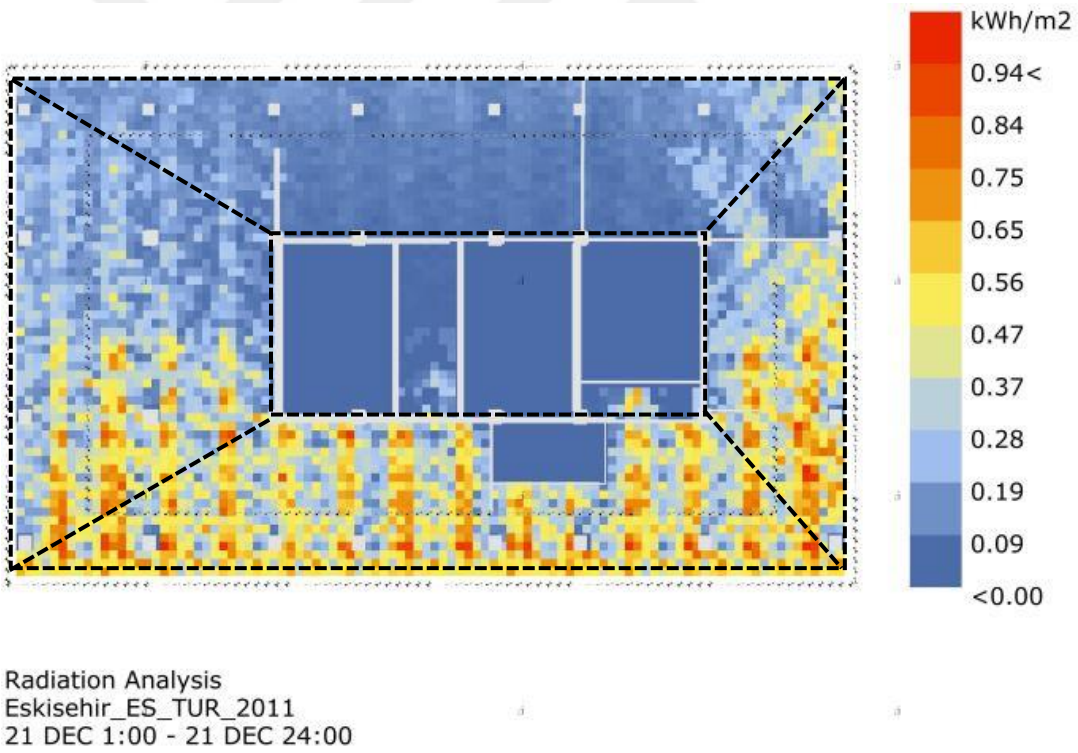

Figure 65: Type B Facade, Winter Radiation graphs (21st of December), Level 1.

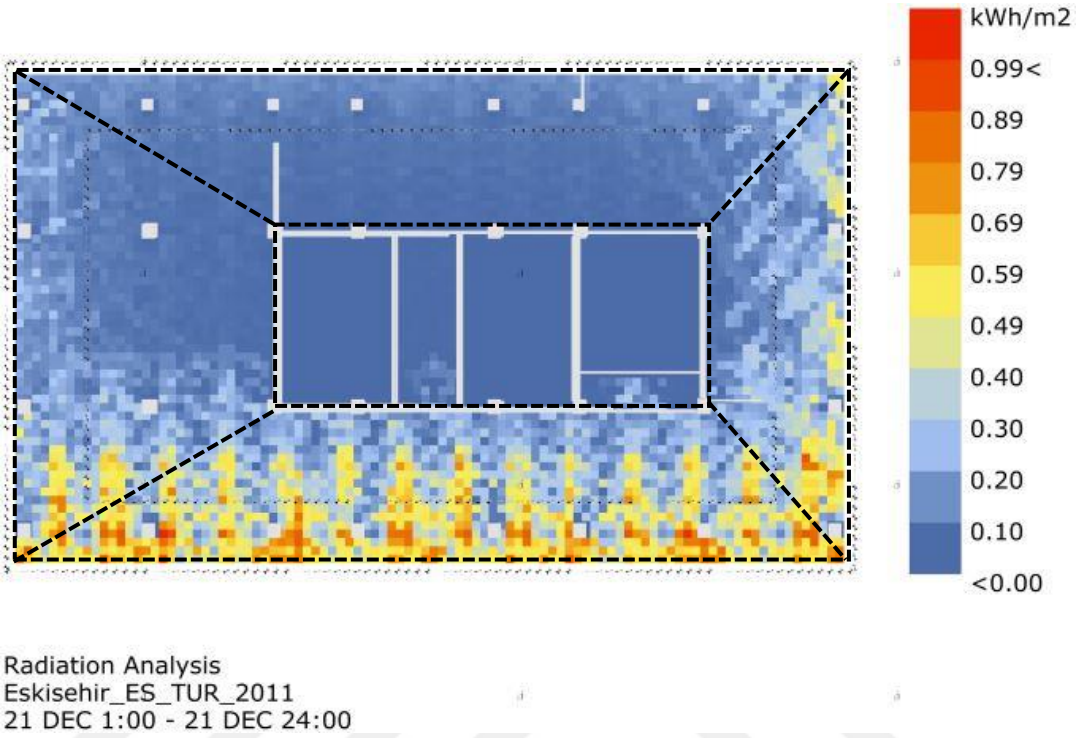

Figure 66: Type B Facade, Winter Radiation graphs (21st of December), Level 2.

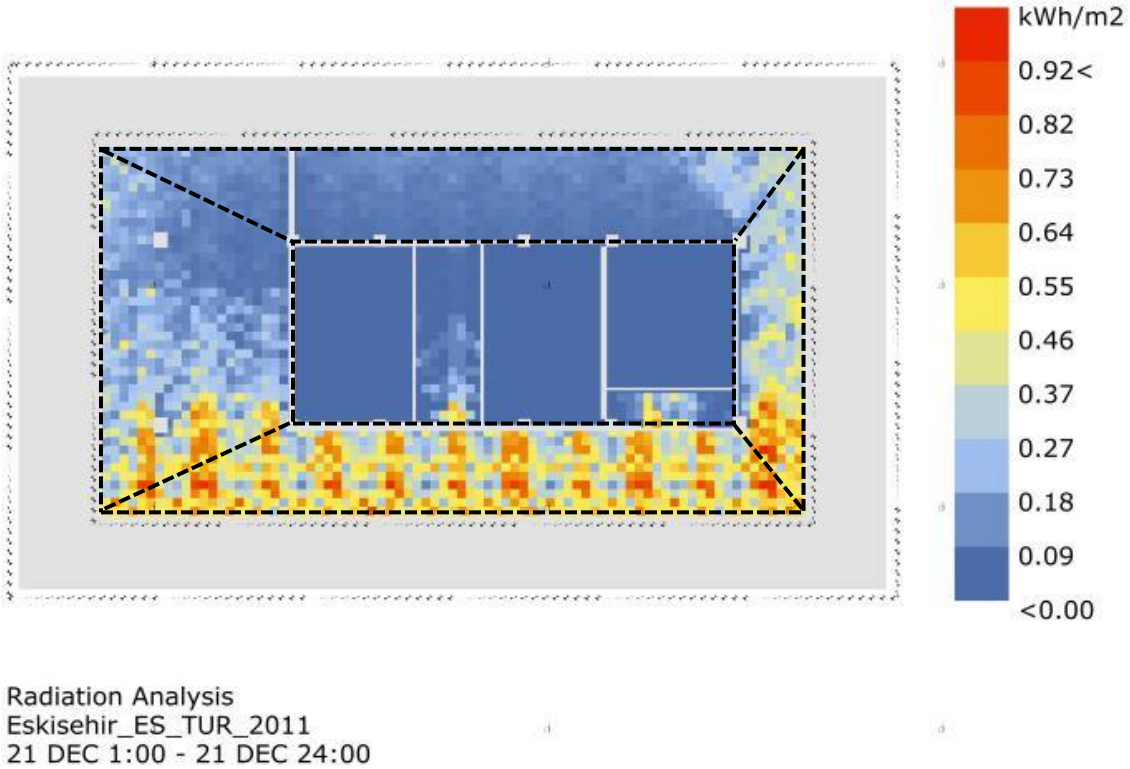

Figure 67: Type B Facade, Winter Radiation graphs (21st of December), Level 3.

The overall radiation results on winter for façade B are similar to pattern A in that they provided more radiation distribution on the interior spaces of the building compared to the base model. Although the radiation decreased in average value significantly in this pattern, it reached deeper office parts. The graphs recorded for pattern B presented close radiation values as the graphs provided for pattern A.

5.3.4 Type C Facade Building Model

a- Summer (Incident) radiation graphs:

In this simulation results, like patterns A and B, this façade pattern allows the radiation to reach deeper spaces in the office building but scored lower average radiation values than the base case model. In pattern C simulation, the first level has lower radiation levels than the original building. The southern part has the highest radiation level reached 3.74 kWh/m2 (figure 67). The western and eastern side values were reduced to 2.24 kWh/m2. The northern side radiation reached 1.12 kWh/m2. The second level shows a slight decrease in the radiation values compared to the original building. The southern areas recorded a radiation level at almost 3.19 kWh/m2. Radiation reached almost 1.91 kWh/m2 on eastern parts, and less than 2.23 kWh/m2 on the western wing (Figure 68). Compared to the base model, the third level recorded a decrease in radiation, especially in the south. The radiation on the southern side was decreased down to less than 3.20 kWh/m2. However, the northern and eastern parts received more radiation than the base case model. (Figure 69).

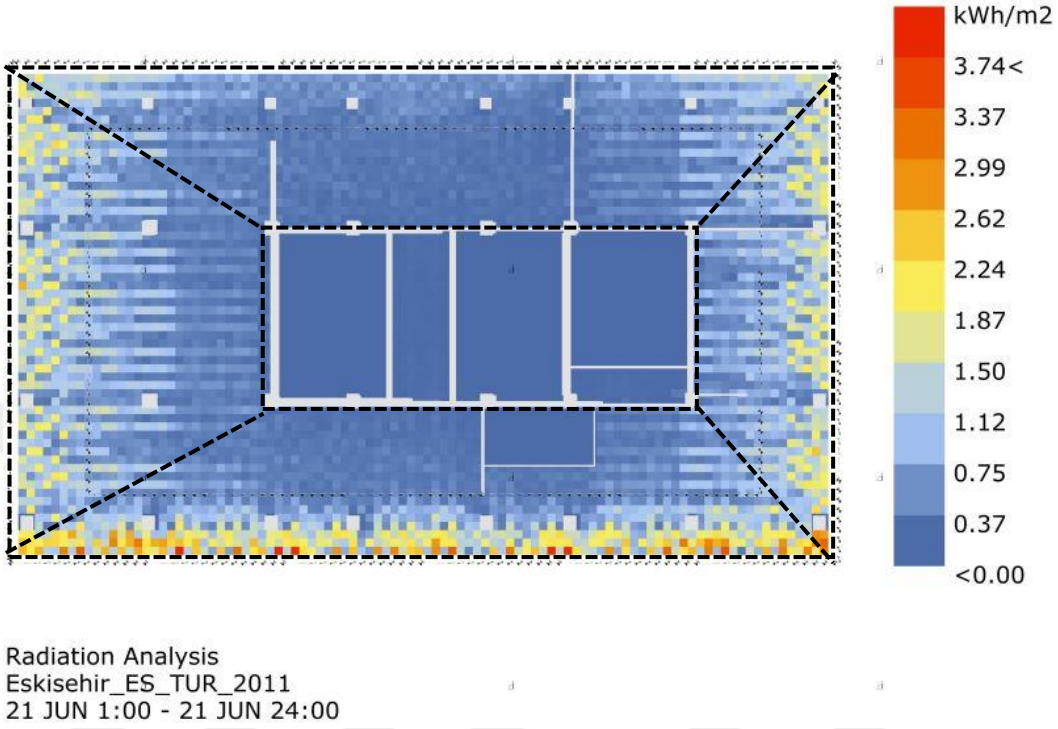

Figure 68: Type C Facade, Summer Radiation graphs (21st of June), Level 1.

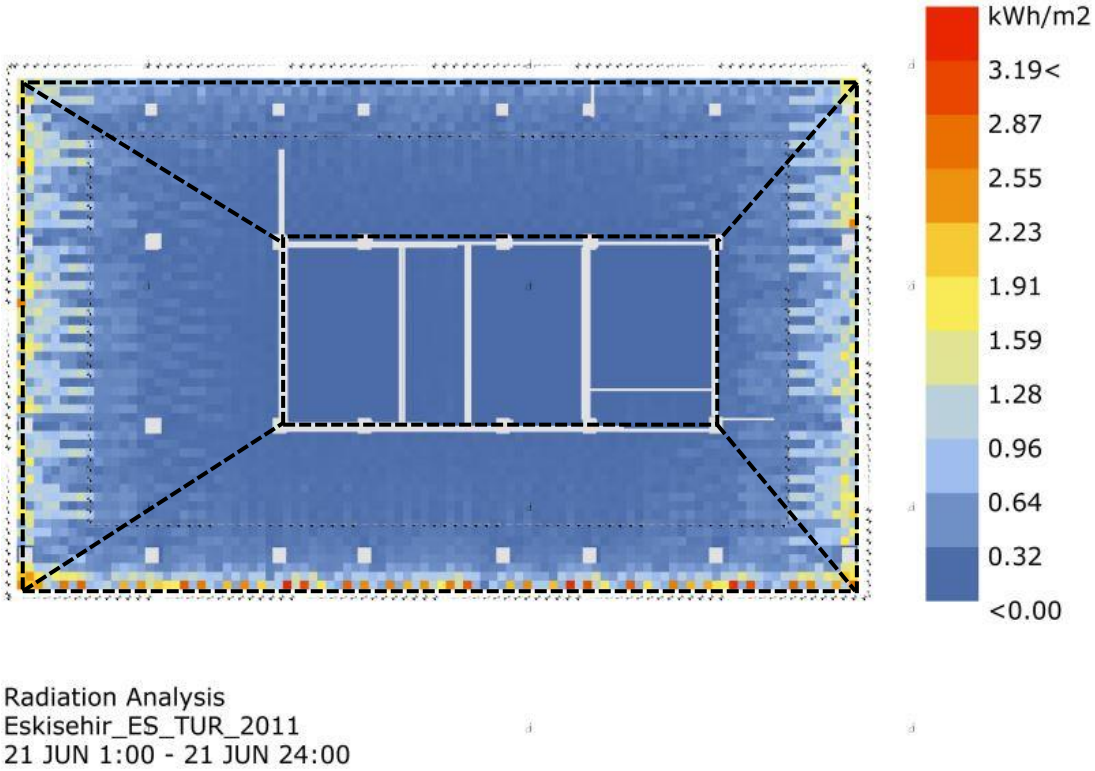

Figure 69: Type C Facade, Summer Radiation graphs (21st of June), Level 2.

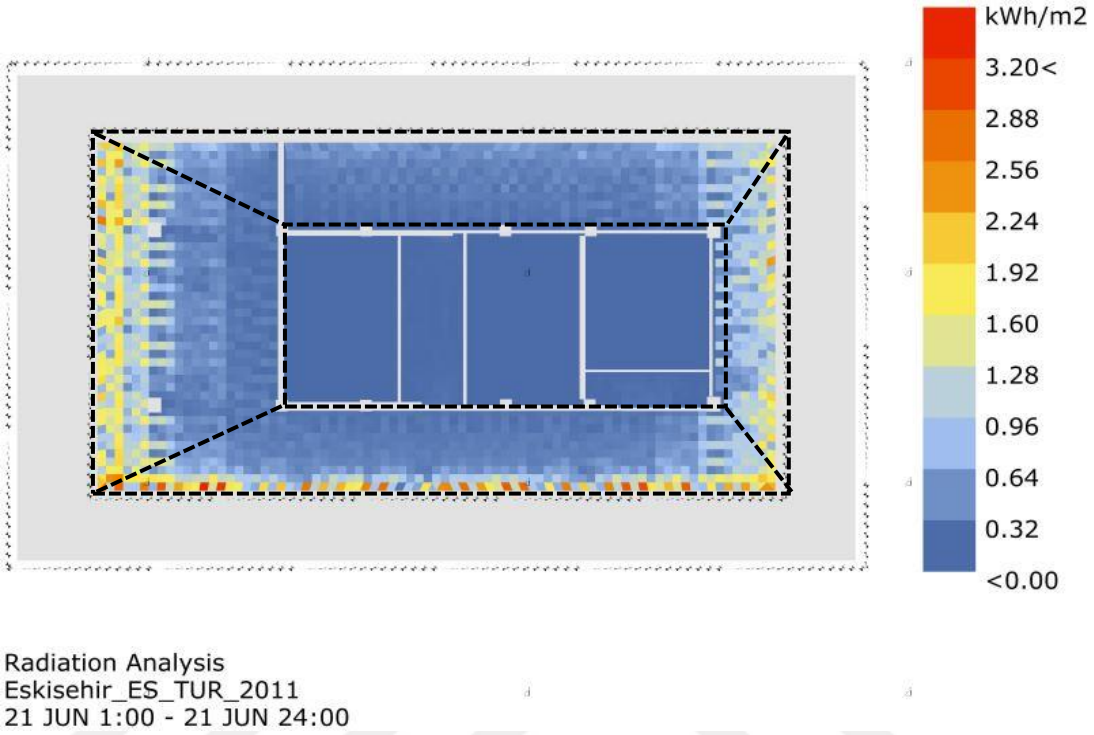

Figure 70: Type C Facade, Summer Radiation graphs (21st of June), Level 3.

Pattern C has the same numbers of panels, panel gap, and dimensions as pattern A but a different panel rotation degree. On the other hand, compared to Pattern B, Pattern C has a different number of panels, panel dimension, panel rotation angle, and gap. Compared to the other two tested iterations, the first level for pattern C scored lower radiation levels than Pattern A and higher radiation levels compared to Pattern B. However, Pattern C scored higher radiation on the second and third levels than Patterns A and B. This result is because pattern C consists of wider panels with wider gaps that provide a higher ratio of the void than solid.

b- Winter (Incident) radiation graphs:

In comparison with the original base model winter graphs, Pattern C decreased the radiation levels notably (figure 70). Radiation levels on the first level do not exceed 0.90 kWh/m2 in the southern area. The western façade records incident value up to 0.63 kWh/m2. The eastern facade receives radiation of 0.72 kWh/m2 (Figure 70).

The second level receives lower radiation than the base model. The southern part records 0.89 kWh/m2. The radiation reaches shallower parts than the first level. Radiation reaches 0.59 kWh/m2 on the east and up to 0.49 kWh/m2 on the west (Figure 71).

The third level's highest radiation is received from the south of 0.97 kWh/m2. The eastern side scored 0.87 kWh/m2, and the western side scored 0.68 kWh/m2. (Figure 72).

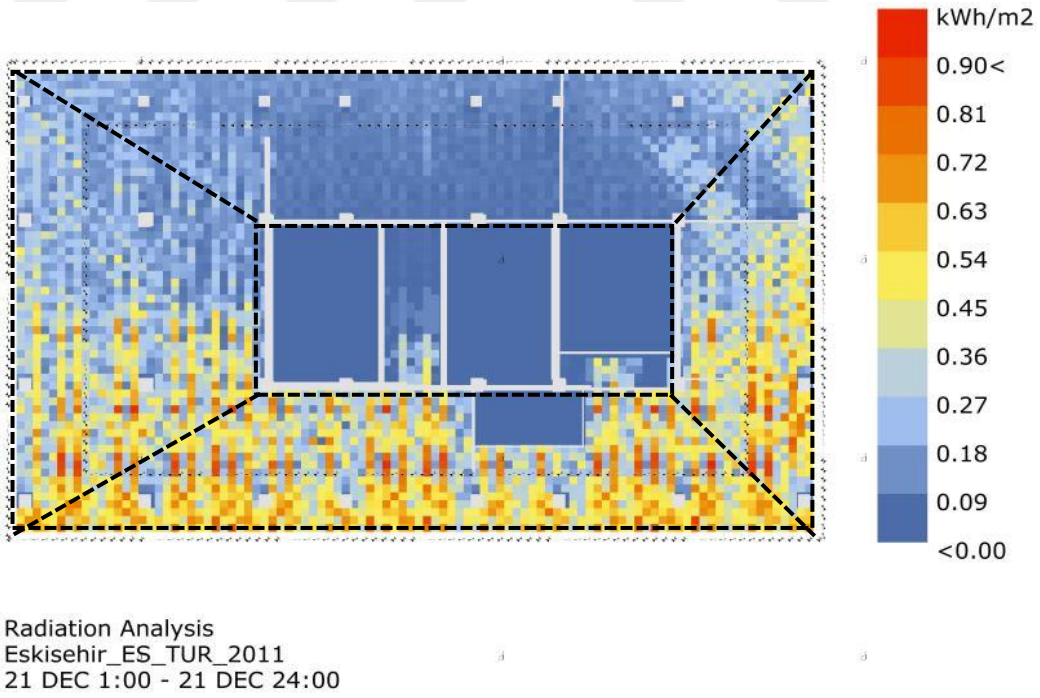

Figure 71: Type C Facade, Winter Radiation graphs (21st of December), Level 1.

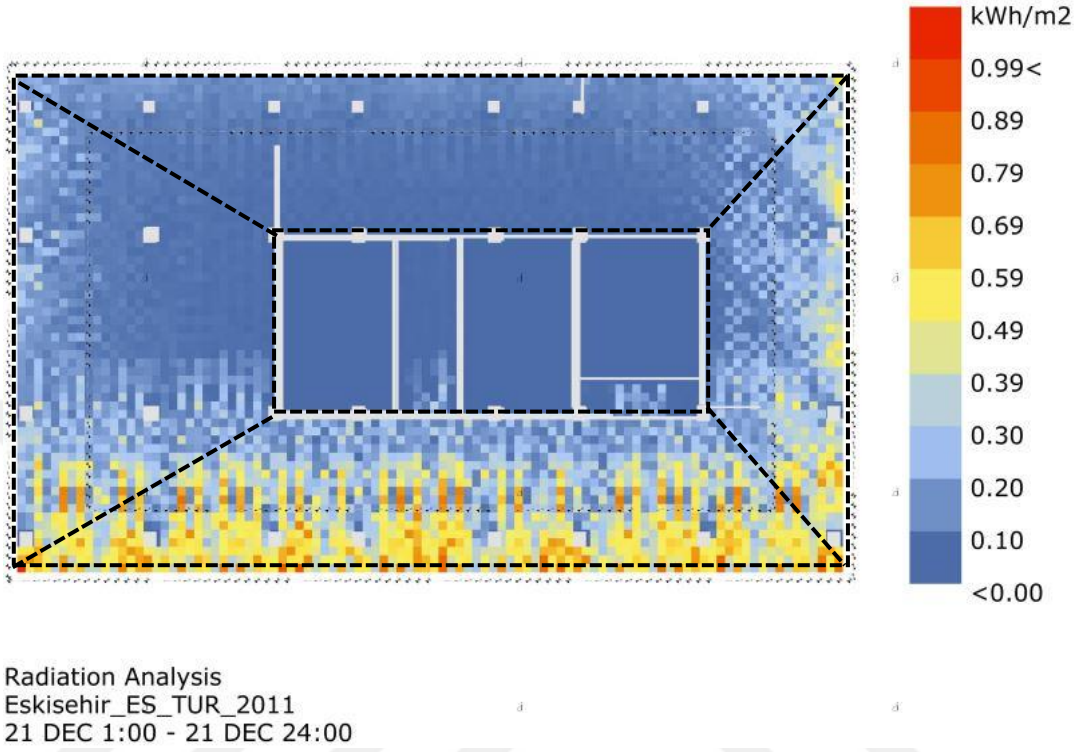

Figure 72: Type C Facade, Winter Radiation graphs (21st of December), Level 2.

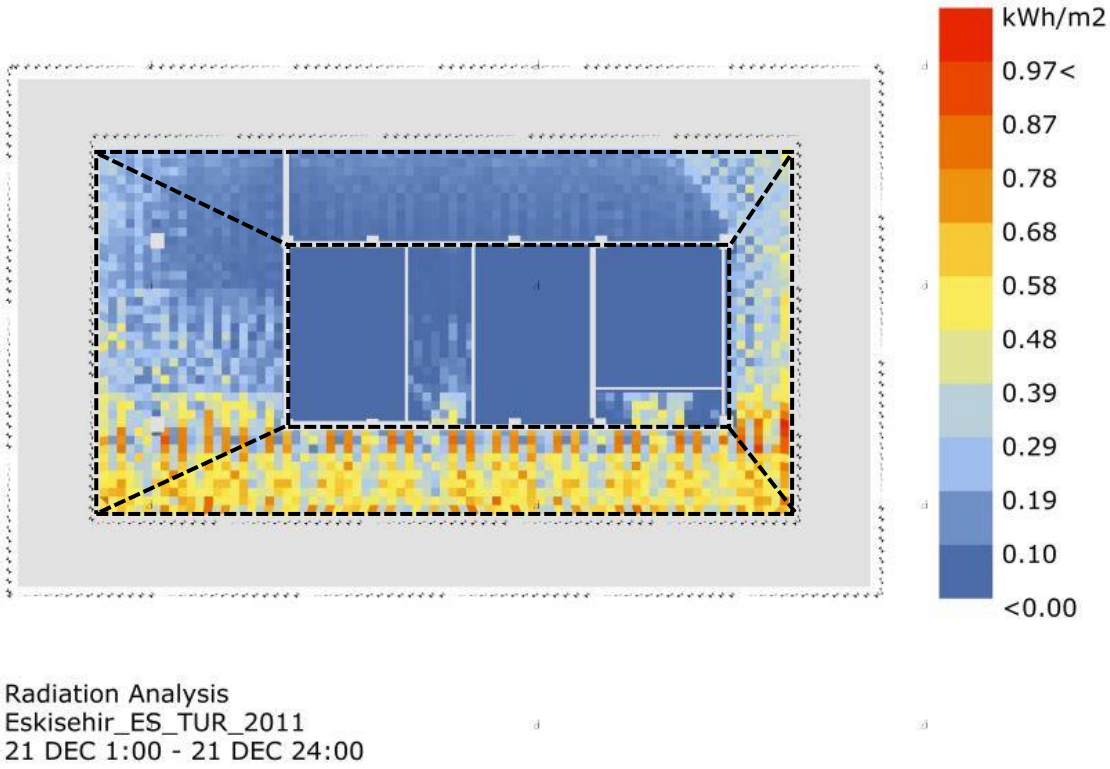

Figure 73: Type C Facade, Winter Radiation graphs (21st of December), Level 3.

Façade C is similar to façade A and B because it provides more radiation distribution on the interior spaces of the building compared to the base model. Although the radiation reached deeper parts of the office, it was still lower than the base model. This façade pattern recorded lower radiation than patterns A and B on the first level. However, the radiation on the second was close to Pattern B results. The third level of this pattern provided higher than patterns A and B.

5.3.5 Type D Facade Building Model

a- Summer (Incident) radiation graphs:

In this simulation results, like patterns A, B, and C, this façade pattern allows the radiation to reach deeper spaces in the office building but still scored lower radiation values than the base case model. The first level graph results have lower radiation levels than the original building, especially in the southern area where it reached 4.32 kWh/m (figure 73). The western and eastern side values were reduced to 2.59 kWh/m2. On the second level, southern areas recorded radiation levels of 3.23 kWh/m2. The eastern and western parts recorded 2.59 kWh/m2 on the eastern parts, and the western wing recorded 2.91 kWh/m2 (Figure 74). The third level recorded the most significant reduction in average radiation value between all three levels. The radiation levels on the southern side were decreased to 3.08 kWh/m2. On the other hand, the northern and eastern facades received more radiation than the base case model. (Figure 75).

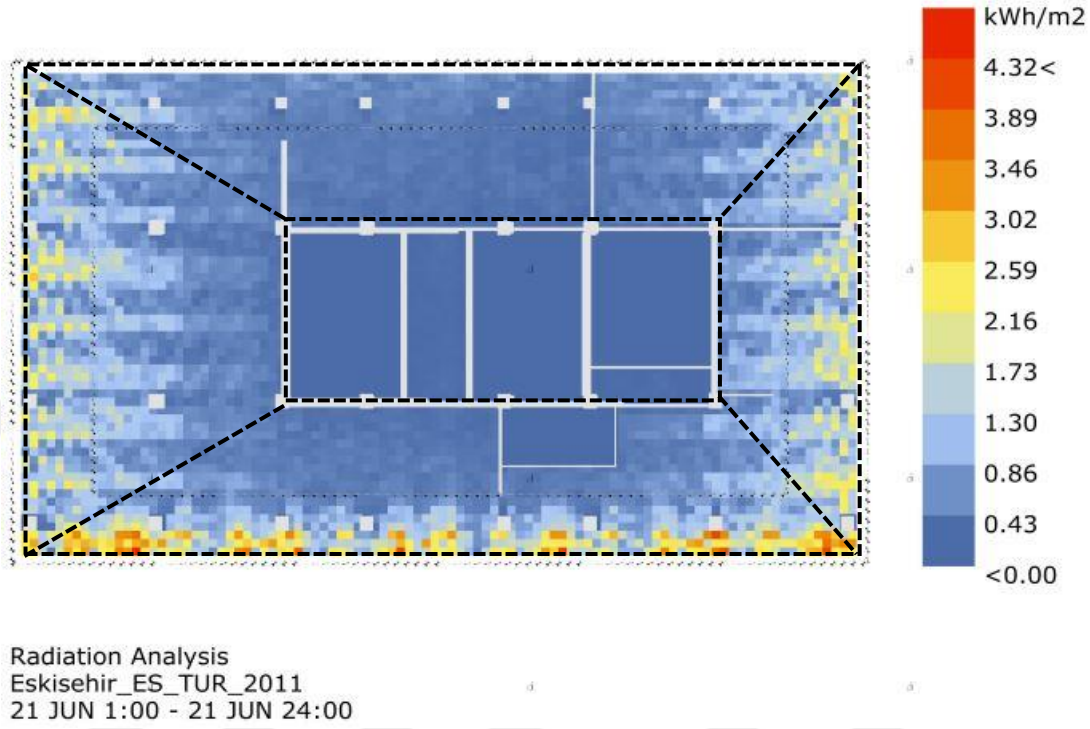

Figure 74: Type D Facade, Summer Radiation graphs (21st of June), Level 1.

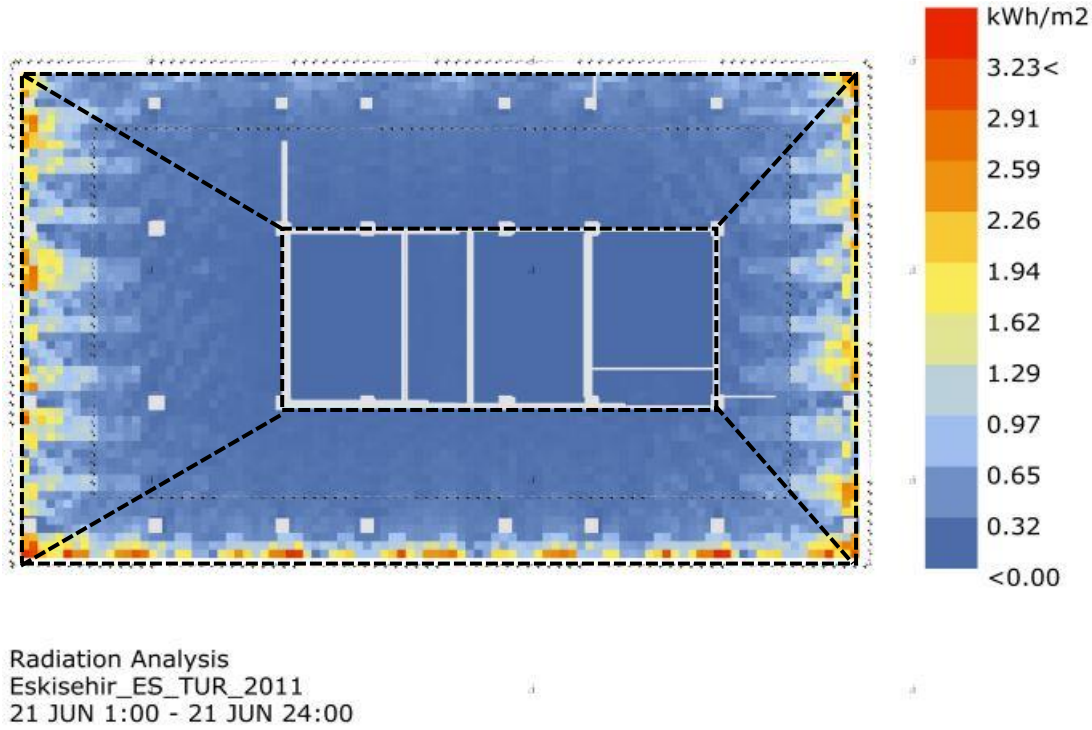

Figure 75: Type D Facade, Summer Radiation graphs (21st of June), Level 2.

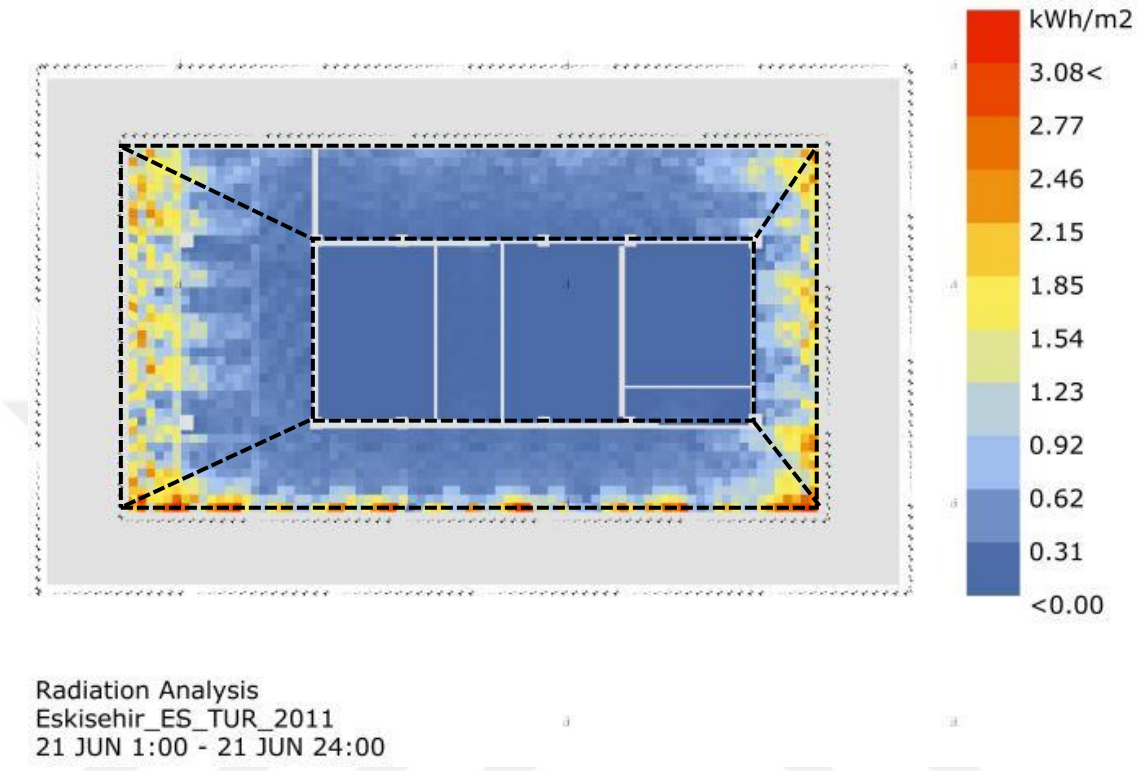

Figure 76: Type D Facade, Summer Radiation graphs (21st of June), Level 3.

Pattern D has the same numbers of panels, gaps, and dimensions as pattern B but a different panel rotation degree. On the other hand, Pattern C has a different number of panels, panel dimensions, and gap compared to Pattern A and C. Compared to the previous three tested iterations, the first level for pattern D scored a comparable radiation level as Pattern A and higher radiation levels compared to Pattern B and C. Pattern D also scored higher radiation on the second level than pattern A, B, and C. On the third level, pattern D scored lower radiation than pattern C, but higher than A and B on the same level. It is because pattern D consists of wider panels with wider gaps and a bigger rotation degree that provides a higher ratio of the void than solid.

a- Winter (Incident) radiation graphs:

In comparison with the original base model winter graphs, Pattern D decreased the radiation levels slightly. Radiation levels on the first level do not exceed 1.03 kWh/m2 on the southern area (Figure 76). The western façade records incident value up to 0.62 kWh/m2. The second level receives higher radiation than the base model. The southern part records a radiation value of around 1.19 kWh/m2. The radiation reaches shallower parts than the first level. The eastern side receives higher value than the western area. Radiation reaches 0.59 kWh/m2 on the east and up to 0.47 kWh/m2 on the west (Figure 77). The third level of this simulation allows the radiation to reach deeper parts than the base case model with a lower radiation average. The highest radiation levels are received from the south, almost reaching 1.02 kWh/m2. The eastern side records nearly 0.61 kWh/m2, and the western side records around 0.41 kWh/m2 (Figure 78).

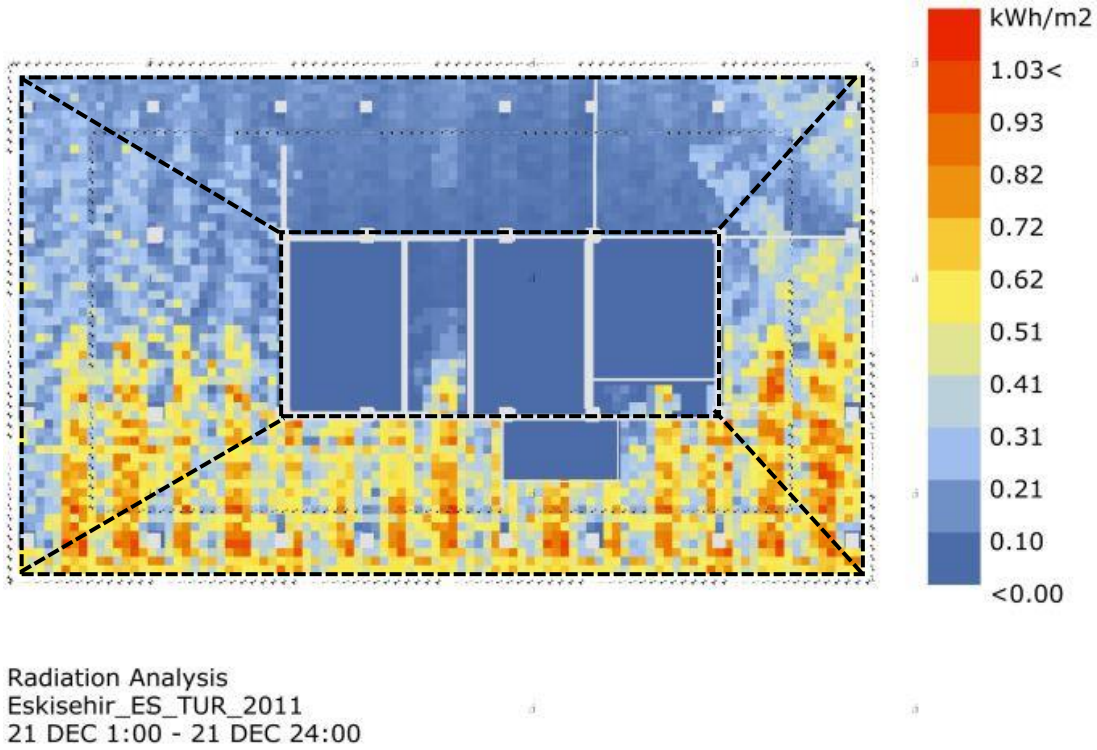

Figure 77: Type D Facade, Winter Radiation graphs (21st of December), Level 1.

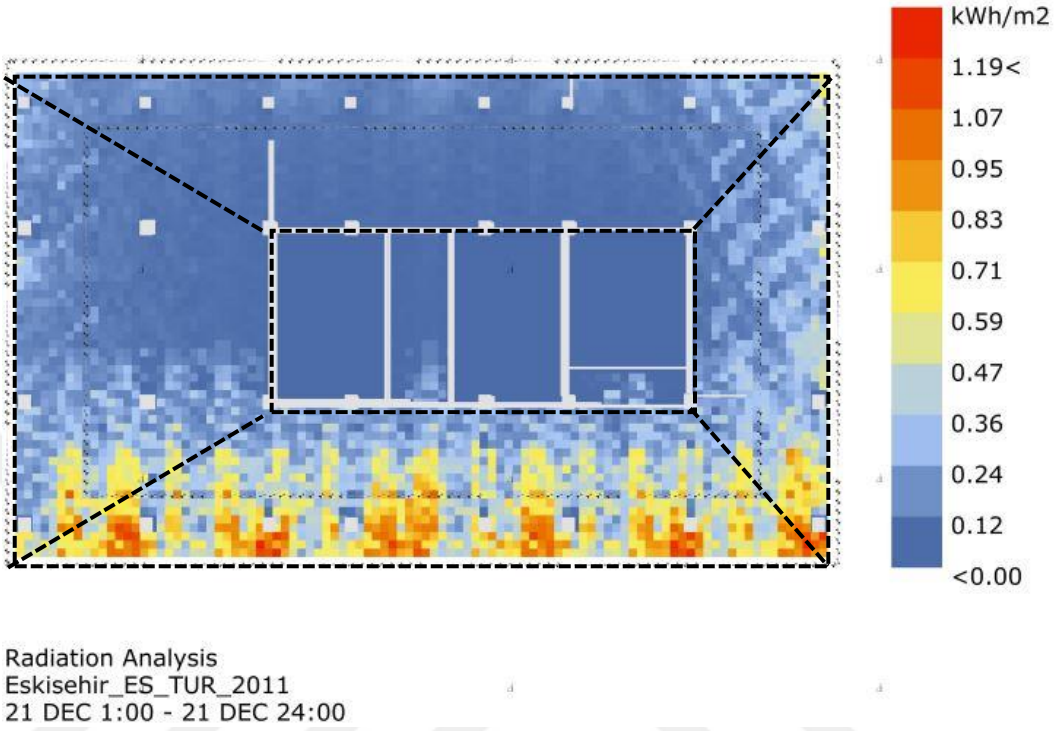

Figure 78: Type D Facade, Winter Radiation graphs (21st of December), Level 2.

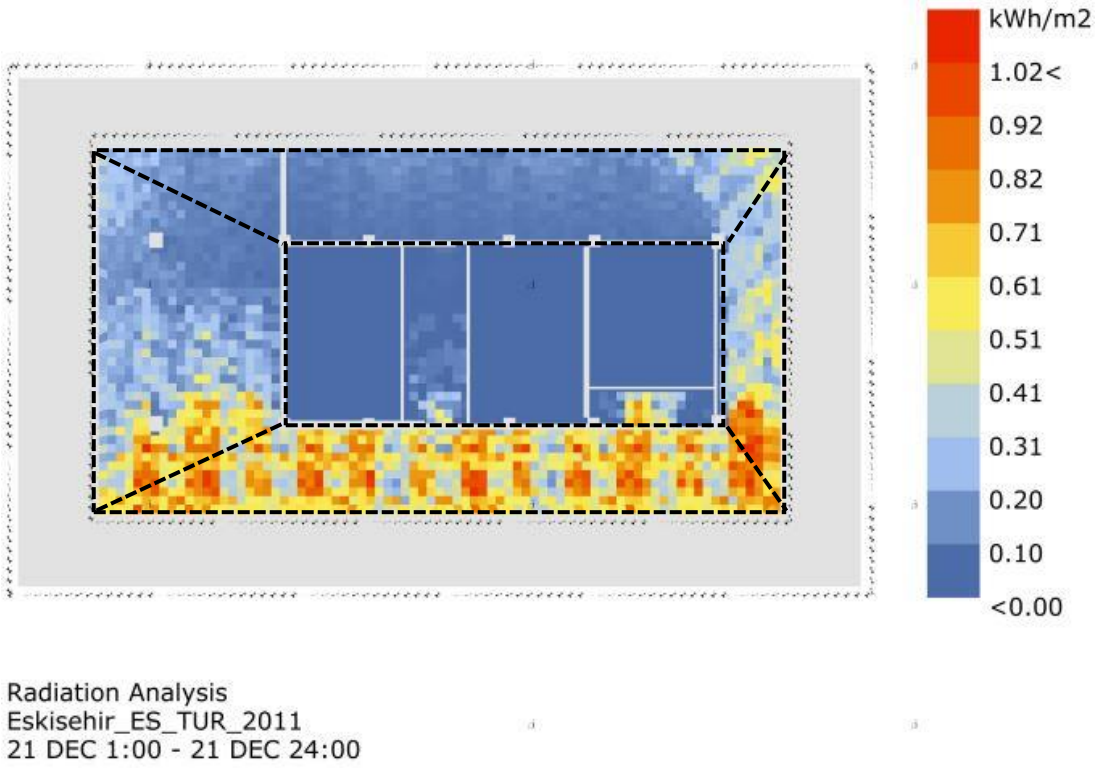

Figure 79: Type D Facade, Winter Radiation graphs (21st of December), Level 3.

Façade D is similar to façade A, B, and C because it provided more radiation distribution on the interior spaces of the building compared to the base model. Although the radiation reached deeper parts of the office, it was higher than the base model on only the second level. This façade pattern recorded higher radiation values than patterns A, B, and C on all levels of the building.

5.3.6 Overall Radiation Results:

According to the numerical data retrieved from the incident simulation (Table 12), the highest average annual radiation value for the building skin facades is located on the Southern elevation. It reaches 365.69 kWh/m2. The least exposed façade to radiation is the Northern elevation, and it receives 122.88 kWh/m2 annually. The highest radiation value received on the surface mesh of the Southern façade is 881.47 kWh/m2. The highest radiation value recorded on the Northern Façade mesh is 296.12 kWh/m2.

Table 12: Base Case Study Facades Annual Radiation values.

Annual Radiation values	North	East	West	South	Roof
Average Annual Radiation (kWh/m2)	122.88	166.85	157.63	365.69	1306.91
Highest Radiation Value (kWh/m2)	296.12	694.88	653.23	881.47	1475.04

According to the summer radiation simulation numerical values in Table 13 below, all four façade pattern proposals have reduced the highest radiation values of the original

base case model received during the peak solar radiation hour. However, the total average radiation has increased on the first and third floors. It can be related to the fact that the four façade iterations have allowed the distribution of more radiation towards the deeper parts of the office. Therefore the average value has increased, but the highest value recorded is lower than the original base model.

The highest radiation value recorded of 0.2 sqm for the first level of the original case study model during summer is 4.6927 kWh/m2. The total average radiation of the base case study model is 0.3173 kWh/m2. Between all four patterns, Pattern D scored the highest radiation value of 4.32 kWh/m2, which is 7.94% less than the highest radiation value of the base model. Pattern D also recorded average radiation of 0.5113 kWh/m2, which is 61.14% higher than the total average value for the base model.

The lowest value of maximum radiation on the first level, during peak hour, reached 3.0779 kWh/m2 by pattern B. This pattern also provides the highest radiation value reduction up to 34.41% less than the highest radiation value of the base model. Pattern B provides the lowest average radiation between all patterns, around 0.4280 kWh/m2, 34.88% higher than the original base case study radiation value.

Pattern A recorded the highest total average radiation value amongst all four iterations on the first level, and it reached 0.7224 kWh/m2. The total radiation recorded is almost 127.67 % higher than the base case building. The pattern’s highest radiation value reached 4.3091 kWh/m2, 8.17% less than the base case study's highest radiation value on the first level.

Pattern C's recorded highest radiation value on the first level reached 3.7408 kWh/m2, almost 20.28 % less than the base case radiation value on that level. The pattern's total average radiation reached 0.4446 kWh/m2, 40.11 % higher than the highest value of the base case study on the first level.

Unlike the first and third level radiation results, the second level recorded a reduction in both the highest radiation value and total average radiation. The highest radiation value recorded for the base case model on the second level reached 3.5249 kWh/m2. The total average radiation for the second level of the base case was 0.2914 kWh/m2.

Pattern D recorded the highest radiation value on the second level amongst all four façade iterations. It reached 3.2341 kWh/m2, which is 8.24% less than the highest radiation value recorded on the second level of the base case model. At the same time, pattern D recorded the highest total average radiation on the second level. It reached 0.2728 kWh/m2, 6.38% lower than the base case model. Pattern D records the lowest reduction amongst all four patterns on the second level.

Pattern A scored the lowest among all four patterns' highest radiation value. The highest radiation reached 2.4711 kWh/m2, almost 29.89 % lower than the base case's highest radiation value. Pattern A provides the highest reduction amongst all four patterns on the second level.

On the second level, pattern B recorded the highest radiation value that reached 2.8063 kWh/m2, which is 20.38% less than the base case model. The pattern's average

radiation reached 0.2253 kWh/m2, almost 22.68% less than the total average radiation of the base case model on the second level.

Like the first level, the third level recorded an overall reduction in the highest radiation value after applying all four iterations on the model. However, it was noticed that there was an increase in the total average radiation percentage. The highest radiation value scored on the third level of the base case model reached 5.0741 kWh/m2. The overall average radiation on the third level reached 0.2761 kWh/m2.

Pattern C scored the highest radiation value of all four iterations on the third level of almost 3.1963 kWh/m2, which is 37% less than the highest radiation value of the base case model. The pattern provided average radiation of almost 3.299 kWh/m2, which is around 19.48% higher than the average radiation of the base case model on the third level.

Pattern A recorded the lowest peak radiation value amongst all four iterations. It reached 2.8013 kWh/m2, which is 44.79% lower than the highest radiation value of the base case model on the third level. The pattern also recorded the lowest average radiation of all four patterns, almost 0.3156 kWh/m2, 14.30% less than the average radiation of the base case model on the third level.

The highest radiation value recorded by pattern B on the third level reached 2.9693 kWh/m2, which is 41.58% less than the highest radiation value of the base case model on that level. On the other hand, pattern B scored an average radiation value of 0.3214 kWh/m2, which is 16.40% higher than the base case model average radiation on the third level.

Pattern D recorded the highest average radiation between all four iterations on the third level. It reached 0.3781 kWh/m2, almost 36.94 % higher than the base case model average radiation value. The pattern scored 3.0780 kWh/m2 as the highest radiation value, which is calculated as 39.33 less than the highest radiation value of the base case model on the third level.

The different façade designs provided different average radiation values. The first level recorded the highest increase in average radiation value between all levels. The second level recorded a reduction in both total average radiation and the highest radiation value. The third floor recorded the highest reduction in total radiation value and the lowest increase in the average radiation value in all four façade iterations between all levels.

Table 13: Summer Simulation Radiation values.

		Base Case Study	Pattern A	Pattern B	Pattern C	Pattern D
Level 1	**Highest radiation value (kWh/m2)**	4.6927	4.3091	3.0779	3.7408	4.3200
	Total Highest Radiation difference %	-	- 8.17	- 34.41	- 20.28	- 7.94
	Average Radiation (kWh/m2)	0.3173	0.7224	0.4280	0.4446	0.5113
	Total Average Radiation difference %	-	+127.67	+34.88	+40.11	+61.14

Level 2	**Highest radiation value (kWh/m2)**	3.5249	2.4711	2.8063	3.1895	3.2341
	Total Highest Radiation Difference %	-	-29.89	-20.38	-9.51	-8.24
	Average Radiation (kWh/m2)	0.2914	0.2183	0.2253	0.2317	0.2728
	Total Average Radiation difference %	-	- 25.08	-22.68	- 20.48	- 6.38
Level 3	**Highest radiation value (kWh/m2)**	5.0741	2.8013	2.9693	3.1963	3.0780
	Total Highest Radiation difference %	-	- 44.79	- 41.58	- 37.00	- 39.33
	Average Radiation (kWh/m2)	0.2761	0.3156	0.3214	0.3299	0.3781
	Total Average Radiation difference %	-	+14.30	+16.40	+19.48	+36.94

The average radiation values for the summer season were compared with each other in Figure 79. Compared to the original building results, all four simulations increased their average radiation values, especially on the first and third levels. The second level recorded an overall decrease in average radiation value in all four iterations of the façade. Pattern A scored the highest average radiation values on the first and lowest on the second and third

levels. Pattern B scored the lowest average radiation on the first level. Pattern D scored the highest average radiation on the second and third levels.

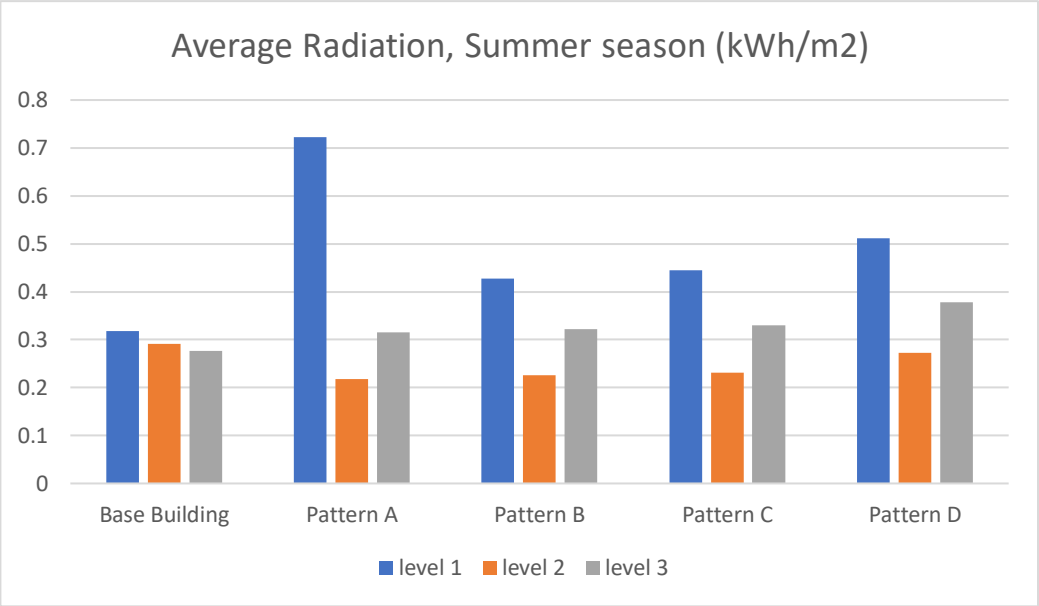

Figure 80: Average Radiation chart, summer season.

The highest radiation values for the summer season were compared in Figure 80. In comparison with the original building results, all four simulations recorded a decrease in their highest radiation values compared to the base case model. The highest radiation value of pattern B on the first level was the lowest amongst all the other four iterations. Pattern D scored the highest radiation value between all four facades on the first level. For the second level, the lowest value was recorded by façade A, and the highest value was provided by façade D. The highest radiation on the third level of façade A was recorded as the lowest between all the façade options on that level. The highest value was provided by façade C (figure 80).

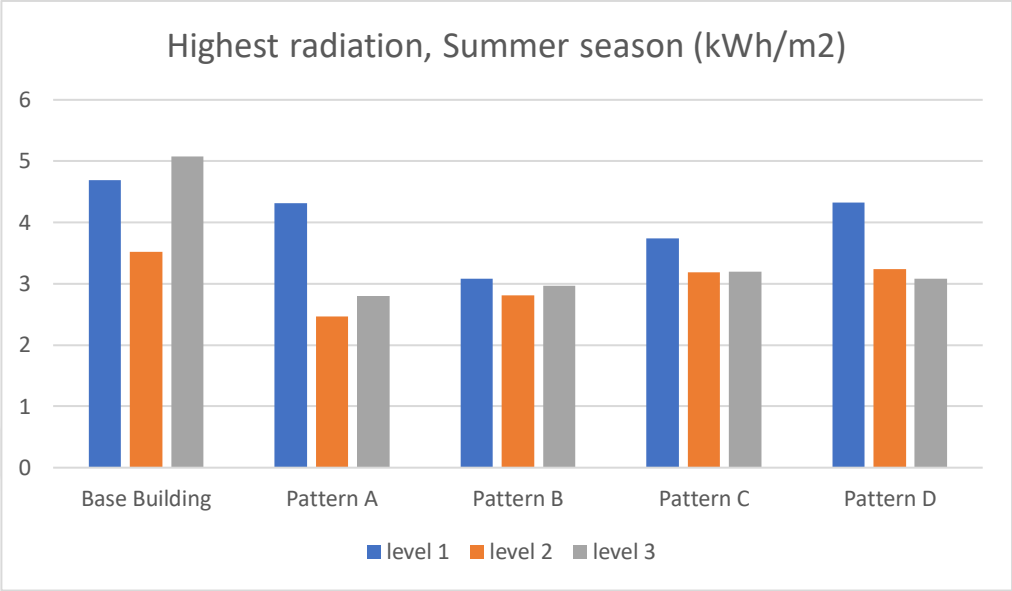

Figure 81: Average Radiation chart, summer season.

According to the winter radiation simulation numerical values in Table 14, all four façade patterns reduced the highest radiation values of the original base case model received during the building's peak solar radiation hour. However, the total average radiation has increased on the first and third floors. It can be related to the fact that the four façade iterations have allowed the distribution of more radiation into the deeper parts of the office. Therefore the average value increased, but the highest value recorded is lower than the original base model.

The highest radiation value recorded for the first level of the original case study model, during winter, is 1.1920 kWh/m2. The average radiation of the base case study model on the first level is 0.1638 kWh/m2.

On the first level, between all patterns, the highest radiation value scored by Pattern D reached 1.0286 kWh/m2, which is 13.70% less than the highest radiation value of the base

case model on the same level. This façade pattern also scored the highest average radiation of 0.2326 kWh/m2 and provided a total increase of 42% than the original model on that level.

Pattern C provided the lowest value of highest radiation during peak hour on the first level at almost 0.8982 kWh/m2, which is around 24.64 % less than the highest radiation value recorded for the base case model on the same level. The pattern's average radiation reached 0.1974 kWh/m2, which is 20.51% more than the total average radiation of the base case model on the first level.

Pattern A records the lowest average radiation on the first level, almost at 0.1888 kWh/m2, which is 15.26% more than the average radiation of the original base case model on the first level. The pattern's highest radiation value on the first level reached 0.9394 kWh/m2, which is 21.19 % less than the highest radiation value for the original base case model at that same level.

Unlike the first and third level radiation results, the second level recorded a reduction in both the highest radiation value and total average radiation except for pattern D. The highest radiation value recorded for the base case model on the second level reached 1.0781 kWh/m2. The total average radiation for the second level of the base case was 0.1552 kWh/m2.

Pattern D recorded the highest radiation value on the second level amongst all four façade iterations. It reached 1.1867 kWh/m2, which is 10.07% more than the highest radiation value recorded on the second level of the base case model. At the same time, pattern D recorded the highest total average radiation on the second level. It reached 0.1681 kWh/m2,

9.77% higher than the base case model. Pattern D records the lowest reduction amongst all four patterns on the second level.

Pattern A scored the lowest among all four patterns' highest radiation value. The highest radiation reached 0.8663 kWh/m2, almost 19.64 % lower than the base case's highest radiation value. Pattern A provides the highest reduction amongst all four patterns on the second level.

On the second level, pattern B recorded the highest radiation value that reached 0.9878 kWh/m2, 8.37 % less than the base case model. The pattern's average radiation reached 0.1419 kWh/m2, almost 10.07 % less than the total average radiation of the base case model on the second level.

Like the first level, the third level recorded an overall reduction in the highest radiation value after applying all four iterations on the model. However, it was noticed that there was an increase in the total average radiation percentage. The highest radiation value scored on the third level of the base case model reached 1.2631 kWh/m2. The overall average radiation on the third level reached 0.1176 kWh/m2.

Pattern D scored the highest radiation value of all four iterations on the third level of almost 1.0210 kWh/m2, 19.16 % less than the highest radiation value of the base case model. The pattern provided the highest average radiation of all four patterns, at almost 0.2041 kWh/m2, around 73.55 % higher than the average radiation of the base case model on the third level.

Pattern A recorded the lowest peak radiation value amongst all four iterations. It reached 0.9140 kWh/m2, 27.63 % lower than the highest radiation value of the base case model on the third level. The pattern also recorded the lowest average radiation of all four patterns, almost 0.1698 kWh/m2, 44.38 % more than the average radiation of the base case model on the third level.

The highest radiation value recorded by pattern C on the third level reached 0.9699 kWh/m2, which is 23.21 % less than the highest radiation value of the base case model on that level. Pattern B scored an average radiation value of 0.1741 kWh/m2, 48.04 % higher than the base case model average radiation on the third level.

The different façade designs provided different average radiation values. The third level recorded the highest increase in average radiation value between all levels. The second level recorded a reduction in both total average radiation and highest radiation value, except for pattern D. The third floor recorded the highest reduction in total highest radiation value and the lowest increase in the average radiation value in all four façade iterations between all levels.

Table 14: Winter Simulation Radiation Values (red is the highest, and green is the lowest for each row).

		Base Case Study	Pattern A	Pattern B	Pattern C	Pattern D
Level 1	**Highest radiation value (kWh/m2)**	1.1920	0.9394	0.9534	0.8982	1.0286
	Total Highest	-	-21.19	-20.01	-24.64	-13.70

	Radiation difference %					
	Average Radiation (kWh/m2)	0.1638	0.1888	0.1968	0.1974	0.2326
	Total Average Radiation difference %	-	+15.26	+20.14	+20.51	+42.00
Level 2	**Highest radiation value (kWh/m2)**	1.0781	0.8663	0.9878	0.9864	1.1867
	Total Highest Radiation difference %	-	-19.64	-8.37	-8.50	+10.07
	Average Radiation (kWh/m2)	0.1552	0.1320	0.1419	0.1403	0.1681
	Total Average Radiation difference %	-	-17.57	- 10.07	- 11.28	+ 9.77
Level 3	**Highest radiation value (kWh/m2)**	1.2631	0.9140	0.9154	0.9699	1.0210
	Total Highest Radiation difference %	-	-27.63	-27.52	-23.21	-19.16

	Average Radiation (kWh/m2)	0.1176	0.1698	0.1699	0.1741	0.2041
	Total Average Radiation difference %	-	+44.38	+44.47	+ 48.04	+73.55

The average radiation values for the winter season were compared with each other in Figure 81. Compared to the original building results, all four simulations increased their average radiation values, especially on the first and third levels. The second level recorded an overall decrease in average radiation value in all iterations of the façade, except for pattern D. Pattern D scored the highest average radiation on all three levels. Pattern A scored the lowest average radiation on the second and third levels.

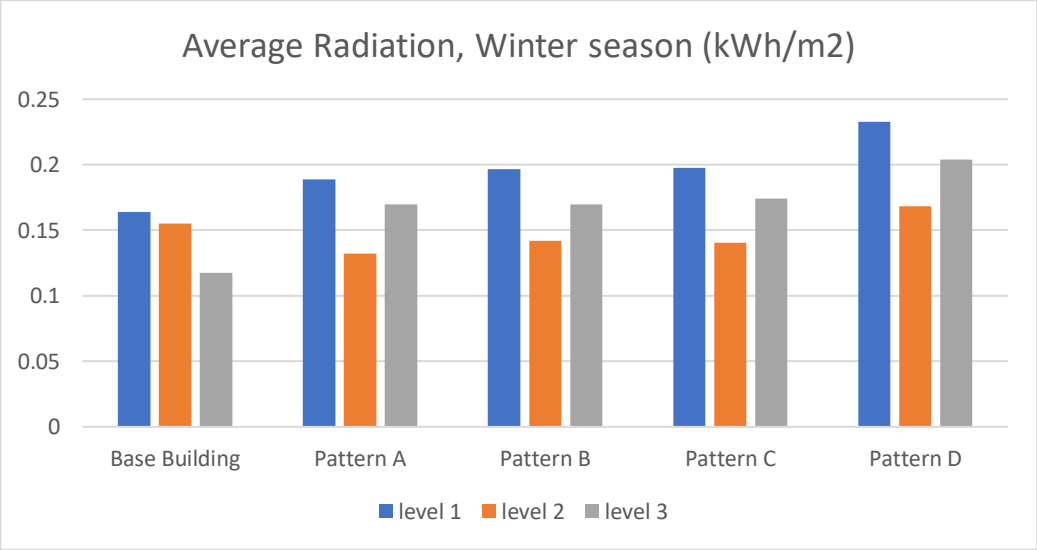

Figure 82: Average radiation chart, winter season.

The highest radiation values for the summer season were compared with each other in Figure 82. In comparison with the original building results, all four simulations recorded a decrease in their highest radiation values compared to the base case model, except for pattern D on the second level. For the first level, the lowest value was recorded by pattern C and the highest by pattern D. For the second level. The highest value was recorded by pattern D, and the lowest by pattern A. Pattern A also recorded the lowest value for the third level.

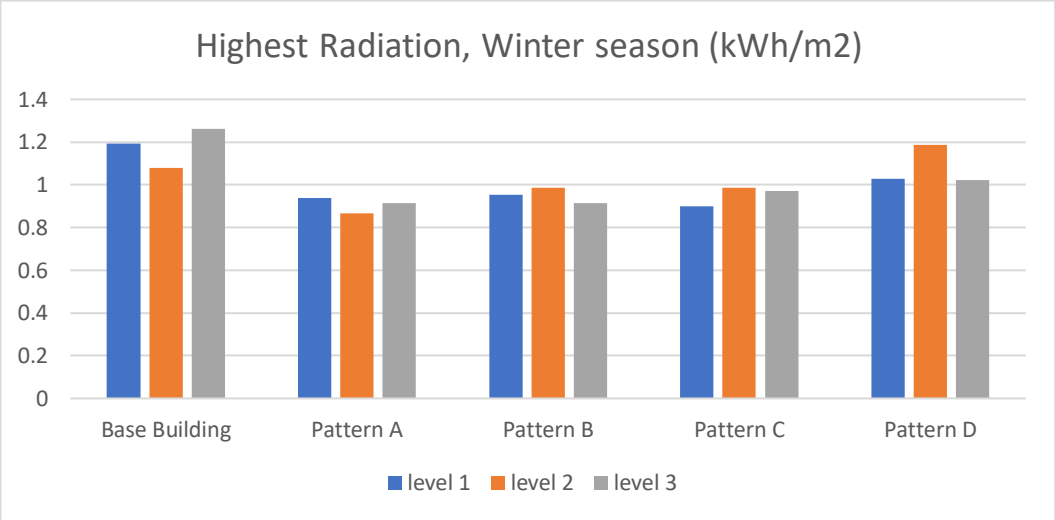

Figure 83: Highest radiation chart, winter season.

The average radiation reduction was calculated for each pattern to compare their effect on the building as a whole (on all three levels combined). Table 15 presents Pattern A, B, C, and D results.

Table 15: Average and highest radiation difference percentage in both season's summer and winter

Façade pattern type	Pattern A	Pattern B	Pattern C	Pattern D

Average summer radiation difference %	+38.96	+9.53	+ 39.11	+ 91.7
Highest radiation difference (summer) %	-27.61	-32.12	-22.26	-18.50
Average winter radiation difference %	+ 14.02	+ 18.18	+ 19.09	+41.77
Highest radiation difference (winter)%	-22.82	-18.63	-18.78	-7.59

According to the results in table 15, façade Pattern type D resulted in the highest average radiation increase rate in both seasons, winter and summer. Pattern D had the least reduction on the highest radiation value in both seasons between all four patterns. This façade type consists of 14 panels, each with a width of 400 mm, and gap of 200 mm, and a rotation of 8° for each panel. The rotation degree is the highest amongst all four iterations and permits more light to penetrate the façade into the interior spaces.

Façade Pattern type B resulted in the lowest average radiation increase rate in the summer. This façade type is similar to façade D in terms of the number of panels, width, and distance between each panel. However, this façade pattern had a lower rotation angle of 4°. The average radiation percentage increase rate was lower than Pattern D. Façade B also provided the highest decrease of peak radiation value during the summer compared to the other façade iterations.

Façade Pattern type A resulted in the lowest average radiation increase rate in winter. Between all four patterns, pattern A had the lowest increase on the average radiation value in winter and the highest decrease of the peak radiation value during winter. This façade type

consists of 7 panels, each with a width of 800 mm and a gap of 400 mm, and rotation of 4° for each panel. The rotation degree is the lowest amongst all four iterations. It restricts the light that penetrates the façade into the interior spaces.

The results confirm that the dimensions, orientation, and gaps between the panels have an evidential influence on the admitted radiation levels into the building. The use of wider panels provides a more concentrated area of solid panels. It controls the radiation levels admitted into the building. Moreover, the rotation angle plays a significant role too. The higher the rotation degree is, the more light is admitted into the building and the higher the radiation levels are. However, the relationship between radiation levels and the gaps between the panels is still unclear.

With the reduction of the radiation levels penetrating the façade into the interior, as provided in table 15, the lower the heat gain, the better the thermal quality inside the building would be. This reduction in heat gain will reduce the total energy consumption, especially in the southern and eastern parts of the building, where the radiation rates were very high and made thermal comfort hard to achieve before the application of the façade skin patterns.

5.4 Daylight Simulation

Each floor plan had been divided into four wings with a (dashed line) to study the effect each pattern has on each interior part of the building. The cyan/red colored outlines indicate areas that receive daylight lower than 500

5.4.1 Case Study Building Base Model

Windows in this model do not have any sun shading elements applied. The site does not include any surrounding buildings. Therefore, there is no extra external shading from neighboring buildings.

a- Summer Daylight graphs:

a.1 Summer Daylight at 10 am

The first level receives the highest daylight on the north-eastern and south-eastern sides. The eastern part receives up to 5000 lux(figure 83). The average lux on level one is 2150 lux, and the median value is 991 lux.

The second level receives a higher daylight than the first level. The highest amount of daylight is located on the east, reaching up to 5000 lux. The southern part receives 3000 lux (figure 84). The average lux on level two is 2354 lux, and the median value is 1110 lux.

On the third level, the highest daylight on the eastsouth reaches up to 8000 lux. The middle area's daylight reaches 700 lux. On the northern and northeast areas, the floor plan records lower than 500 lux, the needed amount for an office area (figure 85). The average lux on level three is 1695 lux, and the median value is 93 lux.

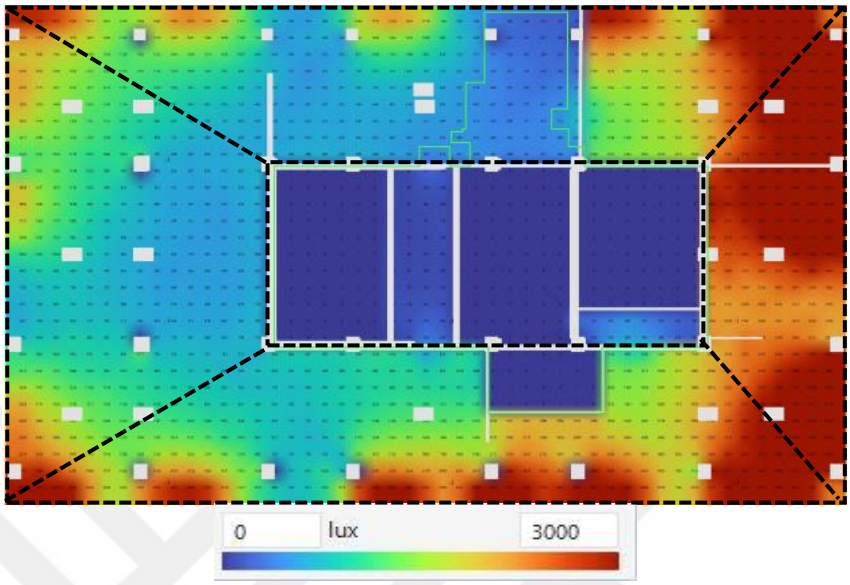

Figure 84: Base case, 21st June, 10 am, level 1.

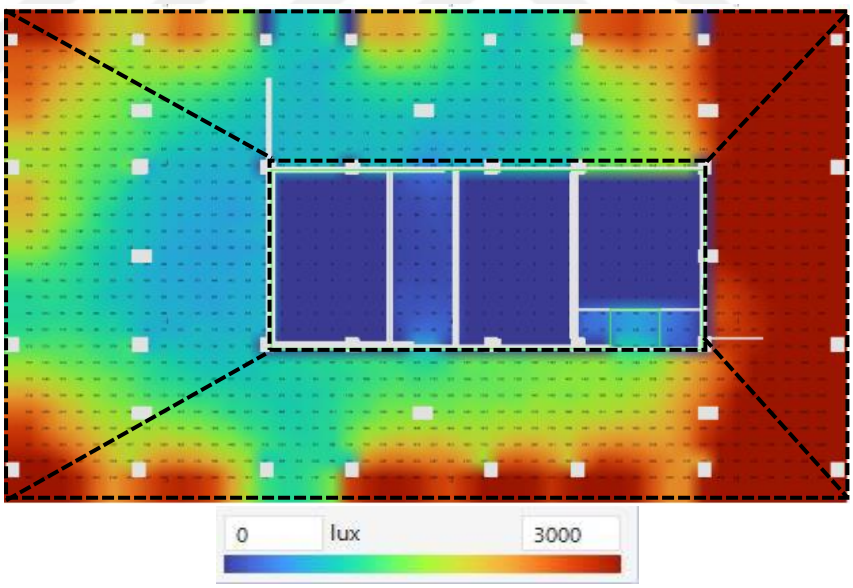

Figure 85: Base case, 21st June, 10 am, level 2.

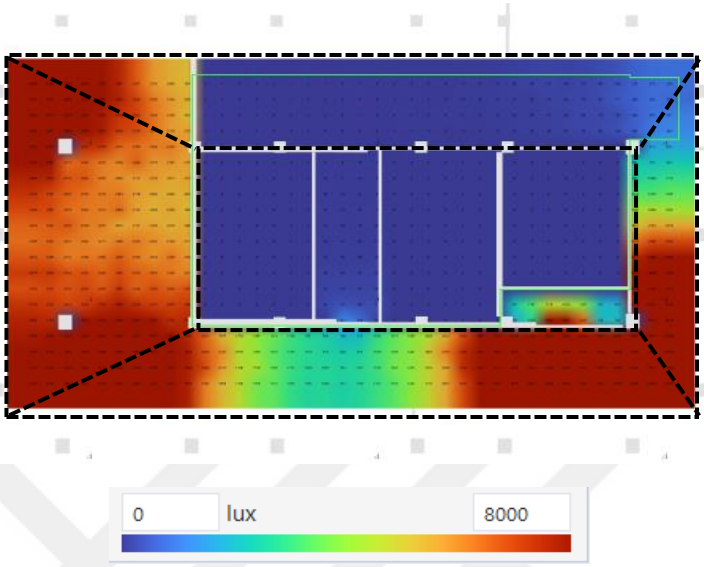

Figure 86: Base case, 21st June, 10 am, level 3.

a.2 Summer Daylight at 12 pm

The first level of the base case building receives the highest amount of daylight on the southern side. On the deeper parts of the floor plan, the daylight reaches 800 lux. The inner areas receive between 800 to 700 lux (figure 86). The average lux on level one is 1262 lux, and the median value is 1191 lux.

The second level receives a higher daylight amount than the first level. The highest amount of daylight on the eastern reaches 4000 lux. The southern part receives up to 4500 lux. In the middle and northern parts, the daylight reaches between 700 to 900 lux. (Figure 87). The average lux on level two is 1473 lux, and the median value is 1354 lux.

The highest daylight on the third level on the eastsouth reaches 8000 lux. The western side of the building receives up to 6000 lux (figure 88). The average daylight on level three is 1960 lux, and the median value is 85 lux.

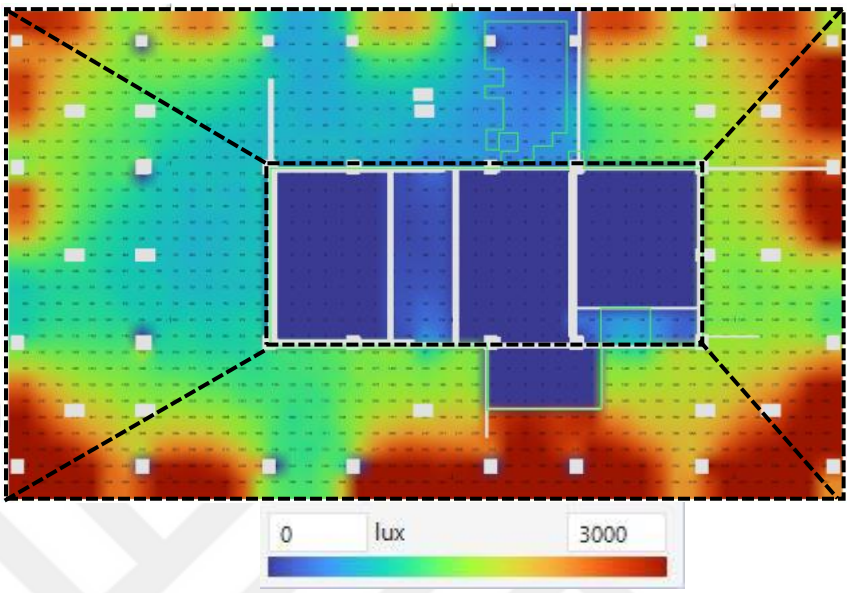

Figure 87: Base case, 21st June, 12 pm, level 1.

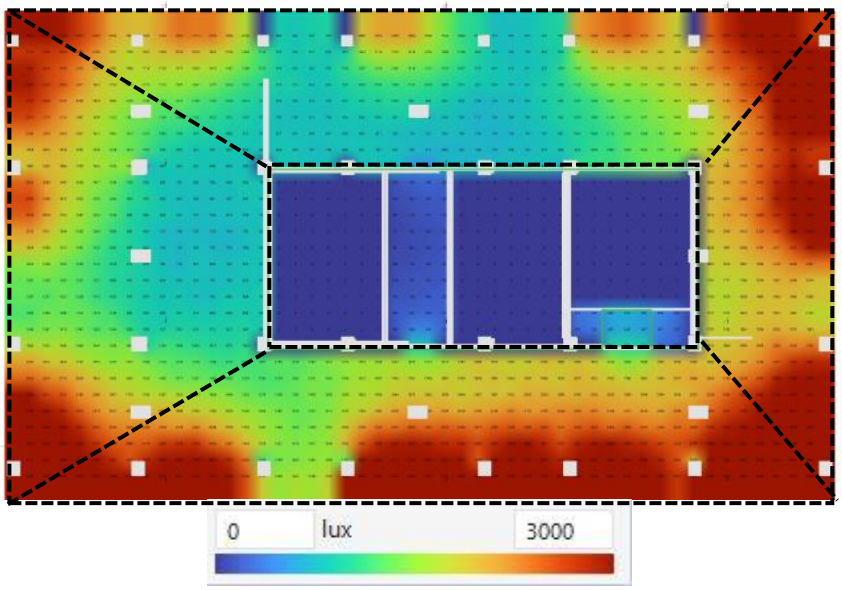

Figure 88: Base case, 21st June, 12 pm, level 2.

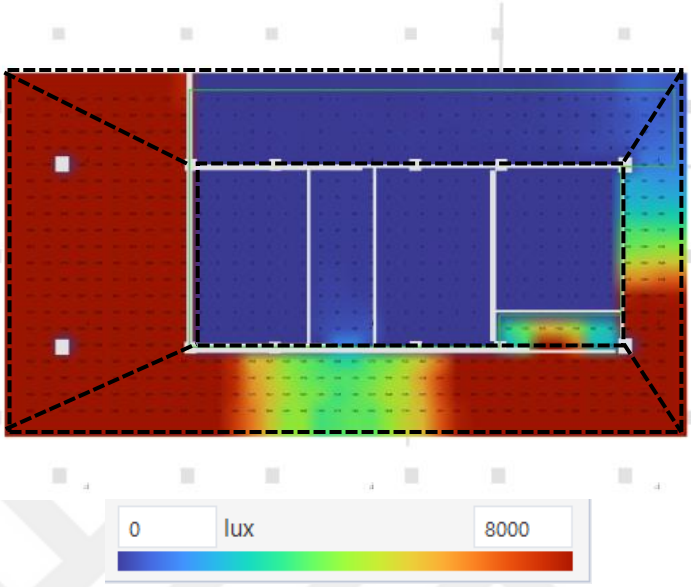

Figure 89: Base case, 21st June, 12 pm, level 3

a.3 Summer Daylight at 2 pm

The first level receives the highest daylight on the southern and western sides. The southern part receives up to 5000 lux. The daylight reaches lower than 500 lux on the northern side, outlined in cyan line (figure 89). The average lux on level one is 1254 lux, and the median value is 1175 lux.

The second level receives higher daylight than the first level. The highest amount of daylight on the south reaches up to 5000 lux (figure 90). The average lux on level two is 1496 lux, and the median value is 1425 lux.

On the western side, the highest daylight on the third level reaches up to 9000 lux. The southeast side of the building receives up to 6000. The northern and northeast areas record the lowest daylight values, lower than 500 lux (figure 91). The average daylight on level three is 2295 lux, and the median is 75 lux.

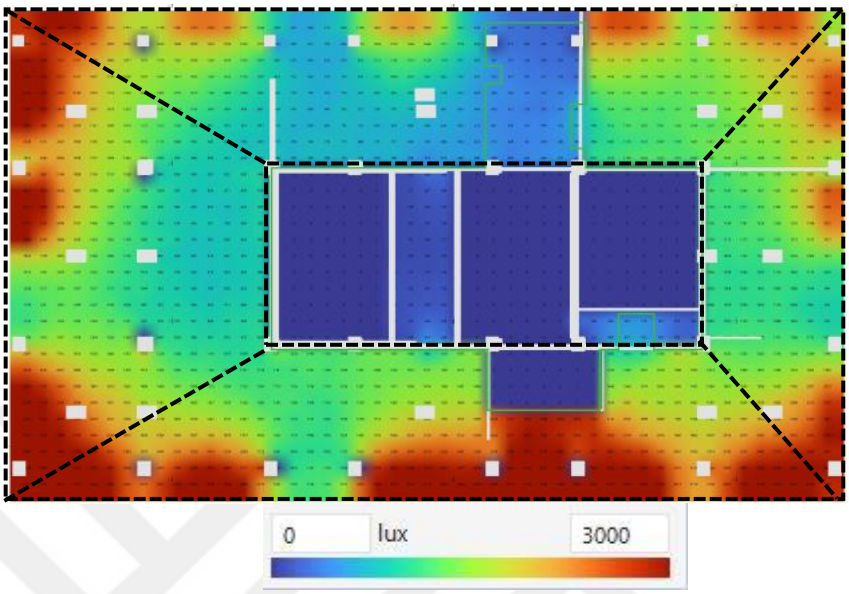

Figure 90: Base case, 21st June, 2 pm, level 1.

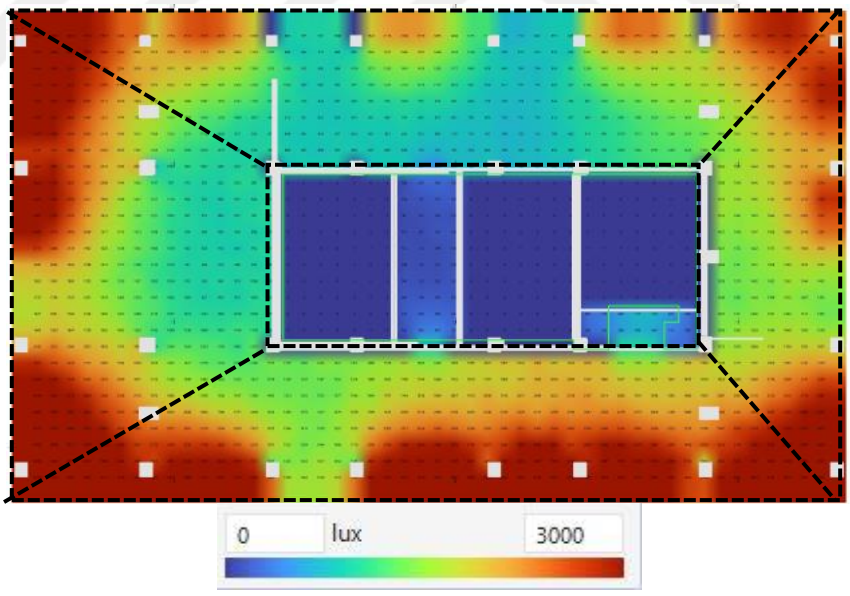

Figure 91: Base case, 21st June, 2 pm, level 2.

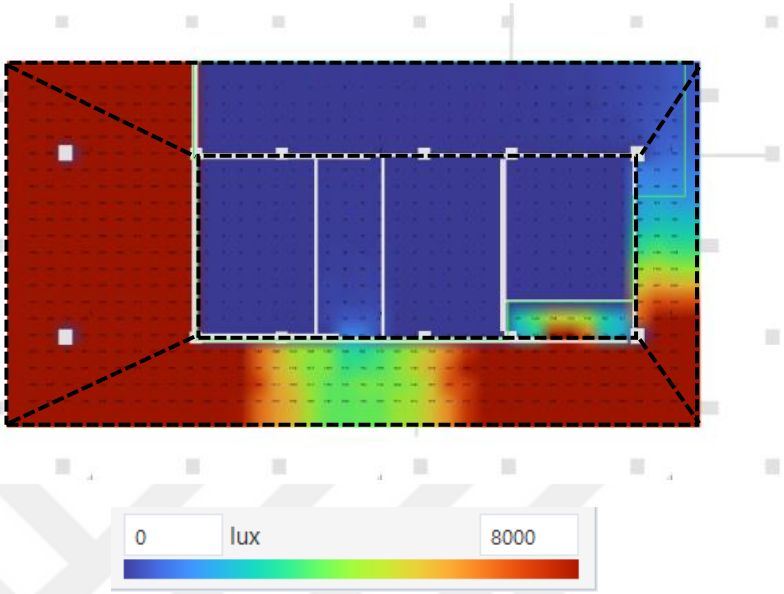

Figure 92: Base case, 21st June, 2 pm, level 3.

b- Winter Daylight graphs:

b.1 Winter Daylight at 10 am

The first level receives average daylight of less than 500 lux during winter. Only the areas closest to the windows receive daylight higher than 500 lux (Figure 92). The average lux on level one is 286 lux, and the median value is 178 lux.

Similar to the first level, the second level receives average daylight of less than 500 lux. However, it records a bigger area with a daylight value higher than 500 lux (Figure 93). The average lux on the second level is 227 lux, and the median value is 217 lux.

Similar to the first and second levels, the third level receives average daylight of less than 500 lux during winter (Figure 94). A big part of the northern area receives almost 0 lux. The west records the highest value up to 1500 lux presented in green spots on the floor plan. The average lux on the third level is 239 lux, and the median value is 6 lux.

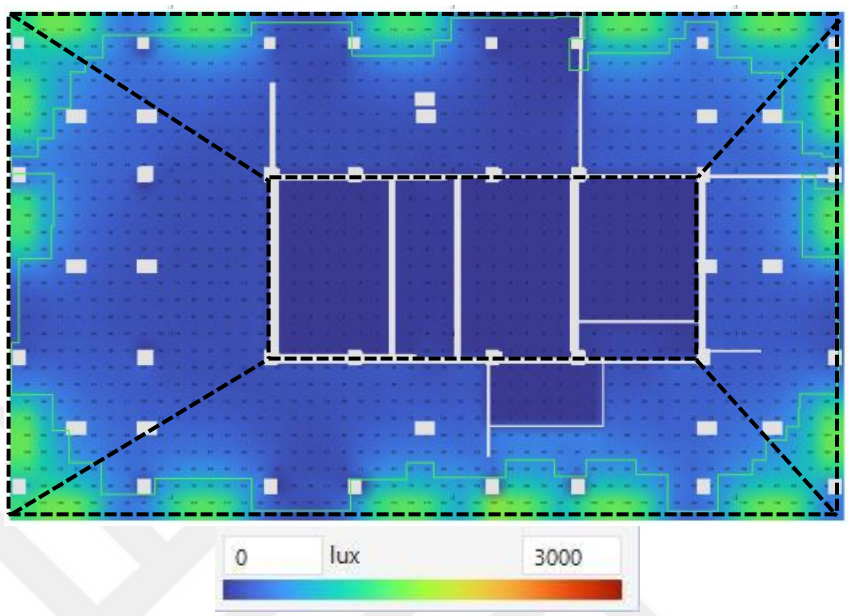

Figure 93: Base case, 21st December, 10 am, level 1.

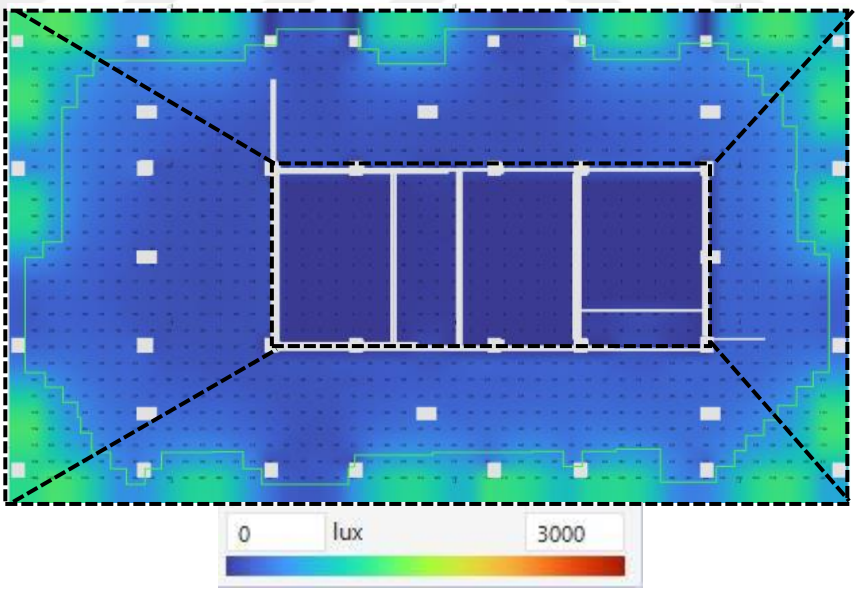

Figure 94: Base case, 21st December, 10 am, level 2.

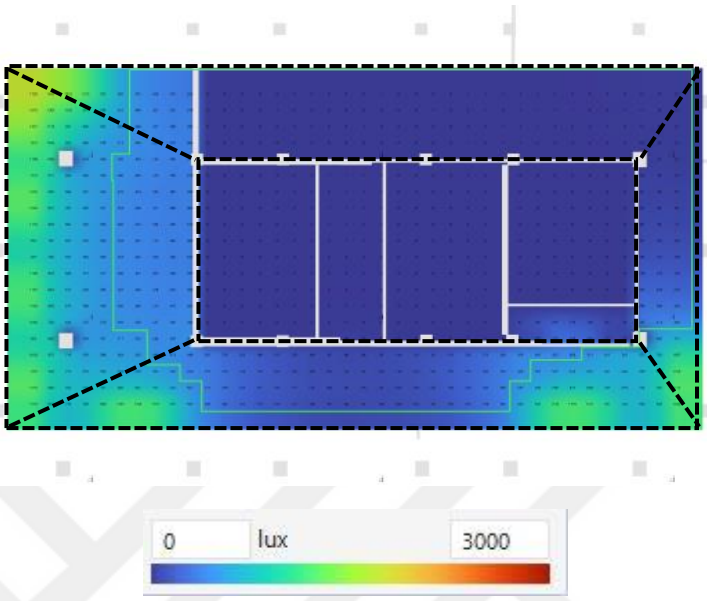

Figure 95: Base case, 21st December, 10 am, level 3.

b.2 Winter Daylight at 12 pm

The first level received daylighting lower than 500 lux (Figure 95). The south records the highest value, almost around 1900 lux. The average lux on level one is 444 lux, and the median value is 290 lux.

The second level, receives an average daylight value of less than 500. However, it receives a bigger area with daylight higher than 500 lux (Figure 96). The average lux on the second level is 452 lux, and the median value is 348 lux.

The third level received average daylight of less than 500 lux. However, it receives a bigger area with daylight higher than 500 lux, especially on the western side of the building (Figure 97). A big part of the northern and northeast areas receive almost 0 lux. The average lux on the third level is 392 lux, and the median is 11 lux.

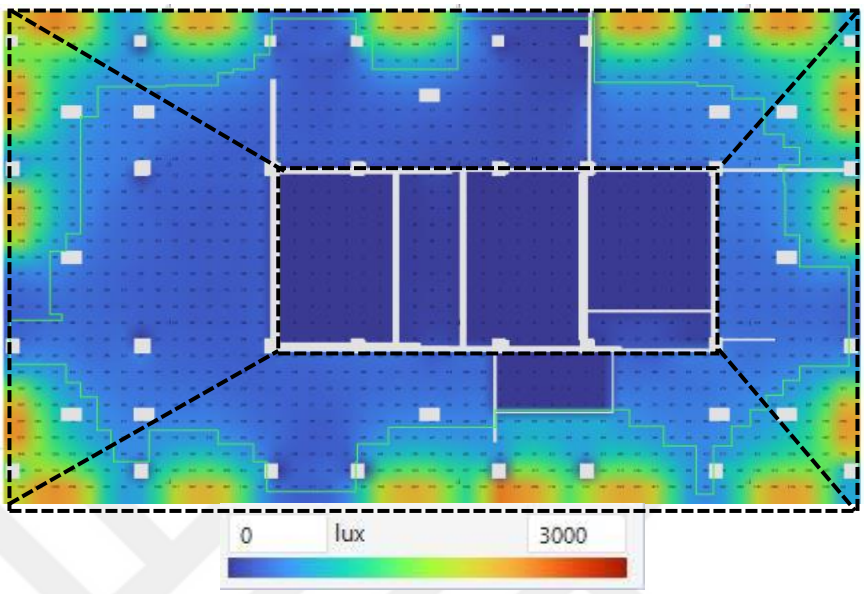

Figure 96: Base case, 21st December, 12 pm, level 1.

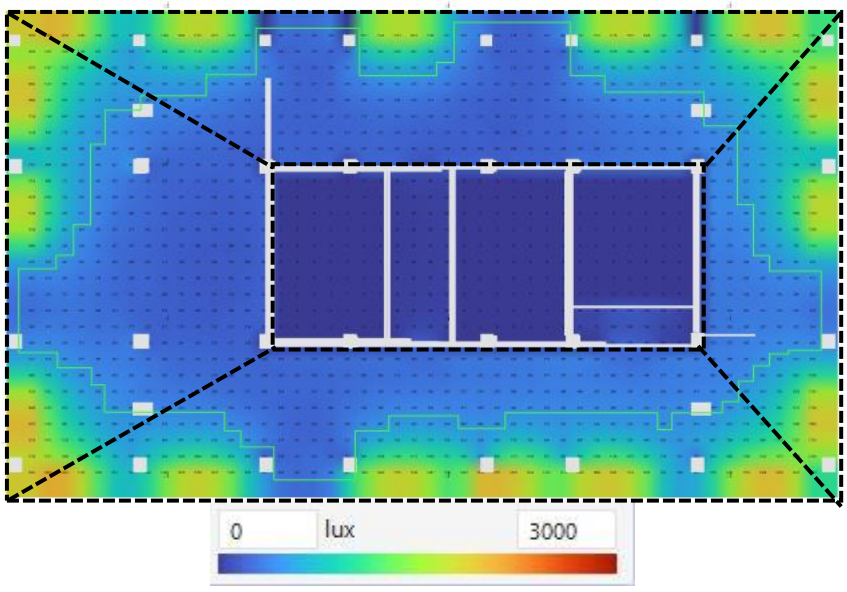

Figure 97: Base case, 21st December, 12 pm, level 2.

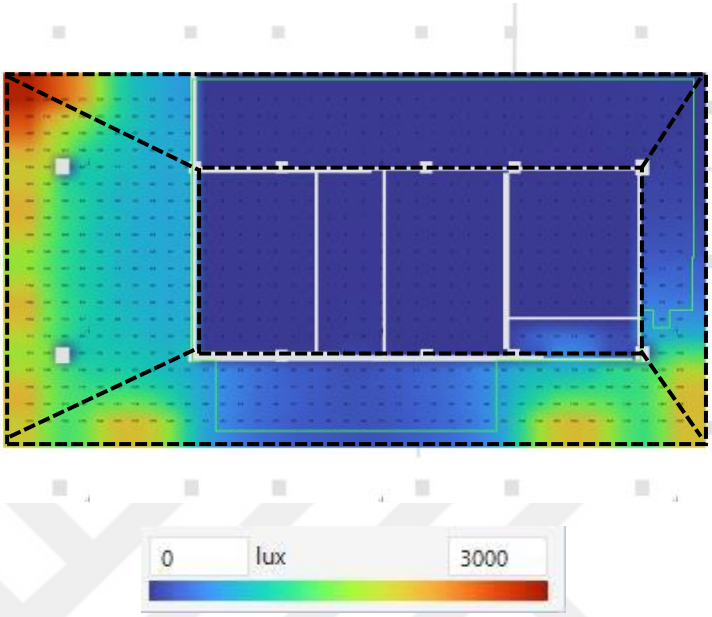

Figure 98: Base case, 21st December, 12 pm, level 3.

b.3 Winter Daylight at 2 pm

During winter, the first level receives a lower average daylight value than 12 pm. The average daylighting is still lower than 500 lux. Areas closest to the windows receive daylight values higher than 500 lux (Figure 98). The south records the highest value, around 2000 lux. The average lux on level one is 435 lux, and the median value is 286 lux.

The second level receives average daylight of less than 500 lux during winter. However, it receives a bigger area with daylight higher than 500 lux (Figure 99). The south records the highest value up to 1900 lux. The average lux on the second level is 448 lux, and the median value is 346 lux.

Similar to the first and second levels, the third level receives an average daylight value that is less than 500 lux during winter. However, it receives a bigger area with daylight higher than 500 lux (Figure 100). A big part of the northern and northeast areas receive almost 0

lux. The west records the highest value up to 2700 lux. The southern areas receive daylighting that ranges from 150 to 1000 lux. The average lux on the third level is 392 lux, and the median value is 10 lux.

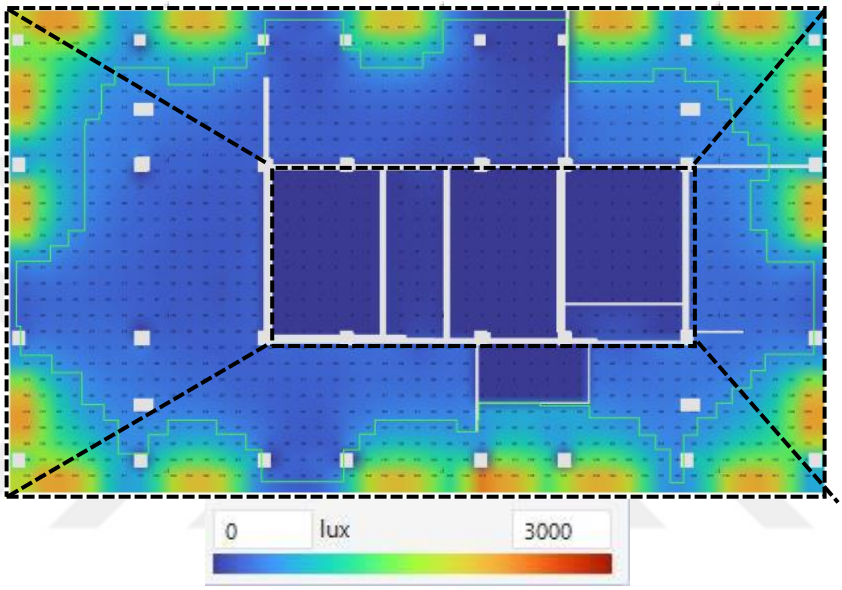

Figure 99: Base case, 21st December, 2 pm, level 1.

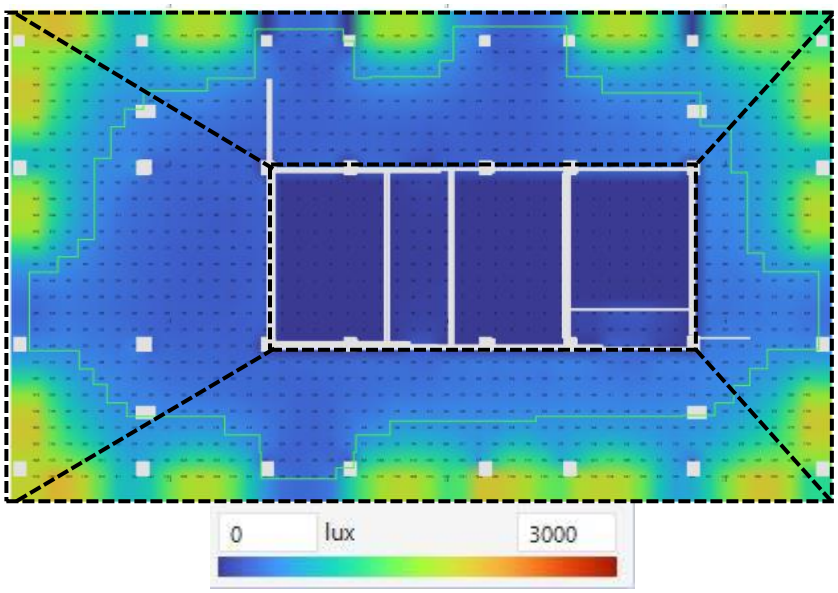

Figure 100: Base case, 21st December, 2 pm, level 2.

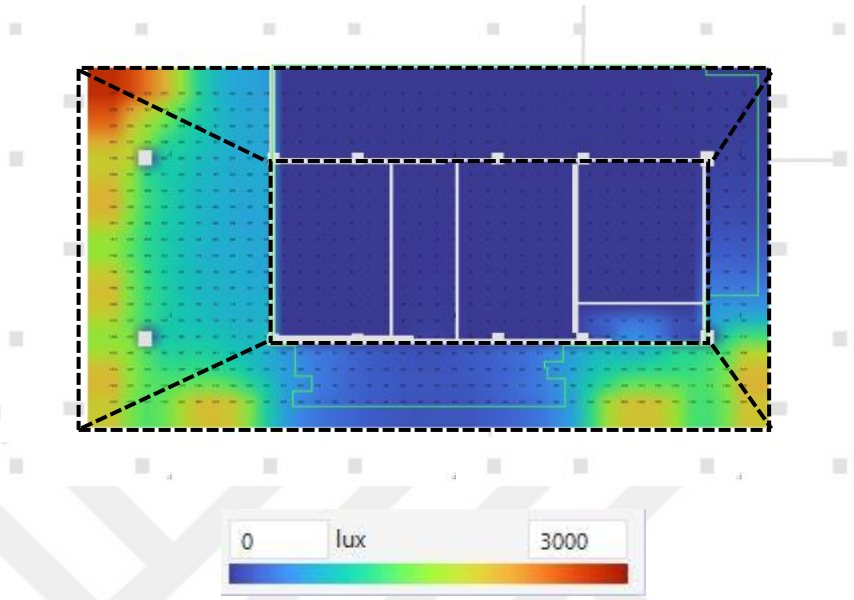

Figure 101: Base case, 21st December, 2 pm, level 3.

5.4.2 Type-A Facade Building Model

a- Summer Daylight graphs:

a.1 Summer Daylight at 10 am

On the first level of pattern A, the highest daylight on the eastern side reached 5000 lux. The inner areas receive daylighting between 700 to 900 lux (figure 101), which is higher and more sufficient than the base case model. The average lux on level one is 2243 lux, and the median value is 1239 lux.

The second level highest daylight is on the east, and it reached up to 5000 lux. The southern part receives significantly less than the base case model (figure 102). The average lux on level two is 2076 lux, and the median is 1382 lux. The highest daylight on the third level is on the eastern side and reaches 10000 lux. The north and northeast parts receive better

daylighting than the base case (figure 103). The average lux on level three is 3592 lux, and the median value is 2611 lux.

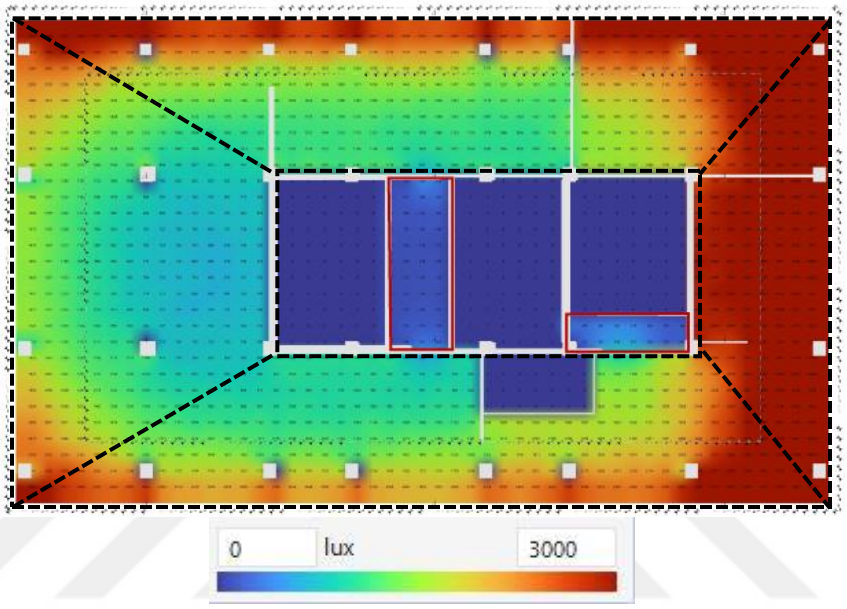

Figure 102: Pattern A, 21st June, 10 am, level 1.

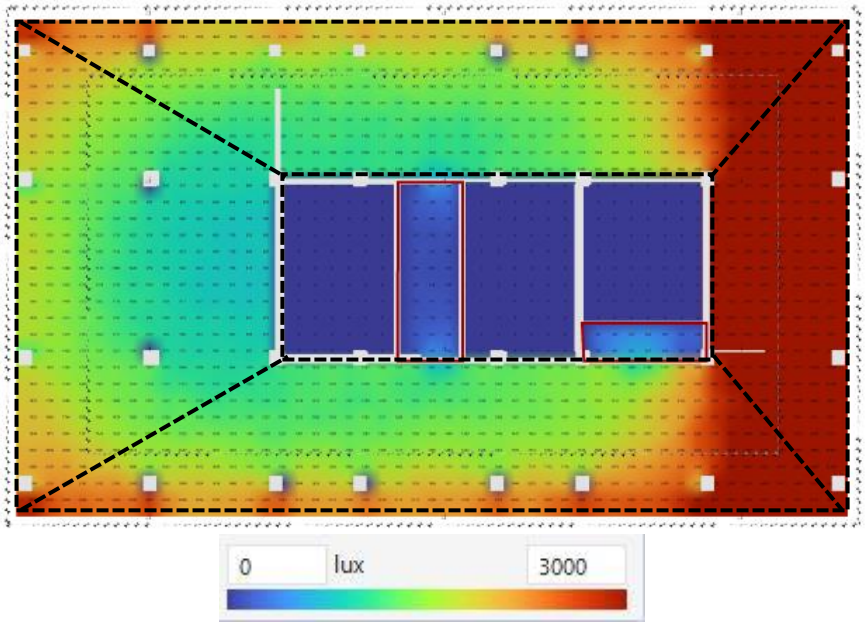

Figure 103: Pattern A, 21st June, 10 am, level 2.

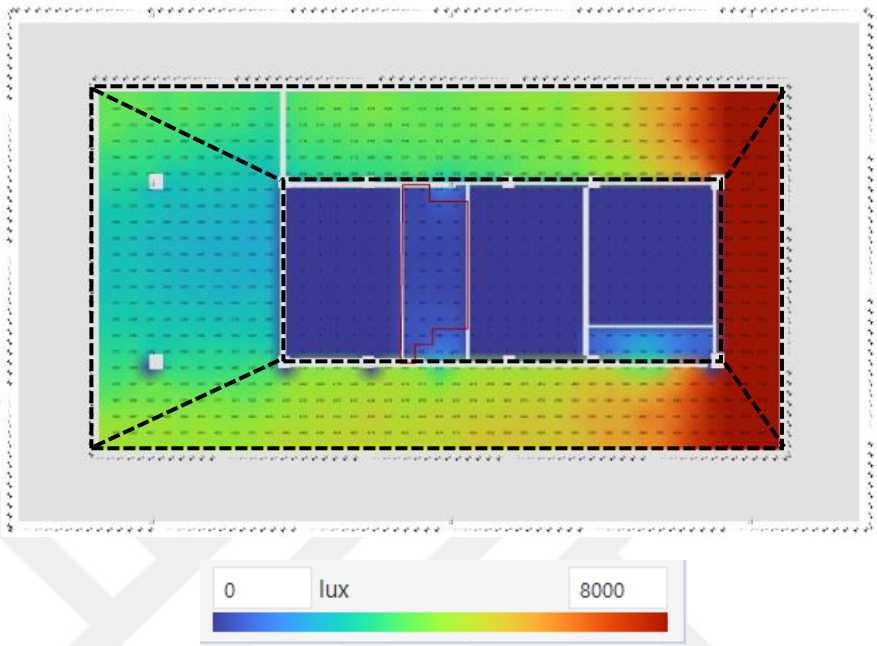

Figure 104: Pattern A, 21st June, 10 am, level 3.

a.2 Summer Daylight at 12 pm

The first level highest daylight is on the eastern side, which reached up to 5000 lux (figure 101). This pattern provides lower daylighting, on the south and east, compared to the base case model. The average lux on level one is 1562 lux, and the median value is 1262 lux. The second level highest daylight is located on the south and reached 3000 lux (figure 105). The average lux on level two is 1534 lux, and the median value is 1647 lux. On the third level, the highest daylight is on the eastern side, where it reached up to 9000 lux case (figure 106). The average lux on level three is 3409 lux, and the median value is 3461 lux.

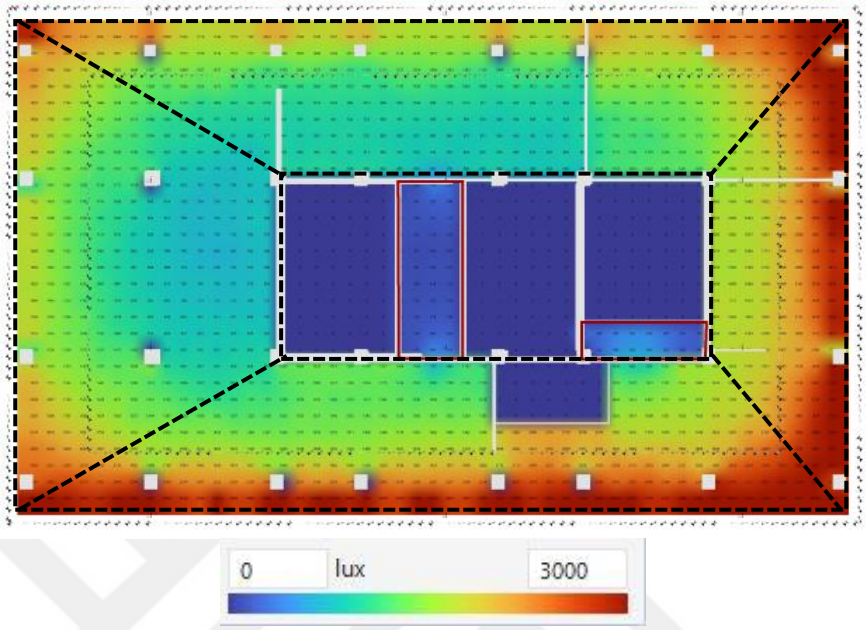

Figure 105: Pattern A, 21st June, 12 pm, level 1.

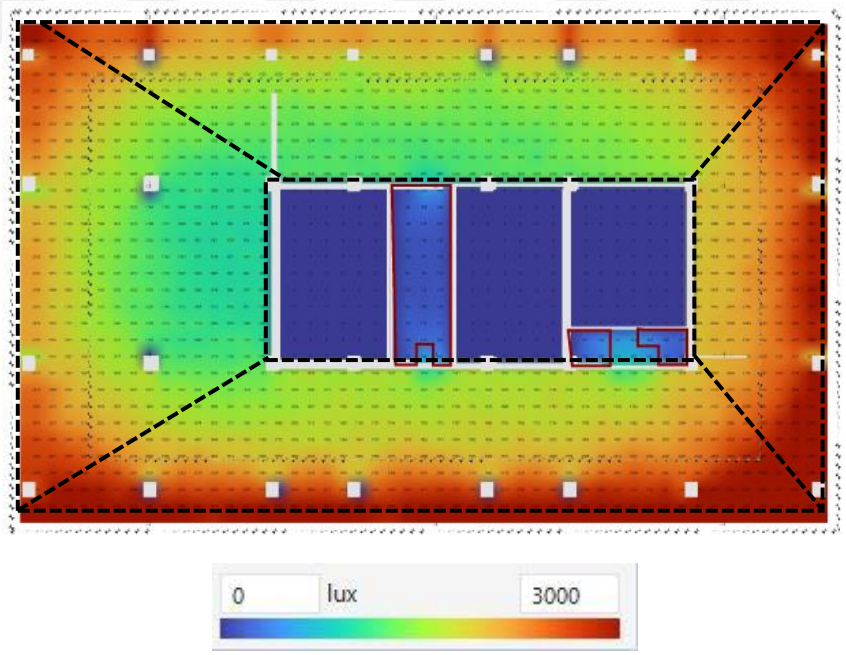

Figure 106: Pattern A, 21st June, 12 pm, level 2.

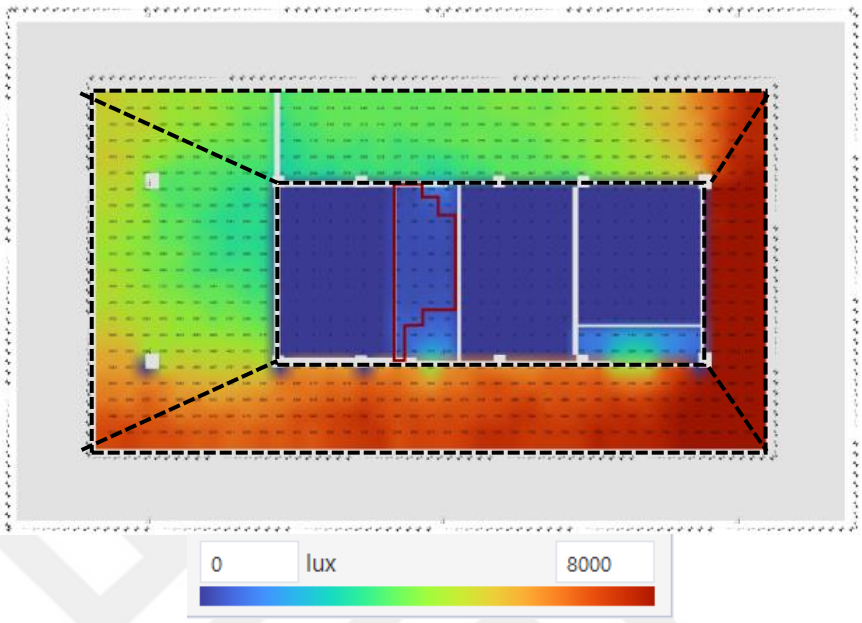

Figure 107: Pattern A, 21st June, 12 pm, level 3.

a.3 Summer Daylight at 2 pm

The first level average lux is 1760 lux, and the median value is 1316 lux. On the first level, the average and median value for pattern A are higher than the results recorded for the base case model (Figure 107).The average lux on level two is 1566 lux, and the median value is 1697 lux (Figure 108). The average lux on level three is 3520 lux, and the median value is 3758 lux (Figure 109).

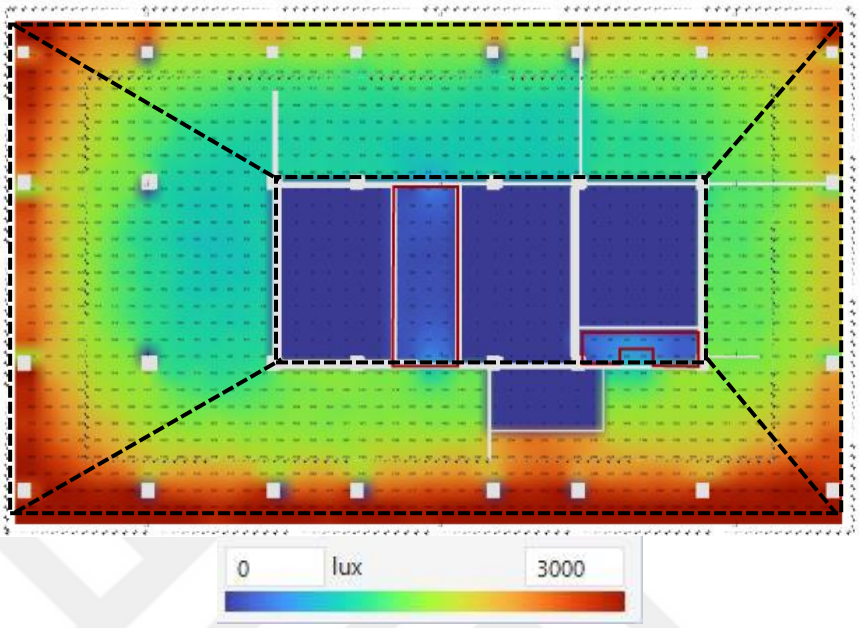

Figure 108: Pattern A, 21st June, 2 pm, level 1.

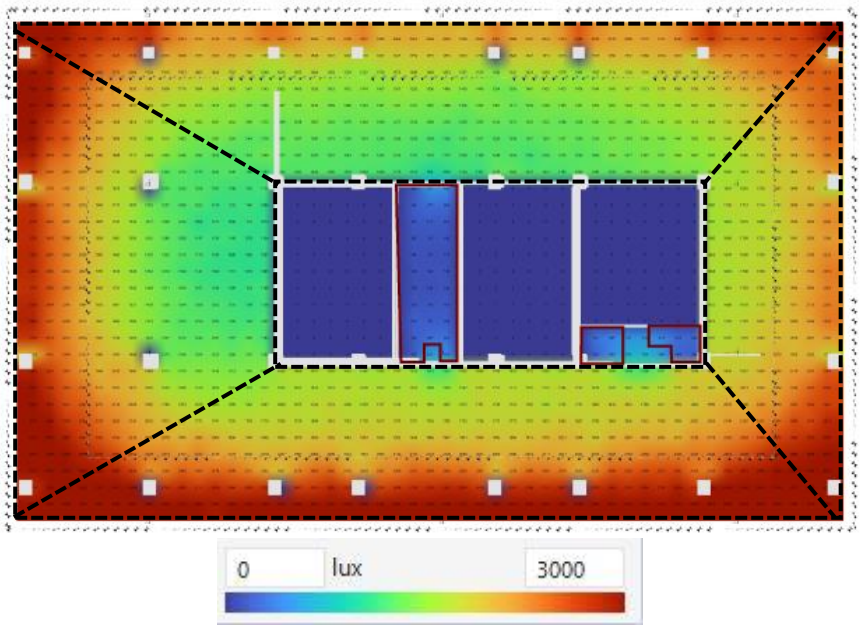

Figure 109: Pattern A, 21st June, 2 pm, level 2.

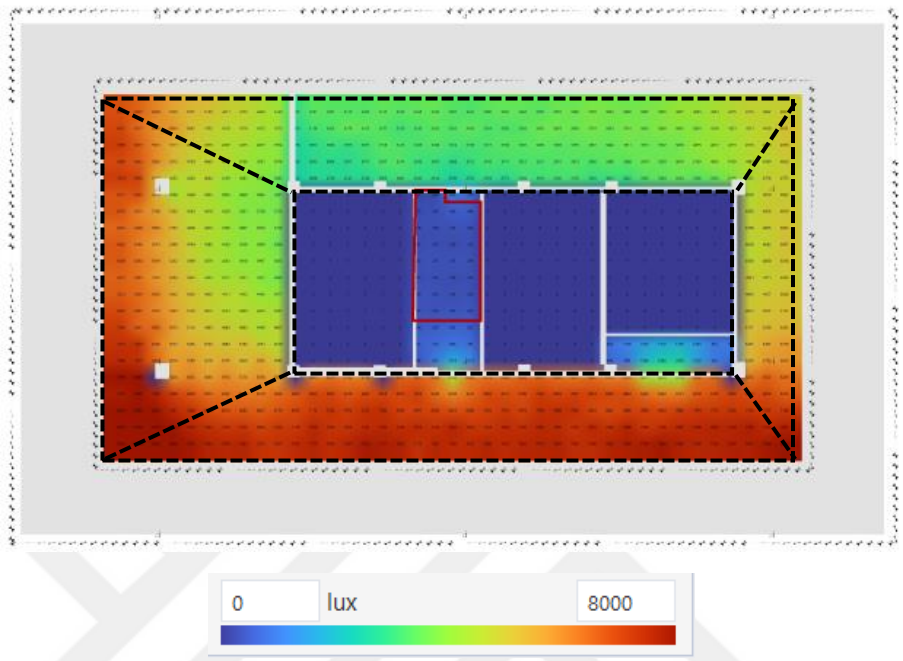

Figure 110: Pattern A, 21st June, 2 pm, level 3.

b- Winter Daylight graphs:

b.1 Winter Daylight at 10 am

In comparison with the base case model, this pattern reduces the lux value received on all sides on the first level (Figure 110). The average lux on level one is 235 lux, and the median value is 207 lux. Compared to the base case model, this pattern reduces the lux value received on the floor wings but increases the lux towards the inner floor areas on the second level (Figure 111). The average lux on level two is 251 lux, and the median is 243 lux. This pattern increased the lux received on the third level (Figure 112).

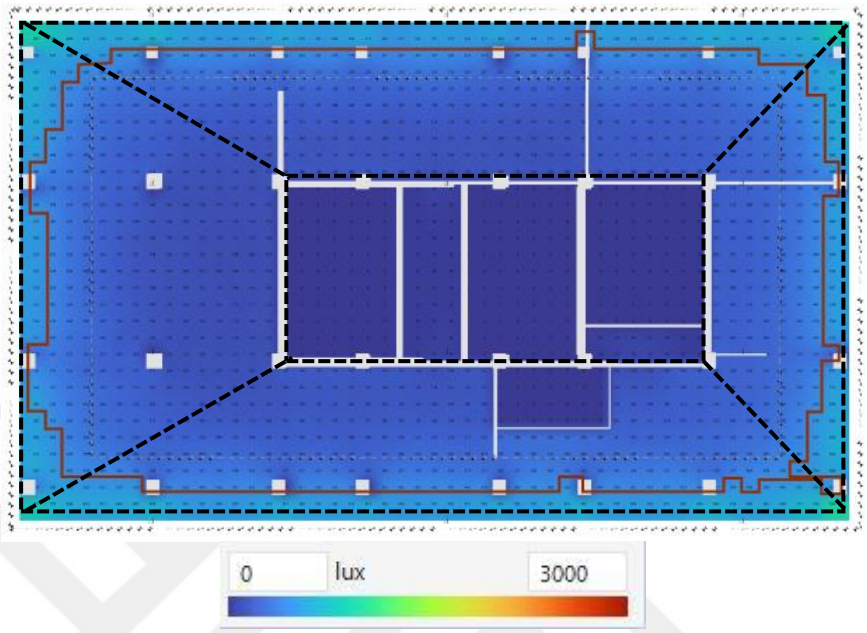

Figure 111: Pattern A, 21st December, 10 am, level 1.

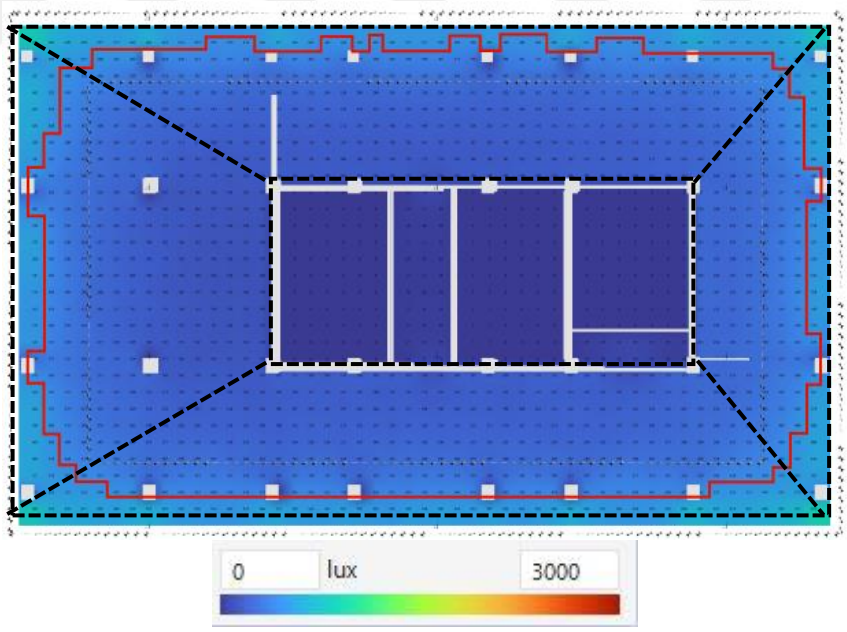

Figure 112: Pattern A, 21st December, 10 am, level 2.

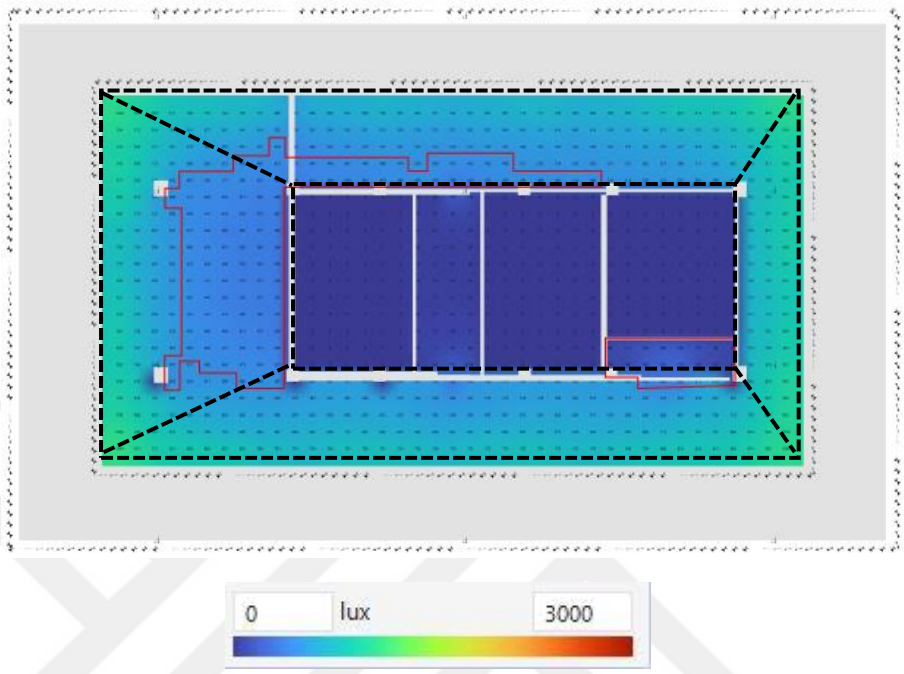

Figure 113: Pattern A, 21st December, 10 am, level 3.

b.2 Winter Daylight at 12 pm

In comparison to the base case model, on the first level, this façade pattern reduces the lux value received on all sides and increases the value on the deeper areas (Figure 113). The average lux on level one is 390 lux, and the median value is 345 lux. The average lux on level two is 418 lux, and the median value is 402 lux (figure 114). The average lux on level three is 694 lux, and the median value is 845 lux (figure 115).

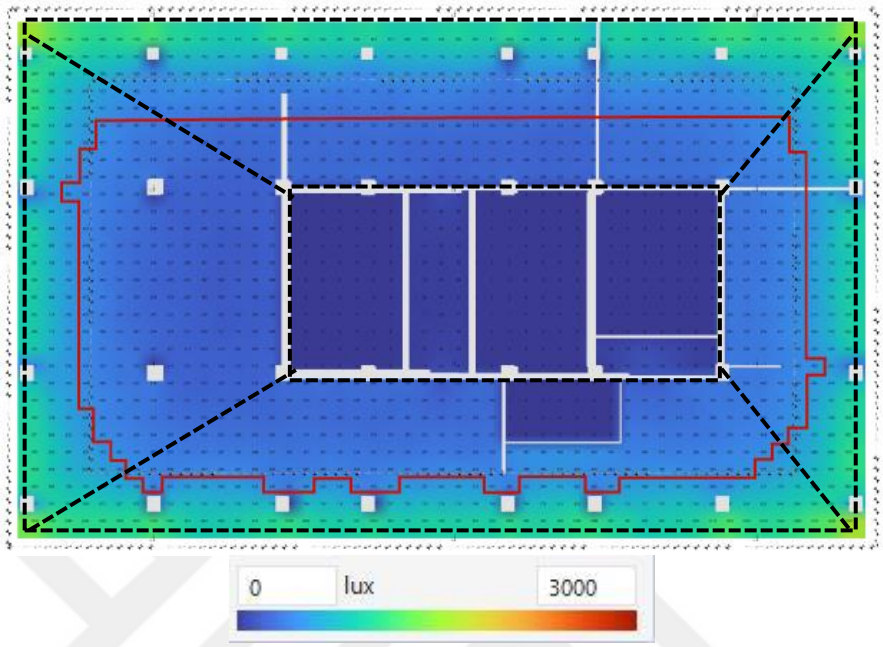

Figure 114: Pattern A, 21st December, 12 pm, level 1.

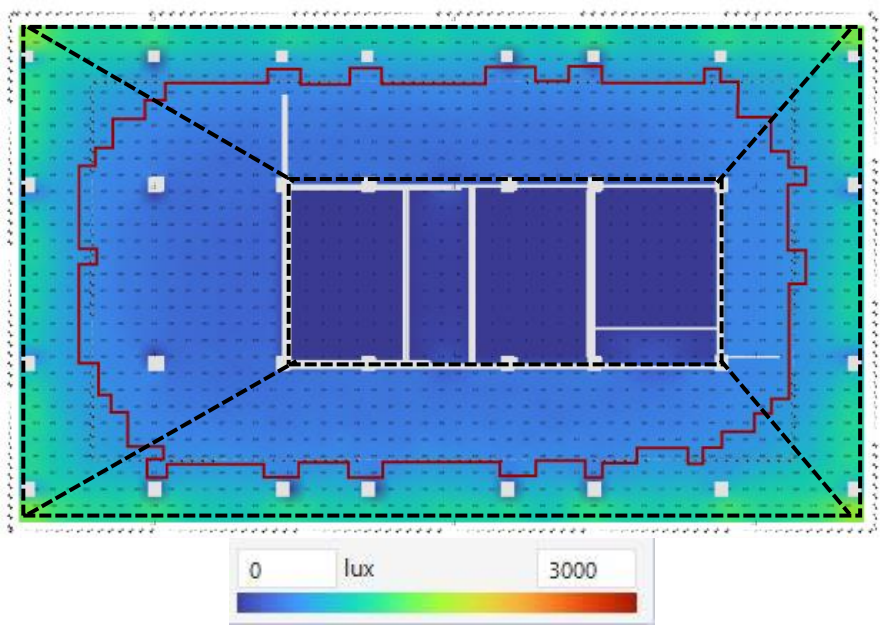

Figure 115: Pattern A, 21st December, 12 pm, level 2.

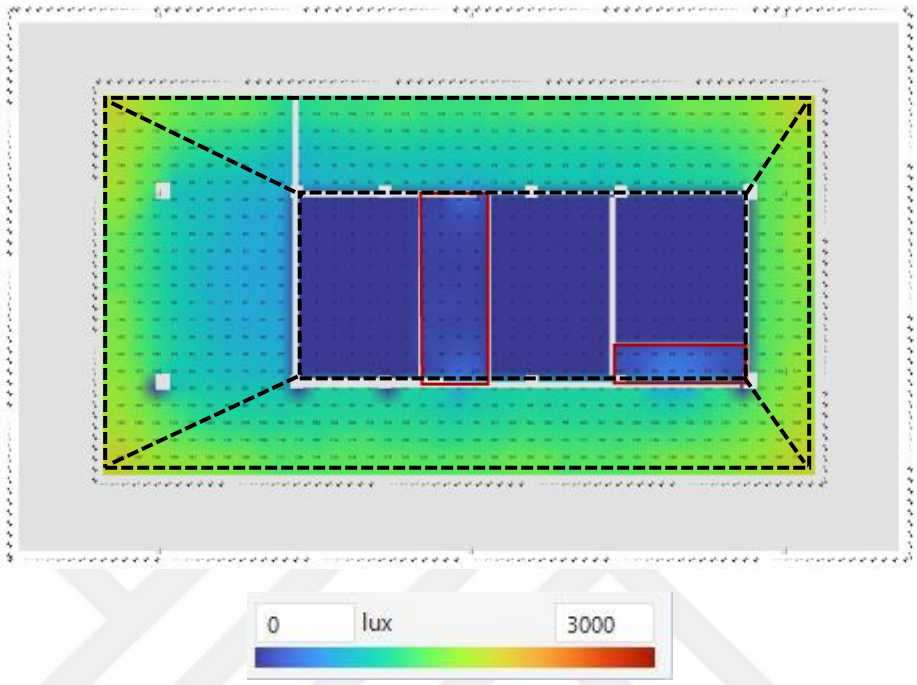

Figure 116: Pattern A, 21st December, 12 pm, level 3.

b.3 Winter Daylight at 2 pm

In comparison to the base case model, on the first level, this façade pattern reduces the lux value received on all edges and increases it on the deeper floor area. (Figure 116). The average lux on level one is 384 lux, and the median value is 336 lux. The average lux on level two is 412 lux, and the median value is 398 lux (figure 117). The average lux on level three is 683 lux, and the median value is 832 lux (figure 118).

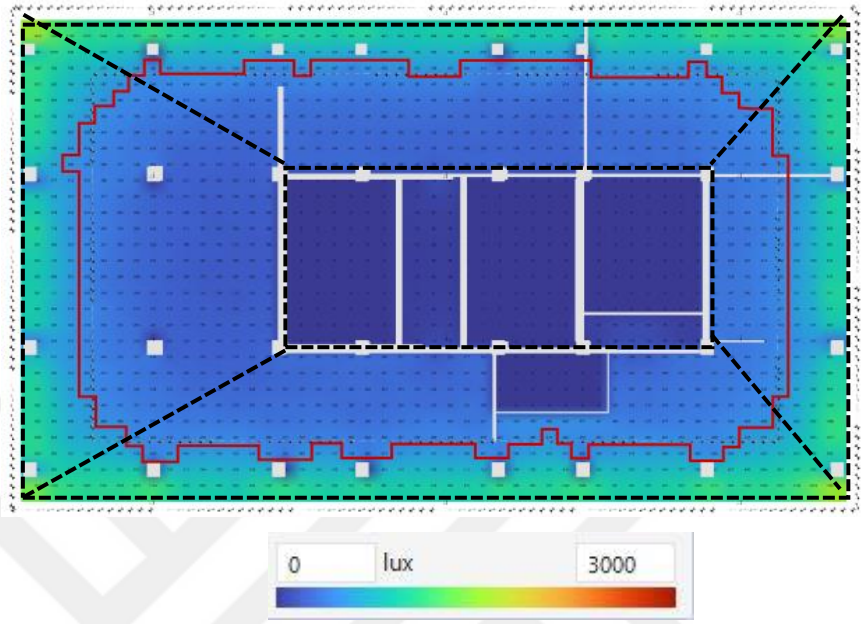

Figure 117: Pattern A, 21st December, 2 pm, level 1.

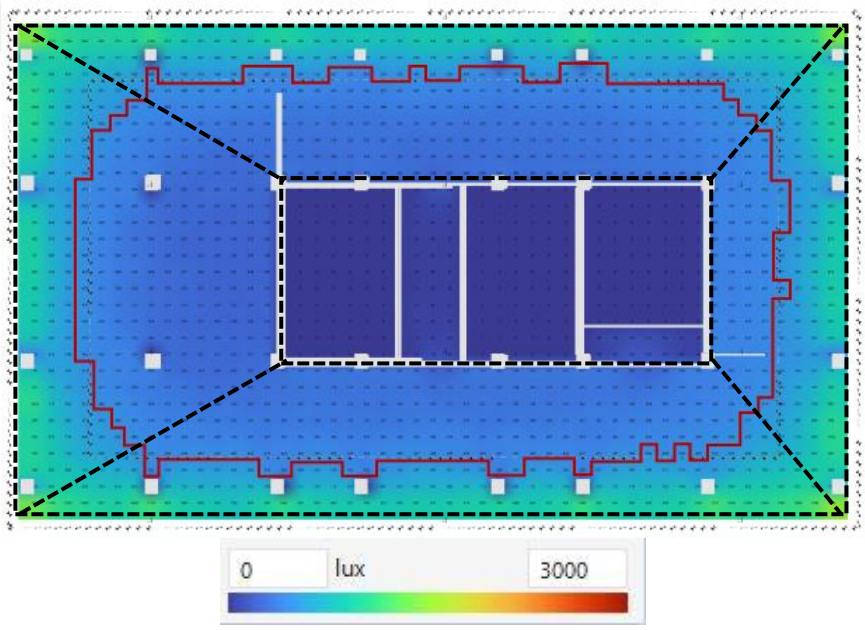

Figure 118: Pattern A, 21st December, 2 pm, level 2.

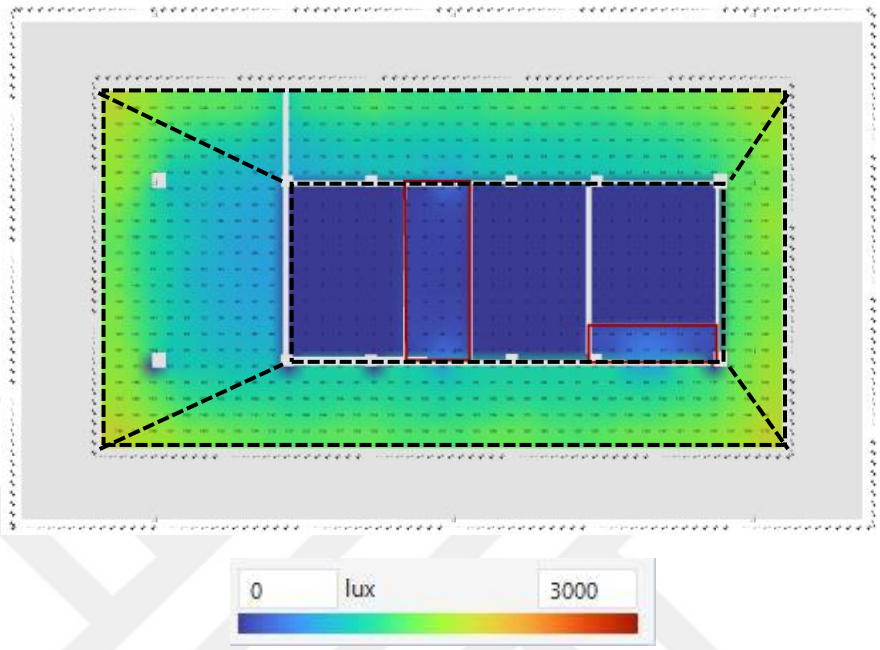

Figure 119: Pattern A, 21st December, 2 pm, level 3.

5.4.3 Type-B Facade Building Model

a- Summer Daylight graphs:

a.1 Summer Daylight at 10 am

In comparison to the base case model, this pattern increases the daylight value on the inner deeper parts of the floor (Figure 119). The average lux on level one is 2148 lux, and the median value is 1066 lux. The average lux on level two is 2220 lux, and the median value is 1472 lux (figure 120). The average lux on level three is 3901 lux, and the median value is 2881 lux (figure 121).

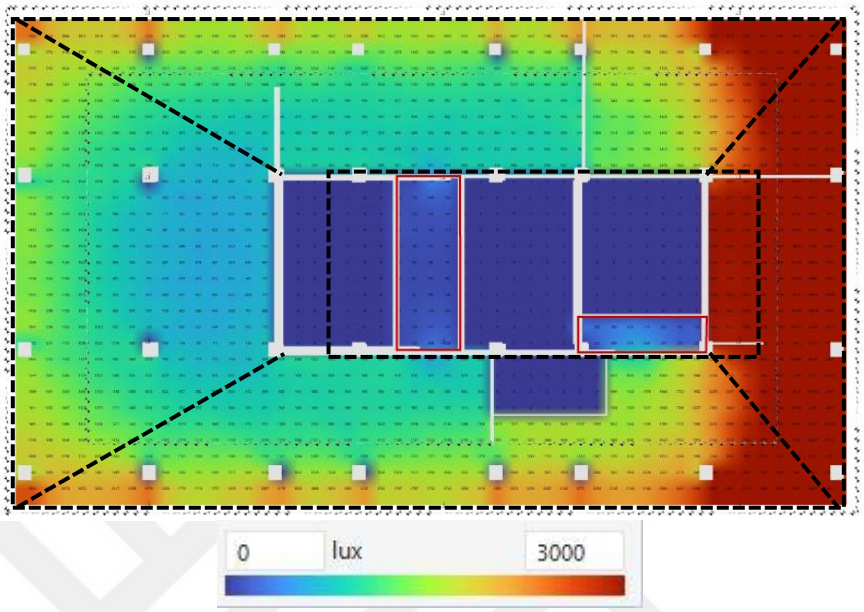

Figure 120: Pattern B, 21st June, 10 am, level 1.

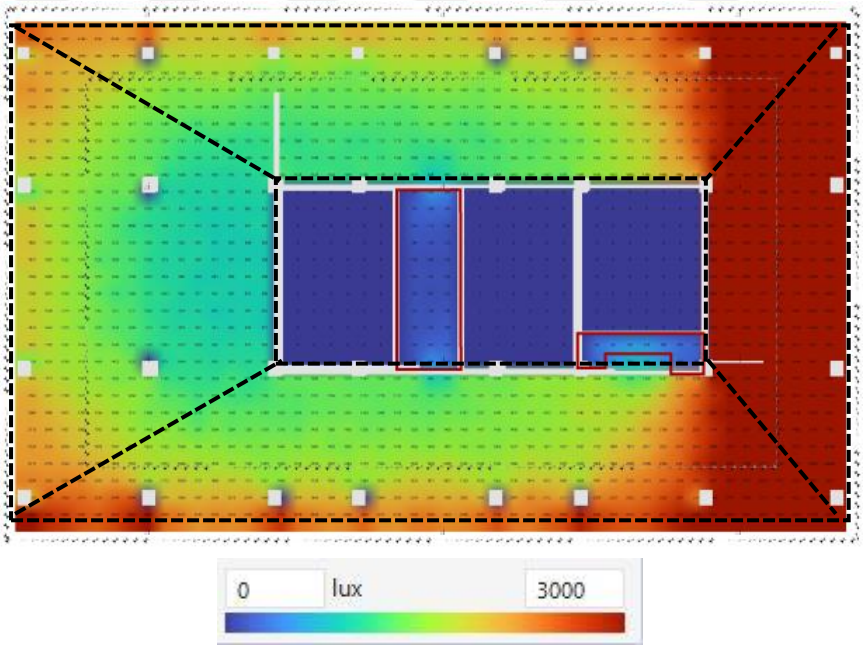

Figure 121: Pattern B, 21st June, 10 am, level 2.

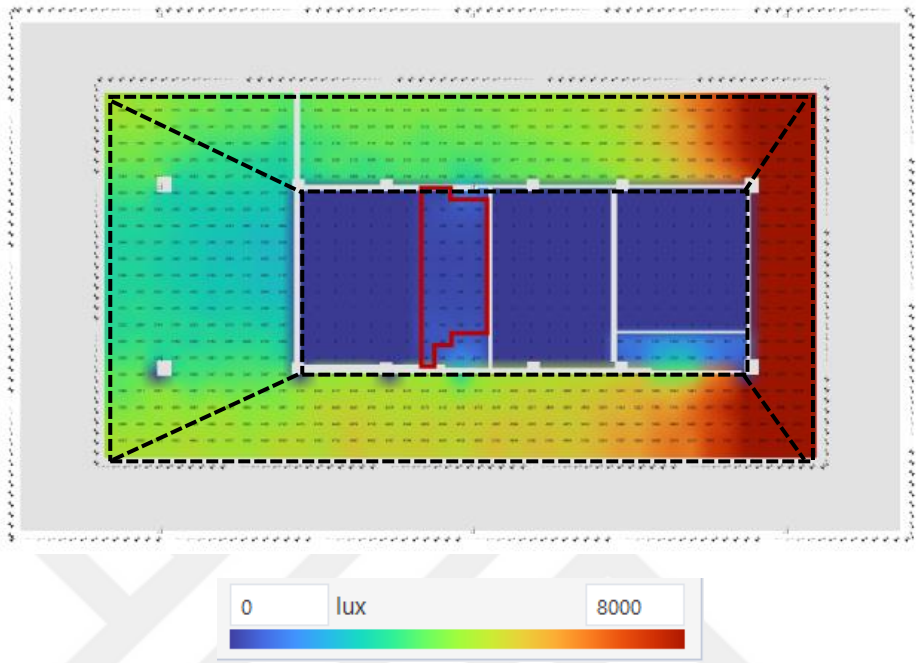

Figure 122: Pattern B, 21st June, 10 am, level 3.

a.2 Summer Daylight at 12 pm

Compared to the base case model, this façade pattern increases the daylighting value received on all four wings on the first level (Figure 122). The average lux on level one is 1615 lux, and the median value is 1339 lux. The average lux on level two is 1663 lux, and the median value is 1788 lux (figure 123). The average lux on level three is 3620 lux, and the median value is 3662 lux (figure 124).

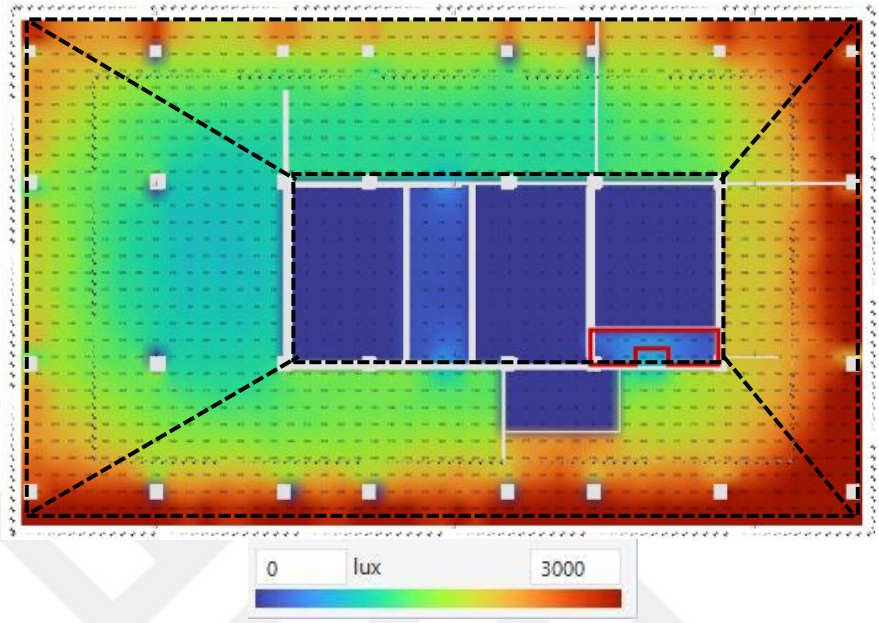

Figure 123: Pattern B, 21st June, 12 pm, level 1.

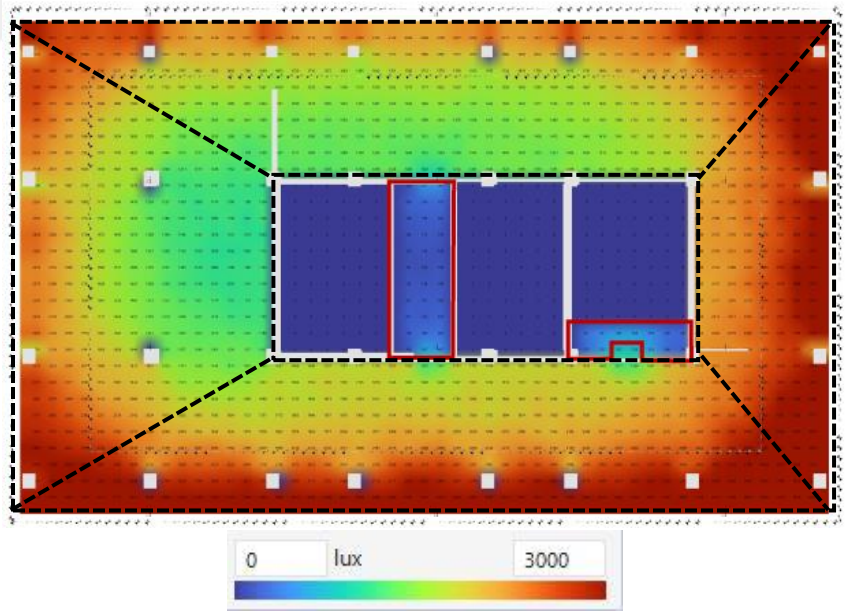

Figure 124: Pattern B, 21st June, 12 pm, level 2.

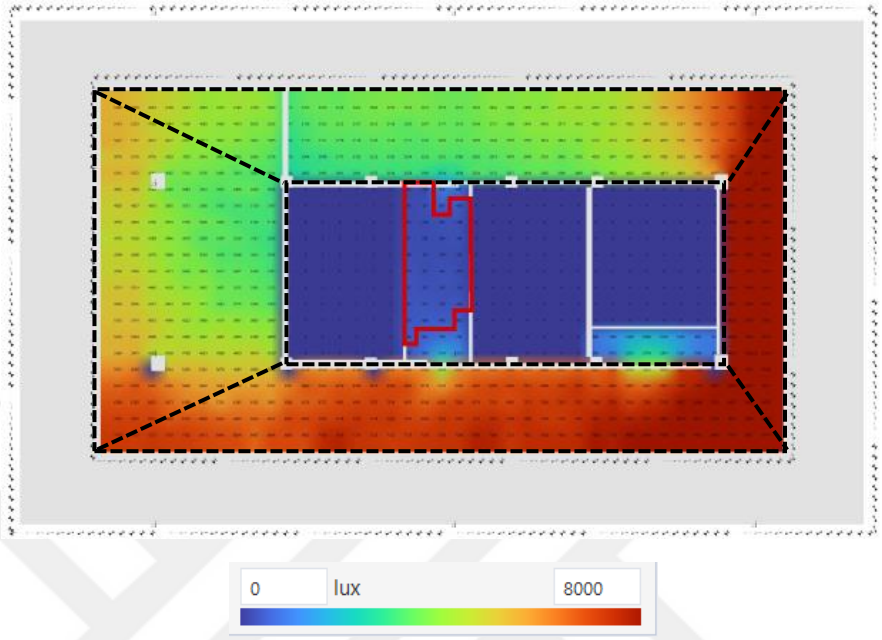

Figure 125: Pattern B, 21st June, 12 pm, level 3.

a.3 Summer Daylight at 2 pm

In comparison to the base case model, pattern B increases the daylight value received on all four sides (Figure 125). The average lux on level one is 2030 lux, and the median value is 1426 lux. The average and median value for pattern B on the first level, are higher than base case model. The average lux on level two is 1707 lux, and the median value is 1855 lux (figure 126). The average lux on level three is 3726 lux, and the median value is 3934 lux (figure 127).

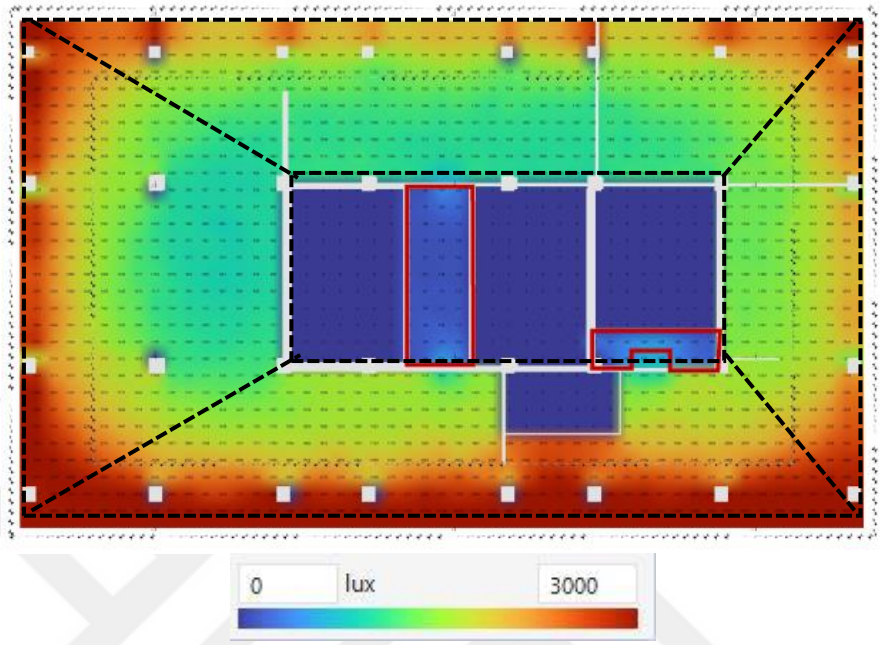

Figure 126: Pattern B, 21st June, 2 pm, level 1.

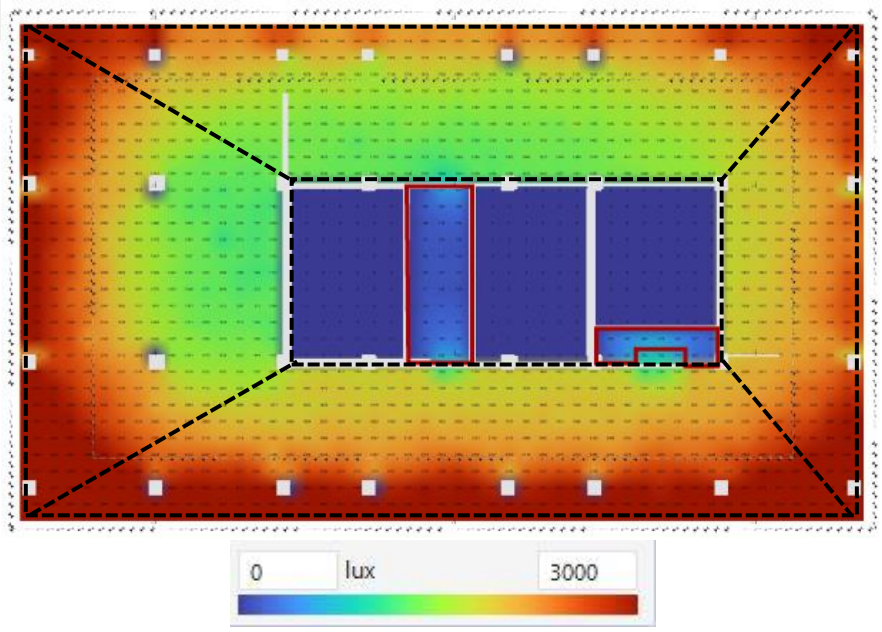

Figure 127: Pattern B, 21st June, 2 pm, level 2.

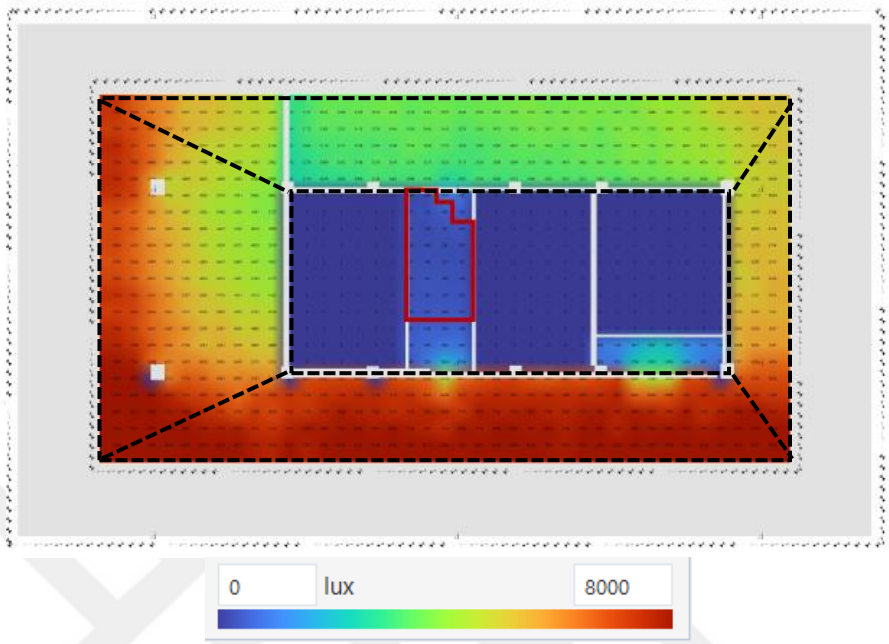

Figure 128: Pattern B, 21st June, 2 pm, level 3.

b- Winter Daylight graphs:

b.1 Winter Daylight at 10 am

This façade pattern increases the lux value received on all four wings closest to the glazing. This pattern increases the daylight on the inner parts of the plan (Figure 128). The average lux on level one is 256 lux, and the median value is 226 lux. The average lux on level two is 269 lux, and the median value is 258 lux (figure 129). The average lux on level three is 435 lux, and the median value is 528 lux (figure 130).

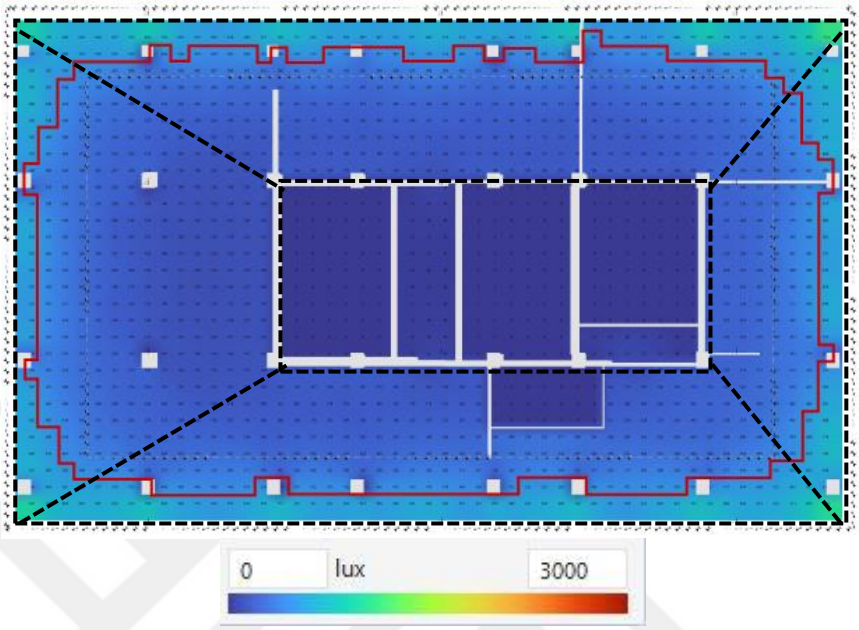

Figure 129: Pattern B, 21st December, 10 am, level 1.

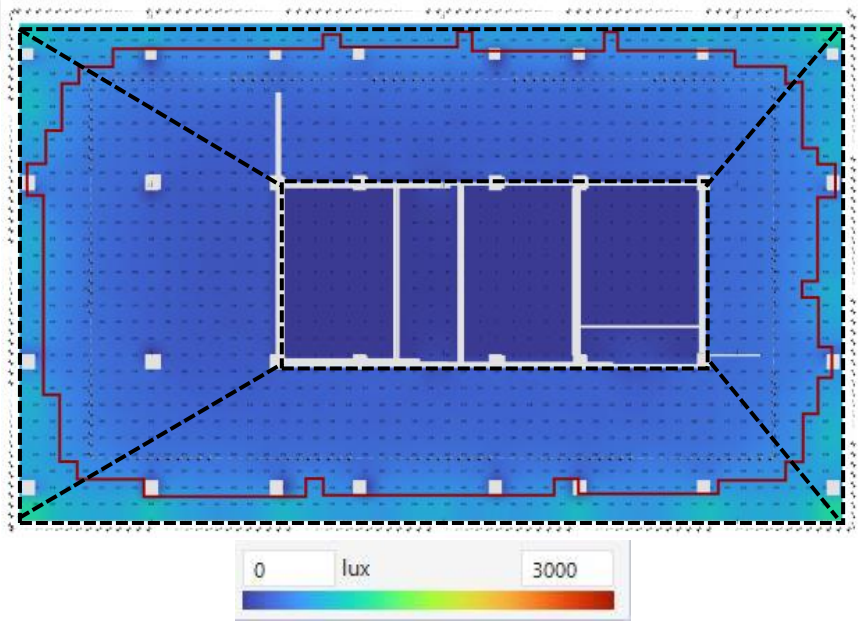

Figure 130: Pattern B, 21st December, 10 am, level 2.

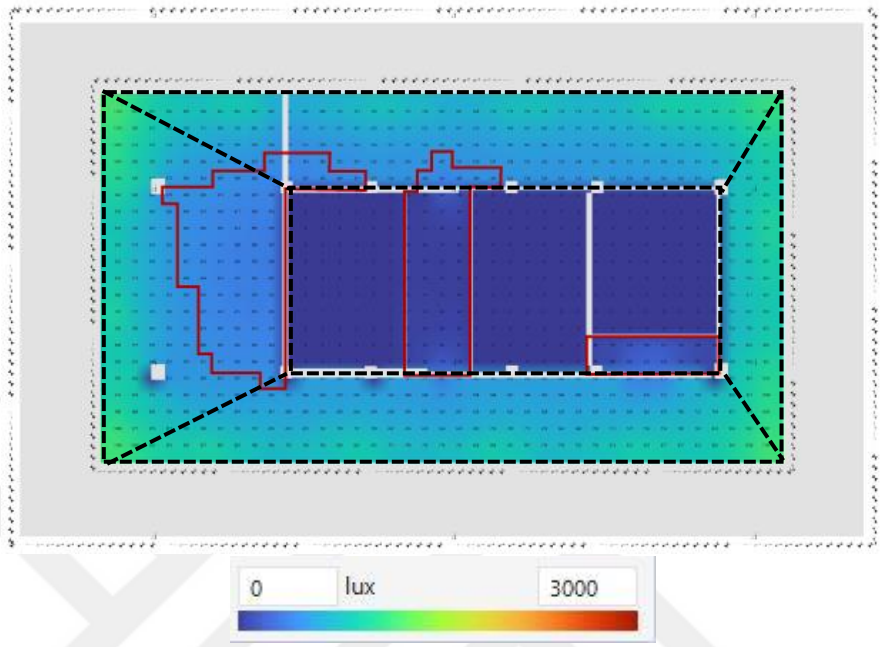

Figure 131: Pattern B, 21st December, 10 am, level 3.

b.2 Winter Daylight at 12 pm

Compared to the base case model, this façade pattern increases the lux value received on all four wings and on the inner parts of the plan (Figure 131). The average lux on level one is 426 lux, and the median value is 376 lux. The average lux on level two is 448 lux, and the median value is 430 lux (figure 132). On the second level, the average value is similar to the base case model, but the median value is lower. The average lux on level three is 724 lux, and the median value is 878 lux (figure 133).

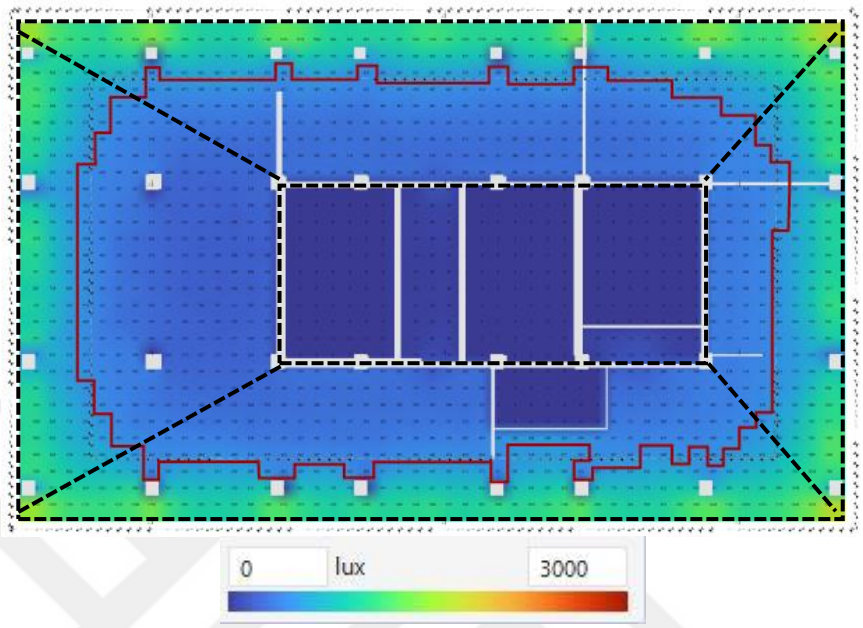

Figure 132: Pattern B, 21st December, 12 pm, level 1.

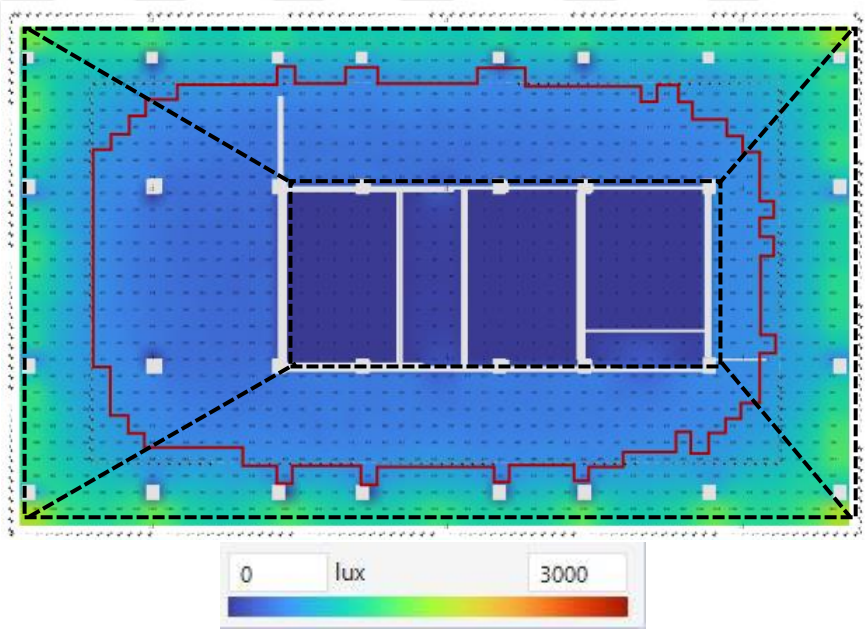

Figure 133: Pattern B, 21st December, 12 pm, level 2.

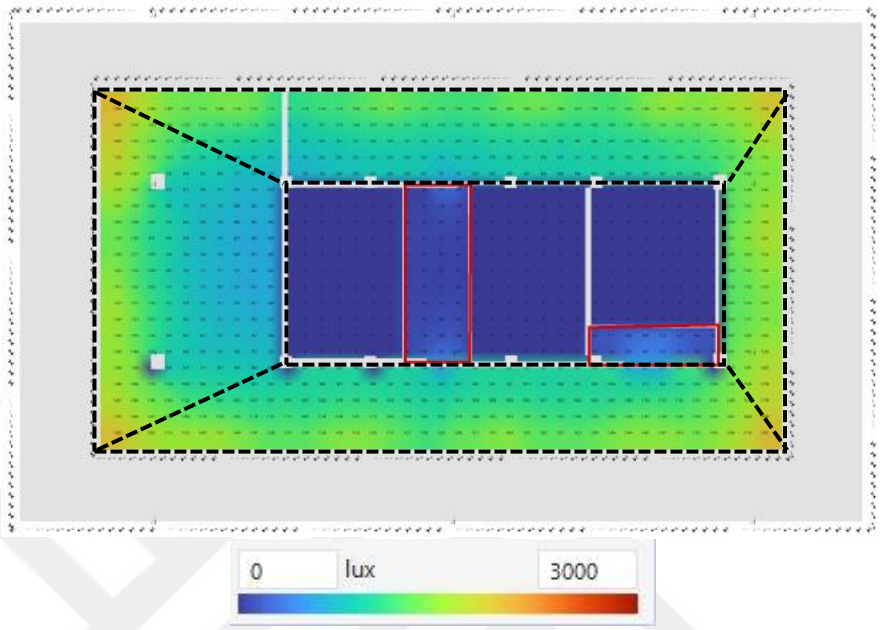

Figure 134: Pattern B, 21st December, 12 pm, level 3.

b.3 Winter Daylight at 2 pm

Compared to the base case model, this façade pattern increases the value of lux value received on all four wings (Figure 134). The average lux on level one is 418 lux, and the median value is 367 lux. The average lux on level two is 440 lux, and the median value is 422 lux (figure 135). The average lux on level three is 714 lux, and the median value is 864 lux (figure 136).

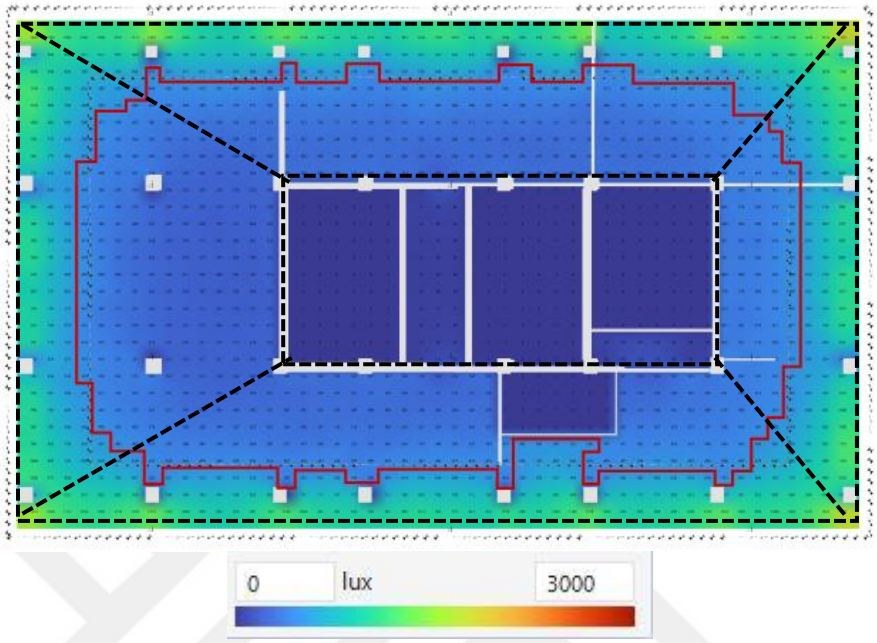

Figure 135: Pattern B, 21st December, 2 pm, level 1.

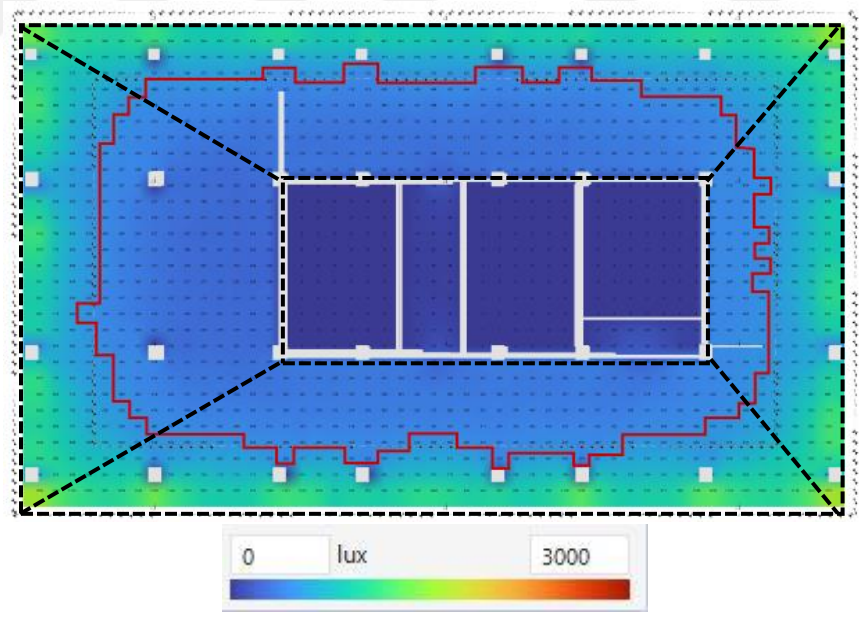

Figure 136: Pattern B, 21st December, 2 pm, level 2.

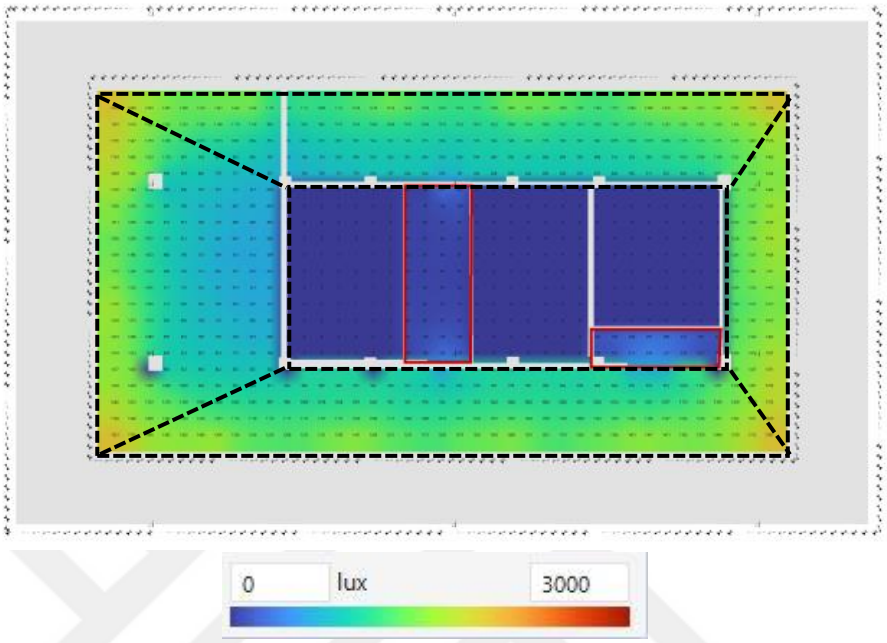

Figure 137: Pattern B, 21st December, 2 pm, level 3.

5.4.4 Type-C Facade Building Model

a- Summer Daylight graphs:

a.1 Summer Daylight at 10 am

In comparison to the base case model, this façade pattern increases the lux value received on all four wings and on the inner deeper parts of the floor (Figure 137). The average lux on level one is 2273 lux, and the median value is 1055 lux. The average lux on level two is 2311 lux, and the median value is 1457 lux (figure 138). The average lux on level three is 3901 lux, and the median value is 2881 lux (figure 139).

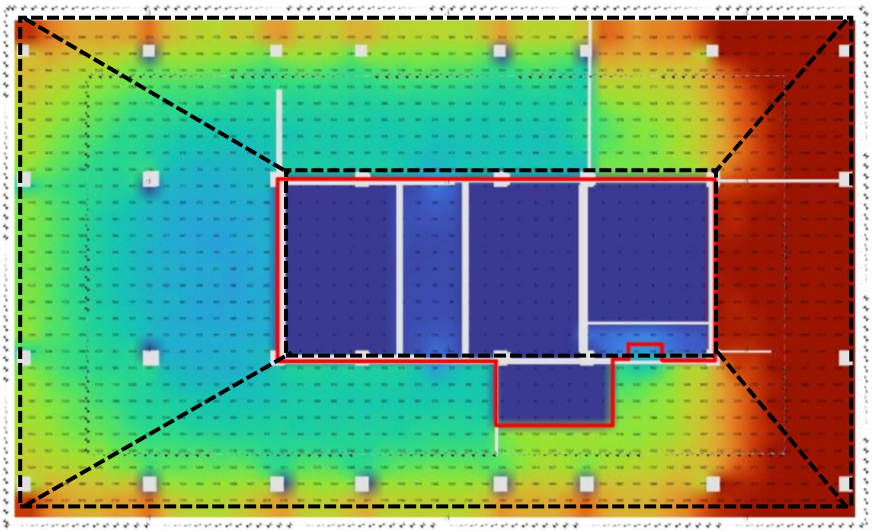

Figure 138: Pattern C, 21st June, 10 am, level 1.

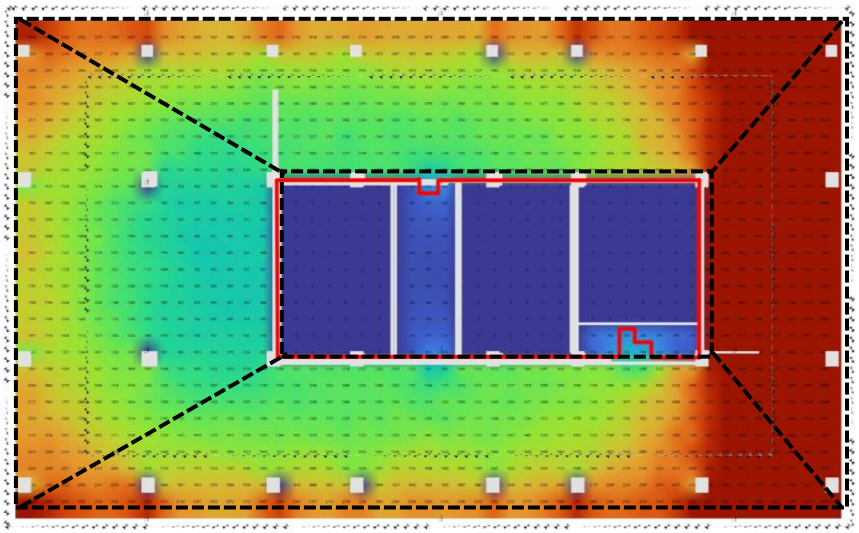

Figure 139: Pattern C, 21st June, 10 am, level 2.

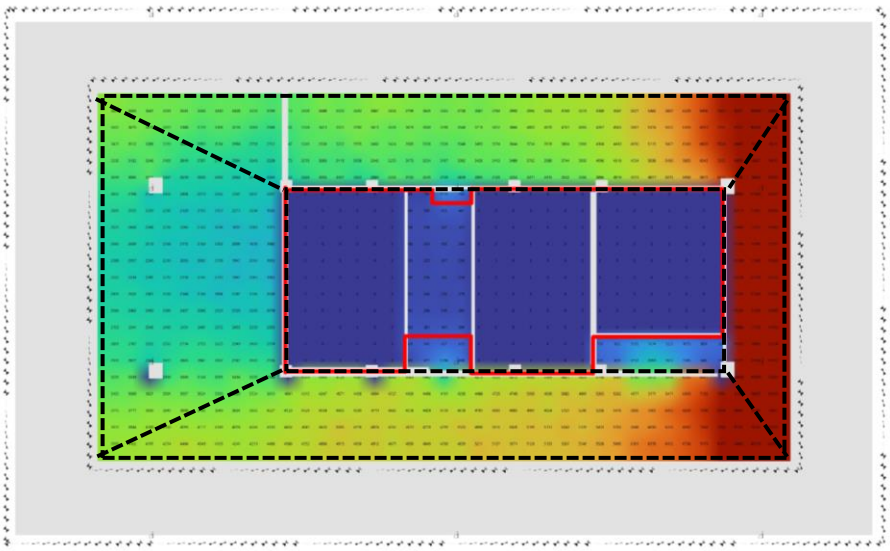

Figure 140: Pattern C, 21st June, 10 am, level 3.

a.2 Summer Daylight at 12 pm

In comparison to the base case model, this façade pattern increases lux value received on all four wings and on the inner deeper parts of the floor (Figure 140). The average lux on level one is 1607 lux, and the median value is 1314 lux. The average lux on level two is 1629 lux, and the median value is 1751 lux (figure 141). The average lux on level three is 3563 lux, and the median value is 3592 lux (figure 142).

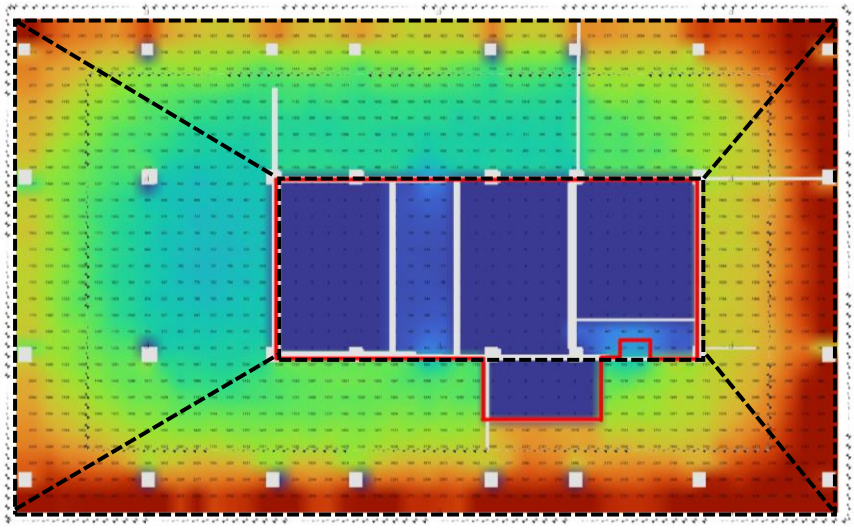

Figure 141: Pattern C, 21st June, 12 pm, level 1.

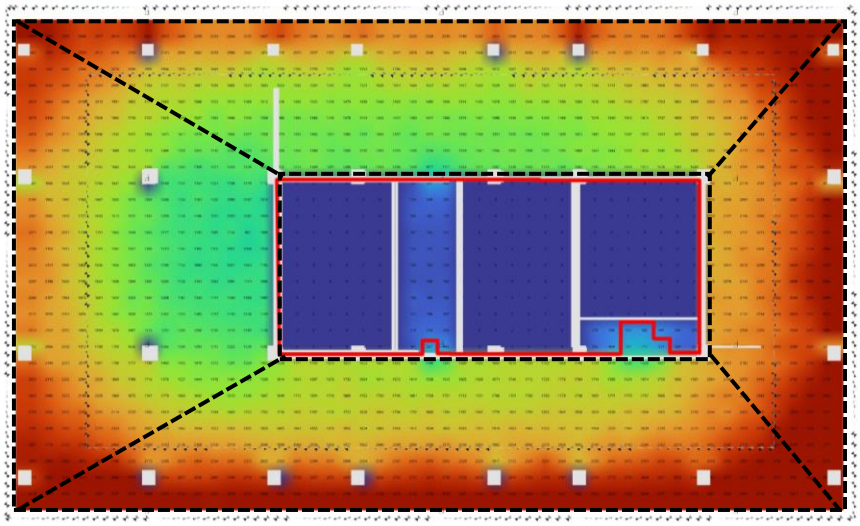

Figure 142: Pattern C, 21st June, 12 pm, level 2.

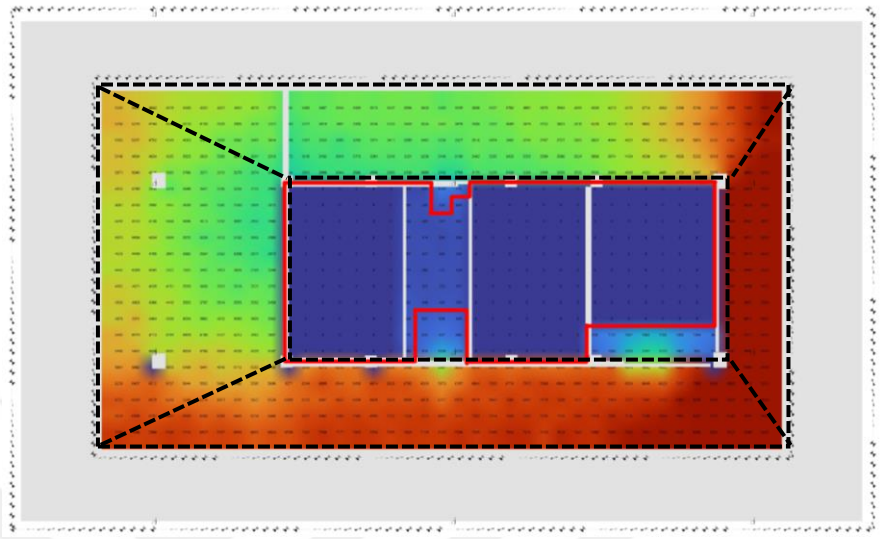

Figure 143: Pattern C, 21st June, 12 pm, level 3.

a.3 Summer Daylight at 2 pm

In comparison to the base case model, this façade pattern increases lux value received on all four wings and on the inner deeper parts of the floor (Figure 143). The average lux on level one is 1952 lux, and the median value is 1376 lux. The average lux on level two is 1668 lux, and the median value is 1819 lux (figure 144). The average lux on level three is 3664 lux, and the median value is 3861 lux (figure 145).

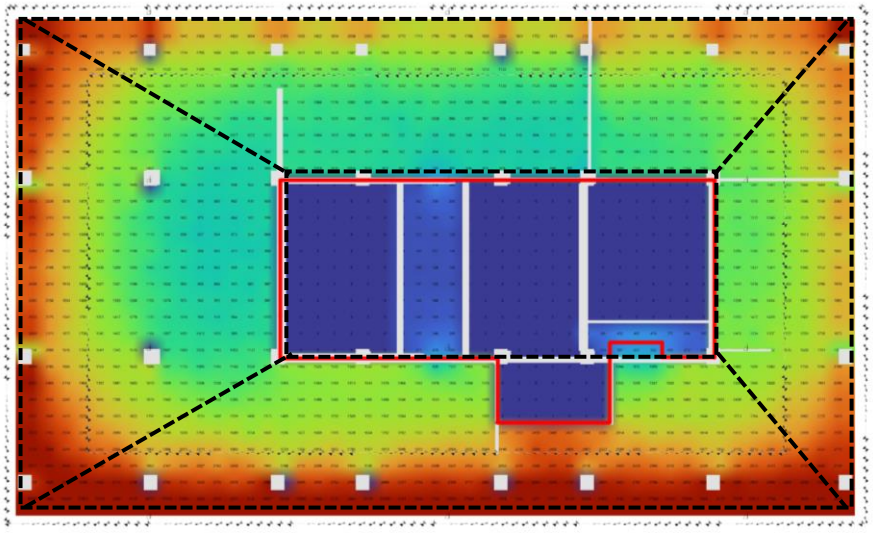

Figure 144: Pattern C, 21st June, 2 pm, level 1.

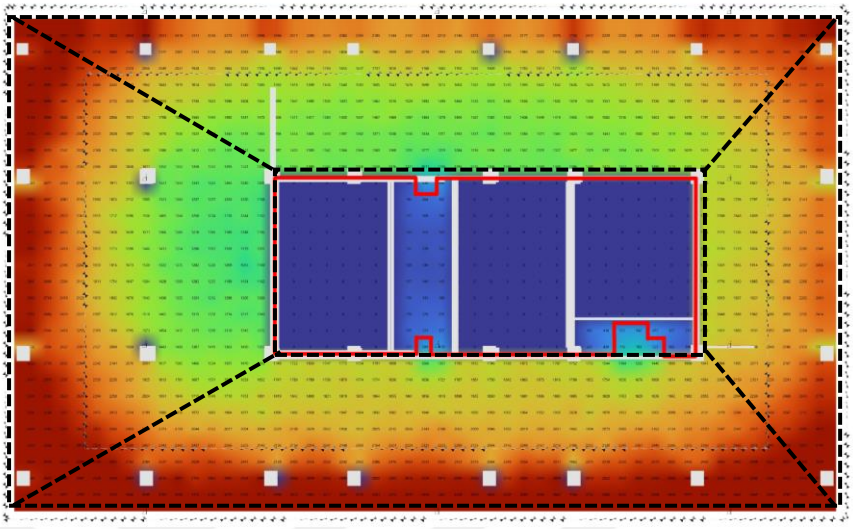

Figure 145: Pattern C, 21st June, 2 pm, level 2.

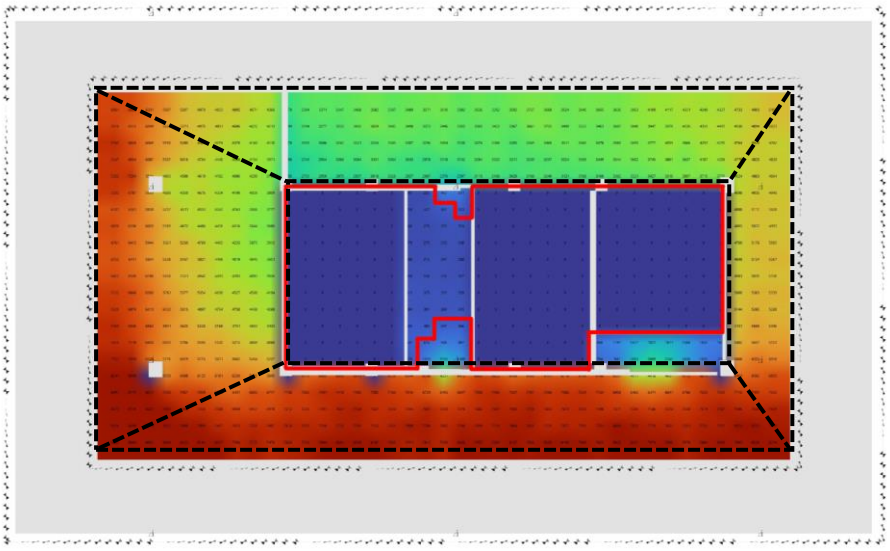

Figure 146: Pattern C, 21st June, 2 pm, level 3.

b- Winter Daylight graphs:

b.1 Winter Daylight at 10 am

In comparison to the base case model, this façade pattern reduced the value of lux value received on all four wings (Figure 146). The average lux on level one is 248 lux, and the median value is 219 lux. The average lux on level two is 266 lux, and the median value

is 254 lux (figure 147). The average lux on level three is 431 lux, and the median value is 531 lux (figure 148).

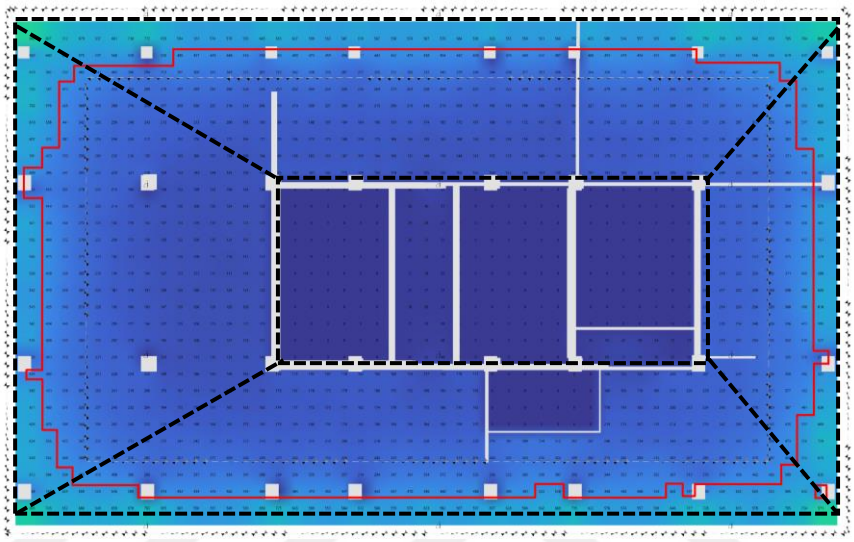

Figure 147: Pattern C, 21st December, 10 am, level 1.

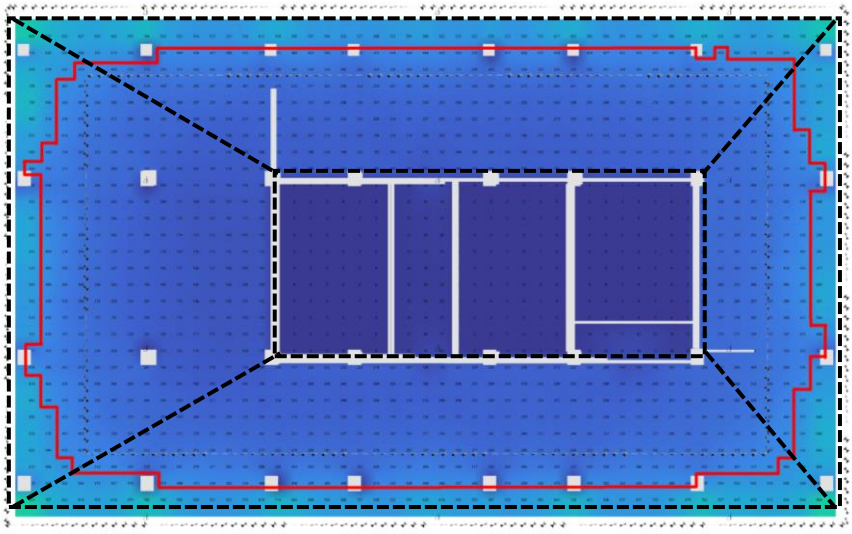

Figure 148: Pattern C, 21st December, 10 am, level 2.

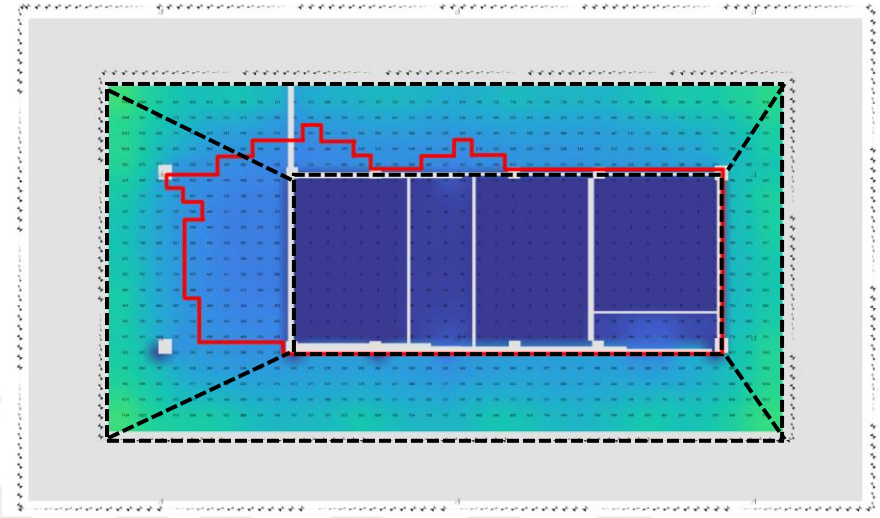

Figure 149: Pattern C, 21st December, 10 am, level 3.

b.2 Winter Daylight at 12 pm

The average lux on level one is 412 lux, and the median value is 364 lux (Figure 149). The average value for pattern C on the first level, is lower than base case model, but the median value is higher. The average lux on level two is 442 lux, and the median value is 423 lux (figure 150). The average lux on level three is 717 lux, and the median value is 876 lux (figure 151).

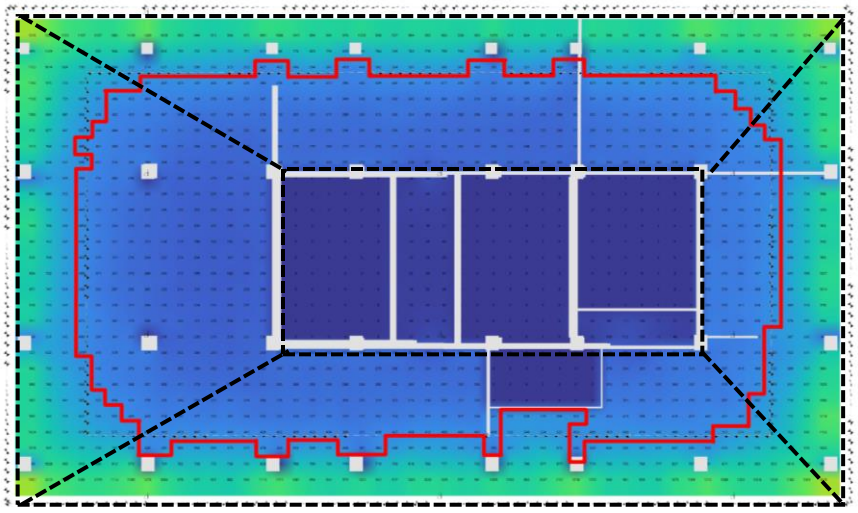

Figure 150: Pattern C, 21st December, 12 pm, level 1.

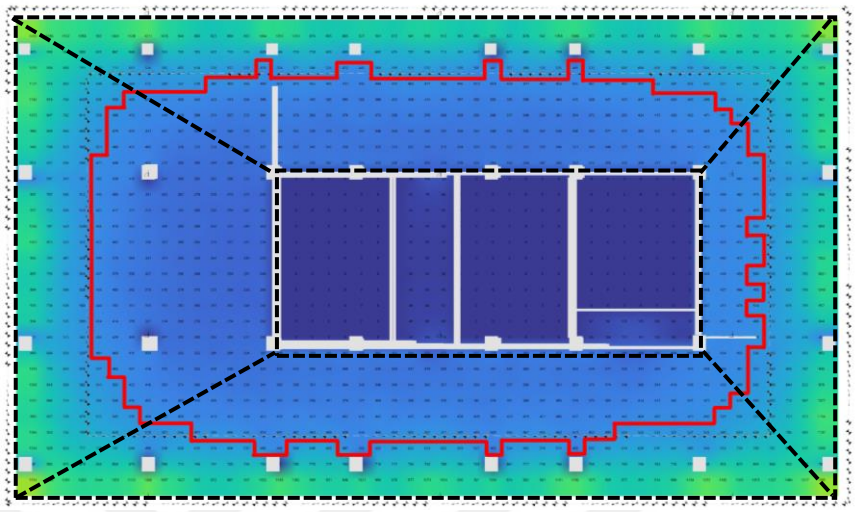

Figure 151: Pattern C, 21st December, 12 pm, level 2.

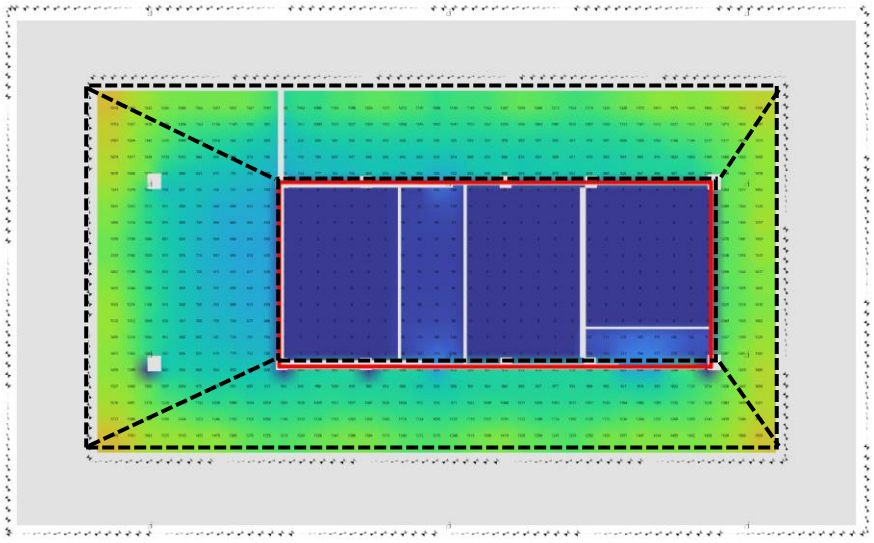

Figure 152: Pattern C, 21st December, 12 pm, level 3.

b.3 Winter Daylight at 2 pm

The average lux on level one is 406 lux, and the median value is 356 lux (Figure 152). The average lux on level two is 435 lux, and the median value is 417 lux (figure 153). The average lux on level three is 706 lux, and the median value is 861 lux (figure 154).

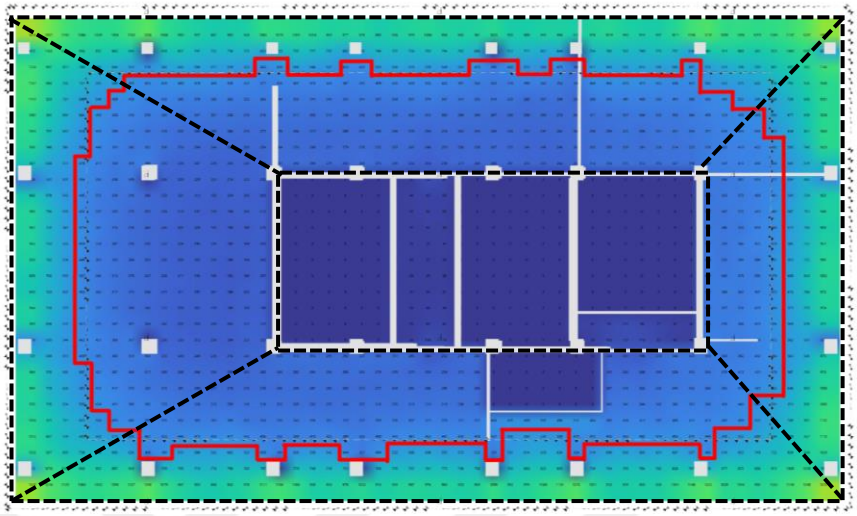

Figure 153: Pattern C, 21st December, 2 pm, level 1.

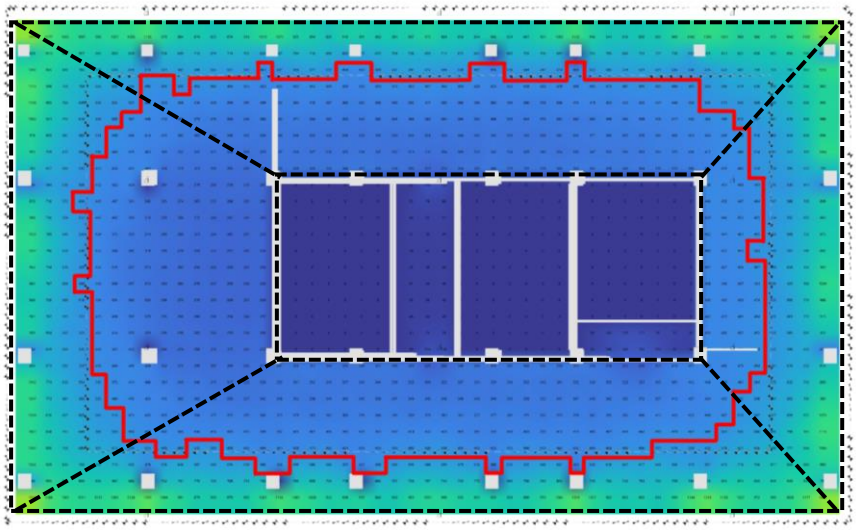

Figure 154: Pattern C, 21st December, 2 pm, level 2.

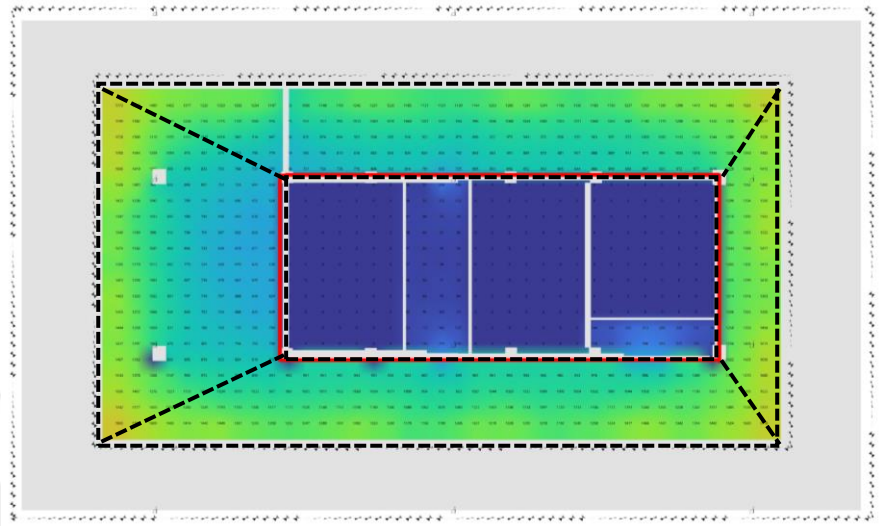

Figure 155: Pattern C, 21st December, 2 pm, level 3.

5.4.5 Type-D Facade Building Model

a- Summer Daylight graphs:

a.1 Summer Daylight at 10 am

The average lux on level one is 2655 lux, and the median value is 1183 lux (Figure 155). The average lux on level two is 2723 lux, and the median value is 1740 lux (figure 156). The average lux on level three is 4715 lux, and the median value is 3154 lux (figure 157).

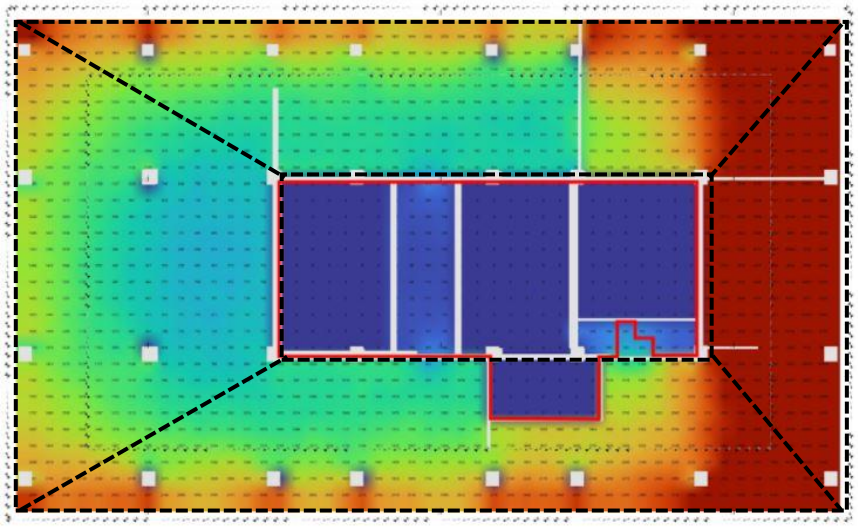

Figure 156: Pattern D, 21st June, 10 am, level 1.

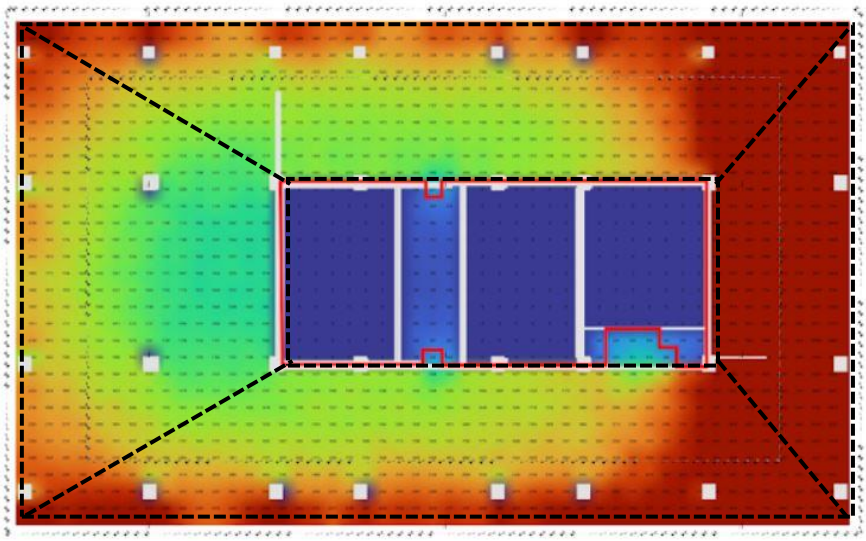

Figure 157: Pattern D, 21st June, 10 am, level 2.

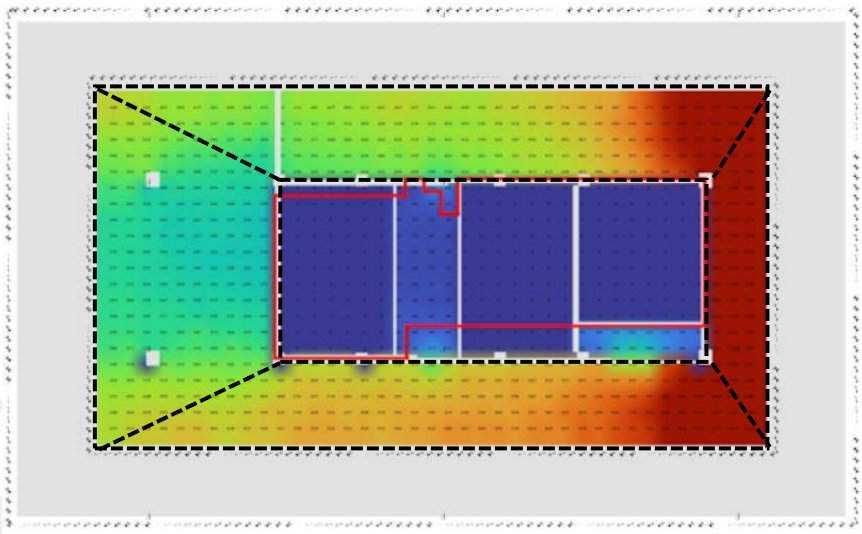

Figure 158: Pattern D, 21st June, 10 am, level 3

a.2 Summer Daylight at 12 pm

The average lux on level one is 1829 lux, and the median value is 1497 lux (Figure 158). The average lux on level two is 1933 lux, and the median value is 2089 lux (figure 159). The average lux on level three is 4085 lux, and the median value is 4115 lux (figure 160).

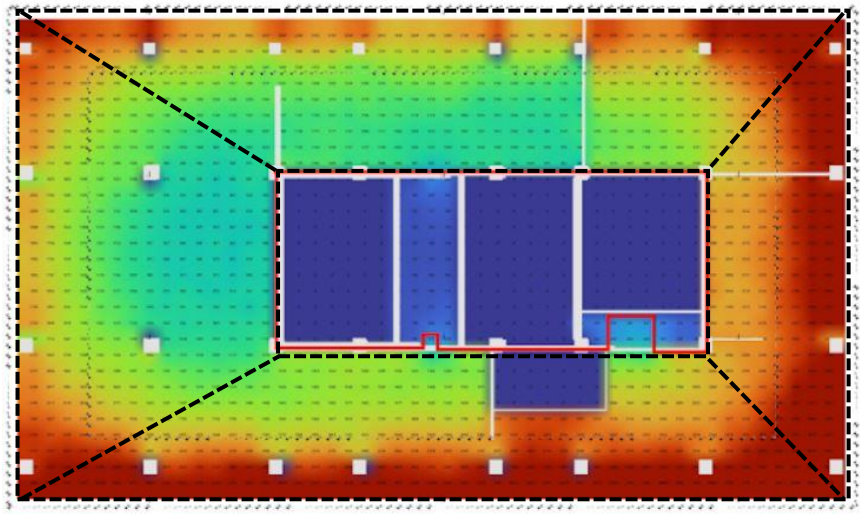

Figure 159: Pattern D, 21st June, 12 pm, level 1.

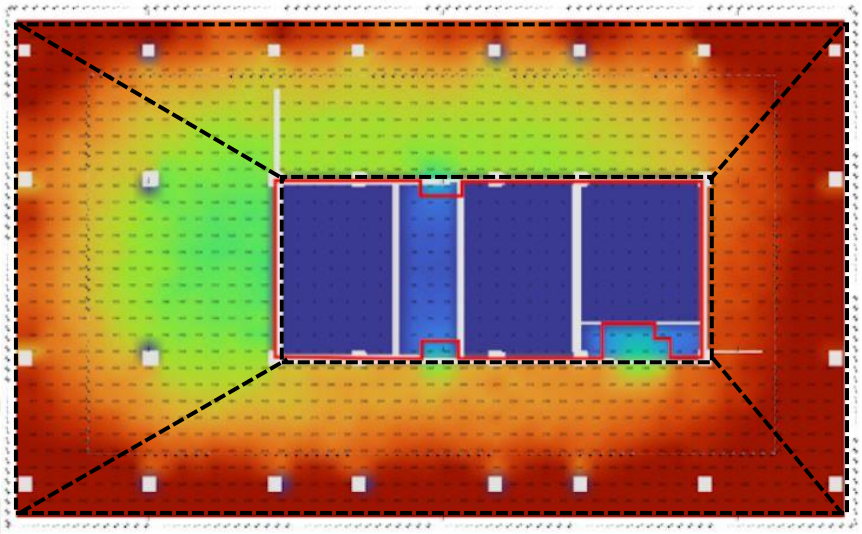

Figure 160: Pattern D, 21st June, 12 pm, level 2.

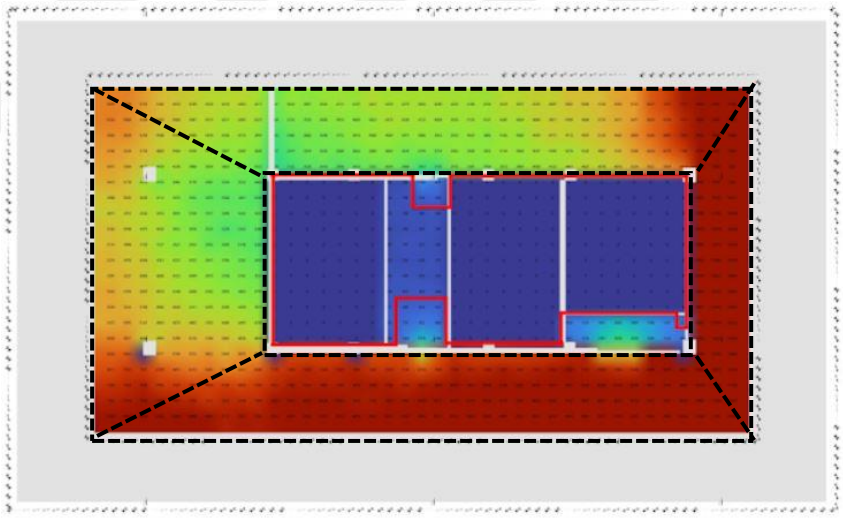

Figure 161: Pattern D, 21st June, 12 pm, level 3.

a.3 Summer Daylight at 2 pm

The average lux on level one is 2235 lux, and the median value is 1569 lux (Figure 161). The average lux on level two is 1971 lux, and the median value is 2137 lux (figure 162). The average lux on level three is 4241 lux, and the median value is 4439 lux (figure 163).

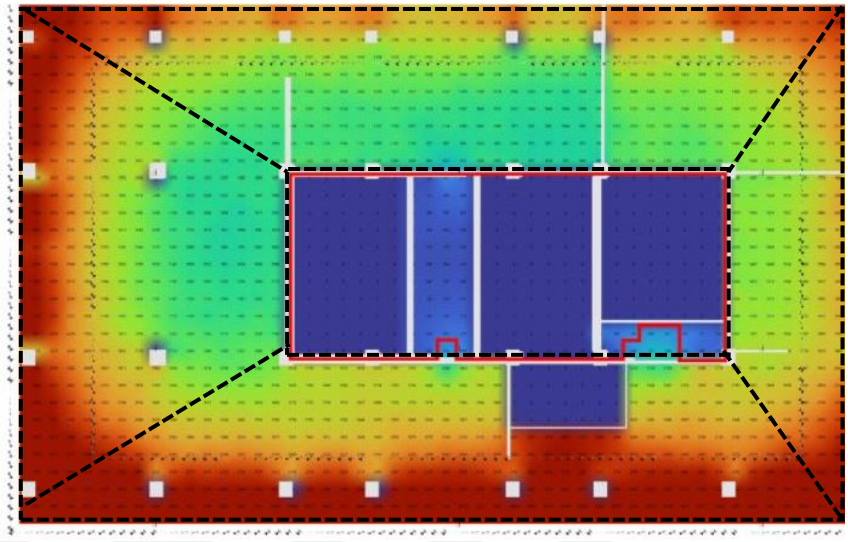

Figure 162: Pattern D, 21st June, 2 pm, level 1.

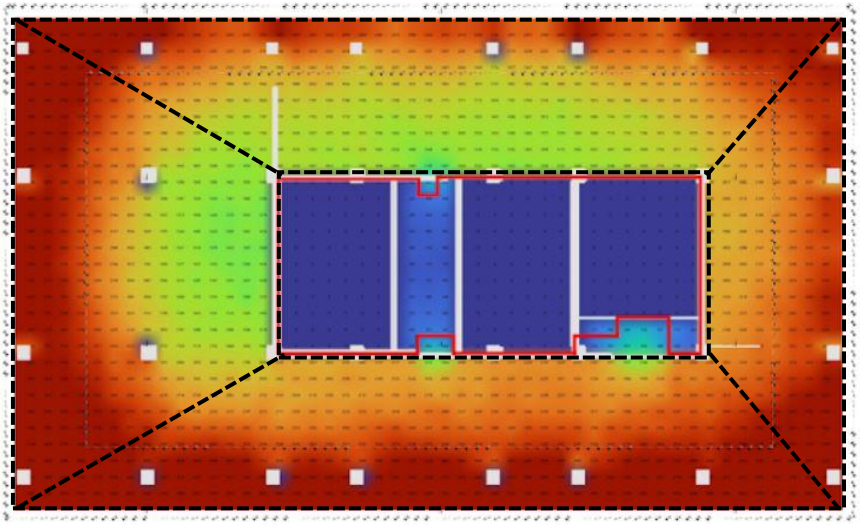

Figure 163: Pattern D, 21st June, 2 pm, level 2.

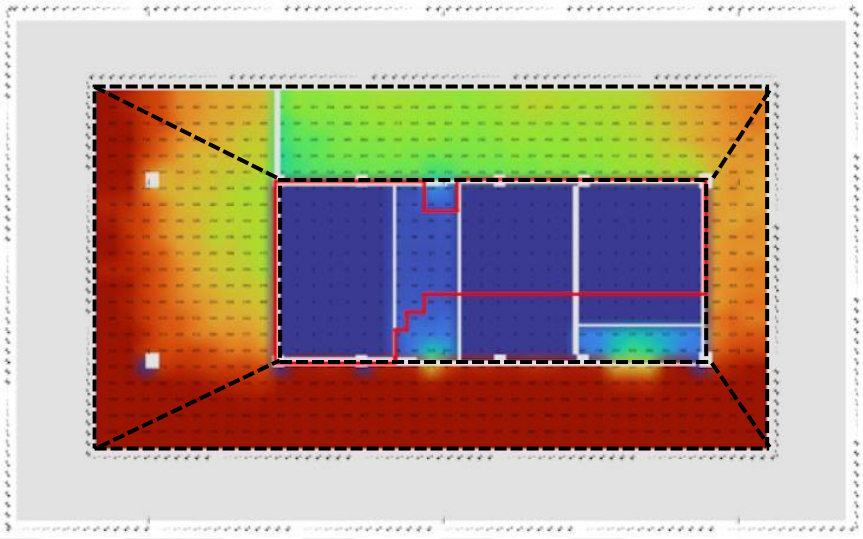

Figure 164: Pattern D, 21st June, 2 pm, level 3.

b- Winter Daylight graphs:

b.1 Winter Daylight at 10 am

The average lux on level one is 294 lux, and the median value is 259 lux (Figure 164). The average lux on level two is 311 lux, and the median value is 299 lux (figure 165). The average lux on level three is 500 lux, and the median value is 607 lux (figure 166).

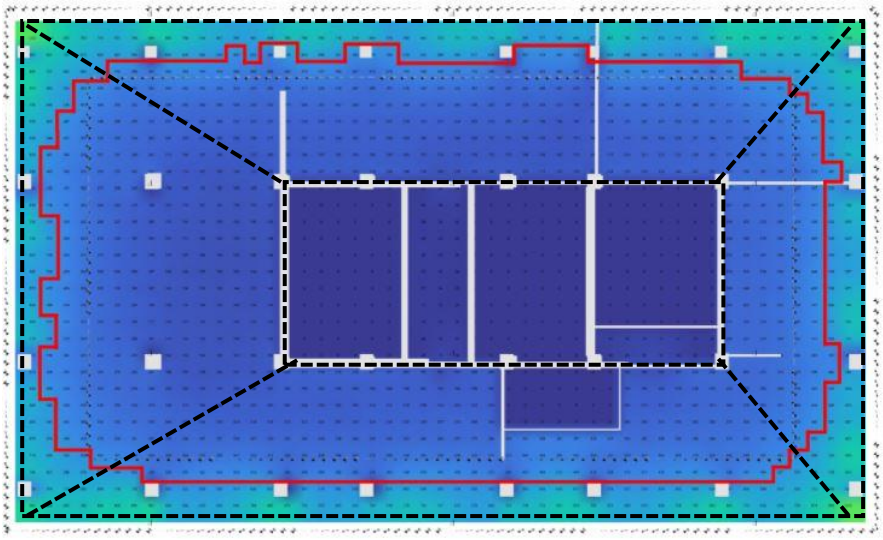

Figure 165: Pattern D, 21st December, 10 am, level 1.

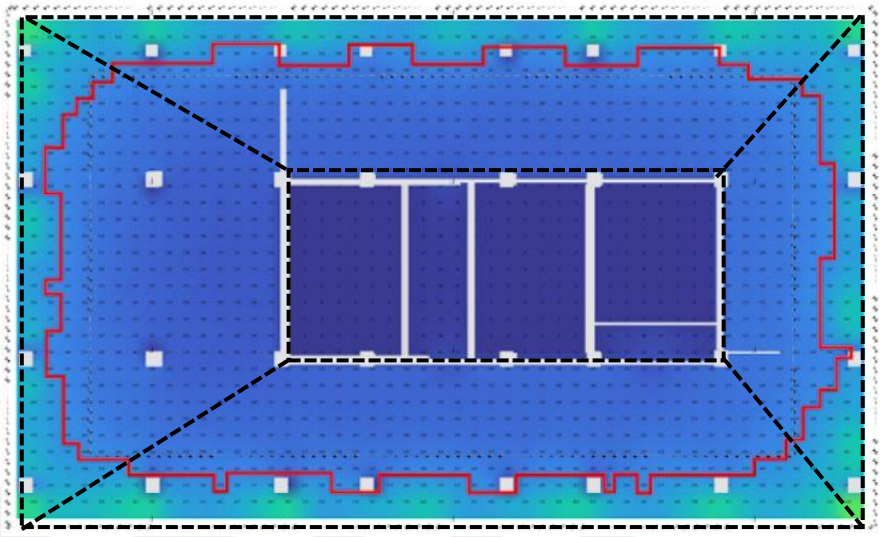

Figure 166: Pattern D, 21st December, 10 am, level 2.

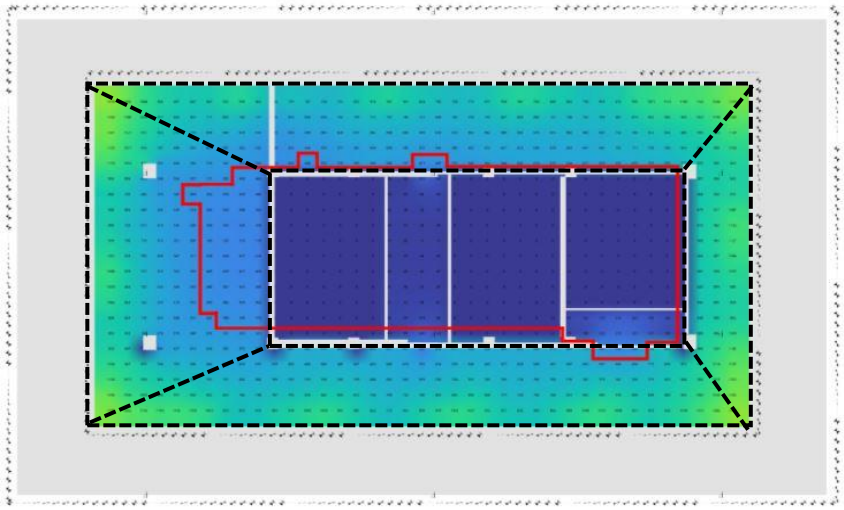

Figure 167: Pattern D, 21st December, 10 am, level 3.

b.2 Winter Daylight at 12 pm

The average lux on level one is 448 lux, and the median value is 431 lux (Figure 167). The average lux on level two is 517 lux, and the median value is 498 lux (figure 168).The average lux on level three is 833 lux, and the median value is 1000 lux (figure 169).

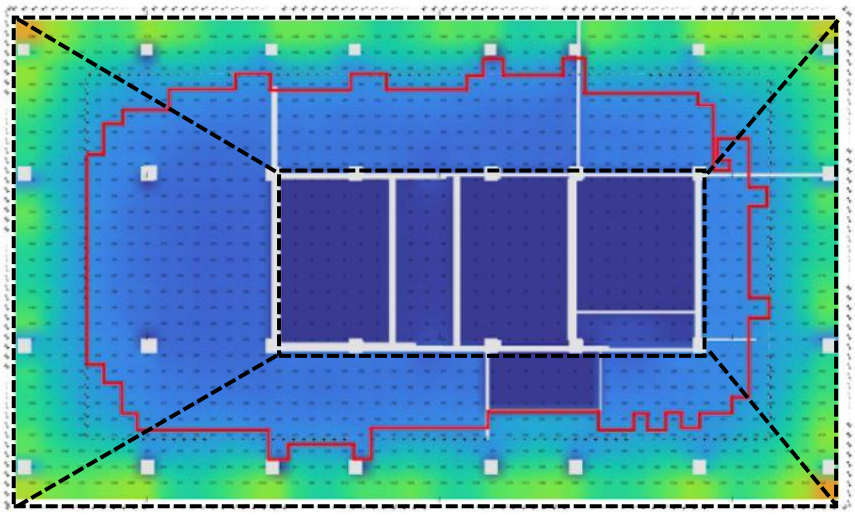

Figure 168: Pattern D, 21st December, 12 pm, level 1.

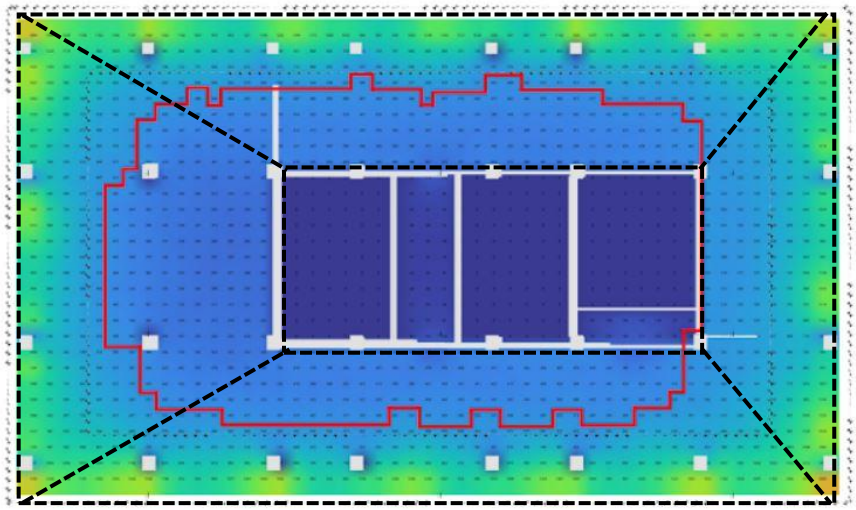

Figure 169: Pattern D, 21st December, 12 pm, level 2.

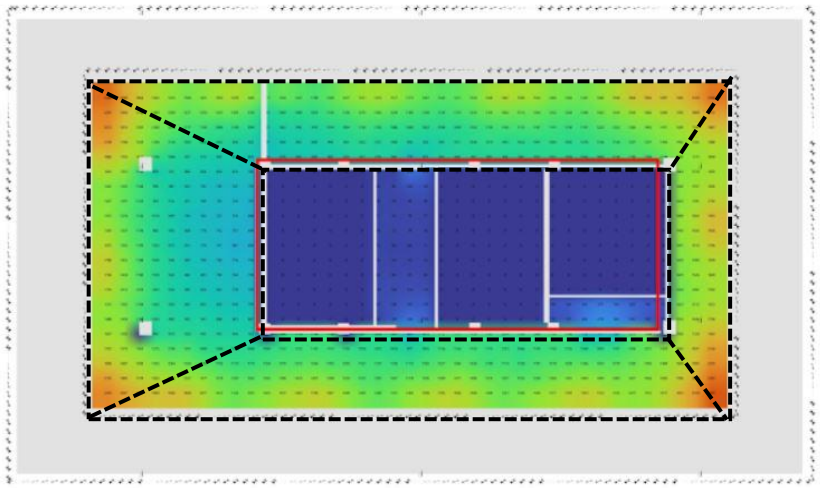

Figure 170: Pattern D, 21st December, 12 pm, level 3.

b.3 Winter Daylight at 2 pm

The average lux on level one is 481 lux, and the median value is 426 lux (Figure 170). The average lux on level two is 509 lux, and the median value is 489 lux (figure 171). The average lux on level three is 820 lux, and the median value is 990 lux (figure 172).

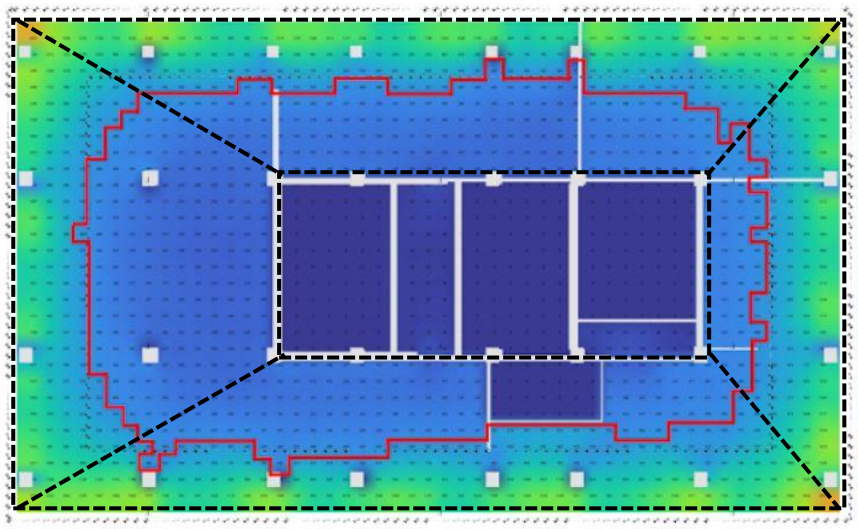

Figure 171: Pattern D, 21st December, 2 pm, level 1.

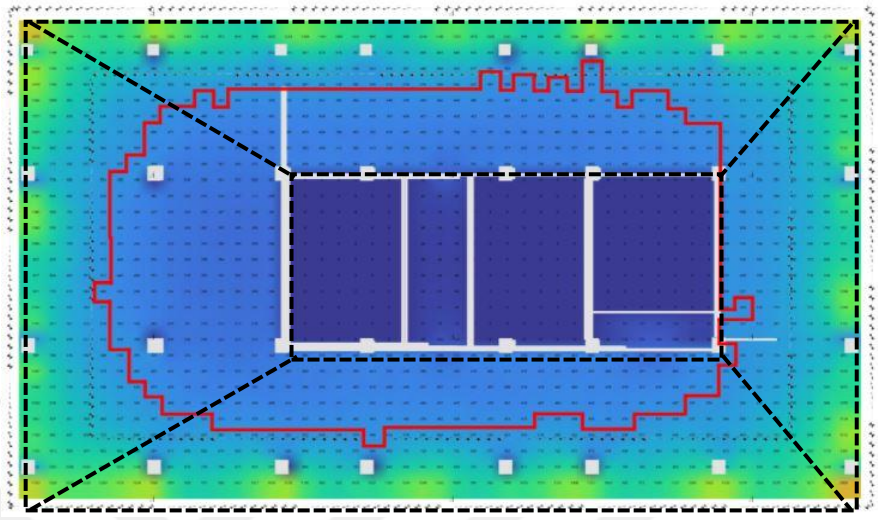

Figure 172: Pattern D, 21st December, 2 pm, level 2.

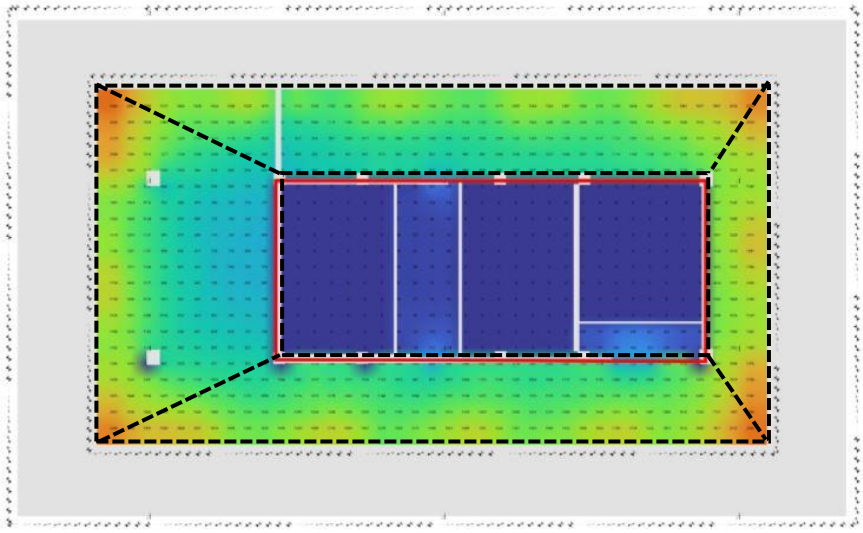

Figure 173: Pattern D, 21st December, 2 pm, level 3.

5.4.5 Overall Daylighting Simulation

According to the summer daylight simulation numerical values in Table 16, all four façade pattern proposals have increased the average values of the daylight of the original base case model received during the three different timings in the day, except for a few cases during 10 am on the first and second level. However, all four façade patterns increased the

median daylighting values unanimously, without any exceptions. It can be related to the fact that the different solid to the void ratio of each four façade iterations have allowed the distribution of more daylight towards the deeper parts of the office resulted in increasing the lux value and the median value in many cases with few exceptions for all four cases.

On the first level, pattern D scored the highest average daylight value between all four patterns on all three timings of 10 am, 12 pm, and 2 pm. Those average daylight values are higher than the base case model by 23.48%, 44.92%, and 78.23%. Pattern D also scored the highest median daylight value at 12 pm and 2 pm. Those median daylight values are higher than the base case model by 25.69% and 33.53%. The pattern scored a median daylight value of 1183 lux at 10 am, 19.37% higher than the base case model.

Pattern A scored the lowest average daylight value, on the first level, between all four patterns at 12 pm and 2 pm. Those values are higher than the base case model by 23.77% and 40.35%. Pattern A also scored the lowest median daylight value at 12 pm and 2 pm. Those median daylight values are still higher than the base case model by 5.96% and 12%, respectively. The pattern scored average daylight of 4.32% higher than the base model. Pattern A scored the highest median daylight value at 10 am, on the first level is 25.03% higher than the base case model.

Pattern B recorded the lowest average daylight value on the first level, in summer, at 10 am, which is 0.09% lower than the average daylight value of the base case model. Pattern C recorded the lowest median daylight value on the first level, in summer, at 10 am, which is 6.46% higher than the median daylight value of the base case model.

On the second level, pattern D scored the highest average daylight value between all four patterns on all three timings of 10 am, 12 pm, and 2 pm. Those values are higher than the base case model by 15.68%, 31.23%, and 31.75%. Pattern D also scored the highest median daylight value at 10 am, 12 pm, and 2 pm. Those median daylight values are higher than the base case model by 56.76%, 54.28% and 50%.

Pattern A scored the lowest average daylight value, on the second level, between all four patterns at 10am, 12 pm, and 2 pm. The average daylight value, recorded at 10 am, is 11.81% lower than the recorded average daylight value for the base case model. The values recorded at 12 pm and 2 pm are 4.14% and 4.69% higher than the recorded average daylight value for the base case model. Pattern A also scored the lowest median daylight value at 10 am, 12 pm, and 2 pm. Those median daylight values are still higher than the base case model by 24.50%, 21.64%, and 19.09%.

Unlike the first level, pattern C records a decrease in average daylight value on the second level at 10 am. The average daylight value of pattern C at 10 am on the second level is 1.83% less than the average daylight value recorded for the base case model. However, pattern C records average daylight values at 12 pm and 2 pm that are higher than the base case model by 10.59% and 11.50%.

On the third level, between all four patterns, pattern D scored the highest average daylight value on all three timings of 10 am, 12 pm and 2 pm. Those values are higher than the base case model by 178.17%, 108.42%, and 84.79%. Pattern D also scored the highest median daylight value at 10 am, 12 pm, and 2 pm. Those median daylight values are higher than the base case model by 3291.40%, 4741.17% and 5818.67%.

On the third level, pattern A scored the lowest average daylight value between all four patterns at 10 am, 12 pm, and 2 pm. The values recorded are 111.91%, 73.93%, and 53.37% higher than the recorded average daylight value for the base case model. Pattern A also scored the lowest median daylight value at 10 am, 12 pm, and 2 pm. Those median daylight values are still higher than the base case model by 2707.53%, 3971.76%, and 4910.67%.

The different façade designs provided different average daylight values. All four patterns record an increase of average and median daylight values on three levels, with some exceptions for the average daylight value for pattern A on the second level at 10 am. The average daylight value for pattern B on the first and second level at 10 am. The average daylight value of pattern C on the second level at 10 am. The third level records the highest increase in average and median daylight values.

Table 16: summer Daylight simulation results, 21st of June, (red is the highest value and green is the lowest value between the four façade patterns).

			Base Case Study	Pattern A	Pattern B	Pattern C	Pattern D
Level 1	**Average Daylight Value (Lux)**	**10 am**	2150	2243	2148	2273	2655
		12 pm	1262	1562	1615	1607	1829
		2 pm	1254	1760	2030	1952	2235
	Average Daylight Difference %	**10 am**	-	+4.32	-0.09	+5.72	+23.48
		12 pm	-	+23.77	+27.97	+27.33	+44.92
		2 pm	-	+40.35	+61.88	+55.66	+78.23
	Median Daylight (Lux)	**10 am**	991	1239	1066	1055	1183
		12 pm	1191	1262	1339	1314	1497
		2 pm	1175	1316	1426	1376	1569
	Median Daylight	**10 am**	-	+25.03	+7.57	+6.46	+19.37
		12 pm	-	+5.96	+12.42	+10.33	+25.69

	Difference %	**2 pm**	-	+12	+21.36	+17.11	+33.53
Level 2	**Average Daylight Value (Lux)**	**10 am**	2354	2076	2220	2311	2723
		12 pm	1473	1534	1663	1629	1933
		2 pm	1496	1566	1707	1668	1971
	Average Daylight Difference %	**10 am**	-	-11.81	-5.69	-1.83	+15.68
		12 pm	-	+4.14	+12.90	+10.59	+31.23
		2 pm	-	+4.68	+14.10	+11.50	+31.75
	Median Daylight (Lux)	**10 am**	1110	1382	1472	1457	1740
		12 pm	1354	1647	1788	1751	2089
		2 pm	1425	1697	1855	1819	2137
	Median Daylight Difference %	**10 am**	-	+24.50	+32.61	+31.26	+56.76
		12 pm	-	+21.64	+32.05	+29.32	+54.28
		2 pm	-	+19.09	+30.18	+27.65	+50.00
Level 3	**Average Daylight Value (Lux)**	**10 am**	1695	3592	3901	3890	4715
		12 pm	1960	3409	3620	3563	4085
		2 pm	2295	3520	3726	3664	4241
	Average Daylight Difference %	**10 am**	-	+111.9	+130.15	+129.50	+178.2
		12 pm	-	+73.93	+84.69	+81.79	+108.4
		2 pm	-	+53.37	+62.35	+59.65	+84.79
	Median Daylight (Lux)	**10 am**	93	2611	2881	2787	3154
		12 pm	85	3461	3662	3592	4115
		2 pm	75	3758	3934	3861	4439
	Median Daylight Difference %	**10 am**	-	+2708	+2998	+2897	+3291
		12 pm	-	+3972	+4208	+4126	+4741
		2 pm	-	+4911	+5145.	+5048	+5819

According to the winter daylight simulation numerical values in Table 17 below, all four façade pattern proposals have increased the average values of the daylight of the original base case model received during the three different timings in the day, except for a few cases

on the first and second level. However, all four façade patterns increased the median daylighting values unanimously, without any exceptions.

On the first level, pattern D scored the highest average daylight value between all four patterns on all three timings of 10 am, 12 pm, and 2 pm. Those average daylight values are higher than the base case model by 2.80 %, 0.90%, and 10.57%. Pattern D also scored the highest median daylight value at 10 am, 12 pm, and 2 pm. Those median daylight values are higher than the base case model by 45.51%, 48.62%, and 48.62%.

On the first level, pattern A scored the lowest average daylight value between all four patterns at 10 am, 12 pm, and 2 pm. Those values are lower than the base case model by 17.83%, 12.16%, and 11.72%. Pattern A also scored the lowest median daylight value at 10 am, 12 pm, and 2 pm. However, those median daylight values are higher than the base case model by 16.29%, 18.96%, and 17.48%, respectively.

On the second level, pattern D scored the highest average daylight value between all four patterns on all three timings of 10 am, 12 pm, and 2 pm. Those average daylight values are higher than the base case model by 37.00 %, 14.38%, and 13.62%. Pattern D also scored the highest median daylight value at 10 am, 12 pm, and 2 pm. Those median daylight values are higher than the base case model by 37.79%, 43.10%, and 41.33%.

On the second level, pattern A scored the lowest average daylight value between all four patterns at 10 am, 12 pm and 2 pm. The pattern recorded an average daylight value of 251 lux at 10 am, higher than the base case model by 10.57%. However, the pattern scored an average daylight value of 418 lux at 12 pm, and 412 lux at 2 pm, which is 7.52% and

8.04% lower than the base case model average daylight values. Pattern A also scored the lowest median daylight value at 10 am, 12 pm, and 2 pm. However, those median daylight values are higher than the base case model by 11.98%, 15.52%, and 15.03%, respectively.

On the third level, pattern D also scored the highest average daylight value on all three times: 10 am, 12 pm, and 2 pm. Those average daylight values are higher than the base case model by 109.21%, 112.50%, and 109.18%. Pattern D also scored the highest median daylight value at 10 am, 12 pm, and 2 pm. Those median daylight values are higher than the base case model by 100017%, 8991%, and 9800%.

Pattern A scored the lowest average daylight value, on the third level, between all four patterns at 10 am, 12 pm, and 2 pm. Those values are higher than the base case model by 74.48%, 77.04%, and 74.23%. Pattern A also scored the lowest median daylight value at 10 am, 12 pm, and 2 pm. However, those median daylight values are higher than the base case model by 8350%, 7582%, and 8220%, respectively.

The different façade designs provided different average daylight values during winter. All four patterns record an increase of average and median daylight values on three levels, except for the average daylight value for patterns A, B and C on the first and second levels. All four patterns increased the median daylight on all three levels significantly. The third level records the highest increase in average and median daylight values.

Table 17: Winter Daylight simulation results, 21st of December, (red is the highest value and green is the lowest value between the four façade patterns).

	Base Case Study	**Pattern A**	**Pattern B**	**Pattern C**	**Pattern D**

Level 1	**Average Daylight Value (Lux)**	**10 am**	286	235	256	248	294
		12 pm	444	390	426	412	448
		2 pm	435	384	418	406	481
	Average Daylight Difference %	**10 am**	-	-17.83	-10.49	-13.29	+2.80
		12 pm	-	-12.16	-4.05	-7.21	+0.90
		2 pm	-	-11.72	-4.00	-6.67	+10.57
	Median Daylight (Lux)	**10 am**	178	207	226	219	259
		12 pm	290	345	376	364	431
		2 pm	286	336	367	356	426
	Median Daylight Difference %	**10 am**	-	+16.29	+26.97	+23.03	+45.51
		12 pm	-	+18.96	+29.66	+25.52	+48.62
		2 pm	-	+17.48	+28.32	+24.48	+48.95
Level 2	**Average Daylight Value (Lux)**	**10 am**	227	251	269	266	311
		12 pm	452	418	448	442	517
		2 pm	448	412	440	435	509
	Average Daylight Difference %	**10 am**	-	+10.57	+18.50	+17.18	+37.00
		12 pm	-	-7.52	-0.88	- 2.21	+14.38
		2 pm	-	-8.04	-1.79	-2.90	+13.62
	Median Daylight (Lux)	**10 am**	217	243	258	254	299
		12 pm	348	402	430	423	498
		2 pm	346	398	422	417	489
	Median Daylight Difference %	**10 am**	-	+11.98	+18.89	+17.05	+37.79
		12 pm	-	+15.52	+23.56	+21.55	+43.10
		2 pm	-	+15.03	+21.97	+20.52	+41.33
Level 3	**Average Daylight Value (Lux)**	**10 am**	239	417	435	431	500
		12 pm	392	694	724	717	833
		2 pm	392	683	714	706	820
	Average Daylight Difference %	**10 am**	-	+74.48	+82.01	+80.33	+109.2
		12 pm	-	+77.04	+84.69	+82.91	+112.5
		2 pm	-	+74.23	+82.14	+80.10	+109.2
		10 am	6	507	528	531	607

	Median Daylight (Lux)	**12 pm**	11	845	878	876	1000
		2 pm	10	832	864	867	990
	Median Daylight Difference %	**10 am**	-	+8350	+8700	+8750	+10017
		12 pm	-	+7582	+7882	+7864	+8991
		2 pm	-	+8220	+ 8540	+8570	+9800

All average and median values are presented in figures 173, 174, 175 and 176 for comparison between each façade pattern on each level. The average and median daylight differences during summer and winter were calculated and summarized in table 18 below.

The average daylight values for the summer season are presentedin figure 173. Compared to the original building results, all four simulations increased their average daylight values, especially on the third level. Pattern D scored the highest average daylight values on all three levels. Pattern A scored the lowest average daylight values on all three levels compared to the other four patterns (figure 173).

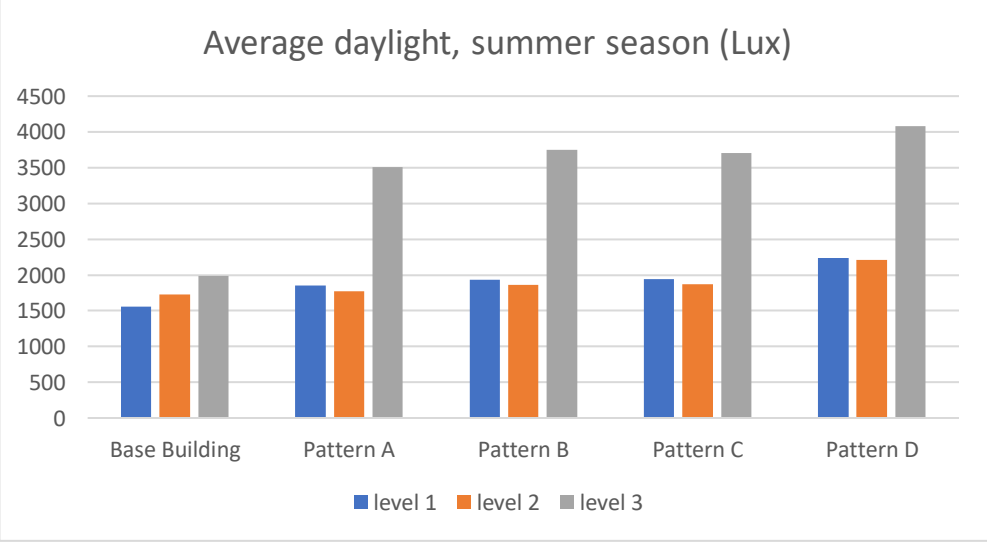

Figure 174: Average values of each level, during summer.

The median daylight values for the summer season are represented in figure 174. Compared to the original building results, all four simulations increased their median daylight values, especially on the third level. Pattern D scored the highest median daylight values on all three levels. Pattern A scored the lowest median daylight values on all three levels compared to the other four patterns (figure 174).

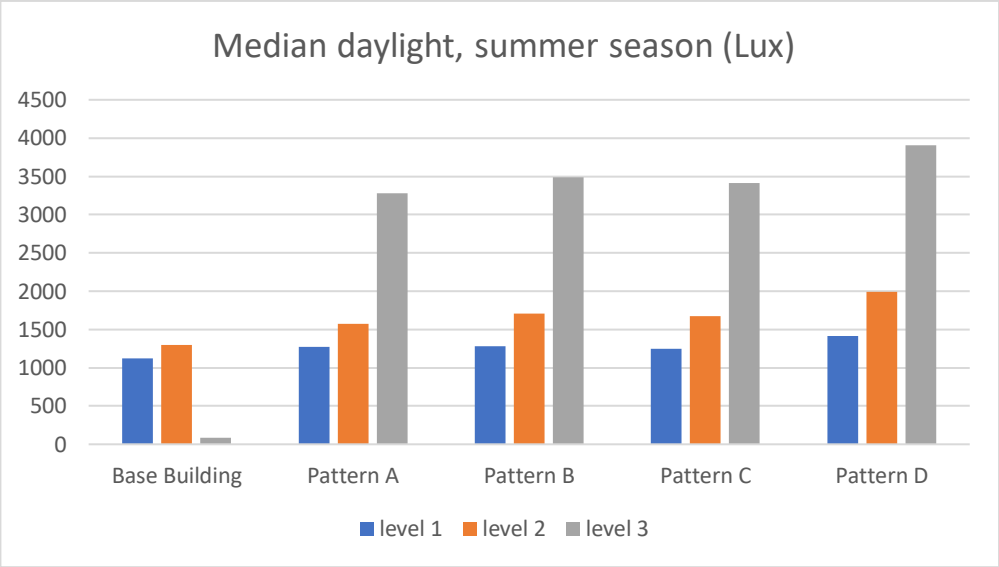

Figure 175: Median values of each level, during summer.

The average daylight values for the winter season were compared in figure 175. Compared to the original building results, all four simulations increased their average daylight values on the third level. Pattern D scored the highest average daylight values on all three levels. Pattern A scored the lowest average daylight values on all three levels compared to the other four patterns (figure 175). Pattern A, B, and C provided a lower average daylight value than the base case building on the first level. Pattern A recorded a lower average daylight value than the base case building on the second level.

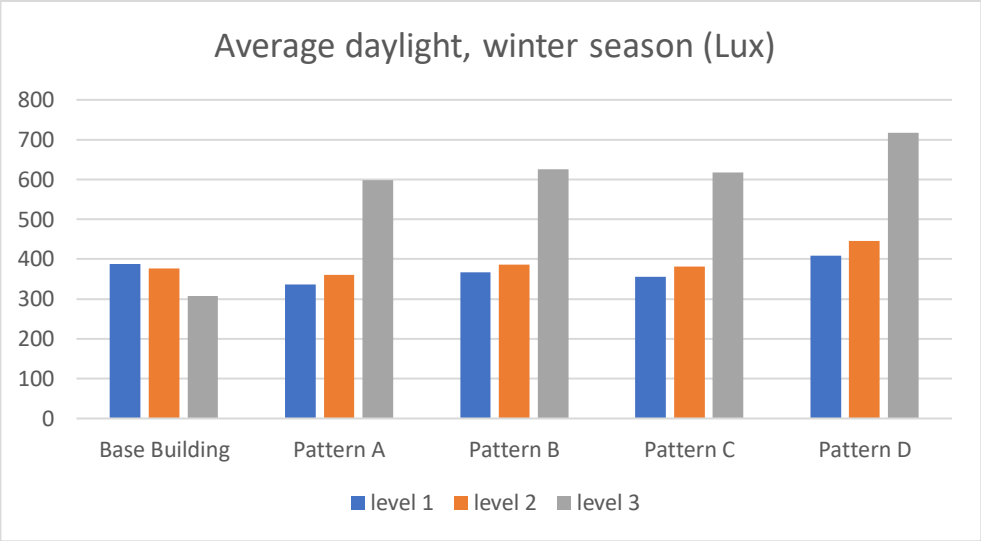

Figure 176: Average values of each level, during winter.

The median daylight values for the winter season were compared in figure 176. Compared to the original building results, all four simulations increased their median daylight values, especially on the third level. Pattern D scored the highest median daylight values on all three levels. Pattern A scored the lowest median daylight values on all three levels compared to the other four patterns (figure 176). The median daylighting value on the third level on all four patterns increased significantly from 9 lux to 500 lux.

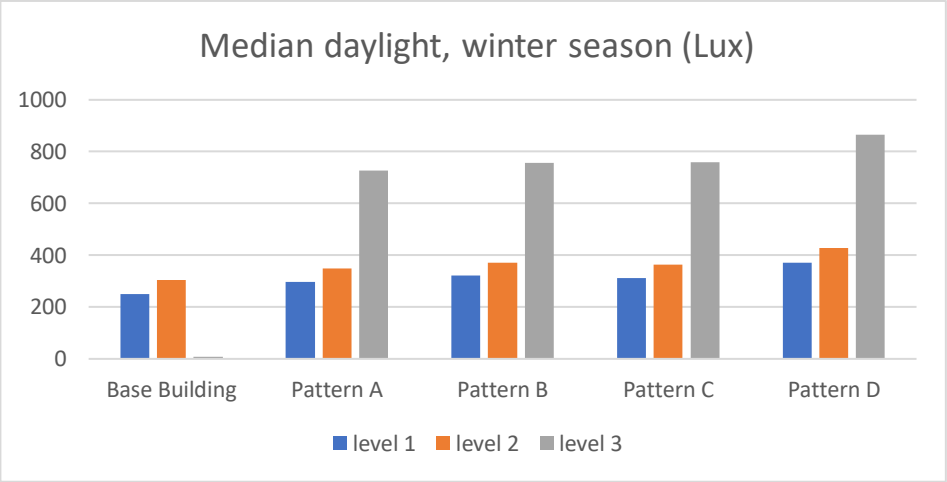

Figure 177: Median values of each level during winter.

The average and median daylight differences during summer and winter were calculated and summarized in table 18 below for each floor. Those percentages are presented to compare each façade pattern on all three levels to study their effect on the entire floor during the day.

According to daylight data calculated in table 18, during summer, pattern A provides the lowest increase of average daylight percentage on all levels during the day. The pattern scored an increase of 22.81%, 6.75%, and 79.73%, respectively. Pattern A also scored the lowest increase in median daylight percentage during the day on all levels. The pattern recorded an increase of 11.3%, 21.74%, and 3863.32%, respectively.

Pattern D provides the highest increase in average and median daylight percentage amongst all four patterns, on all levels during the entire day in summer. The pattern scored an increase of 48.88%, 78.66%, and 123.79% in average daylight value, respectively. The

pattern also recorded the highest increase in median daylight percentage during the entire day on all levels. The pattern recorded a rise of 26.20%, 53.68%, and 4617.08%, respectively.

Both patterns B and C recorded a higher average and median result than pattern A and a lower result than pattern D on all levels during the summer. Pattern B recorded a higher increase in average and median daylight values than pattern C on all levels. Pattern B scored average daylight of 29.92%, 7.10%, and 92.49, respectively. The pattern also scored median daylight of 13.78%, 31.61%, and 4117.14%.

Pattern C recorded an average daylight increase of 29.57% on the first level, 6.88% on the second level, and 90.31% on the third level. The pattern recorded median daylight values of 13.4% on the first level, 29.41% on the second level, and 4023.55% on the third level.

According to daylight data calculated in table 18, during winter, pattern A provides the lowest values of average daylight percentage on all levels during the entire day. The pattern scored a decrease of 13.90% on the first level, a reduction of 1.66% on the second level, and an increase of 75.25% on the third level. However, pattern A increased the total median daylight average on all three levels and scored the lowest increase in median daylight percentage during the entire day between all other patterns. The pattern recorded a rise of 17.58% on the first level, 14.18% on the second level, and 8050.67% on the third level.

Pattern D provides the highest increase in average and median daylight percentage amongst all four patterns, on all levels during the entire day in winter. The pattern scored an increase in average daylight of 4.76%, 21.67%, and 110.30%, respectively. The pattern also

recorded the highest increase in median daylight percentage during the entire day on all levels. The pattern recorded a rise of 47.69%, 40.74%, and 9602.67%, respectively.

Table 18: average and median daylight values of each level.

Daylight difference (per level)		Pattern A	Pattern B	Pattern C	Pattern D
Average daylight difference (summer) %	**Level 1**	+22.81	+29.92	+29.57	+48.88
	Level 2	+6.75	+7.10	+6.88	+78.66
	Level 3	+79.73	+92.40	+90.31	+123.79
Median daylight difference (summer) %	**Level 1**	+11.33	+13.78	+13.4	+26.20
	Level 2	+21.74	+31.61	+29.41	+53.68
	Level 3	+3863.32	+4117.14	+4023.55	+4617.08
Average daylight difference (winter) %	**Level 1**	-13.90	-6.18	-9.05	+4.76
	Level 2	-1.66	+5.28	+4.02	+21.67
	Level 3	+75.25	+82.94	+81.11	+110.30
Median daylight difference (winter) %	**Level 1**	+17.58	+28.32	+24.34	+47.69
	Level 2	+14.18	+21.47	+19.71	+40.74
	Level 3	+8050.67	+8374	+8394	+9602.67

The average and median daylight differences during summer and winter were calculated and summarized in table 19 below for each pattern. The values are presented for comparison between each façade pattern on all three levels and study their effect on the building as a whole.

Table 19: average and median daylight values pf each pattern.

Façade pattern type	Pattern A	Pattern B	Pattern C	Pattern D
Average daylight difference (summer) %	+36.47	+43.14	+42.21	+83.78
Median daylight difference (summer) %	+1299.80	+1387.51	+1354.75	+1565.65
Average daylight difference (winter) %	+19.90	+27.35	+25.36	+45.58
Median daylight difference (winter)%	+2694.14	+2807.93	+2812.68 %	+3230.37

According to the results in table 19, façade Pattern type D recorded the highest average daylight increase rate in both seasons, winter and summer. Between all four patterns, pattern D had the highest increase in the median daylight value in both seasons. The façade type consists of a highly concentrated geometry of 14 panels, each with a width of 400 mm and gap of 200 mm, and rotation of 8° for each panel. The rotation degree is the highest amongst all four iterations. It permits more light to penetrate the façade into the interior spaces.

According to the results in table 19, façade Pattern type A recorded the lowest average daylight increase rate in both seasons, summer and winter. Pattern A had the lowest increase on the median daylight value in summer and winter between all four patterns. This façade type consists of a less concentrated geometry of 7 panels, each with a width of 800 mm and a gap of 400 mm, and rotation of 4° for each panel. The rotation degree is the lowest amongst all four iterations and restricts the light penetrating the façade into the interior spaces.

According to the results in table 19, façade Pattern types B and C resulted in a significant increase in average and median daylight rates in both seasons as well.

The results confirm that the dimensions, orientation, and gaps between the panels have an evidential influence on the admitted daylight levels into the building. The use of wider panels provides a more concentrated area of solid panels and controls the daylight levels admitted into the building. Moreover, the rotation angle plays a significant role too. The higher the rotation degree is, the more light is admitted into the building and the higher the daylight levels are. However, the relationship between daylight levels and the gaps between the panels is still unclear.

5.5 Daylight and Radiation results

A study in figures 177 and 178 was conducted to compare the average radiation values to the average daylight values of patterns A, B, C, and D and their individual effect on the building as a whole.

According to figures 177 and 178, pattern D façade provides the highest average radiation and daylight in summer and winter seasons. However, the data is not as consistent when it comes to patterns A and B. In figure 177, pattern B provides lower average radiation than pattern A but higher average daylight in summer. On the other hand, pattern A in figure 178 provides lower average radiation than pattern B and a lower average daylight in winter. In both seasons, summer and winter, Pattern B provide higher average daylighting than pattern C and lower average radiation. The figures are more consistent in both seasons for patterns C and D.

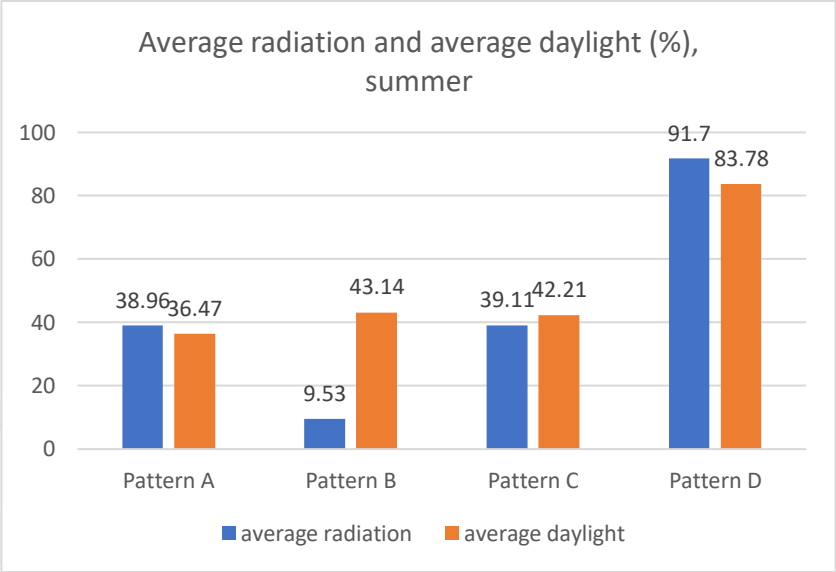

Figure 178: Average radiation and average daylight, summer.

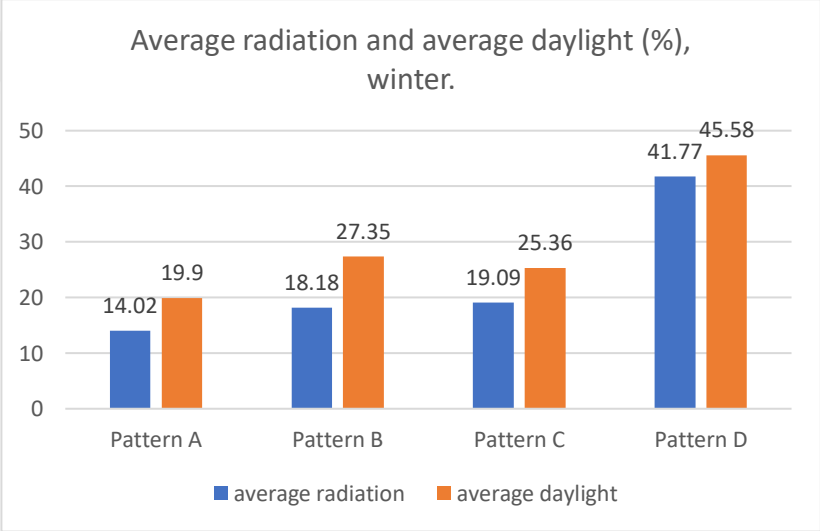

Figure 179: Average radiation and average daylight, winter.

5.6 Proposed model

According to the study conducted and the analysis of each wing on each floor of the building, the following tables below were proposed to present a high-performance model that would maintain indoor thermal comfort within an acceptable range and provide the recommended illuminance needed for the office building. The tables highlight and recommend the best

performance on each side of the building. In some cases, some patterns share similar results on the same façade side.

Table 20: Model proposal for best thermal performance.

Radiation performance		East	South	west	North
Level 1	**Summer**	Pattern c	Pattern c	Pattern c	Pattern a Pattern c
	Winter	Pattern c	Pattern c	pattern c	Pattern a Pattern c
Level 2	**Summer**	Pattern c	Pattern a Pattern c	Pattern c	Pattern c
	Winter	Pattern c	Pattern a Pattern c	Pattern c	Pattern c
Level 3	**Summer**	Pattern c	Pattern c	Pattern c	Pattern c
	Winter	Pattern c	Pattern a Pattern c	Pattern c	Pattern c

Table 21: Model proposal for best daylight performance.

Daylight performance			East	South	west	North
Level 1	**10 am**	**Summer**	Pattern c	Pattern c	Pattern c	Pattern c
		Winter	Pattern d	Pattern d	Pattern d	Pattern d
	12 pm	**Summer**	Pattern c	Pattern c	Pattern c	Pattern c
		Winter	Pattern a	Pattern a	Pattern a	Pattern a
	2 pm	**Summer**	Pattern c	Pattern c	Pattern c	Pattern c
		Winter	Pattern c	Pattern c	Pattern c	Pattern c
Level 2	**10 am**	**Summer**	Pattern c	Pattern a- c	Pattern a- c	Pattern a- c
		Winter	Pattern d	Pattern d	Pattern d	Pattern d
	12 pm	**Summer**	Pattern c	Pattern c	Pattern c	Pattern a- c
		Winter	Pattern c	Pattern c	Pattern c	Pattern c
	2 pm	**Summer**	Pattern c	Pattern c	Pattern c	Pattern c
		Winter	Pattern c	Pattern c	Pattern c	Pattern c
Level 3	**10 am**	**Summer**	Pattern c	Pattern c	Pattern c	Pattern c
		Winter	Pattern c	Pattern c	Pattern d	Pattern c
	12 pm	**Summer**	Pattern c	Pattern c	Pattern c	Pattern a- c
		Winter	Pattern d	Pattern d	Pattern c	Pattern d
	2 pm	**Summer**	Pattern c	Pattern c	Pattern c	Pattern a- c
		Winter	Pattern a	Pattern a	Pattern a	Pattern a

CHAPTER VI

CONCLUSION

Providing human comfort and occupants' satisfaction is a crucial design factor that ought to be considered during the early design stages. The indoor thermal quality affects the comfort levels and the environmental balance indoors. High radiation values tend to negatively influence the productivity of the occupants due to excessive heating. It will also increase the energy consumption within the building, relying on mechanical cooling alternatives.

DSFs maintain a significant impact on indoor environmental quality due to their effects on the building's thermal performance. This research studies the different thermal and daylight performances of DSF and encourages the application of DSF in temperate Mediterranean climates.

The research provides an in-depth literature study on the origin, implementation, classification, and application of DSF in general and on office buildings in particular. The paper also explores the thermal and daylight performance of the different DSFs categories.

The main purpose of this research is to generate a parametric skin façade and analyze the main characteristics and components that contribute to the transmission of solar radiation incident value and daylighting using algorithmic tools.

The methodology investigated generating 3D parametric skin facades using algorithmic modelling tools. The façade iterations explored the changing ratio from solid to

void by manipulating three rules; panel size, rotation, and gaps in-between. The four different iterations were each applied on all facades located all around the four elevations of the building. Environmental performance tools of Ladybug, in Grasshopper, Rhinoceros aided in the assessment of the solar radiation levels on the building and each iteration separately via Energy-Plus weather data files. ClimateStudio plug-in in Rhinocerous aided in studying the daylight performance in the building. The software assessed the available illuminance indoor and calculated total daylight. This simulation aims to determine whether the amount of daylight provided by each façade iteration is sufficient for each office floor.

The codes in this research provided a real-time analysis that contributes to reducing the gap between qualitative and quantitative radiation and daylighting performance studies. It explored the different solar effects on various skin façade iterations applied on the same 3D spatial context to provide virtual graphic and numerical data that visualize the interior environment and contribute to better-informed design choices.

The major challenge in this research is that simulations are prone to error, and any credible verification demands real physical experimentation and verification. That would be an obstacle, especially in the early design stages, as the decisions need to be taken faster. One other vital restriction was that with simulations used, changing the gap distance between the two façade skins did not affect the results as it should. Another main obstacle was acquiring the precise weather data files for the selected city from Energy-Plus, as the software is short in providing weather files for many cities in Turkey. Another restrain that would be considered a major setback for the study would be the learning curve required to learn the software and understand its components. Usually, existing dialogue boxes are available in

other tools that could run the simulation without the need to code the components or set up an entire configuration. This software requires the user to configure parametric components to run a certain simulation. However, once the configuration is complete, it is possible to use it repeatedly on many other models and projects. One other setback is that there is no method or technique in the code that could aid in determining the radiation value at a certain point on the plan. The simulation provides the numerical radiation value for every point on the mesh, but it is not possible to determine the location of each point and refer the value to it on the plan. One other restriction faced during the simulations is that the mesh size is restrained to a certain size, where the software would crash if the mesh size were set to very low values. The last obstacle observed in this research would be that credible verification requires real physical experimentation. The process would be time-consuming, especially in the early design stages, where decisions must be taken faster.

The study demonstrates that breaking the repetition in the pattern through the solid-void ratio will significantly affect the thermal and daylight performance in indoor spaces.

According to the findings, all four different iterations significantly reduced the highest radiation value indoors compared to the original case study model in both seasons. However, the average radiation value was an increase for almost all floors, which is due to the fact that the façade patterns distributed the incoming radiation into the building, reduced the highest value, and allowed the radiation to penetrate deeper areas of the floor plans.

Façade Pattern D resulted in the highest average radiation increase rate in both summer and winter, by 91.7% in summer and 41.77% in winter. It also decreased the highest radiation value by 18.50% in summer and 7.59% in winter. The lowest increase in the average

radiation value and highest radiation value was recorded by Pattern B in the summer season and pattern A in the winter season. Pattern B recorded an increase of average summer radiation by 9.53% and a decrease of the highest radiation value in summer by 32.12%. Pattern A recorded an increase of average winter radiation by 14.02% and a decrease of the highest radiation value in summer by 22.82%.

The results provided model proposals that would contribute to the overall indoor thermal and daylight performance. The proposals selected the façade patterns that provided the best performance on each side of the building

According to the findings, all four different iterations increased the average daylight indoors significantly compared to the original case study model in both seasons. The patterns also increased the median daylight rate for all floors that is due to the fact that the façade patterns distributed the incoming daylight into the building and allowed the light to penetrate deeper areas of the floor plans.

Façade pattern D resulted in the highest average daylight rate and the highest median daylight rate in both seasons, summer and winter. The pattern increased the average daylight rate by 83.78% in summer and 45.58% in winter. The pattern also increased the median daylight rate by 1565.65% in summer and 3230.37% in winter.

Façade pattern A resulted in the lowest average daylight increase rate and the lowest median daylight increase rate in both seasons, summer and winter. The pattern increased the average daylight rate by 36.47% in summer and 19.90% in winter. The pattern also increased the median daylight rate by 1299.80% in summer and 2694.14% in winter.

The results demonstrated and confirmed that the use of wider panels provides higher concentrated solid areas of panels and controls the radiation levels admitted into the building. Moreover, the rotation angle plays a significant role too. The higher the rotation degree is, the more light is admitted into the building and the higher the radiation levels are. However, the relationship between radiation levels and the gaps between the panels is still unclear.

Although the simulation was run for Eskisehir, Turkey, the parametric methodology applied in this research allows the simulation to be conducted anywhere globally, as long as the weather files are available in the Energy-Plus database.

The results establish an example that computational design technologies integrated with performance analysis tools for complex shading elements are essential in understanding incident radiation admission. The results assist in understanding how DSF's different components and iterations affect the environmental, thermal, and daylight quality in the interior spaces of the building.

Optimizing the façade panels' size, rotation, and gaps between panels and integration with ecological office building would generate wholesome, energy-efficient designs. The DSF would contribute to minimizing thermal radiation at a significant rate and improve the indoor environmental quality and daylighting.

Further studies may explore different gaps of the cavity wall between the outer and inner skin and determine the relationship between available daylight and radiation in

accordance with the different gap parameters. Future studies may interpret different façade ventilation types such as mechanical and mixed.

Further studies can also study the available glare and visual comfort that each façade pattern provides on each side of the building. They may also explore the underlying mathematical concepts in parametric designs and systematically investigate the architectural fields of varying contemporary sciences parameters. Future research should include the digital fabrication, tectonics, and structural performance of the skin façade on different materials while maintaining some constants, such as panel thickness. The studies may also include the various material properties, machine specifications, and performance evaluation. The different results may then be compared, and answer questions related to the skin formation, appearance (size, dimension), and perhaps aesthetics.

Bibliography

[1] B. A. Young, G. Falzone, Z. Wei, G. Sant and L. Pilon, "Reduced-scale experiments to evaluate performance of composite building envelopes containing phase change materials.," *Construction and Building Materials,* pp. 162, 584–595, 2018.

[2] O. Etman, O. Tolba and S. Ezzeldin, "Double skin facades in Egypt between Parametric and Climatic Approaches," in *Computation and Performance-Proceedings of the 31st international conference on Education and Research in Computer Aided Architectural Design in Europe*, Delft, The Netherland, 2013.

[3] Y. K. Cheung, K. W. Chau, K. University of Hong, Tong ji da xue and Zhongguo jian, "International Conference on Tall Buildings," in *Tall buildings: Sixth International Conference on Tall Buildings ; Mini Symposium on Sustainable Cities ; Mini Symposium on Planning, Design and Socio-Economic Aspects of Tall Residential Living Environment, Hong Kong, China, 6-8 December 2005.*, Hong Kong, China, 2005.

[4] M. Shameri, M. Alghoul, O. Elayeb, M. F. Zain, M. Alrubaih, H. Amir and K. Sopian, "Daylighting characterstics of existing double-skin façade office buildings," *Energy and Buildings,* pp. 59, 279-286., 2013.

[5] L. Bellia, F. D. Falco and F. Minichiello, "Effects of solar shading devices on energy requirements of standalone office buildings for Italian climates.," *Applied Thermal Engineering,* pp. 54(1), 190-201, 2013.

[6] S. Mirrahimi, M. F. Mohamed, L. C. Haw, N. L. Ibrahim, W. F. Yusoff and A. Aflaki, "The effect of building envelope on the thermal comfort and energy saving for high-rise buildings in hot–humid climate," *Renewable and Sustainable Energy Reviews,* pp. 53, 1508-1519, 2016.

[7] N. Baker, "Daylight design of buildings," *James & James,* 2002.

[8] A. Tzempelikos, "Advances on daylighting and visual comfort research," *Build. Environ. 113,* p. 1–4, 2017.

[9] H. Plummer, "Light in Japanese Architecture," *A u Pub, Tokyo, Japan,* 1995.

[10] C. Reinhart, "Daylight Performance Predictions, Building Performance Simulation for Design and Operation,," in *Spon Press.*, 2011.

[11] A. Sarkar and S. Bose, "Exploring impact of opaque building envelope components on thermal and energy performance of houses in lower western Himalayans for optimal selection," *Journal of Building Engineering,7,* pp. 170-182, 2016.

[12] ASHRAE, Architectural design impacts, The ASHRAE GreenGuide, second ed., Atlanta: Butterworth-Heinemann, 2006, p. 55–72.

[13] M. Tang, J. Anderson, A. Aksamija and M. Hodge, "Performative Computation-aided Design Optimization," *Enquiry A Journal for Architectural Research,* p. 9(1), 2012.

[14] K. Terzidis, "Algorithms for Visual Design Using the Processing Language," *Wiley Publishing,* 2009.

[15] W. Jabi, "Parametric design for architecture," *Laurence King Publishing,* 2013.

[16] R. Hudson, "Strategies for parametric design in architecture: An application of practice led research," *Bath: University of Bath,* 2010.

[17] M. Turrin, P. V. Buelow and R. Stouffs, "). Design explorations of performance driven geometry in architectural design using parametric modeling and genetic algorithms," *Advanced Engineering Informatics, 25(4),* p. 656–675, 2011.

[18] D. Kim and C. Park, "Corrigendum to "Difficulties and limitations in performance simulation of a double skin façade with EnergyPlus"," *Energy and Buildings. 43,* 2012.

[19] G. Ramos and E. Ghisi, "Analysis of daylight calculated using the EnergyPlus programme," *Renewable and Sustainable Energy Reviews,* 2010.

[20] K. Lagios, J. Niemasz and C. Reinhart, "Animated building performance simulation (abps) – linking rhinoceros/grasshopper with radiance/daysim, in: Pproc. Sim-Build," 2010.

[21] J. Gonzalez and F. Fiorito, "Daylight Design of Office Buildings: Optimization of External Solar Shadings by Using Combined Simulation Methods," *Buildings,* 2015.

[22] A. D. Gracia, A. Castell, L. Navarro, E. Oro and L. F. Cabeza, "Numerical modelling of ventilated facades: A review," *Renewable and Sustainable Energy Reviews, 22,* pp. 539-549, 2013.

[23] A. Sherif, H. Sabry, A. El-zafarany, R. Arafa, T. Rakha and M. Anees, "Balancing the energy savings and daylighting performance of external perforated solar screens: Evaluation of screen opening proportions.," 2011.

[24] A. Pino, W. Bustamante, R. Escobar and F. E. Pino, "Thermal and lighting behavior of office buildings in Santiago of Chile," *Energy and Buildings, 47, 441-449,* 2012.

[25] D. A. Chi, D. Moreno and J. Navarro, "Design optimization of perforated solar façades in order to balance daylighting with thermal performance," *Building and Environment, 125, 383-400,* 2017.

[26] S. M. Hosseini, M. Mohammadi and O. Guerra-Santin, "). Interactive kinetic façade: Improving visual comfort based on dynamic daylight and occupant's positions by 2D and 3D shape changes," *Building and Environment, 165, 106396,* 2019.

[27] A. Rashwan, L. E. Gizawi and S. Sheta, "Evaluation of the effect of integrating building envelopes with parametric patterns on daylighting performance in office spaces in hot-dry climate," *Alexandria Engineering Journal, 58(2), 551-557,* 2019.

[28] E. Oesterle, R. D. Lieb, M. Lutz and W. Heusler, Double-Skin Facades: Integrated Planning, Munich,London, New York:: Prestel Pub, 2001.

[29] K. Ismail and C. Salinas, Non-gray radiative convective conductive modeling of a double glass window with a cavity filled with a mixture of absorbing gases, International Journal of Heat and Mass Transfer, 2006, pp. 2972-2983.

[30] C. A. Lui, X. M. Chen and Y. Y. Wei, "Evolution: the Development of Intelligent Double-skin Facades," *Applied Mechanics and Materials Vols 71-78,* pp. pp 1546-1549, 2011.

[31] O. J. Hendriksen, H. Sorensen, A. Svenson and P. Aaqvist, "Double Skin Facades Fashion or a Step Towards Sustainable Buildings," in *Proceedings of ISES*, Eurosun, 2000.

[32] W. Wang, H. Rivard and R. Zmeureanu, "Floor shape optimization for green building design," *Advanced Engineering Informatics,* pp. 20(4), 363-378, 2006.

[33] E. Aljofi, "The potentiality of reflected sunlight through Rawshan screens," in *international conferenece passive low energy cool. Built Environ., Heliotopos Conferences*, Santorini, Greece, 2005.

[34] W. Ding, Y. Hasemi and T. Yamada, "Natural ventilation performance of a double-skin façade with a solar chimney," *Energy and buildings,* 2005.

[35] S. Kim and K. Song, "Determining Photosensor Conditions of a Daylight Dimming Control System Using Different Double-skin Envelope Configurations," *Indoor and Built Environment,* 2007.

[36] A. Chan, T. Chow, K. Fong and Z. Lin, "Investigation on energy performance of double skin façade in Hong Kong," *Energy and Buildings,* 2009.

[37] G. Andreotti, From single to double skin facades, vol. 50, Via colleoni, 2001, pp. 360-362.

[38] S. Khoshroonejad, a Comparison of Daylight Prediction Methods Msc. Architecture Thesis, Eastern Mideterranean University, 2010.

[39] E. Alakavuk, "Sıcak iklim bölgelerinde çift kabuk cam cephe sistemlerinin tasarımı için kullanılabilecek bir yaklaşım," *DEÜ Fen Bilimleri Enstitüsü,* 2010.

[40] Crespo and M. L. A.. [Online]. Available: http://envelopes.cdi.harvard.edu/envelopes/content/.

[41] B. Alessi, "Double Skin Facade and its Benefits. Dissertation Report," 2009.

[42] W. Streicher, Double Skin Facades in European Buildings, Advances in building Energy Research, 2007.

[43] H. Poirazis, ""Double skin facades; a literature review", A report of IEA SHC Task 34 ECBCS Annex 34," *Department of Construction and Architecture, Lund University, Sweden,* 2006.

[44] A. Fissabre and B. Niethammer, "The Invention of glazed Curtain Wall in 1903 -The Steiff Toy Factory," in *Third International Congress on Construction History, Brandenburg University of Technology Cottbus*, Germany, 2009.

[45] H. Poirazis, "Double skin facades: a literature review," *A report of IEA SHC Task 34 ECBCS Annex 41, Department of Contruction and Architecture, Lund University, Sweden,* 2006.

[46] L. Turner, "Climate and Architecture Report for Honor's Section 8 of MET1010 Introduction," Florida State University, 2003.

[47] H. T. Sa'ad, "The Changing role of the Architect and architecture in the Context of the," *In Nkwogu, U. O. (ed.) Architects and Architecture in Nigeria. AARCHES: Nigeria,* 2001.

[48] IPCC, "The Regional Impacts of Climate Change: An Assessment of Vulnerability," *R.T.Watson, M.C.Zinyowera, R.H.Moss (Eds) Cambridge University Press,* 1997.

[49] K. Harrison and T. Meyer-Boake, "Tectonics of Environmental Skins: The Occidental Chemical Centre," *School of Architecture, University of Waterloo,* p. 6, 2003.

[50] D. Gissen, Big & green: toward sustainable architecture in the 21st century, New York: Princeton Architectural Press, 2002.

[51] A. Bayram, Energy Performance of Double Skin Facades in Intelligent Office Buildings: A Case Study in Germany, The Middle East Technical University, 2003.

[52] M. Wigginton and J. Harris, Intelligent Skins, Oxford: Architecture Press, 2006.

[53] M. Szell, M. Svéd and B. Petró, Transzparens épületszerkezetek., Szerényi és Gazsó Bt., 2001.

[54] U. Pottgiesser, Fassadenschichtungen: Glas Mehrschalige Glaskonstruktionen: Typologie,Energie, Konstruktionen, Projektbeispiele., Bauwerk., 2004.

[55] X. Loncour, M. Deneyer, G. Blasco, P. Flamant and Wouters, Ventilated Double Skin Facades; Classification & Illustration of Facade Concepts, Belgian Building Research Institute, Department of Building Physics, 2004.

[56] T. Herzog, R. Krippner and W. Lang, Facade Construction Manual, Detail, 2018.

[57] A. Gelesz and A. Reith, "Classification and re-evaluation of double skin facades.," *International Review of Applied Sciences and Engineering,* pp. 2(2), 129-136, 2011.

[58] D. Saelens, J. Carmeliet and H. Hens, "Energy Performance Assessment of Multiple-Skin Facades.," *HVAC&R Research,* pp. 9(2), 167–185. , 2003.

[59] . E. Lee, . S. Selkowitz, V. Bazjanac , V. Inkarojrit and C. Kohler, "High-performance commercial building facades.," 2002.

[60] B. Pollard, "Double skin facades, more is less?," *Royal Australian Institute of Architects,* 2009.

[61] P. C. Wong, D. Prasad and M. Behnia, "A new type of double-skin façade configuration for the hot and humid climate.," *Energy and Buildings,* pp. 40(10), 1941–1945., 2008.

[62] M. Gruner, "The potential of façade- integrated ventilation systems in Nordic," *NTNU university,* 2012.

[63] I. Eggers, P. Matthes, J. Panaskova and D. Muller, "Façade integrated hybrid ventilation system for school buildings," *9th international conference and exhibition -Healthy Buildings,* 2009.

[64] B. Alessi, "Double skin facade and its benefits. Dissertation Report," *7th International Line. Copenhagen Technical Academy,* 2008.

[65] A. Compagno, Intelligent Glass Facades: Materials, Practice, Design, Germany: Birkhauser, 2002.

[66] H. Alibaba and M. Ozdeniz, "Energy Performance and Thermal Comfort of Double-Skin and Single-Skin Facades in Warm-Climate Offices," *Journal of Asian Architecture and Building Engineering,* pp. 15(3), 635–642, 2016.

[67] J. Davidson, J. Heinberg and B. Williamson, "Builder's guide to energy efficient homes in Louisiana: Insulation Materiala and Techniques.," *Lousiana department of natural resources, technology assessment division.,* 2007.

[68] R. Zevenhoven, M. Fält and L. P. Gomes, "Thermal radiation heat transfer: Including wavelength dependence into modelling," *International Journal of Thermal Sciences,* pp. 86, 189–197, 2014.

[69] V. Yellamraju, "Evaluation and design of Double Skin Facades for office buildings in hot climates," *Texas: A& M University,* 2004.

[70] D. Fosas, D. A. Coley, S. Natarajan, M. Herrera, M. F. Pando and A. Ramallo-Gonzalez, "Mitigation versus adaptation: Does insulating dwellings increase overheating risk?," *Building and Environment,* pp. 740-759, 2018.

[71] R. Gupta and M. Gregg, "Preventing the overheating of English suburban homes in a warming climate," *Building Research & Information,* pp. 281-300, 2013.

[72] D. M. M. Arons, "Properties and applications of double-skin building facades," *Massachusetts Institute of Technology,* 2000.

[73] Ç. Öztürk, "Gelişmiş Doğal Aydınlatma Sistemleri ve Uygulama Örnekleri.," *Gazi Üniversitesi Yüksek Lisans Tezi,* 2006.

[74] B. Manav, "Light and Health: The Efect of Light on the Biological System," *stanbul Kültür Üniversitesi,* 2007.

[75] N. Baker and K. Steemers, "Daylight Design of Buildings," *James and James (Science Publishers),* 2002.

[76] T. Kazanasmaz , M. Günaydin and S. Binol , "Artificial neural networks to predict daylight illuminance in office buildings," *Building and Environment,* pp. 44(8), 1751–1757, 2009.

[77] . C. Reinhart and . S. Selkowitz, "Daylighting—Light, form, and people. Energy and Buildings," pp. 38(7), 715–717, 2006.

[78] A. A. Buhari and H. Z. Alibaba, "ANALYSIS OF DAYLIGHTING QUALITY IN INSTITUTIONAL LIBRARIES," *International Journal of Electrical and Electronics Research,* pp. Vol. 7, Issue 4, pp: (6-20), 2019.

[79] K. Robertson, "guide on daylighting of buildings," *SCHLCMHC,* 2003.

[80] . I. R. Maestre, J. L. Blázquez , . F. J. Gallero and P. R. Cubilla, "Influence of selected solar positions for shading device calculations in building energy performance simulations," *Energy and Buildings,* pp. 101, 144–152., 2015.

[81] M. Unal, "Çift kabuk cephelerin sistematik analizi ve uygulama örneklerinin incelenmesi. Master Thesis, Mimar Sinan University, Istanbul. (P.110-114)," 2006.

[82] J. Gliner, G. A. Morgan and N. L. Leech, Research methods in applied settings: An integrated approach to design and analysis., Routledge, Taylor & Francis Group. , 2017.

[83] J. D. Freitas, J. Cronemberger, R. M. Soares and C. N. Amorim, "Modelling and assessing BIPV Envelopes using parametric Rhinoceros Plug-ins Grasshopper and Ladybug," *Renewable Energy,* pp. 160, 1468-1479, 2020.

[84] A. Groenewolt, J. Bakker, J. Hofer and Z. Nagy, "Methods for modelling and analysis of bendable photovoltaic modules on irregularly curved surfaces," *International Journal of Energy and Environmental Engineering,* p. 7(3), 2016.

[85] D. B. Crawley, C. O. Pedersen, L. K. Lawrie and F. C. Winkelmann, "EnergyPlus: energy Simulation Program," *ASHRAE J.,* pp. 42(4),49–56., 2000.

[86] M. S. Roudsari, M. Pak and A. Smith, "Ladybug: a parametric environmental plugin for grasshopper to help designers create an environmentally-conscious design," *Proceedings of Building Simulation 2013: 13th Conference of International Building Performance Association,* pp. 26-28, 2013.

[87] D. Ibarra and F. Reinhart, "Solar availability: a comparison study of six irradiation distribution methods," *Proceedings of Building Simulation 2011: 12th Conference of International Building Performance Simulation Association.,* 2011.

[88] Solemma, "ClimateStudio," 2021. [Online]. Available: https://climatestudiodocs.com/.

[89] Poirazis and Harris, "Double Skin Facades for Office Buildings- Literature Review Report," 2004.

[90] E. Gratia and A. De Herde, "The most efficient position of shading devices in a double-skin facade," *Energy and Buildings,* pp. 39364-373, 2007.

[91] W. M. Trochim, J. P. Donnelly and K. Arora, Research Methods: The Essential Knowledge Base, Cengage, 2015.

[92] M. Pidd, Tools for Thinking: Modelling in Management Science, Chichester: John Wiley and Sons Ltd, 2003.

[93] S. A. Kalogirou, Solar Energy Engineering, Elsevier Inc., 2014.

[94] A. E. Dixon and J. D. Leslie, Solar Energy Conversion, 1979.

[95] M. Kottek, J. Grieser, C. Beck, B. Rudolf and F. Rubel, "World map of the Köppen-Geiger climate Classification updated," *Meteorologische Zeitschrift,* pp. 15(3), 259-263, 2006.

[96] O. J. Hendriksen, H. Sorensen, A. Svenson and P. Aaqvist, "Double Skin Facades Fashion or a step towards sustainable buildings.," in *Proceedings of ISES*, Eurosun, 2000.

[97] L. Bellia, F. D. Falco and F. Mnichiello, "). Effects of solar shading devices on energy requirements of standalone office buildings for Italian climates," *Applied Thermal Engineering, 54(1),* pp. 190-201, 2013.

VITA

EDUCATION

Masters of Architecture Student at Architecture Department of Graduate school of Engineering at Ozyegin University, (February 2019- December 2021). Thesis title: Thermal And Daylight Performance of Double-Skin Facades; Case Study of an Office Building.

Bachelor of Architectural sciences at Kulliyah of Architecture and Environmental Design at International Islamic University Malaysia (IIUM), Kuala Lumpur (November, 2017).

ACADEMIC AWARDS

Outstanding Undergraduate student, Rector's List, Department of Architecture, International Islamic University Malaysia, November 2017.

PUBLICATIONS

H. Alsafadi and T. Ashrafian. : Interaction between controlled natural lighting and IEQ: Integrated double skin facades approach applied on an office building. Proceedings of the 17th International Healthy Buildings Conference 21-23 June 2021.